NASA Technical Memorandum 80129

Effect of Several Airframe/Nozzle Modifications on the Drag of a Variable-Sweep Bomber Configuration

Richard J. Re and David E. Reubush

OCTOBER 1979

NASA

NASA Technical Memorandum 80129

Effect of Several Airframe/Nozzle Modifications on the Drag of a Variable-Sweep Bomber Configuration

Richard J. Re and David E. Reubush
Langley Research Center
Hampton, Virginia

National Aeronautics
and Space Administration

**Scientific and Technical
Information Branch**

1979

SUMMARY

An investigation of a 0.06-scale model of a variable-sweep bomber airplane was conducted in the Langley 16-foot transonic tunnel to identify possible modifications to the configuration which would result in reduced drag. The modifications, some of which were tested in combination, included simulated two-dimensional nozzles; staggered and extended nozzles; short, long, and no interfairings between the nozzles; partial and complete wing-glove fairings; glove-fuselage sidefairing; fuselage underfairing; and wing pods. Tests were conducted at Mach numbers from 0.60 to 1.30 at angles of attack in the range from -4° to 12° with the wings swept 25°, 65°, and 67.5°.

Results from this investigation indicate that modifications which reduced the drag of the configuration included simulated two-dimensional nozzles, extended nozzles, wing-glove fairings, and the glove-fuselage sidefairing combined with the fuselage underfairing. Modifications which resulted in little or no change to the configuration drag included the interfairing changes and the staggered nozzles. Wing pods resulted in substantially increased drag.

INTRODUCTION

An airplane which must operate over a range of Mach numbers and altitudes is a design compromise and probably cannot perform as well at any given condition as a configuration optimized for that particular condition. However, geometric features such as variable wing sweep and variable nozzle throat and exit area can bring the configuration closer to the optimum for a particular operating condition. Unfortunately, the variable-geometry features may result in penalties across the flight envelope. For example, variable wing sweep can result in steps and gaps in the wing-glove juncture area which can produce higher drag. Variable exhaust nozzles, when closed down to cruise settings, often have large boattail angles that result in high drag. Also, for twin-engine configurations (or nacelles) with closely spaced exhaust nozzles, the large surface slopes in the gutter beween the nozzles can cause flow separation and result in high drag. The variable-sweep bomber configuration of this investigation is an example of an airplane with some of these problems.

In an effort to provide means to improve the drag characteristics of the configuration, an investigation of various modifications applied to a 0.06-scale model of a variable-sweep bomber was conducted in the Langley 16-foot transonic tunnel. Included in the modifications were wing-glove fairings to smooth out the steps and gaps at the wing-glove juncture; a fuselage underfairing and wing pods (individually and in combination) to improve the Mach 1.0 cross-sectional area distribution; nozzle extensions to smooth out the area distribution and to move the nozzle boattail away from a separation-producing step; simulated two-dimensional nozzles to eliminate the nacelle gutter area and round nozzle boattail; and short, long, and no interfairings to investigate whether the

gutter flow characteristics could be affected by a relatively small modification. In addition, the model was tested with aero-reference nozzles and with the nacelles removed to give an indication of the lower drag limits which might be approachable. The tests were conducted at Mach numbers from 0.60 to 1.30, at angles of attack in the range from -4° to 12°, and with wings swept 25°, 65°, and 67.5°.

SYMBOLS

The forces and moments presented are referenced to the stability axes. The origin of the axis system is at model station 150.55 cm.

$C_{A,B}$ base axial-force coefficient, $\frac{\text{Base axial force}}{qS}$

$C_{A,I}$ nacelle internal axial-force coefficient (four ducts), $\frac{\text{Internal axial force}}{qS}$

C_D drag coefficient, $\frac{\text{Drag}}{qS}$

C_L lift coefficient, $\frac{\text{Lift}}{qS}$

C_{L_α} lift-curve slope measured at $\alpha = 0^{\circ}$, per deg

C_m pitching-moment coefficient, $\frac{\text{Pitching moment}}{qS\bar{c}}$

$C_{m_{C_L}}$ longitudinal stability parameter measured at $C_L = 0$, $\frac{\Delta C_m}{\Delta C_L}$

$C_{m,0}$ pitching-moment coefficient at $C_L = 0$

$\bar{c}$ wing reference chord (mean geometric chord for $\Lambda = 15^{\circ}$), 28.049 cm

M free-stream Mach number

q free-stream dynamic pressure

S wing reference area ($\Lambda = 15^{\circ}$), 0.6509 m^2

α angle of attack of fuselage reference line, deg

α_0 angle of attack for $C_L = 0$, deg

ΔC_D increment of drag coefficient at constant lift coefficient

Λ leading-edge sweepback angle of outboard wing panel, deg

Abbreviations:

L.E. leading edge

MS model station, cm

2-D two dimensional

WIND TUNNEL

This investigation was conducted in the Langley 16-foot transonic tunnel, which is a single-return atmospheric wind tunnel with continuous air exchange. The test section is octagonal in shape with a distance of 4.724 m between opposite walls (equivalent to the area of a circle 4.850 m in diameter) and has axial slots at the wall vertices. The total width of the eight slots in the vicinity of the model is approximately 3.7 percent of the test-section perimeter. The tunnel sting-support system pivots in such a manner that the model remains on or near the test-section center line through the angle-of-attack range. Details of the operation of the tunnel and its flow qualities are presented in reference 1.

MODEL

The model was a 0.06-scale model of a variable-sweep bomber airplane with the fuselage afterbody modified to allow the model to be mounted on a sting support. A three-view drawing of the model is shown in figure 1. The wings could be manually positioned at leading-edge sweep angles from 15° to 67.5°. For this investigation, they were positioned at 25°, 65°, and 67.5°. The wings in the 65° sweep position were shimmed at the wing pivot point such that they approximated a 1g flight condition (incidence angle of the entire wing was decreased by 1.5°). The horizontal tail was fixed at 0°.

During the investigation, the model was configured with a number of modifications and combinations thereof to evaluate their effectiveness in reducing the aircraft drag. Sketches and photographs of model parts and modifications can be found in figures 2 to 7. Shown in figure 2 are sketches of the nacelle and nozzle modifications such as cruise (nonafterburning) and aero-reference nozzles, staggered and extended cruise nozzles, short and long nozzle interfairings and simulated 2-D nozzles. The aero-reference nozzles have been used in previous investigations of this model as a standard to maximize the amount of flow through the nacelle ducts. Here they are used to approximate nozzles in the afterburning mode with little external boattail. Figure 3 presents sketches of the two fuselage fairings investigated. Figure 4(a) shows the wing pods, which were tested at a wing sweep of 67.5°, and figure 4(b) shows a cross-

sectional area distribution of the model with wing pods and fuselage underfairing. Photographs of some model configurations and the glove fairings tested with the wings swept 25° are shown in figure 5. Photographs of the configurations tested with the wings swept 65° and 67.5° are shown in figures 6 and 7, respectively.

TESTS AND METHODS

The model was tested at angles of attack in the range from -4° to 12° at a sideslip angle of 0°. The Mach number range of the tests varied with wing leading-edge sweep as follows: 0.60 to 0.80 at $\Lambda = 25°$; 0.60 to 0.95 at $\Lambda = 65°$; and 0.60 to 1.30 at $\Lambda = 67.5°$. Reynolds number, based on wing reference chord, varied from 2.9×10^6 at a Mach number of 0.60 to 3.6×10^6 at a Mach number of 1.30.

Aerodynamic forces and moments were measured by an internal six-component strain-gage balance. Model angle of attack was obtained by correcting the angle of the model support system for deflection of the sting and balance under aerodynamic loads and for test-section stream angularity. The force data were adjusted to the condition of free-stream static pressure in the balance cavity, at the fuselage base, at the nacelle base (area between the nozzles when the interfairing was removed), and at the base of the aero-reference nozzles. Some examples of the magnitudes of the various pressure adjustments are shown in figure 8 in base axial-force coefficient form. In addition, the force data were also corrected for the internal axial force in the four flow-through ducts of the nacelles. The internal axial force was determined from pressure measurements made during preliminary wind-tunnel tests with external survey rakes mounted at the nacelle bases for the configuration with the cruise and aero-reference nozzles. The internal geometry of the nacelles with the simulated 2-D nozzles was the same as that with the cruise nozzles, so that no additional internal axial-force measurements were necessary for the configuration with simulated 2-D nozzles. For the nacelles with staggered and extended nozzles, internal skin-friction increments were calculated and added to the cruise-nozzle internal axial-force coefficients. The internal axial-force coefficient corrections for the various duct/nozzle combinations are presented in figure 9.

All configurations were tested with fixed boundary-layer transition on the model surfaces. The transition-fixing strips consisted of No. 90 and No. 100 silicon carbide grit positioned as illustrated in figure 10. The location of the strips on the variable-sweep portion of the wings remained the same regardless of wing sweepback angle.

DISCUSSION

25° Wing-Sweep Configurations

The effect of removing the nacelles and of nozzle shape on the longitudinal characteristics of the model with wings swept 25° is shown in figures 11 and 12 for Mach numbers of 0.60, 0.70, 0.75, and 0.80. The model was tested without nacelles (fig. 5(a)) to obtain an estimate of the total drag of the installed

propulsion system. As expected, removal of the nacelles resulted in a large reduction in drag compared with the configuration with the cruise nozzles and short interfairings (referred to hereafter as the basic configuration, fig. 2(a)). The aero-reference nozzles (fig. 2(a)) were tested at these Mach numbers to give an indication of the lowest drag level possible with a complete nacelle installation. (These nozzles approximate an afterburning-nozzle geometry for high Mach numbers and wing sweeps.) Because of their reduced boattail angle, the configurations with aero-reference and simulated 2-D nozzles (figs. 2(d) to (f)) had lower drag levels when compared with the basic configuration. All four of the configurations had about the same lift-curve slope, angle of attack for zero lift, and stability level. The configuration with nacelles off showed a large reduction in pitching-moment coefficient at zero lift $C_{m,0}$ when compared with the basic configuration. The configuration with aero-reference nozzles had a slight reduction in $C_{m,0}$ when compared with the basic configuration and the configuration with simulated 2-D nozzles had essentially the same value of $C_{m,0}$ as the basic configuration.

The effect of either staggering or extending the nozzles (fig. 2(b)) on the longitudinal characteristics of the basic configuration is shown in figures 13 and 14. Staggering or extending the nozzles had little effect on any longitudinal characteristic except drag. The drag of the configuration with staggered nozzles is generally lower than that of the basic configuration (typically $\Delta C_D < 0.0010$) and the drag of the configuration with extended nozzles is lower still (typically $0.0010 < \Delta C_D < 0.0025$). Although the configurations with staggered and extended nozzles do generally reduce the drag (probably by moving the boattailed nozzles farther aft of the disturbances created by the step at the aft end of the glove), they may not be practical because of the possibility of the nozzles scraping the ground on take-off rotation.

Figures 15 and 16 show the effect on the longitudinal characteristics of removing the nozzle interfairing from the basic configuration (cruise nozzles, short interfairing). Except for random minor differences, the removal of the interfairings had no effect on the longitudinal characteristics. Little effect was also found when the short interfairing was replaced with a long interfairing (fig. 2(c)) on the configuration with extended nozzles (figs. 17 and 18).

Figures 19 and 20 present the effect on the longitudinal characteristics of fairing the upper surface of the wing glove with a partial and a complete fairing (figs. 5(b) and (c)) to eliminate the steps and gaps in the wing-glove juncture area. Addition of these fairings produces a small but consistent increase in lift at a given angle of attack and a reduction in drag. The drag of the configuration with the partial glove fairing is lower than the basic configuration (typically $0.0005 < \Delta C_D < 0.0015$) and the configuration with the complete glove fairing is lower still (typically $0.0009 < \Delta C_D < 0.0025$). Also, as expected, the higher the Mach number the more effective the fairings become.

The combined effect of extending the nozzles and adding the complete wing-glove fairing on the longitudinal characteristics of the model is shown in figures 21 and 22. This combined modification reduced the drag of the model for lift coefficients below 0.8 and decreased lift and stability at higher angles of attack for Mach numbers of 0.70, 0.75, and 0.80. The drag reduction, which was the greatest at zero lift, was still significant at typical cruise lift

coefficients. (See, for example, fig. 22(b).) However, there are conditions at which the drag of this configuration is not as low as the drag of either the extended-nozzle configuration or the complete glove-fairing configuration. Also, the measured drag of the configuration with the combined modifications is never as low as the drag calculated using the sum of increments obtained with the separate modifications.

65° Wing-Sweep Configurations

The effect of removing the nacelles and of the various nozzle shapes on the longitudinal characteristics of the model with the wings swept 65° is shown in figures 23 and 24 for Mach numbers of 0.60, 0.80, 0.85, 0.90, and 0.95. The results for these configurations at this wing sweep for Mach numbers from 0.60 to 0.80 are comparable with those for the same configurations with the wings swept 25°. Of interest for the 65° wing-sweep configurations is the effect of the increased Mach number range. For example, the data of figure 24(b) show that addition of the nacelles appears to reduce the Mach number at which the drag rise starts by approximately 0.05. Lift-curve slope and angle of attack for zero lift are virtually the same for all four configurations. The stability level was affected by the configuration changes and by Mach number (fig. 24(a)). As with the 25° wing sweep, the configuration with nacelles off had a lower $C_{m,0}$ than the other three configurations with nacelles on. The configuration with aero-reference nozzles had slightly lower $C_{m,0}$ than the basic configuration or the configuration with simulated 2-D nozzles.

The effect of staggering (fig. 6(c)) and of extending the cruise nozzles with the short interfairing (fig. 6(a)) on the longitudinal characteristics of the model with wings swept 65° (figs. 25 and 26) was also about the same as that for the model with wings swept 25°. The drag of the configuration with staggered nozzles was generally about the same as or slightly lower than that of the basic configuration over the Mach number range, whereas extending the nozzles was more effective in reducing the drag. Extending the nozzles reduced the drag by less than 0.0010 at Mach numbers below 0.90 and by 0.0010 to 0.0020 at Mach numbers of 0.90 and 0.95. Lift-curve slope, angle of attack for zero lift, and pitching moment at zero lift were about the same for the basic configuration as for the configurations with staggered and extended nozzles. The basic configuration generally had a slightly higher stability level than the configurations with staggered or extended nozzles.

The effect of removing the nozzle interfairings on the longitudinal characteristics of the model is shown in figures 27 and 28. Except for minor reductions in drag there was no effect on model longitudinal characteristics when the interfairings were removed. The effect of replacing the short nozzle interfairings with longer ones was investigated for the configuration with extended nozzles. The results of this modification are shown in figures 29 and 30. Except for small random variations, this change had no effect on longitudinal characteristics.

Effect of the addition of a wing-glove fairing (fig. 6(b)) and of a glove-fuselage sidefairing in combination with a fuselage underfairing (figs. 6(d) to 6(h)) on the longitudinal characteristics of the model is shown in figures 31

and 32. These two configurations had drag levels equal to or slightly lower than the basic configuration at Mach numbers less than 0.90. At Mach numbers of 0.90 and 0.95, improvements in area distribution with the glove-fuselage side-fairing and fuselage underfairing (change in area distribution similar to pods, fig. 4(b)) resulted in a reduction in drag. The configuration with a wing-glove fairing continued to produce drag levels which were the same as or slightly lower than the basic configuration, probably because this fairing was designed to fill and fair gaps and steps in the glove area and not significantly affect the area distribution. Neither of these modifications significantly changed any of the other longitudinal characteristics from the basic configuration except for a positive increment in the values of the stability parameter at zero lift $C_{m_{C_L}}$ for some of the lower Mach numbers.

Effect on longitudinal characteristics of combining the glove fairing with the extended nozzles is shown in figures 33 and 34. For this configuration, all longitudinal characteristics remained essentially the same as the basic configuration except the drag, which was reduced at all Mach numbers investigated. This configuration generally gave a drag level equal to that which would be expected by subtracting the sum of the two individual drag reductions from the drag of the basic configuration. This is not the same result as that found for $\Lambda = 25^\circ$, for which the sum of the two individual reductions was generally greater than the reduction measured with the combined modifications. This may be due to the changes in area distribution caused by sweeping the wings combined with the area distribution changes caused by the fairing and extensions.

67.5° Wing-Sweep Configurations

The model with wings swept 67.5° was tested in the basic configuration (cruise nozzles, short interfairings) and configured with wing pods, fuselage underfairing, and a combination of pods and underfairing. The tests were made at Mach numbers of 0.60, 0.80, 0.85, 0.90, 0.95, and 1.30. (Only the combination and the basic configuration were tested at $M = 1.30$.) The effect of these modifications on the longitudinal characteristics of the model is shown in figures 35 and 36. The fuselage underfairing produced drag values which were the same as or slightly lower than the basic configuration, whereas the wing pods and combination of wing pods and underfairing produced drag values which were substantially higher than the basic configuration (high drag of combination due to pods, not underfairing). All four configurations have about the same lift-curve slope. Addition of the fuselage underfairing did not significantly affect the other longitudinal characteristics, whereas addition of the wing pods (either alone or in combination with the underfairing) resulted in an increase in angle of attack for zero lift, a decrease in stability at Mach numbers above about 0.80, and a decrease in pitching moment at zero lift for all subsonic Mach numbers.

The fuselage underfairing and the wing pods were also tested for configurations with the aero-reference nozzles at Mach numbers of 0.85 and 1.30. The effect of these modifications on longitudinal characteristics is shown in figures 37 and 38. As with the configuration with cruise nozzles, the underfairing resulted in drag values which were equal to or slightly lower than the configuration with aero-reference nozzles (unmodified) and had only minor effect on

the other longitudinal characteristics. Addition of the wing pods resulted in significantly higher drag and changes to all the other longitudinal characteristics except C_{L_α}. Although the wing pods were designed to smooth the wing-glove surface as well as to improve the area distribution (fig. 4(b)) the results indicate any drag improvement due to changing the area distribution is overcome by a large drag increase due to local flow problems caused by the pods themselves (fig. 36(b)).

Incremental Drag Comparisons

Typical flight lift coefficients were chosen for the three wing sweeps investigated - 0.63 for $\Lambda = 25^\circ$ and 0.16 for $\Lambda = 65^\circ$ and 67.5° - and incremental drag data were obtained for the various configuration modifications (figs. 39 to 46). The basic configuration used for all these comparisons is the configuration with the wing sweep of interest, nacelles on with cruise nozzles, and short nozzle interfairings. These data are presented in bar chart form without further comment since the effect on drag of various modifications has been previously discussed in this section.

CONCLUDING REMARKS

A 0.06-scale model of a variable-sweep bomber aircraft has been investigated in the Langley 16-foot transonic tunnel to identify possible modifications which would result in reduced drag for the configuration. Tests were conducted at Mach numbers from 0.60 to 1.30 at angles of attack in the range from -4° to 12°, with wings swept 25°, 65°, and 67.5°. When all Mach numbers and wing sweeps are considered, results from this investigation indicate that either the simulated two-dimensional nozzles or the combination of complete glove fairing and extended nozzles gave the largest drag reductions. Other modifications which gave drag reductions include the glove-fuselage sidefairing and fuselage underfairing; the wing-glove fairing; extended nozzles; the partial glove fairing; and staggered nozzles. Results also indicate that nozzle interfairing modification or removal had only minor effects on configuration drag, whereas installation of wing pods significantly increased drag.

Langley Research Center
National Aeronautics and Space Administration
Hampton, VA 23665
August 7, 1979

REFERENCE

1. Corson, Blake W., Jr.; Runckel, Jack F.; and Igoe, William B.: Calibration of the Langley 16-Foot Transonic Tunnel With Test Section Air Removal. NASA TR R-423, 1974.

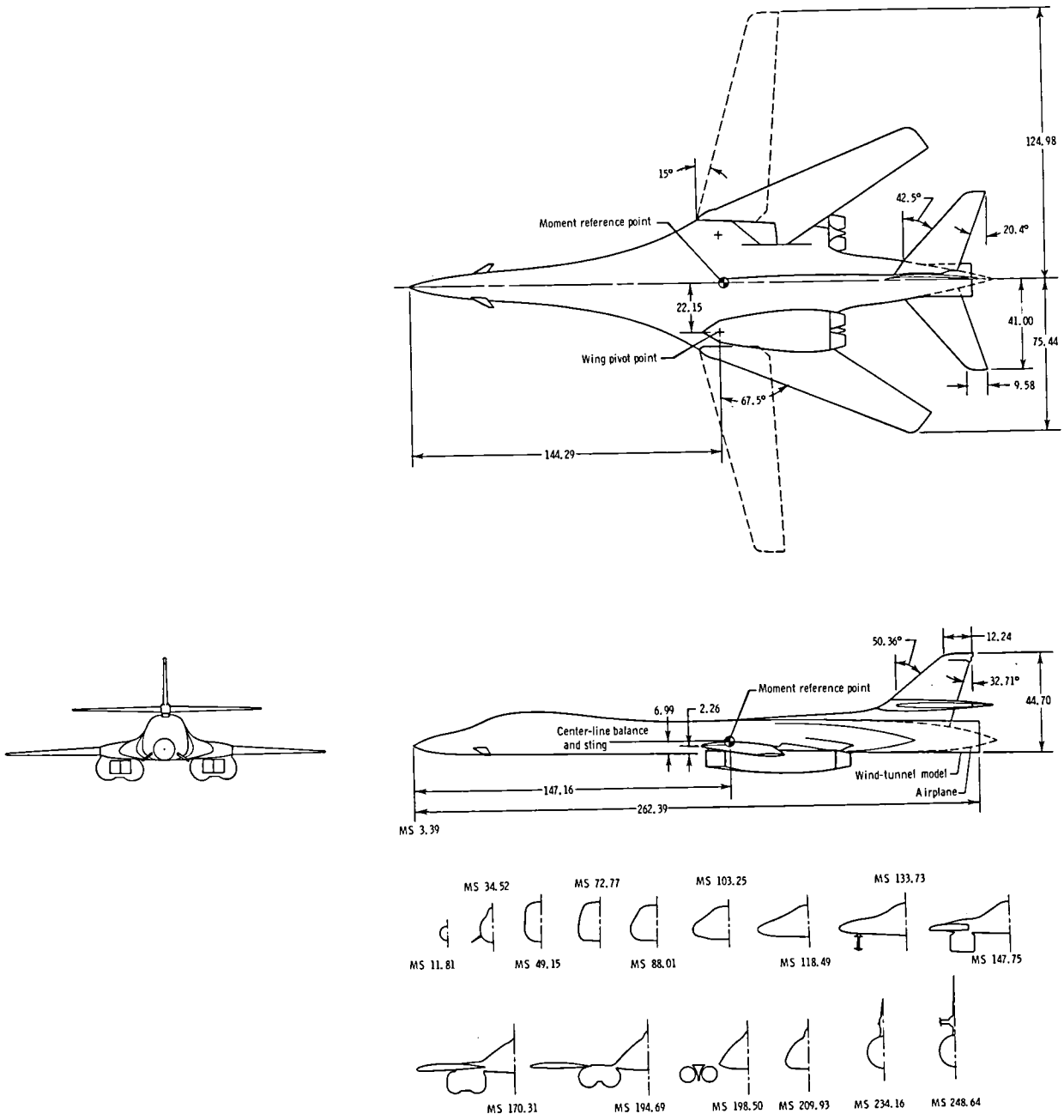

Figure 1.- General arrangement of model with cruise nozzles and short interfairings. All dimensions in centimeters unless otherwise indicated.

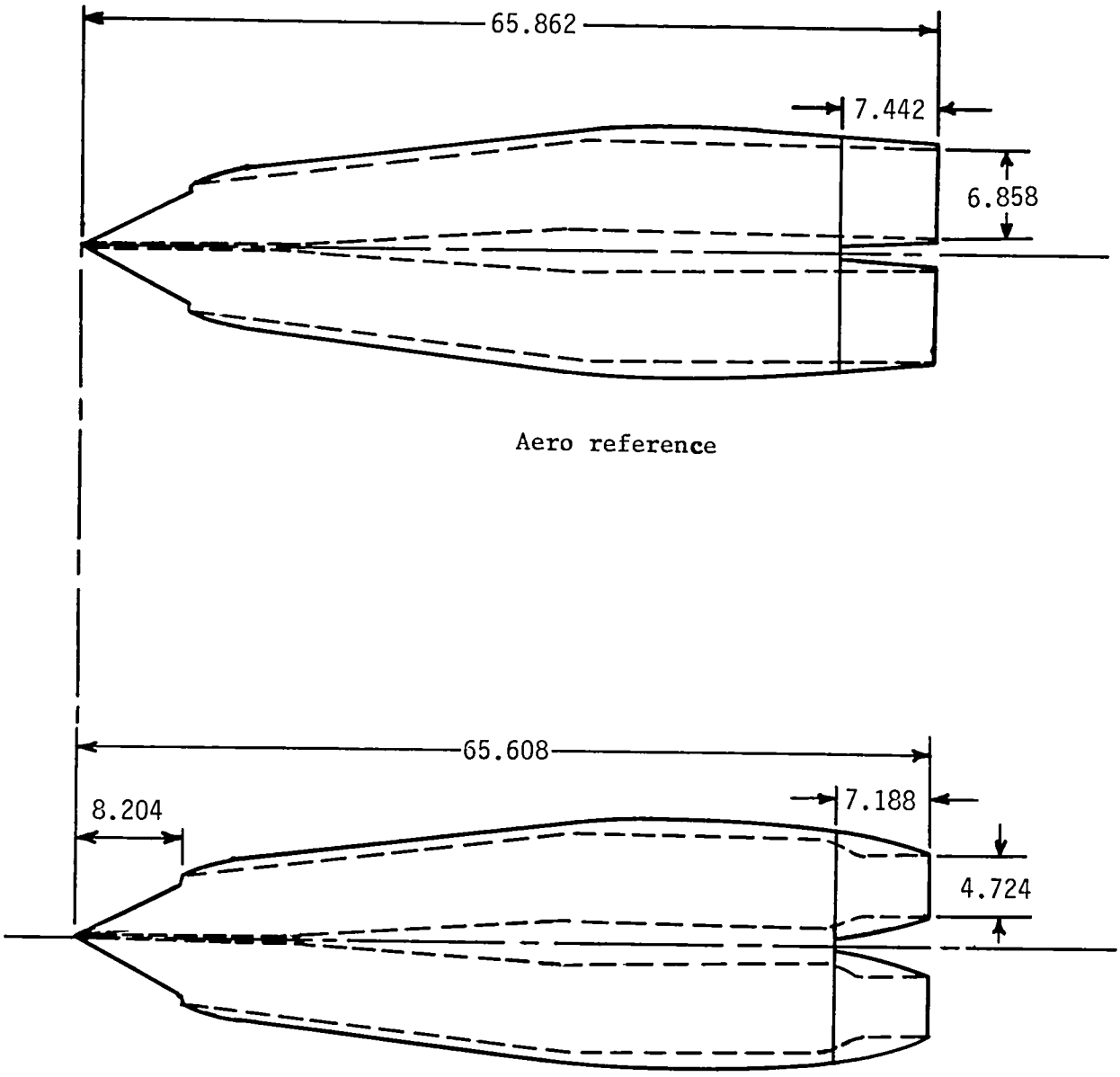

(a) Nacelles with aero-reference and cruise nozzles.

Figure 2.- Nacelle and nozzle configuration variables. All dimensions are in centimeters.

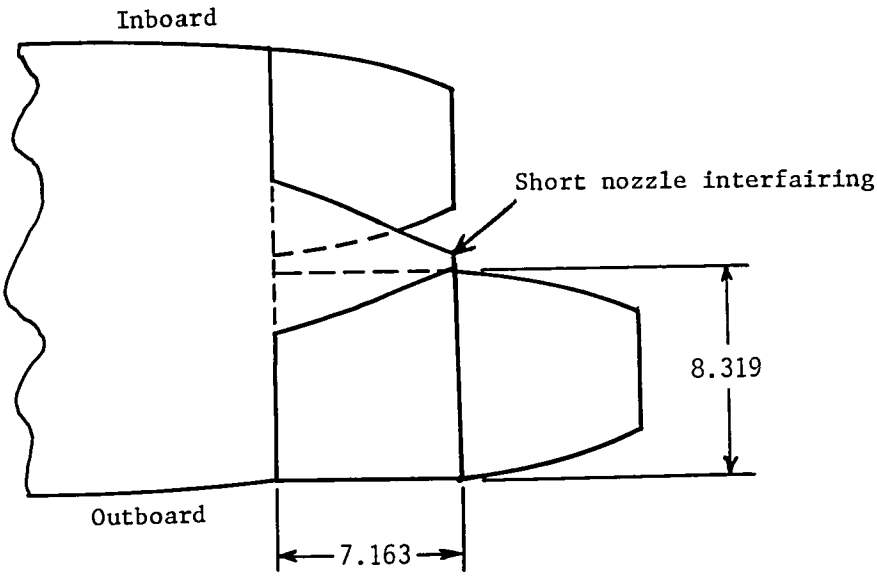

Staggered cruise nozzles

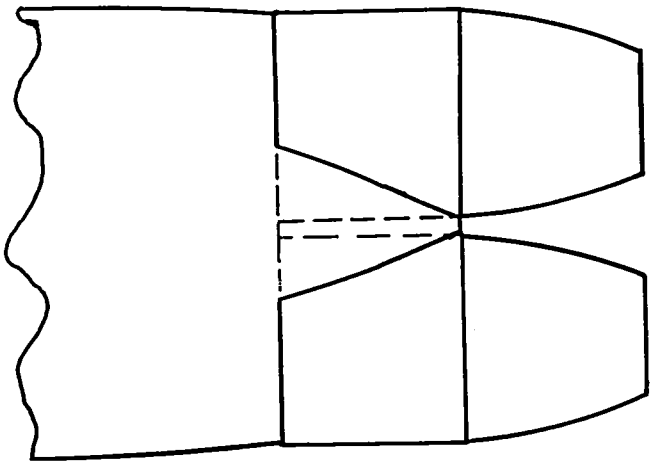

Extended cruise nozzles

TOP VIEW

(b) Staggered and extended cruise nozzles.

Figure 2.- Continued.

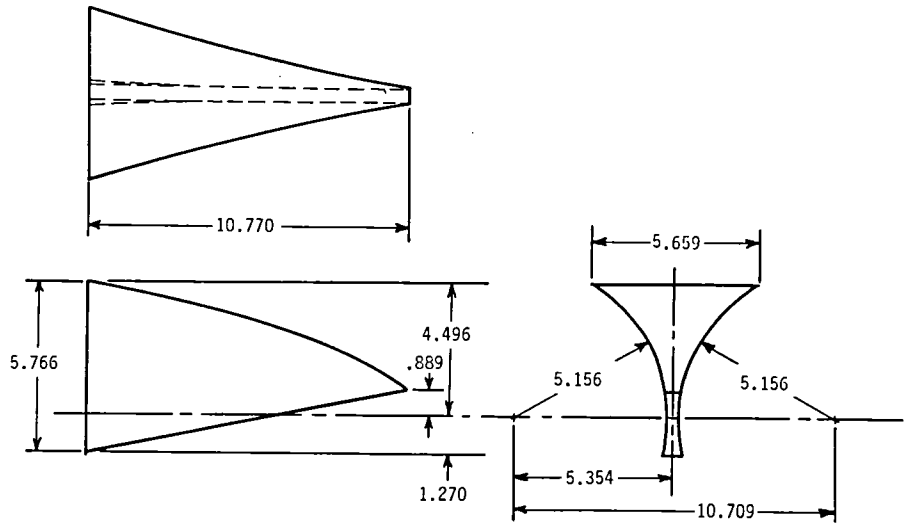

Long interfairing

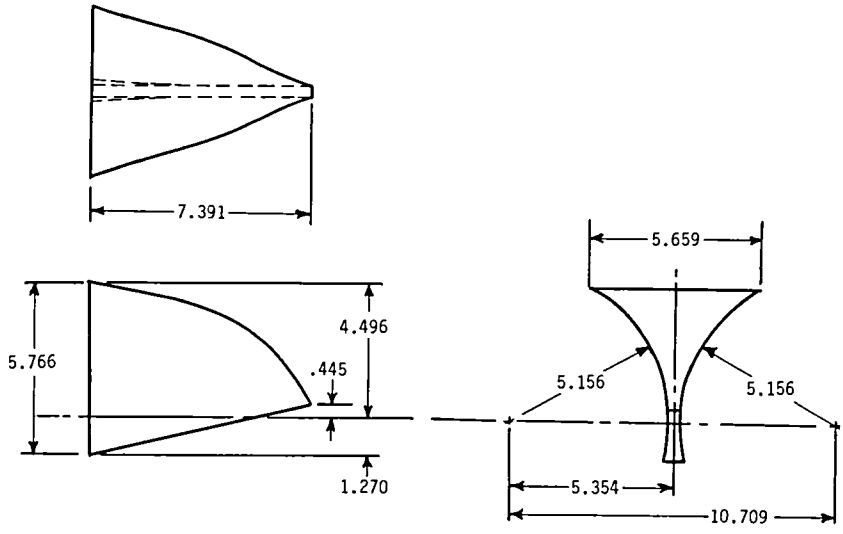

Short interfairing

(c) Short and long nozzle interfairings.

Figure 2.- Continued.

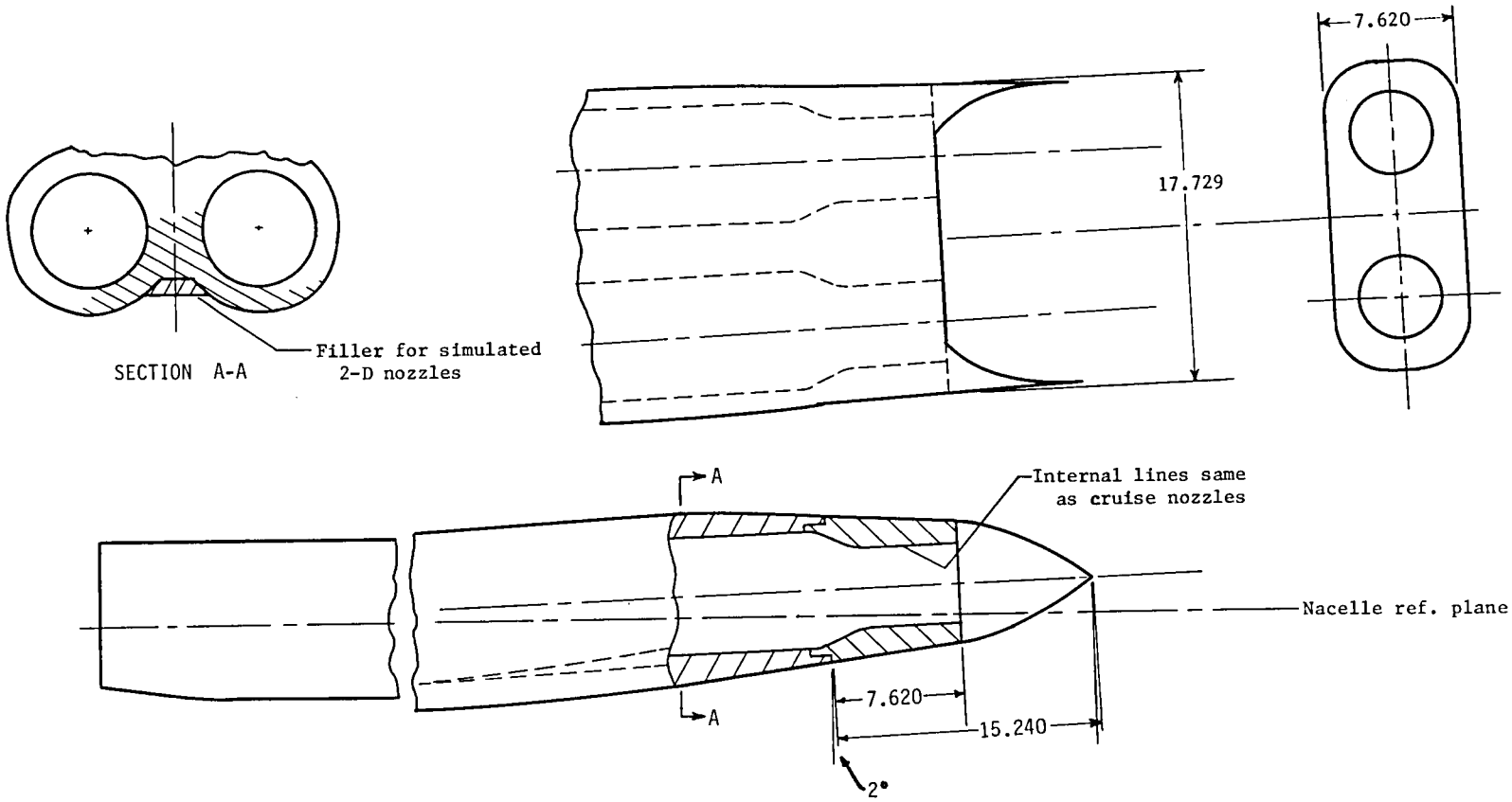

(d) Nacelle with simulated 2-D nozzles.

Figure 2.- Continued.

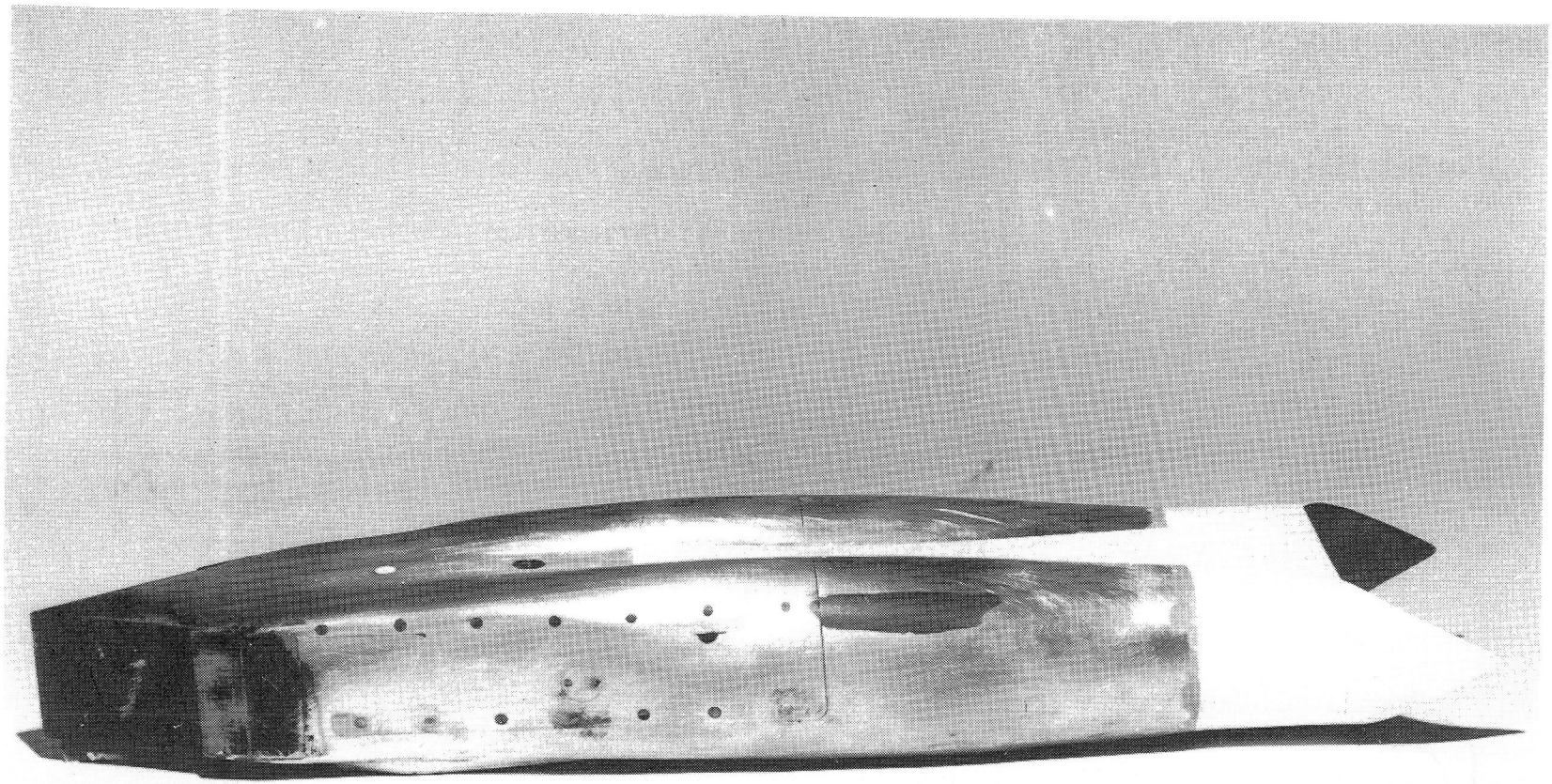

L-75-648

(e) Side below view of nacelle with simulated 2-D nozzles.

Figure 2.- Continued.

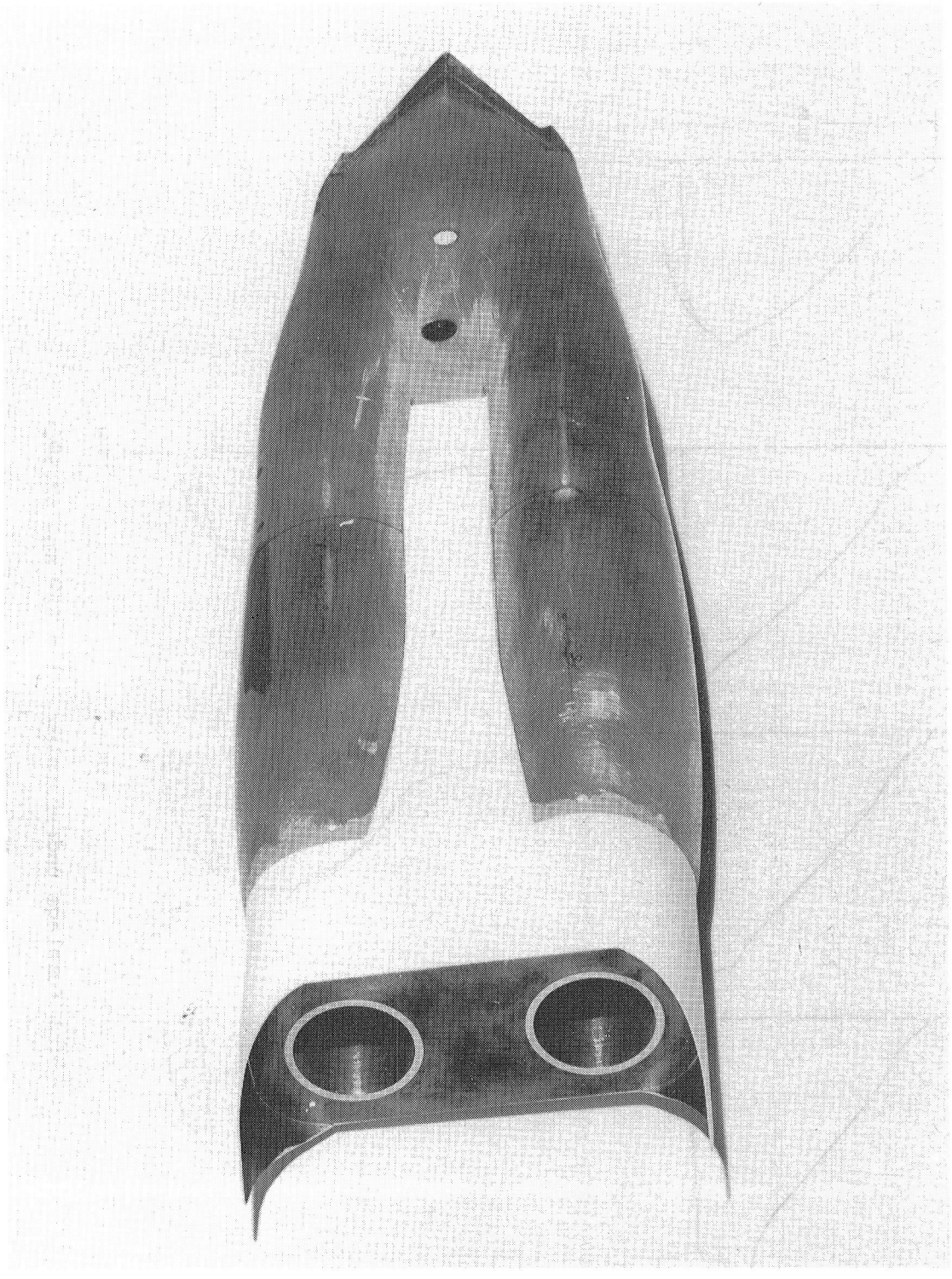

L-75-644

(f) Rear below view of nacelle with simulated 2-D nozzles.

Figure 2.- Concluded.

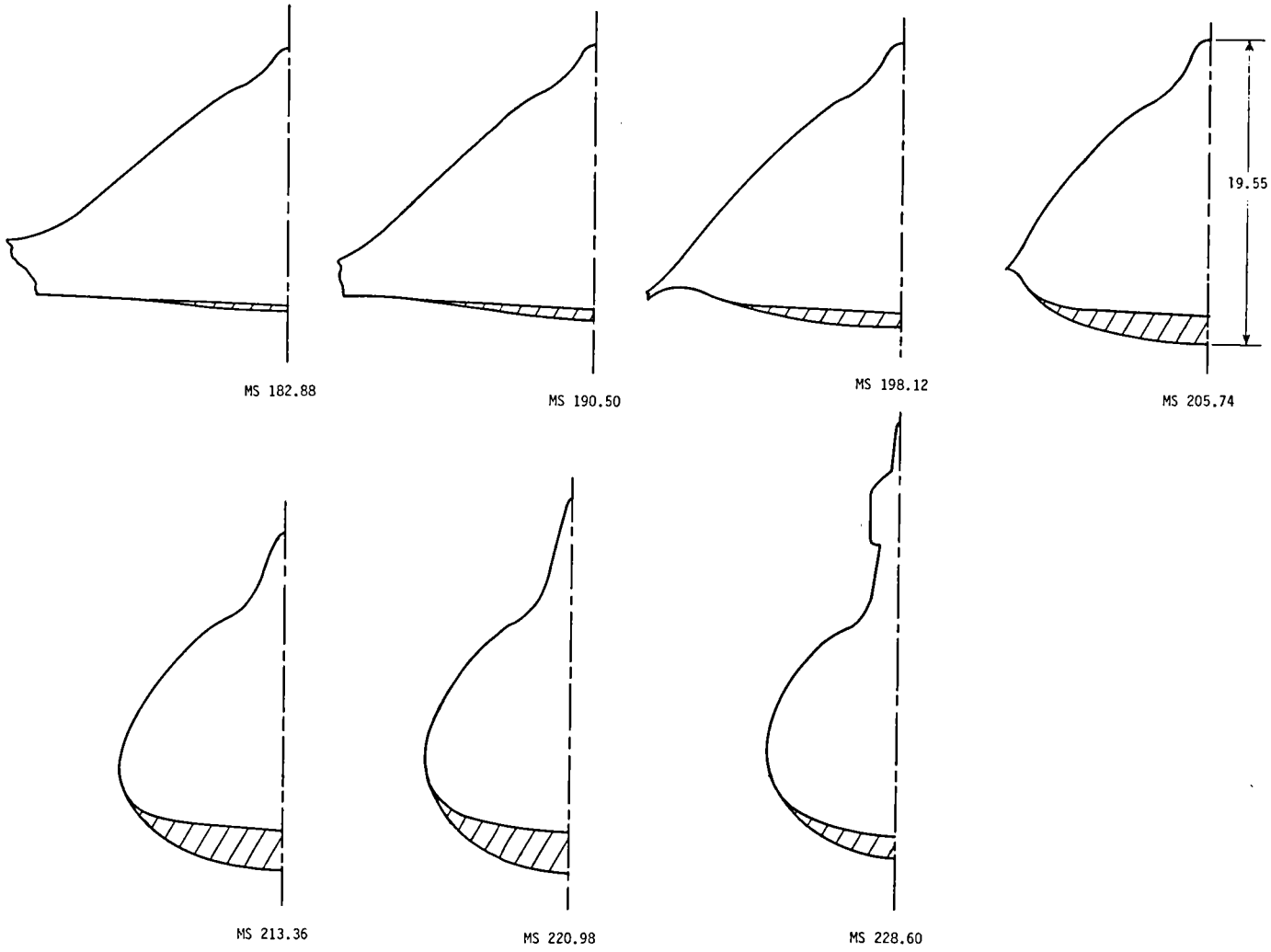

(a) Fuselage underfairing. Λ = 65° and 67.5°.

Figure 3.- Sketches of fuselage fairings. All dimensions are in centimeters.

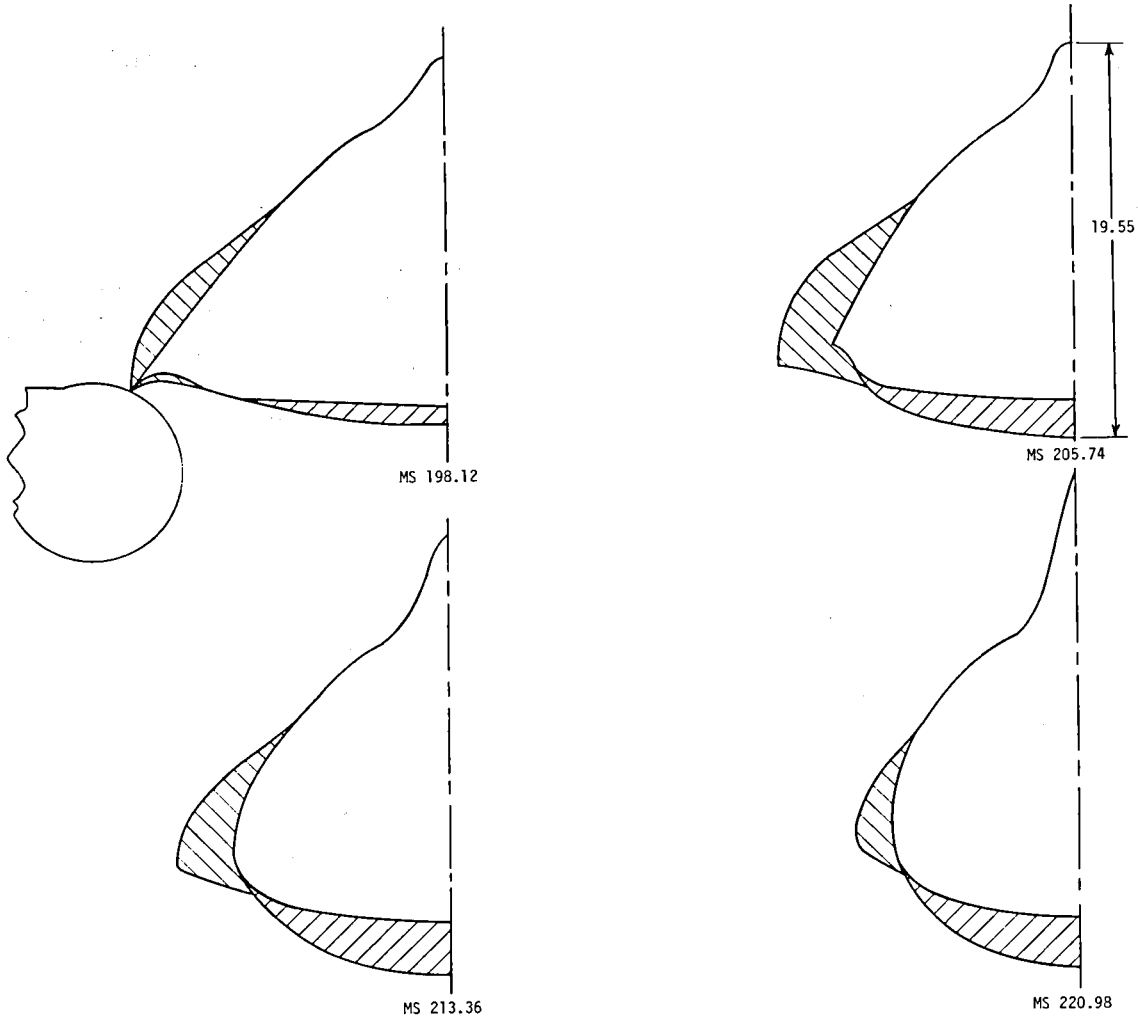

(b) Fuselage sidefairing in combination with fuselage underfairing. $\Lambda = 65^{\circ}$.

Figure 3.- Concluded.

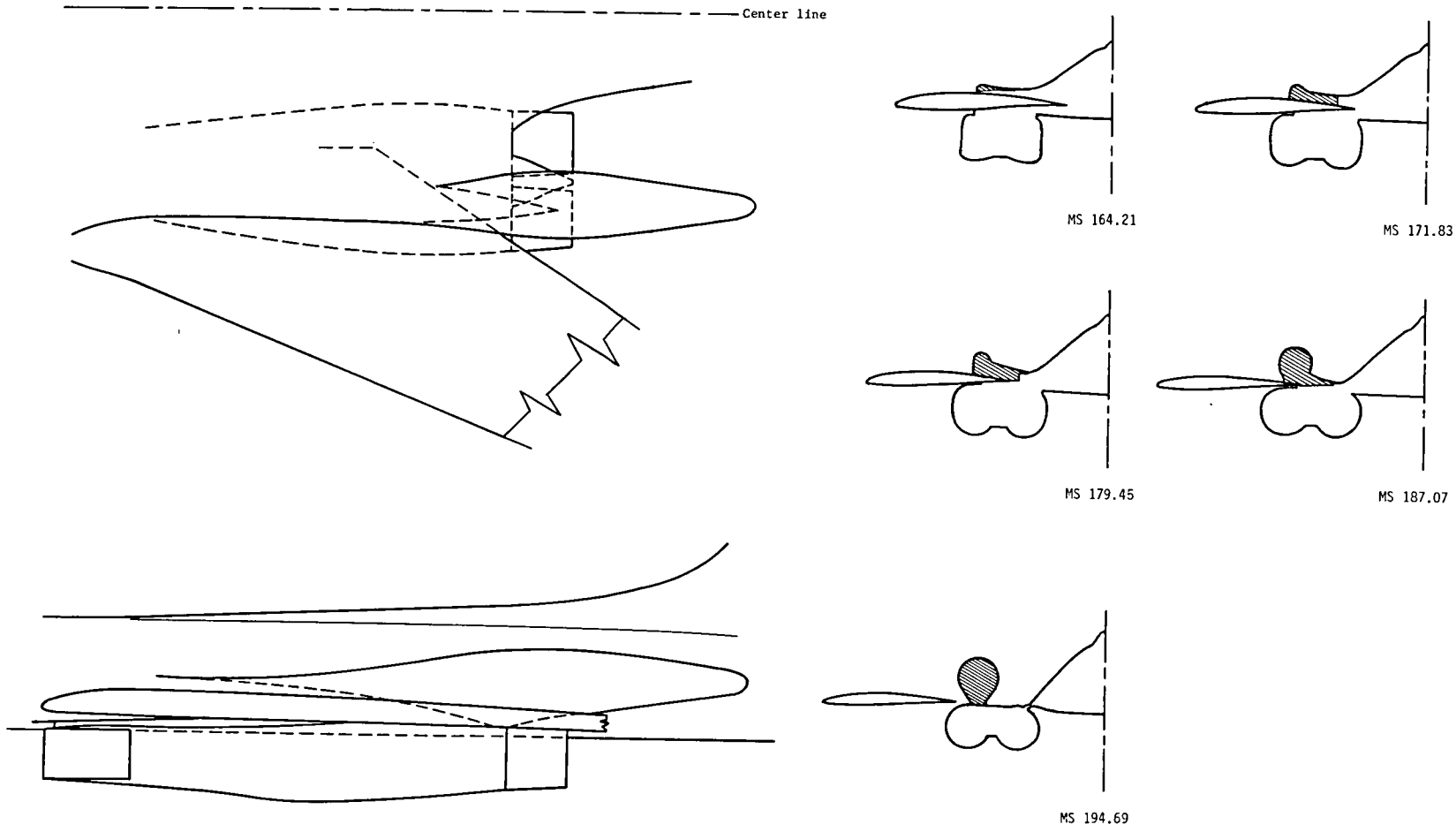

(a) Sketch of model with wing pods.

Figure 4.- Configuration with wing pods. $\Lambda = 67.5^{o}$. All dimensions are in centimeters.

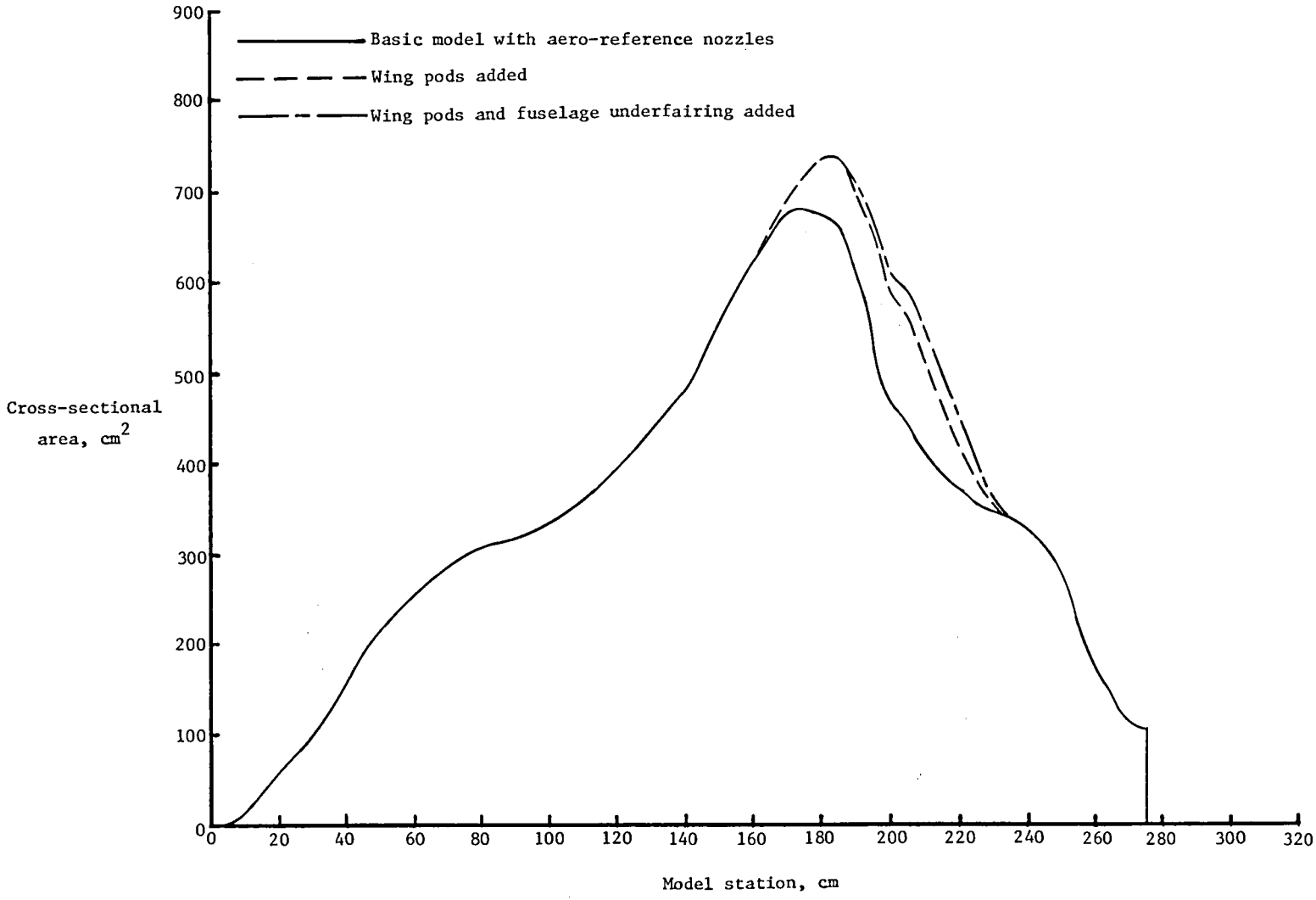

(b) Model cross-sectional area distribution.

Figure 4.- Concluded.

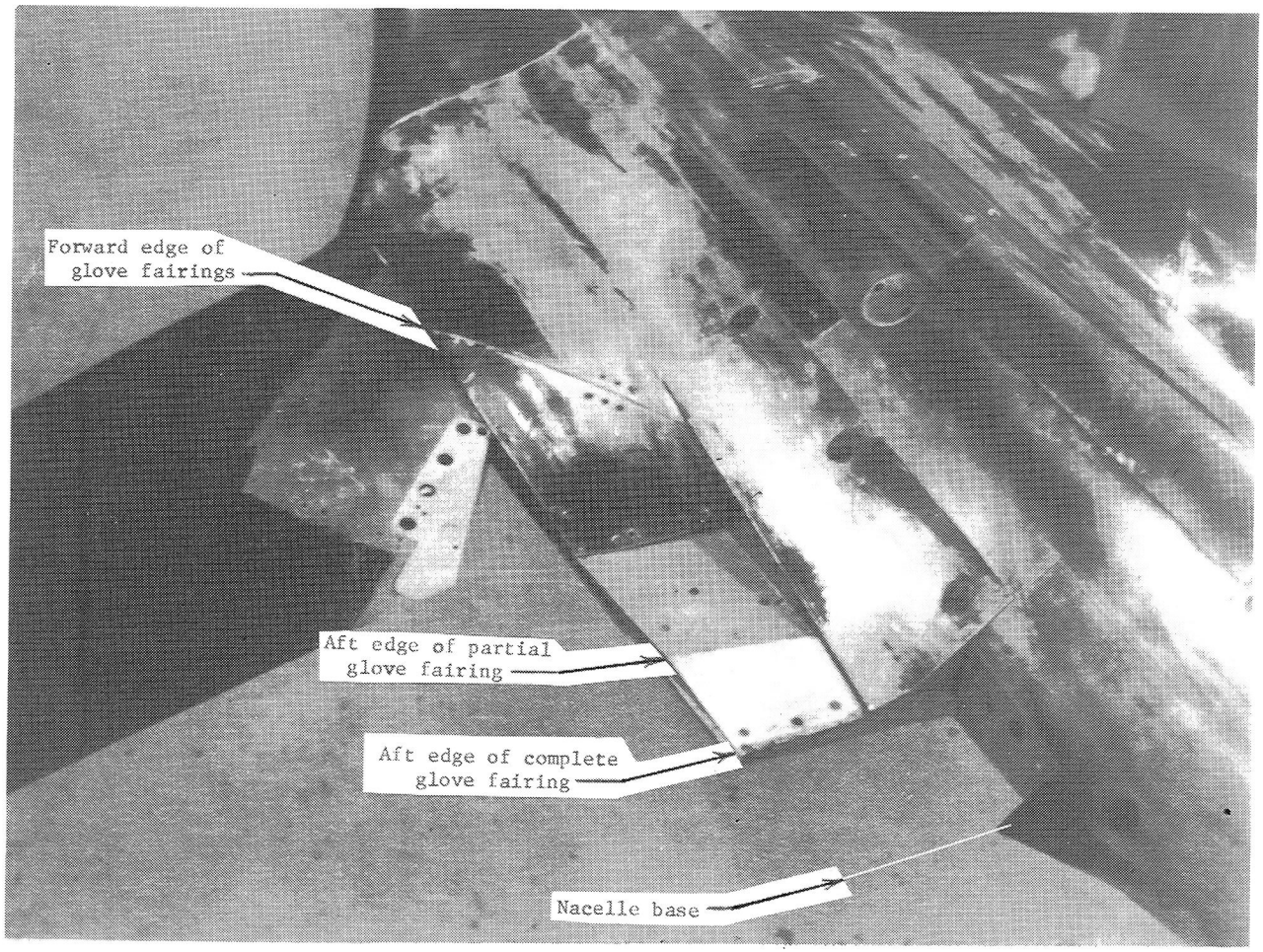

L-79-276

(a) Rear above view of glove-area geometry (unmodified) with nacelle removed.

Figure 5.- Photographs of some model configurations with wings swept 25° and the glove fairings used.

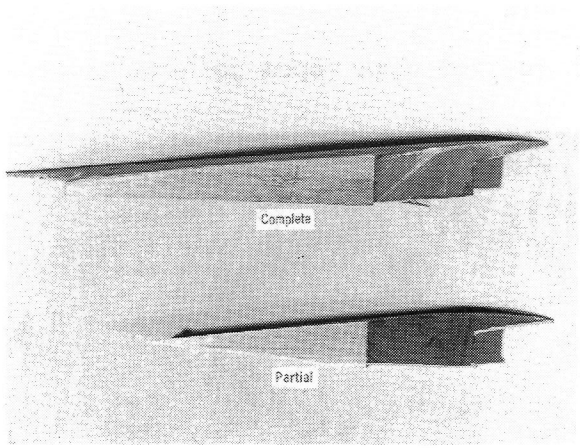

View of inboard side

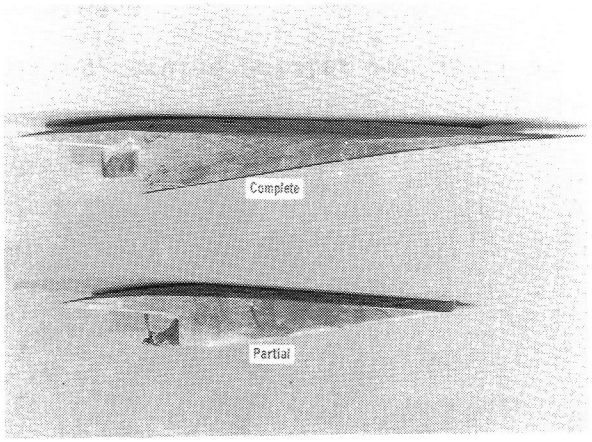

View of outboard side

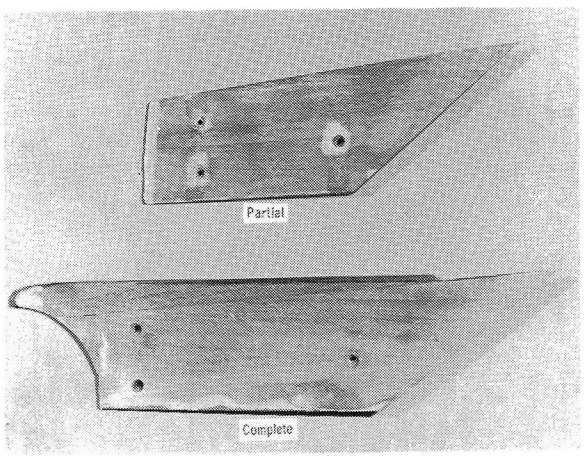

Top view

L-79-277

(b) Partial and complete glove fairings.

Figure 5.- Continued.

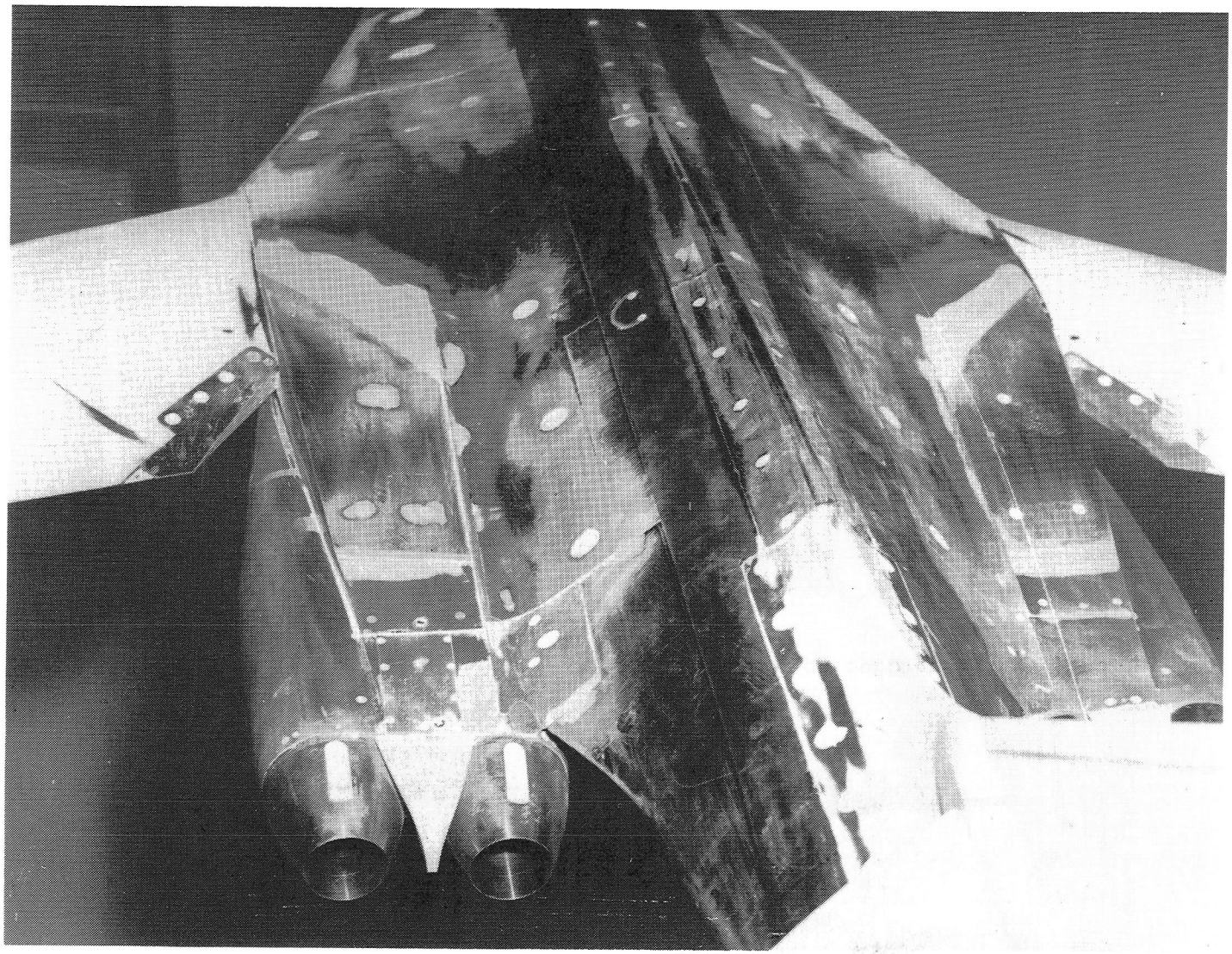

L-75-310

(c) Rear above view of model with partial glove fairing, cruise nozzle, and short interfairing.

Figure 5.- Concluded.

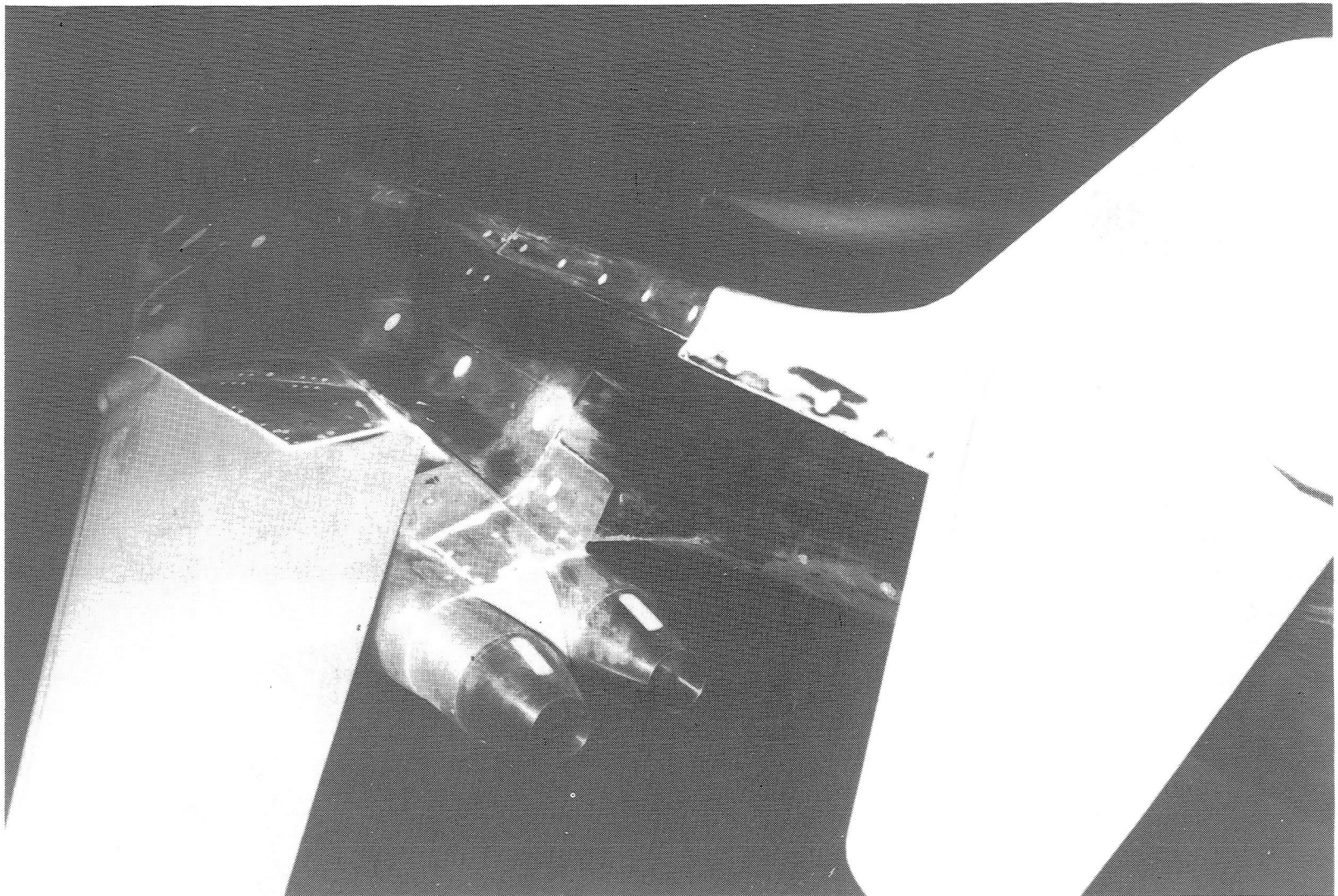

L-79-278

(a) Rear above view of model with extended cruise nozzles and short interfairing.

Figure 6.- Photographs of model configurations with wings swept 65°.

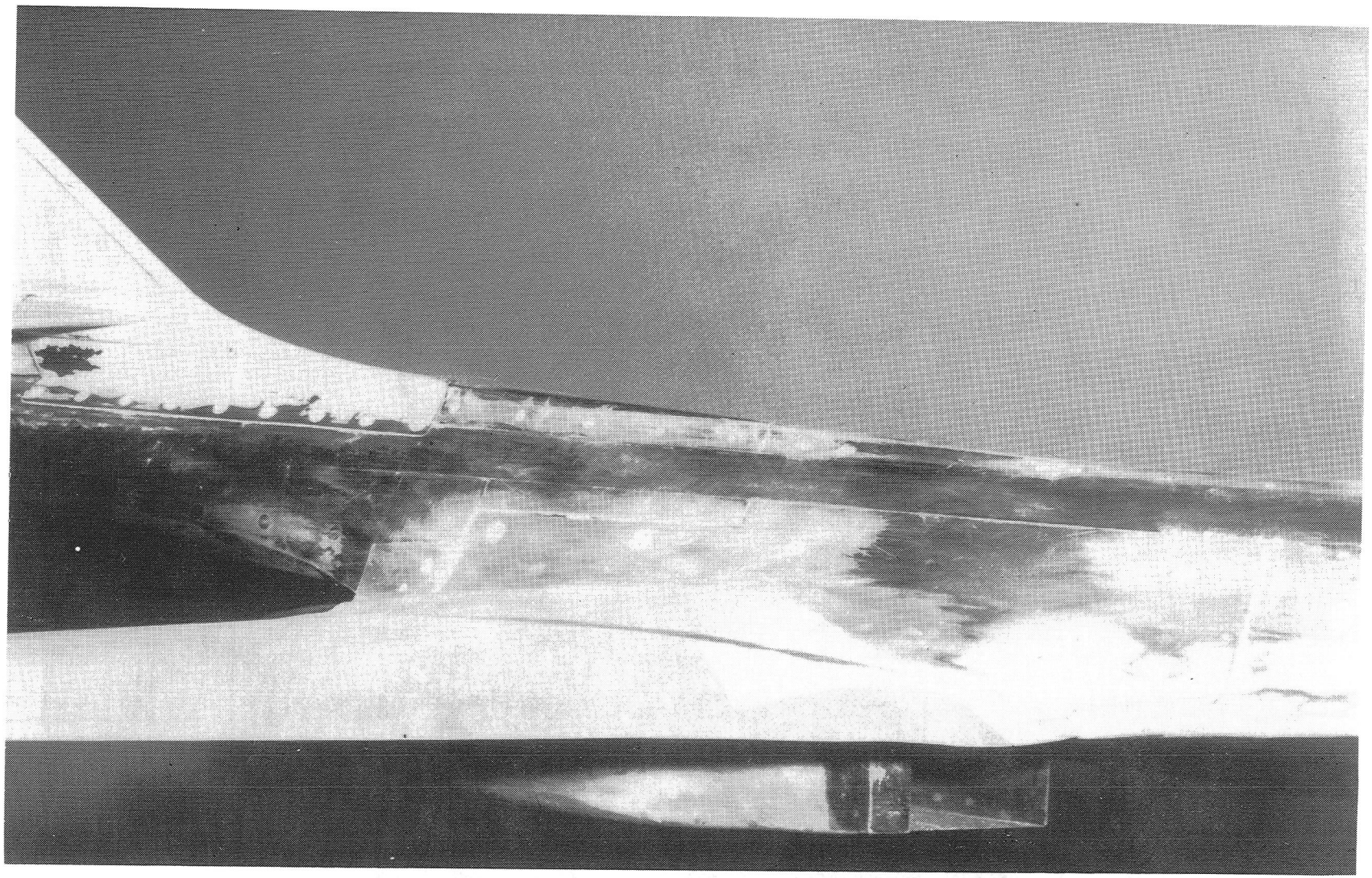

L-79-279

(b) Side view of glove fairing.

Figure 6.- Continued.

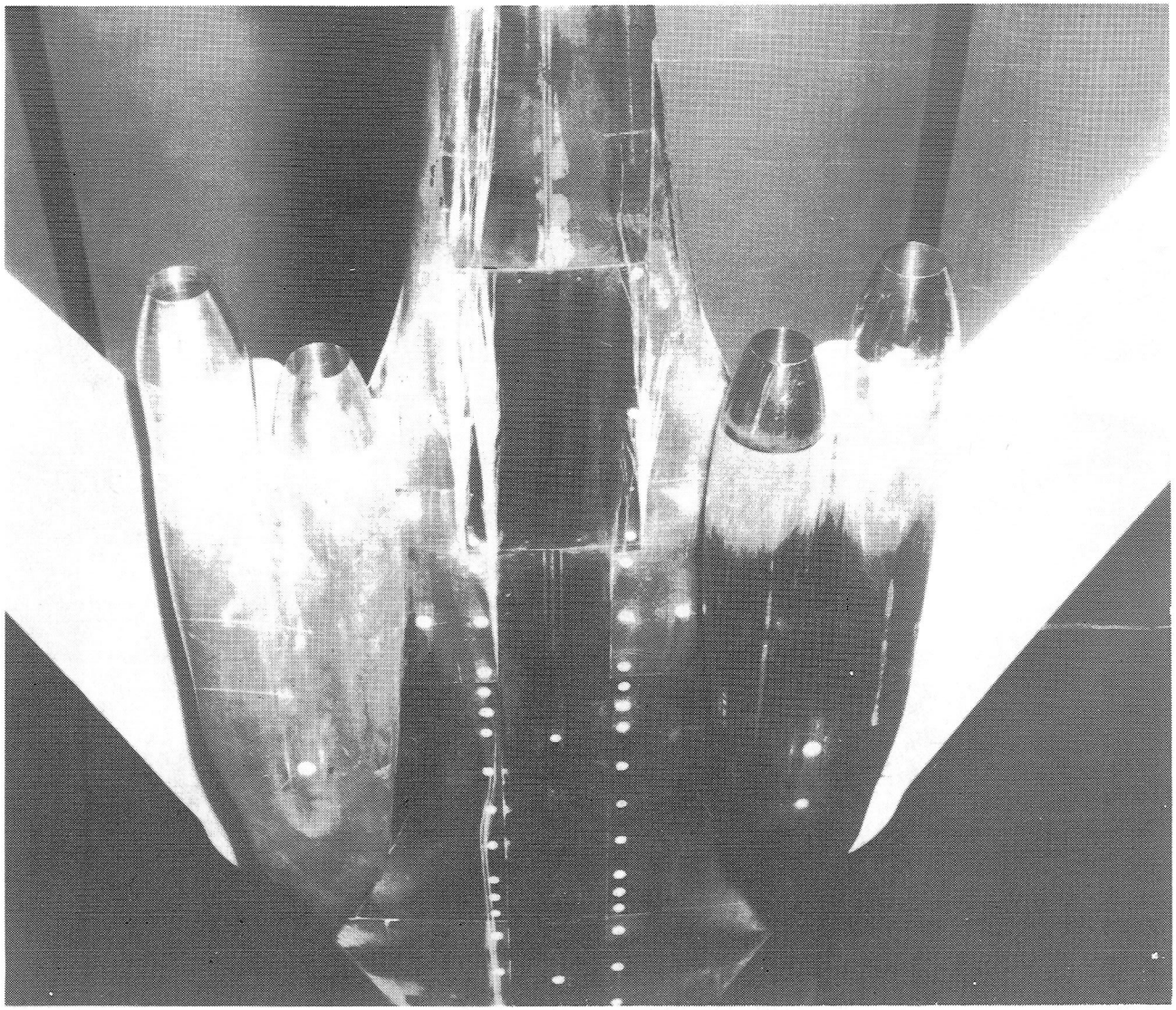

L-79-280

(c) Rear below view of model with staggered cruise nozzles and short interfairing.

Figure 6.- Continued.

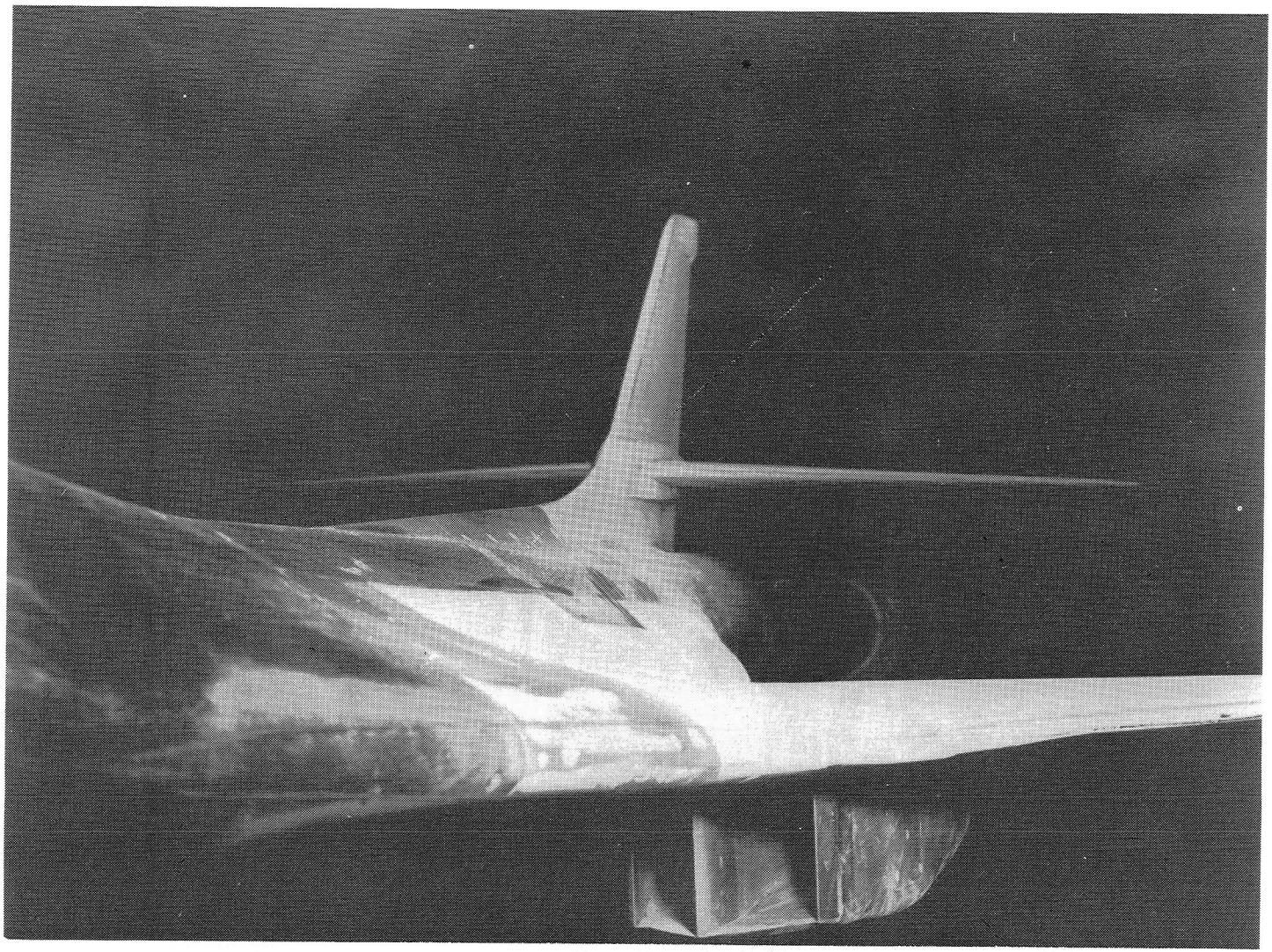

L-75-1017

(d) Front view of model with glove-fuselage sidefairing.

Figure 6.- Continued.

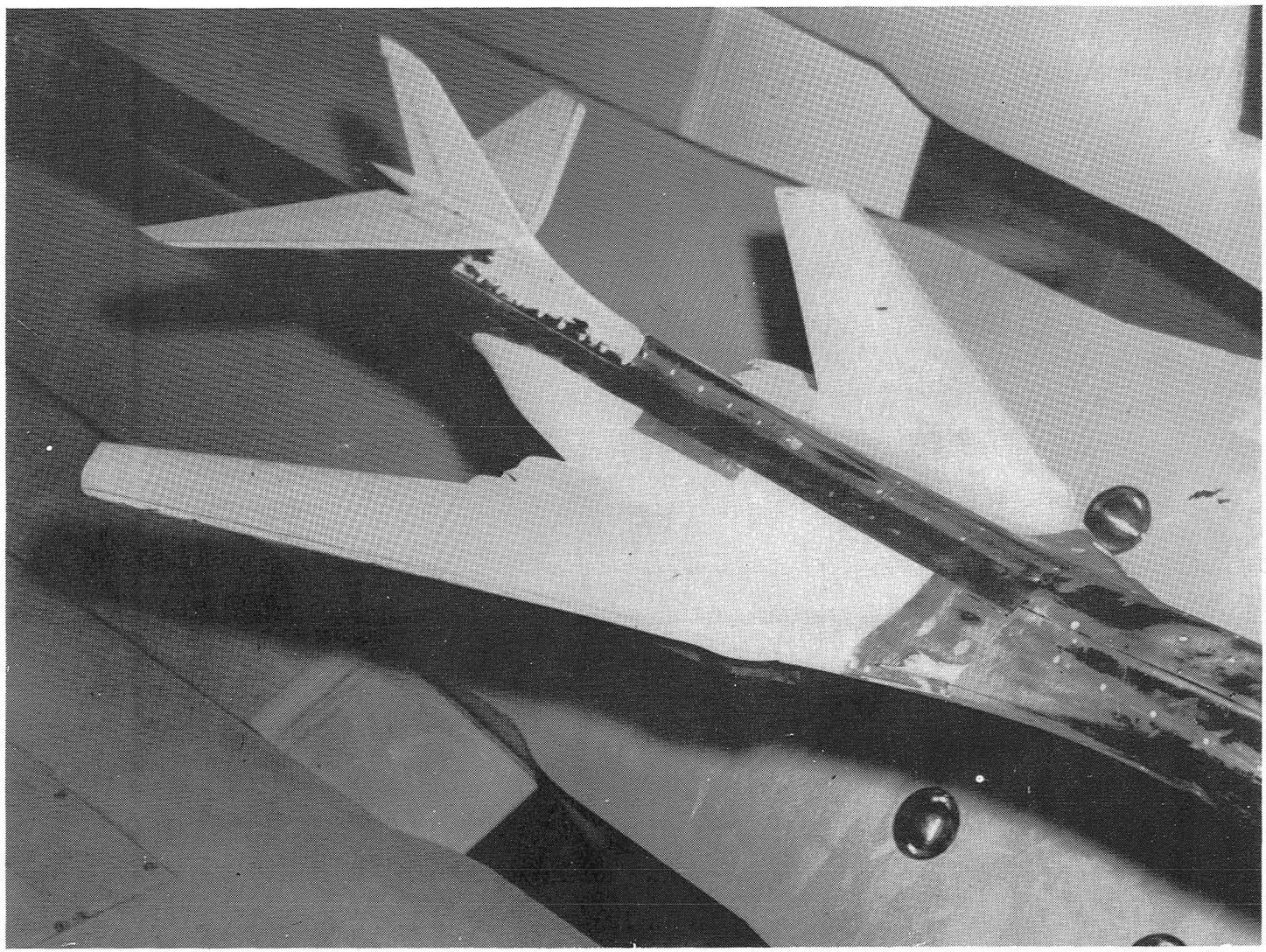

L-75-1018

(e) Front above view of model with glove-fuselage sidefairing, cruise nozzles, and short interfairing.

Figure 6.- Continued.

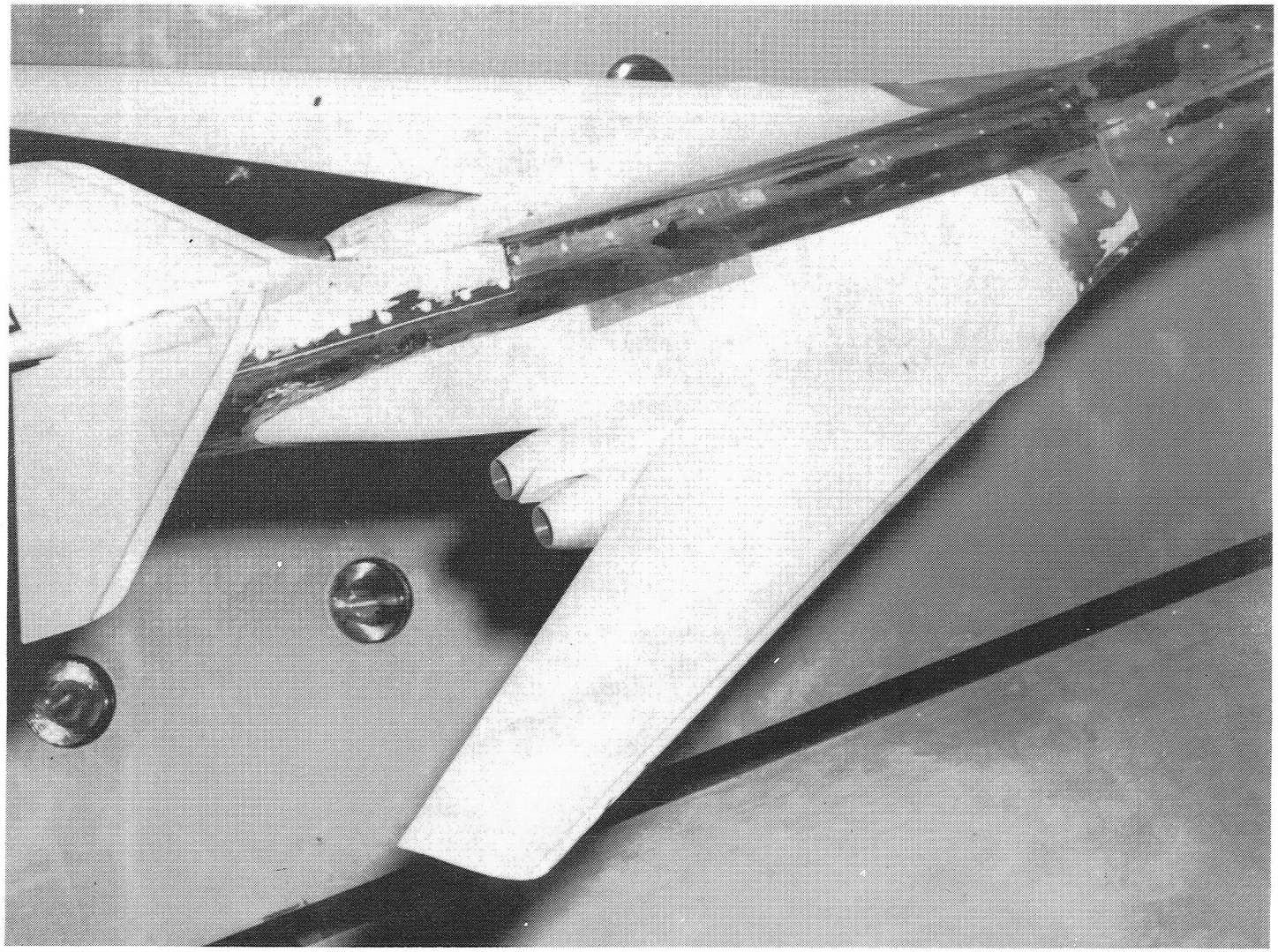

L-75-1020

(f) Rear above view of model with glove-fuselage sidefairing, cruise nozzles, and short interfairing.

Figure 6.- Continued.

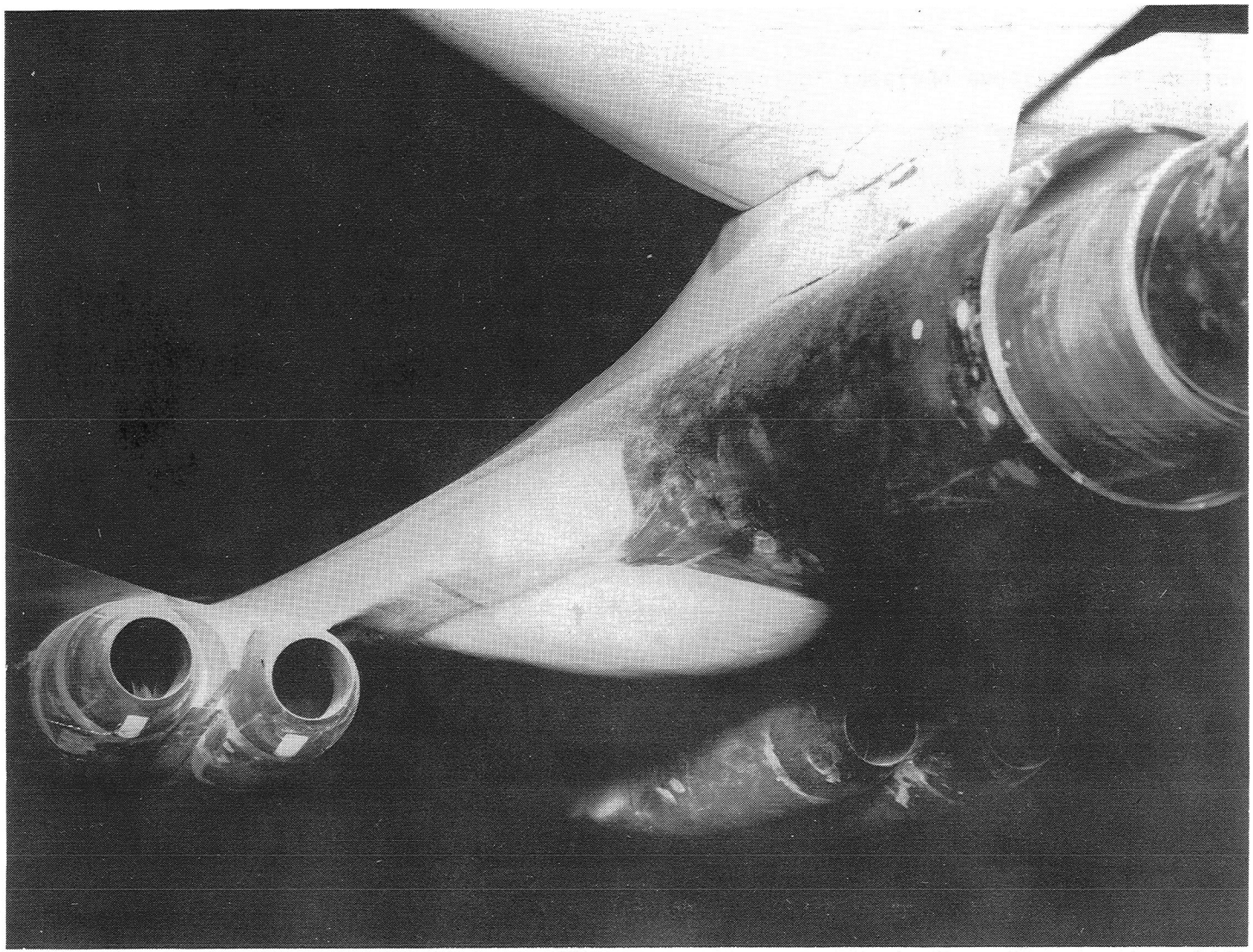

L-75-1021

(g) Rear below view of model with glove-fuselage sidefairing, fuselage underfairing, cruise nozzles, and short interfairing.

Figure 6.- Continued.

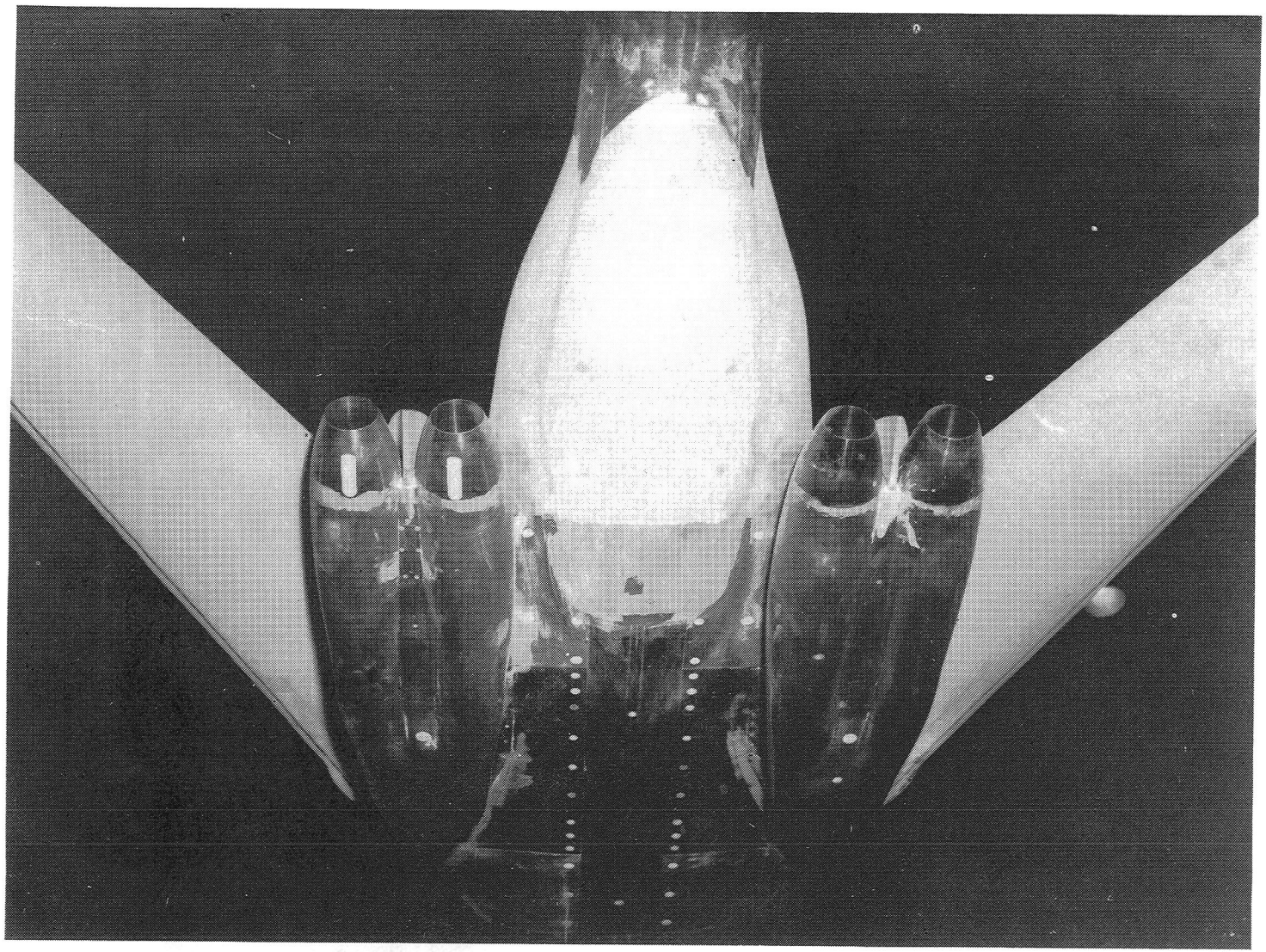

L-75-1022

(h) Rear below view of model with glove-fuselage sidefairing, fuselage underfairing, cruise nozzles, and short interfairing.

Figure 6.- Concluded.

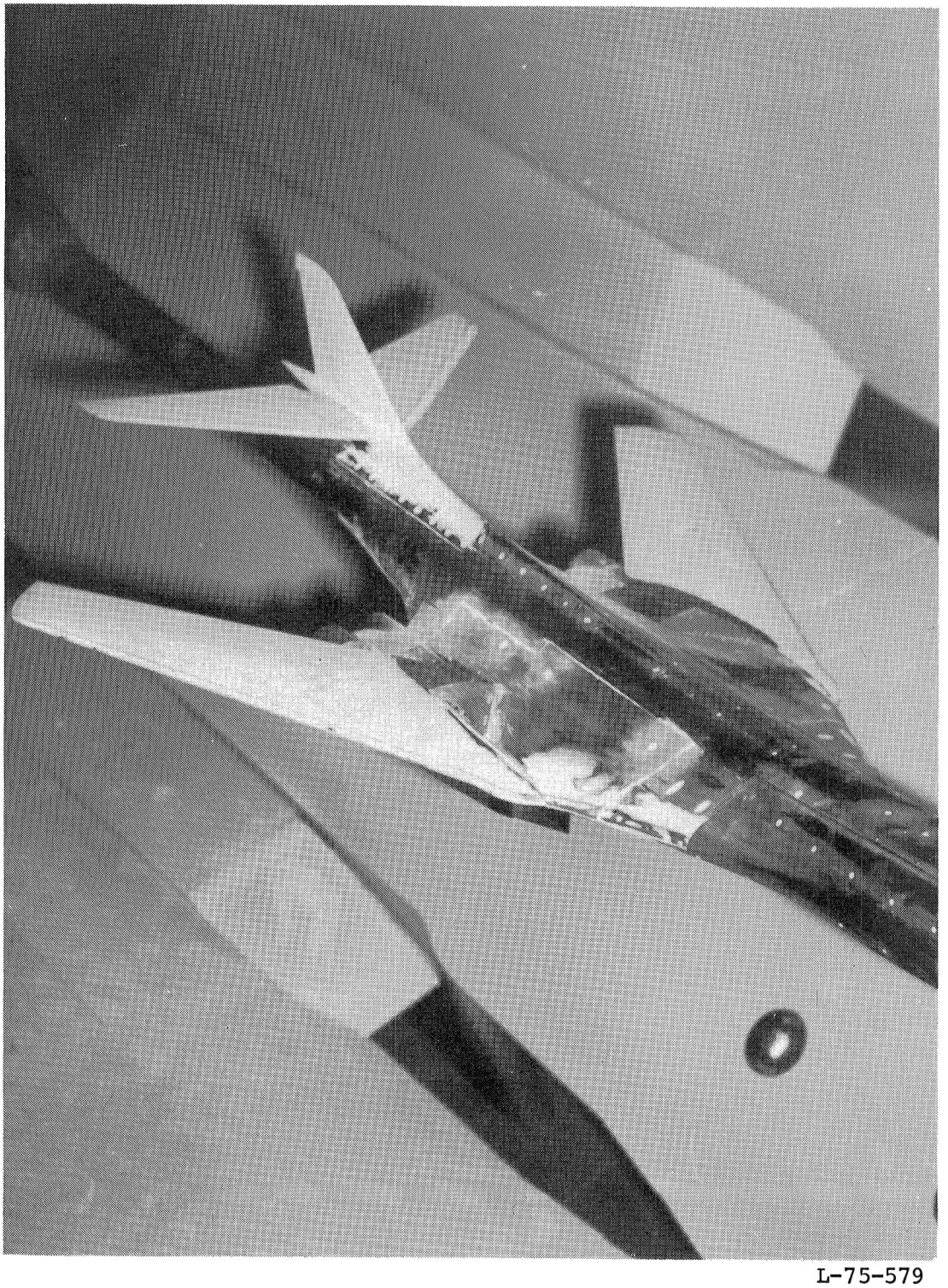

L-75-579

(a) Front above view of model with aero-reference nozzles and short interfairing.

Figure 7.- Photographs of model configurations with wings swept 67.5°.

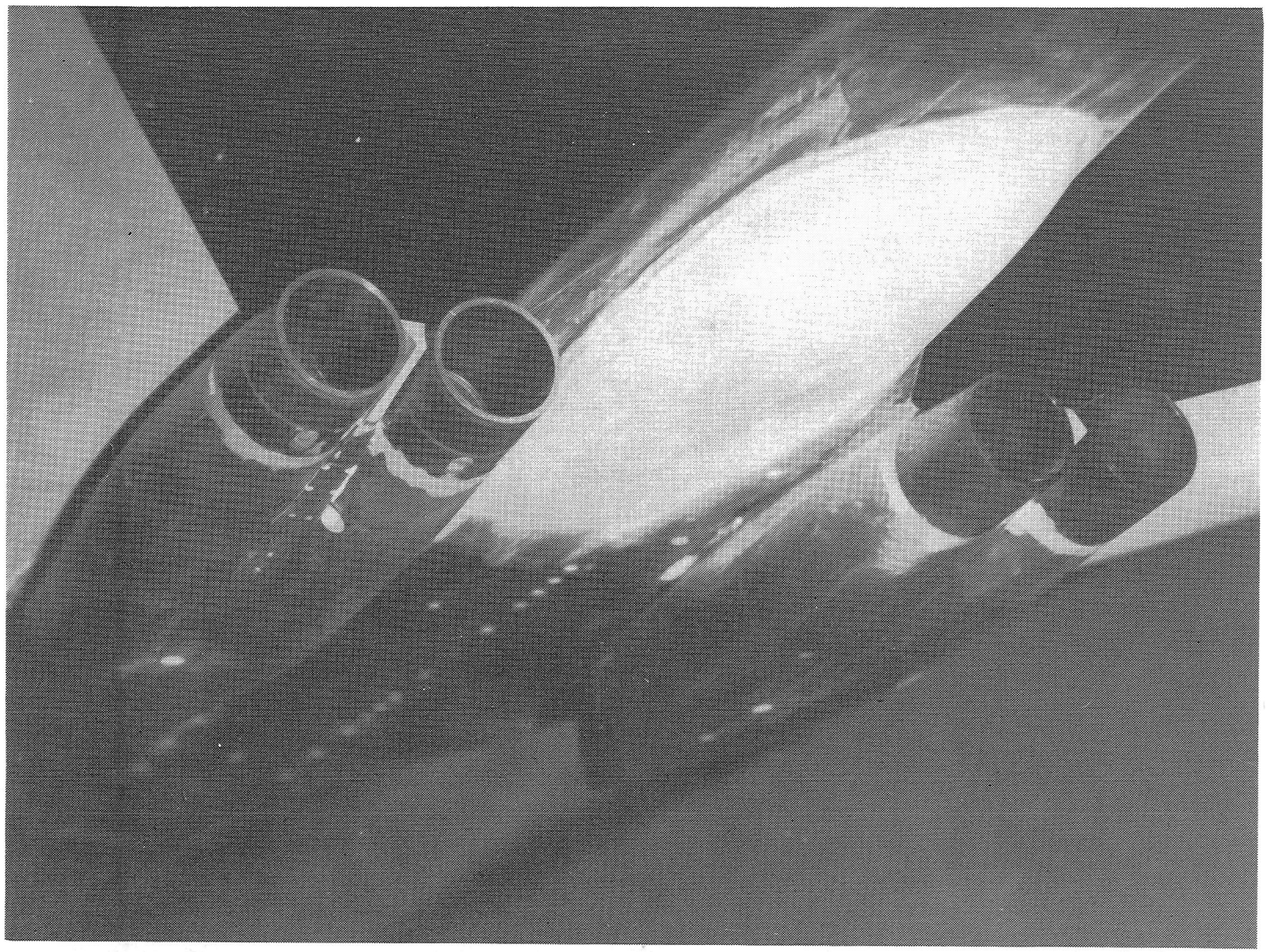

L-75-580

(b) Rear below view of model with fuselage underfairing, aero-reference nozzles, and short interfairing.

Figure 7.- Continued.

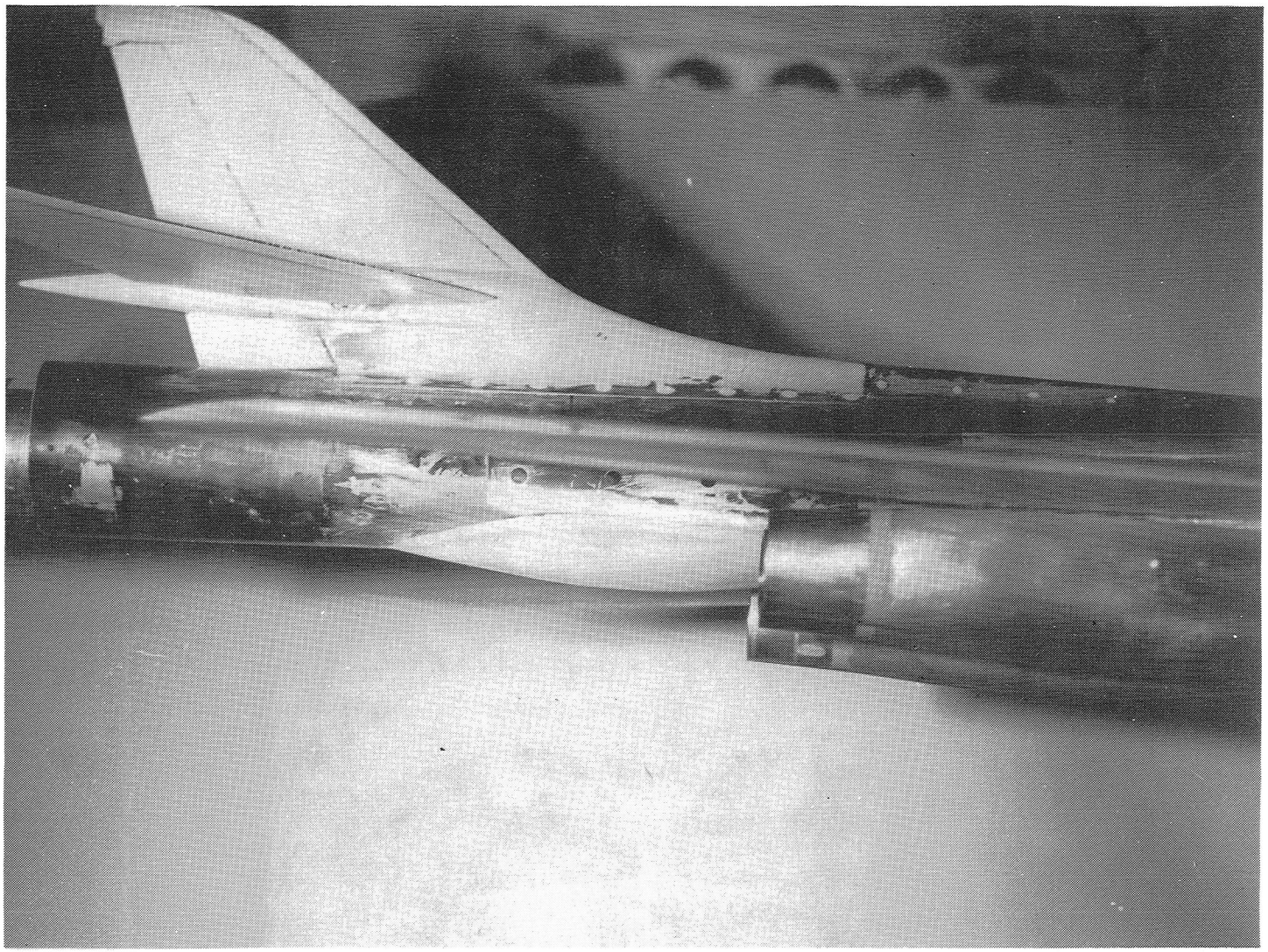

L-75-581

(c) Side view of model with fuselage underfairing and aero-reference nozzles.

Figure 7.- Continued.

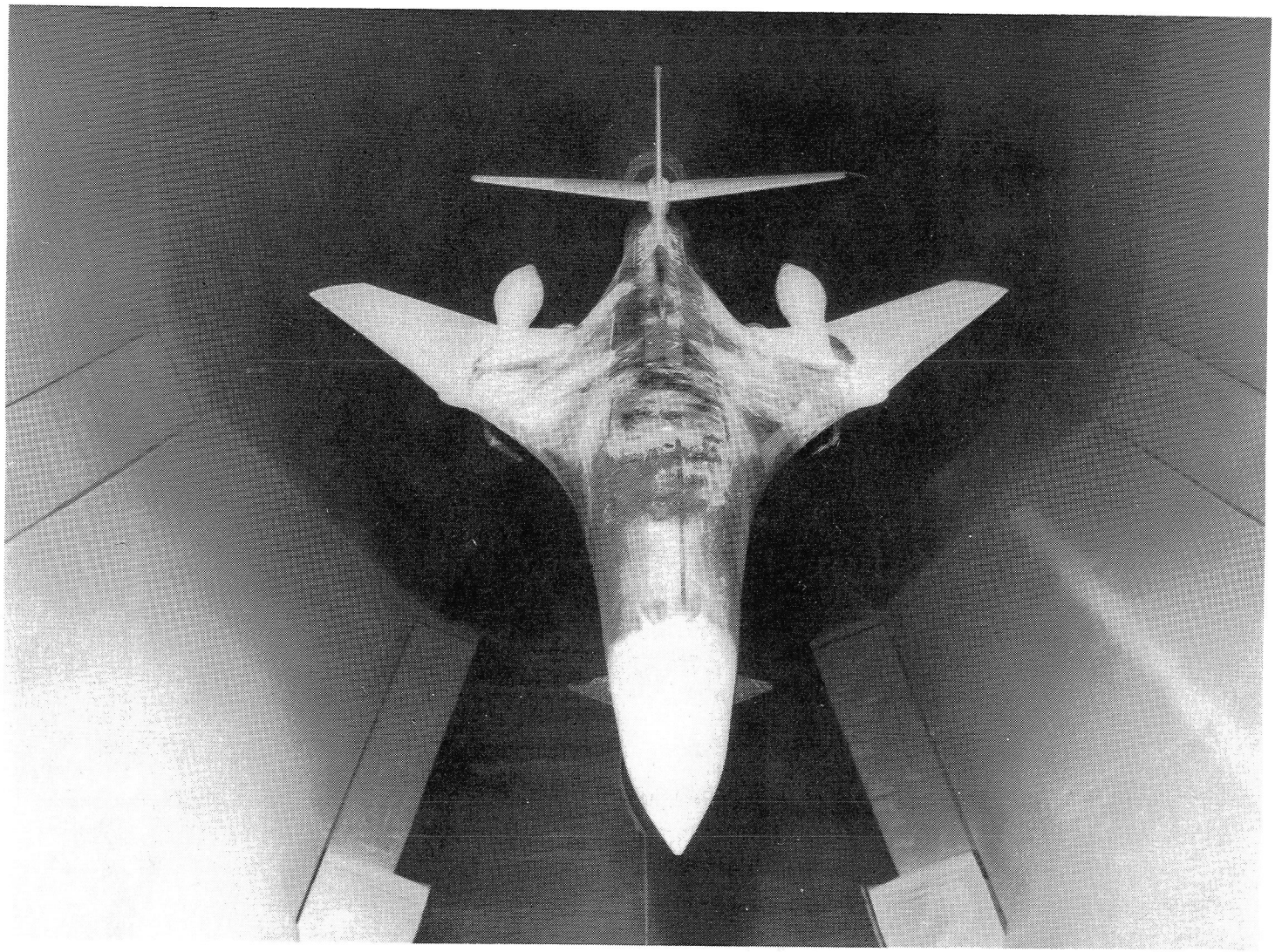

L-75-494

(d) Front above view of model with wing pods.

Figure 7.- Continued.

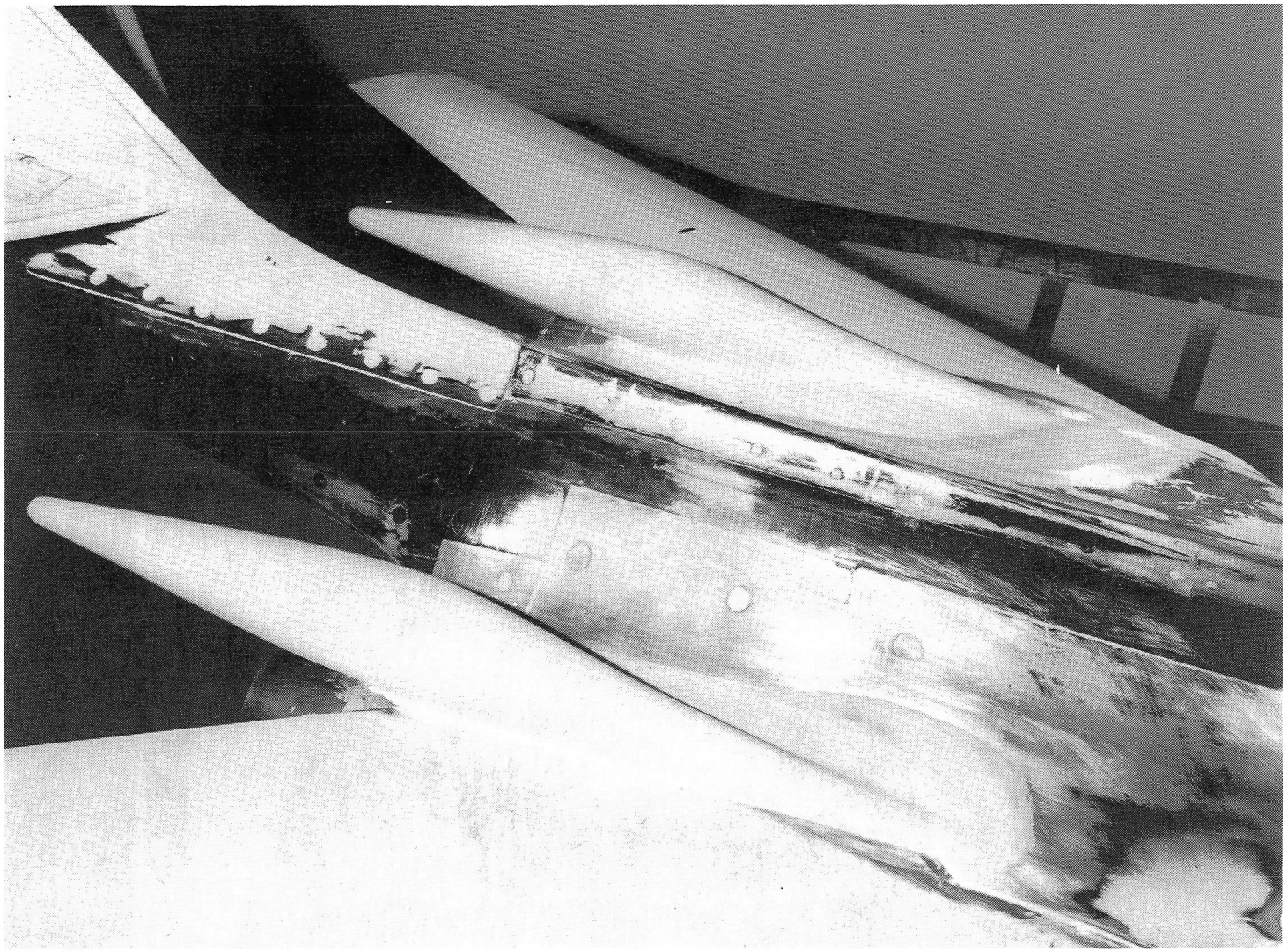

L-75-496

(e) Side above view of model with wing pods and aero-reference nozzles.

Figure 7.- Continued.

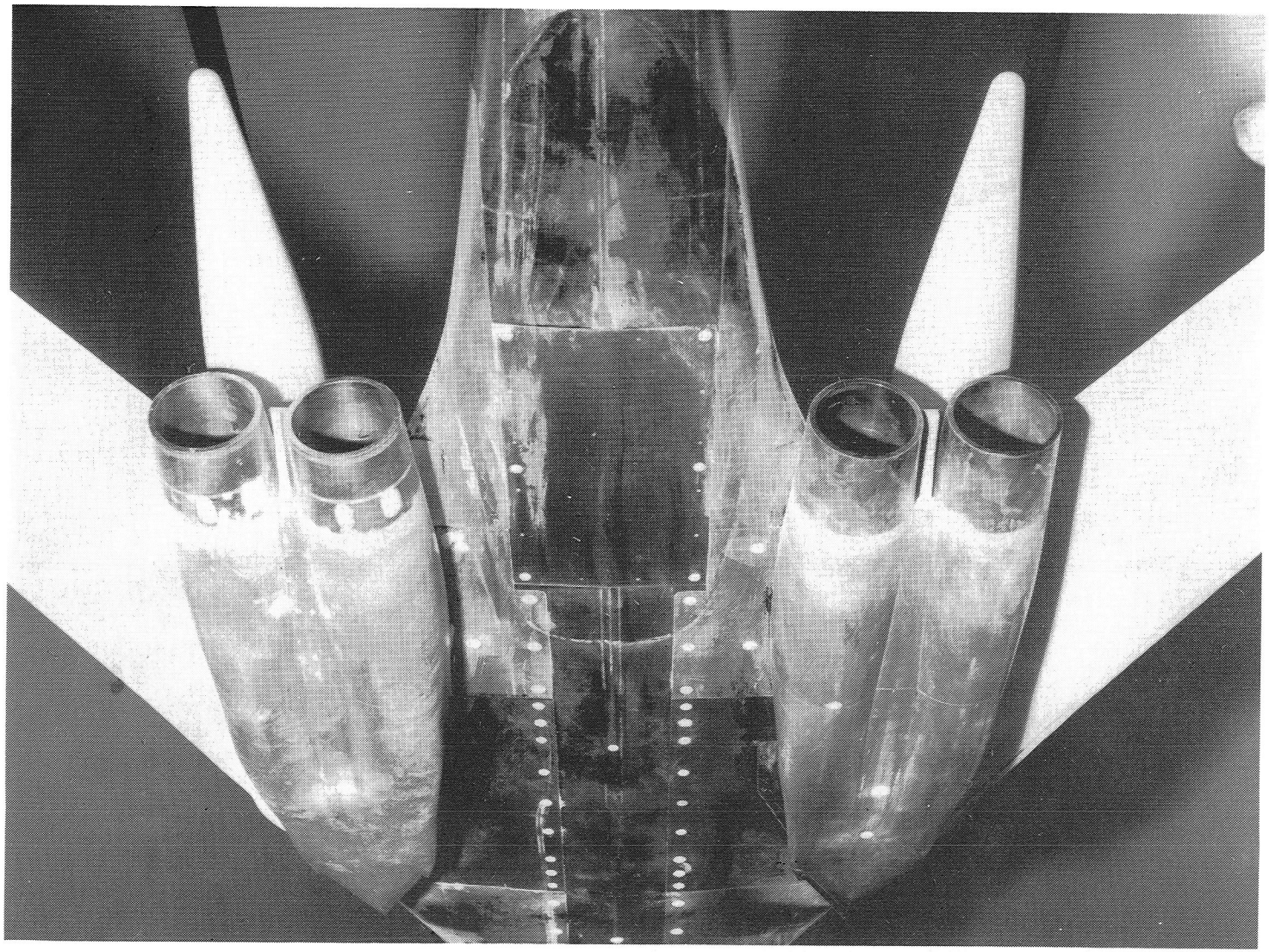

L-75-495

(f) Rear below view of model with wing pods, aero-reference nozzles, and short interfairing.

Figure 7.- Concluded.

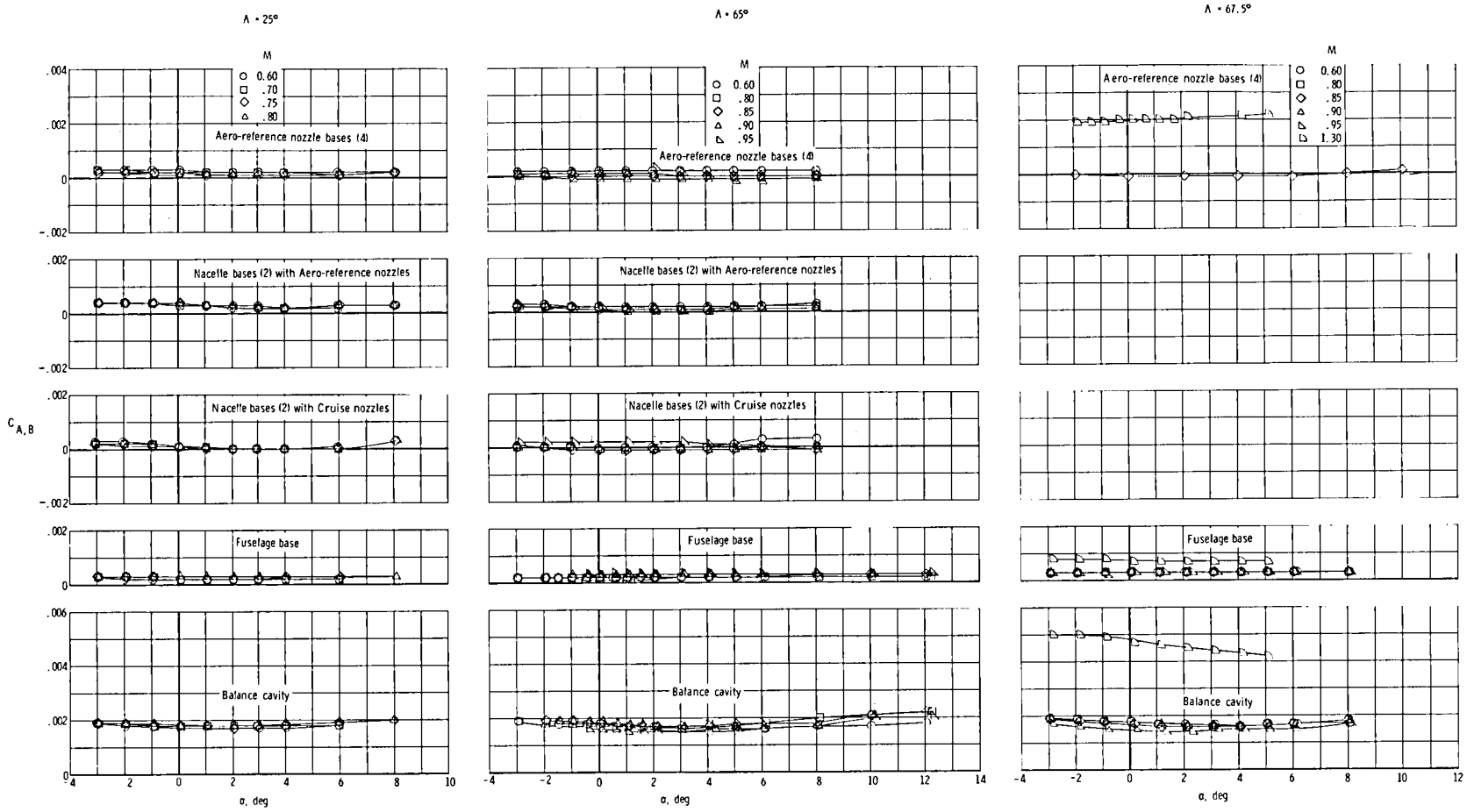

(a) Aero-reference and cruise nozzles.

Figure 8.- Typical variations with angle of attack of base axial force for the model with various wing sweeps and nacelle geometries.

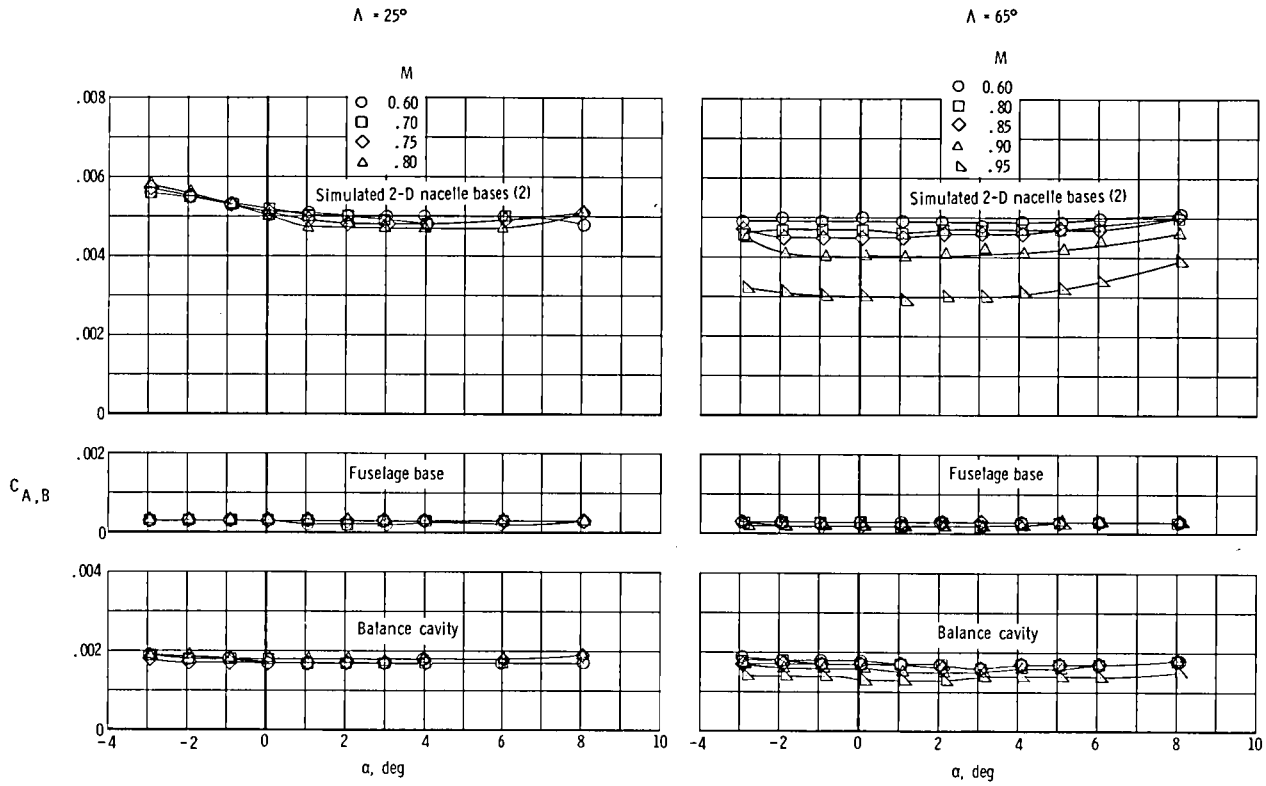

(b) Simulated 2-D nacelles.

Figure 8.- Concluded.

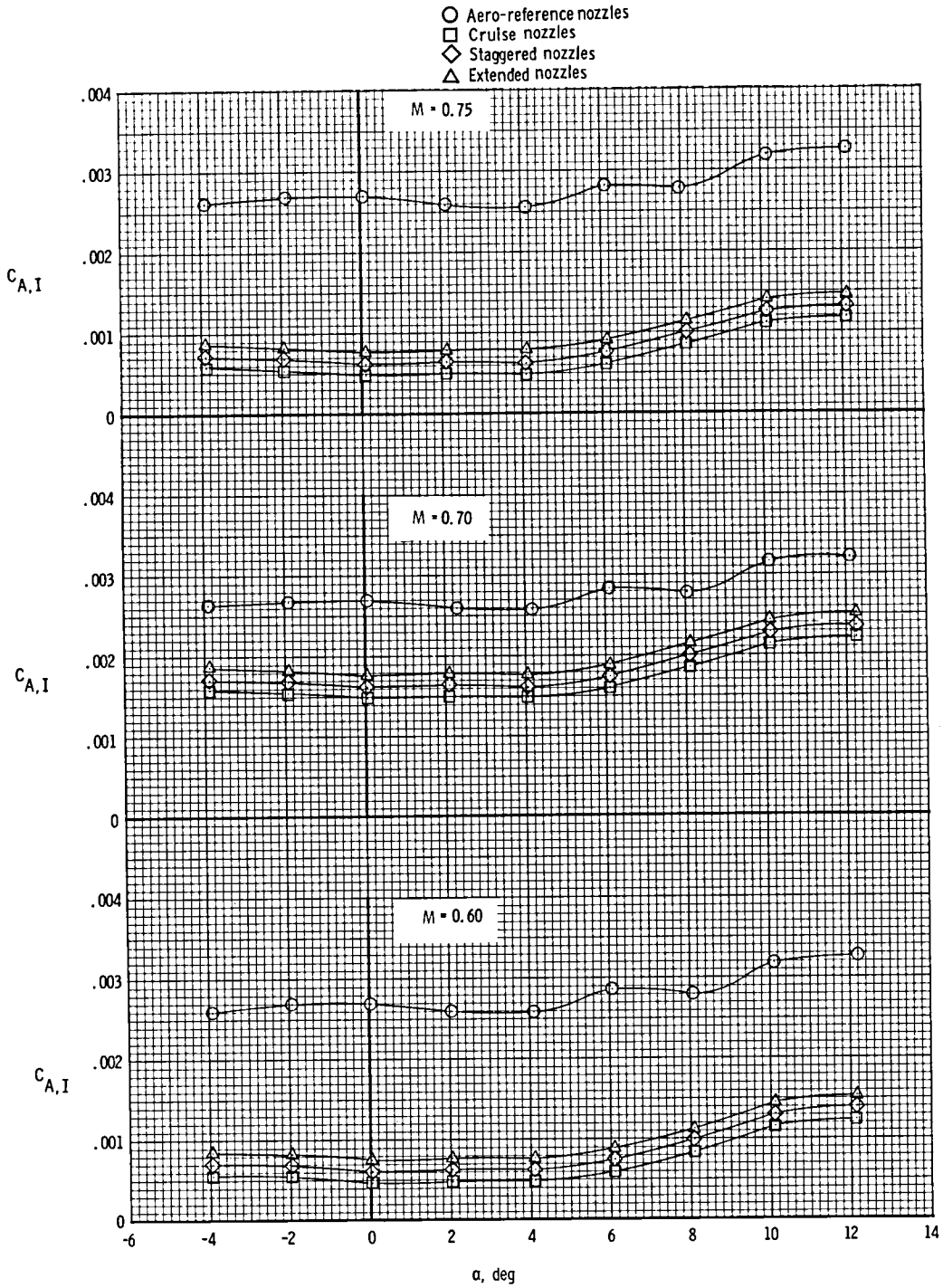

(a) M = 0.60, 0.70, and 0.75.

Figure 9.- Variation of internal axial-force coefficient with angle of attack at various Mach numbers.

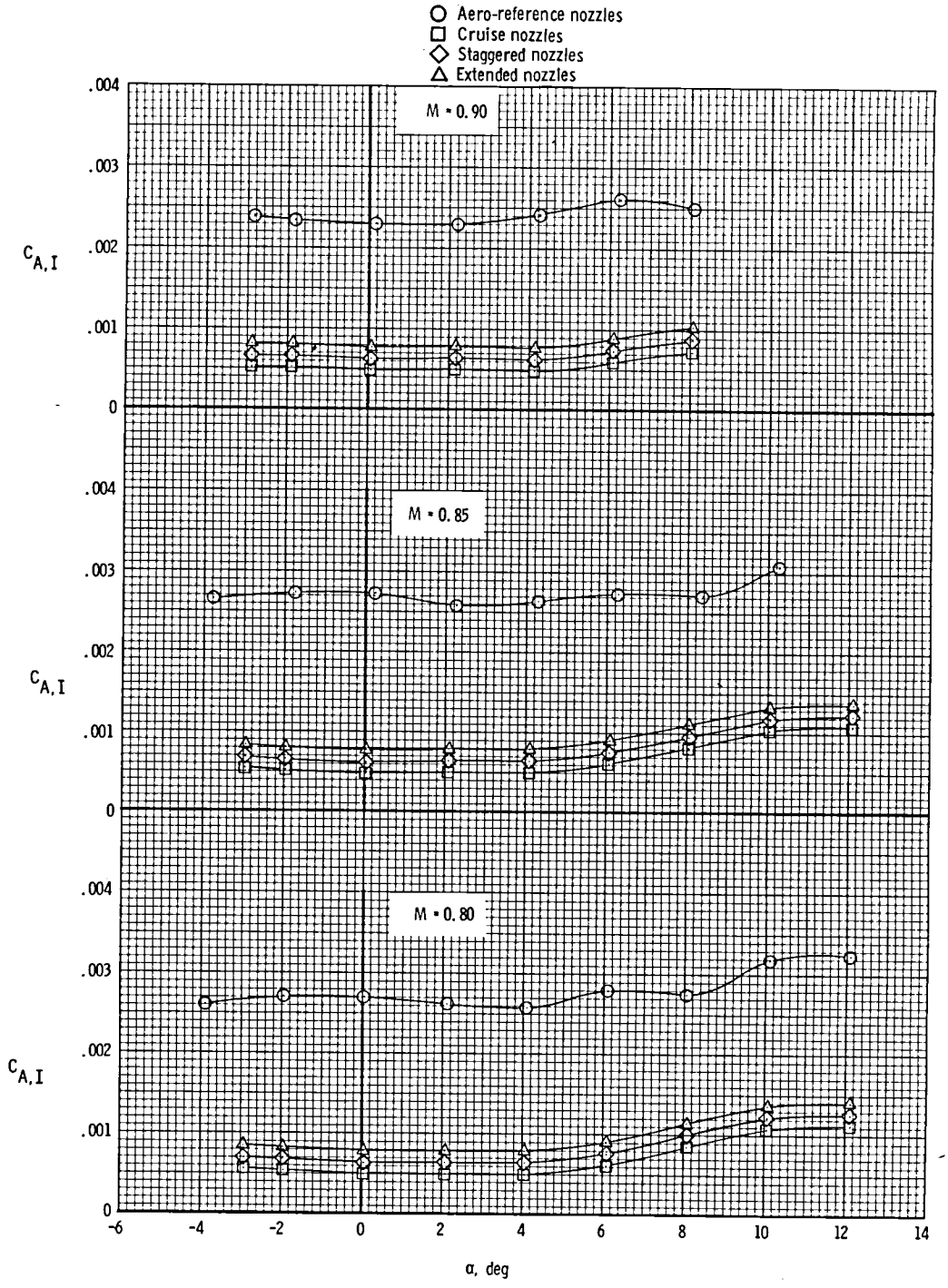

(b) M = 0.80, 0.85, and 0.90.

Figure 9.- Continued.

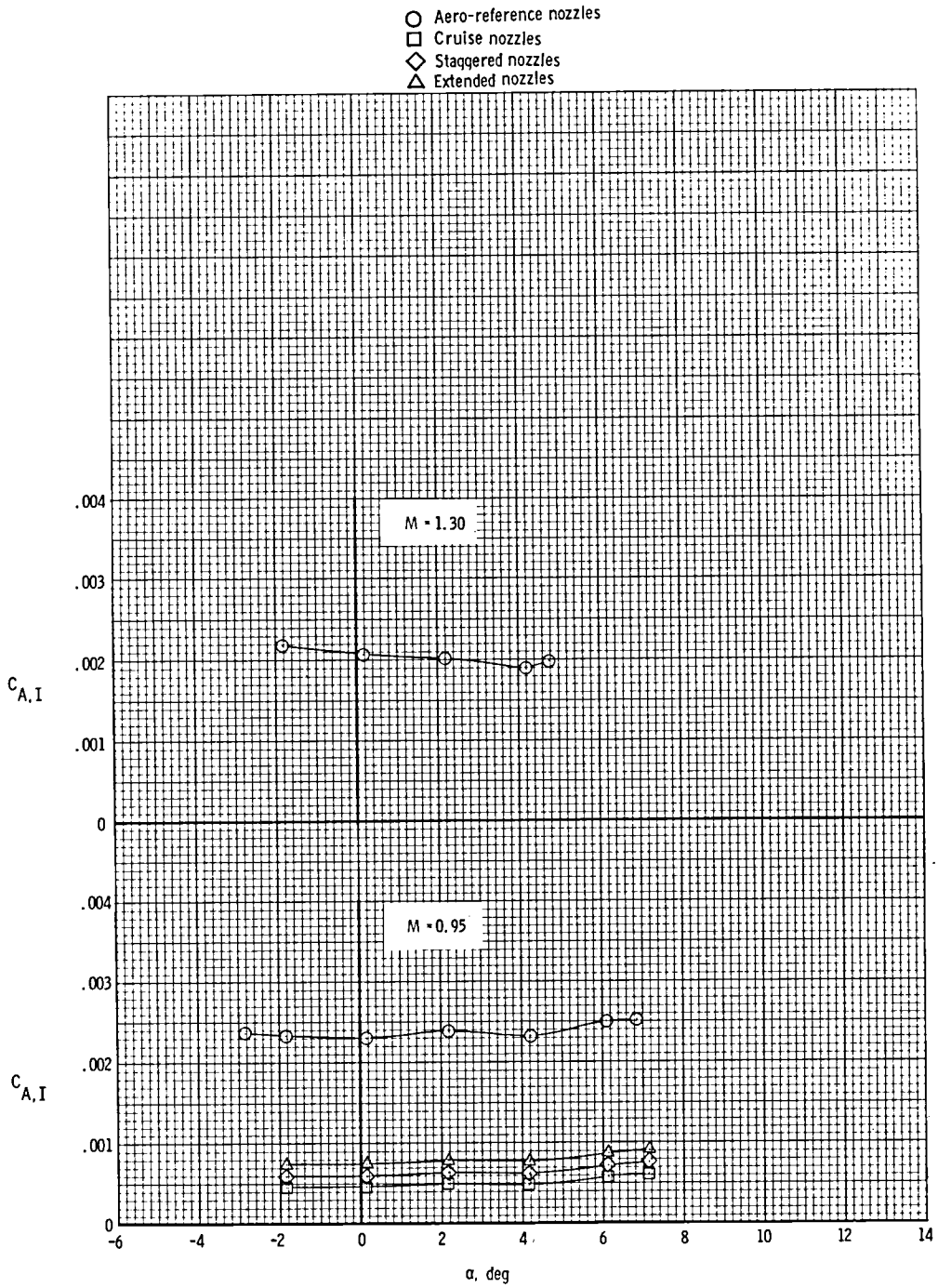

(c) M = 0.95 and 1.30.

Figure 9.- Concluded.

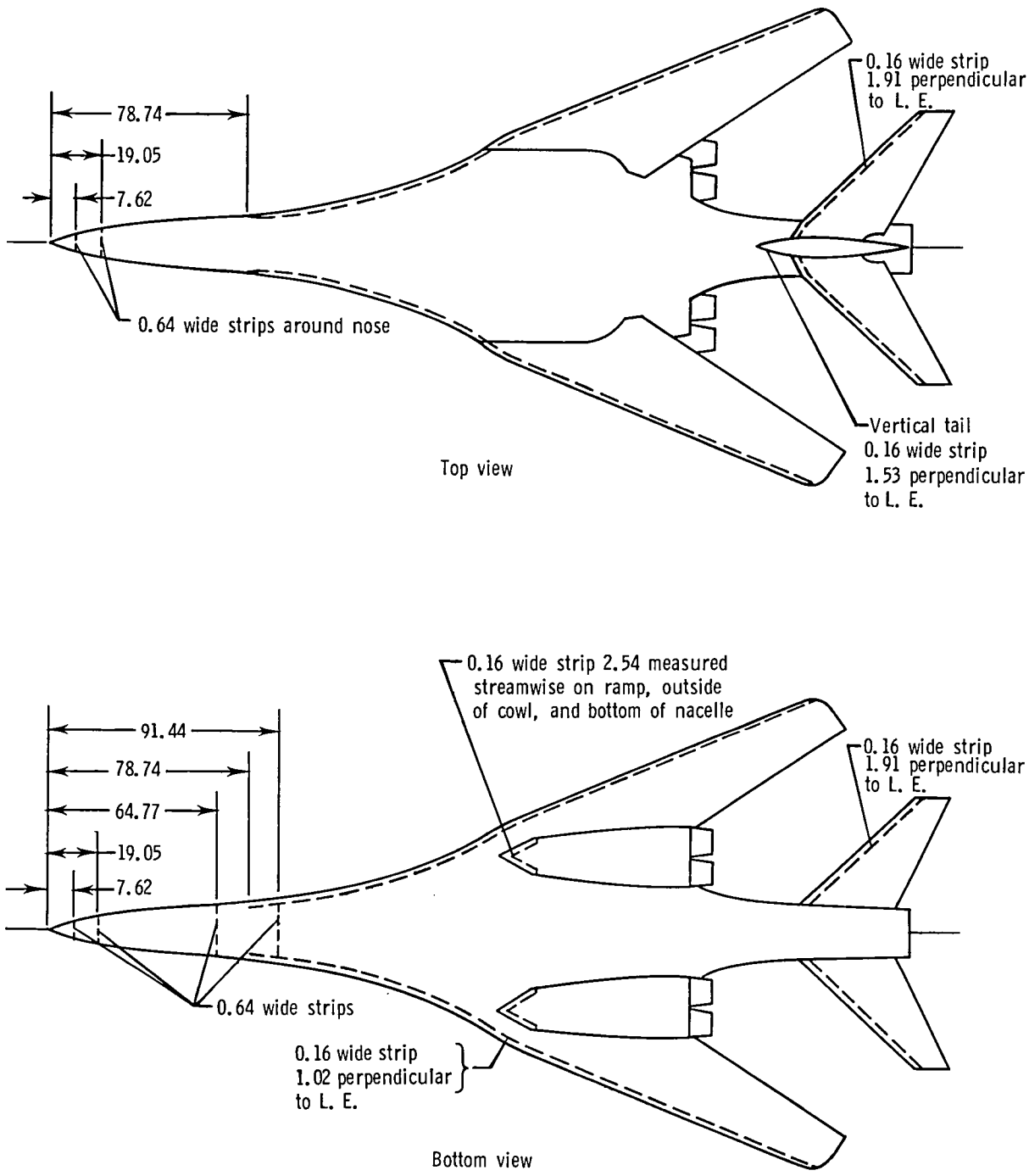

Figure 10.- Transition-strip location. All dimensions are in centimeters.

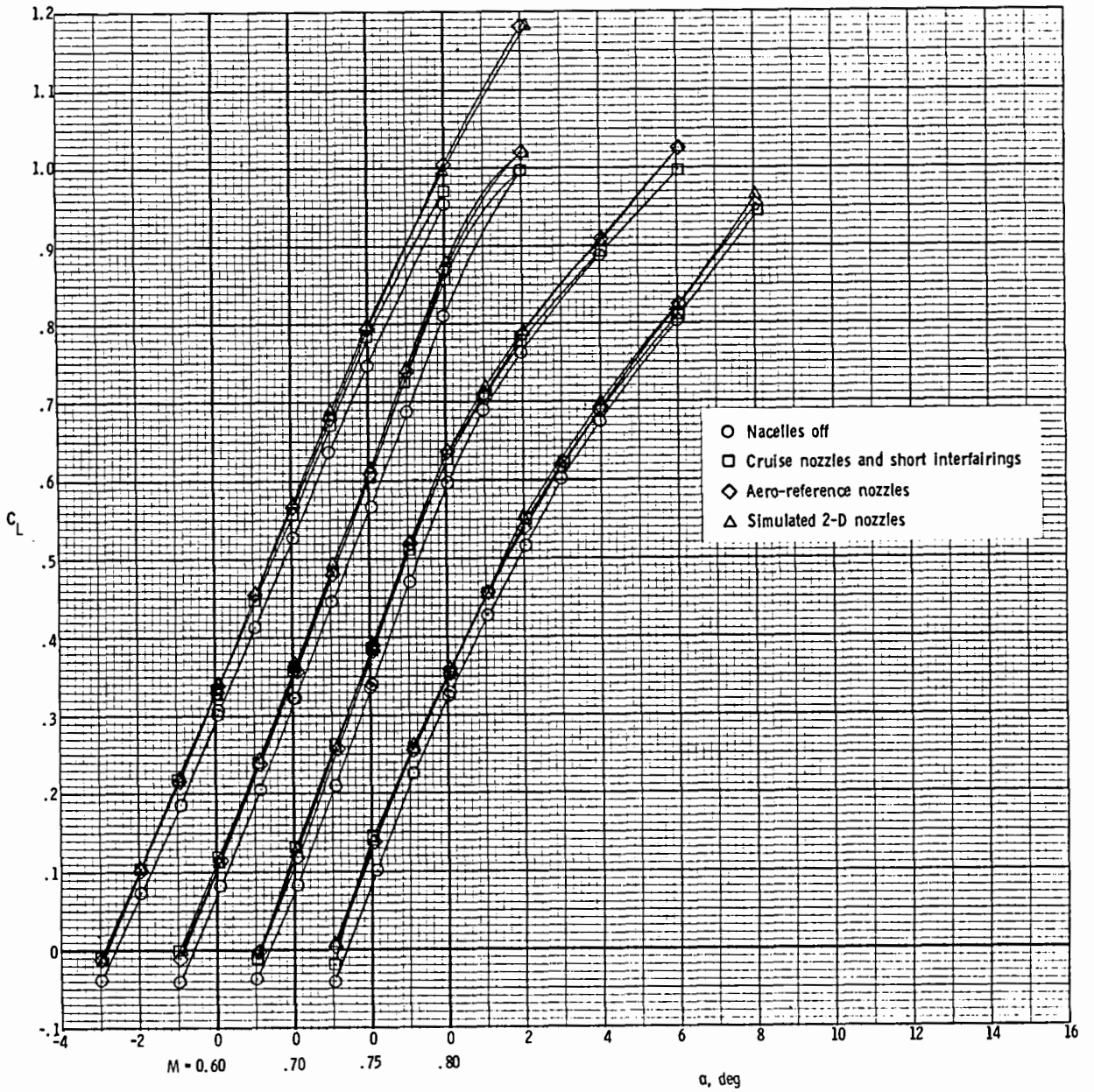

(a) Lift coefficient.

Figure 11.- Effect of nacelles and of nozzle shape on longitudinal aerodynamic characteristics of the model with wings swept 25°.

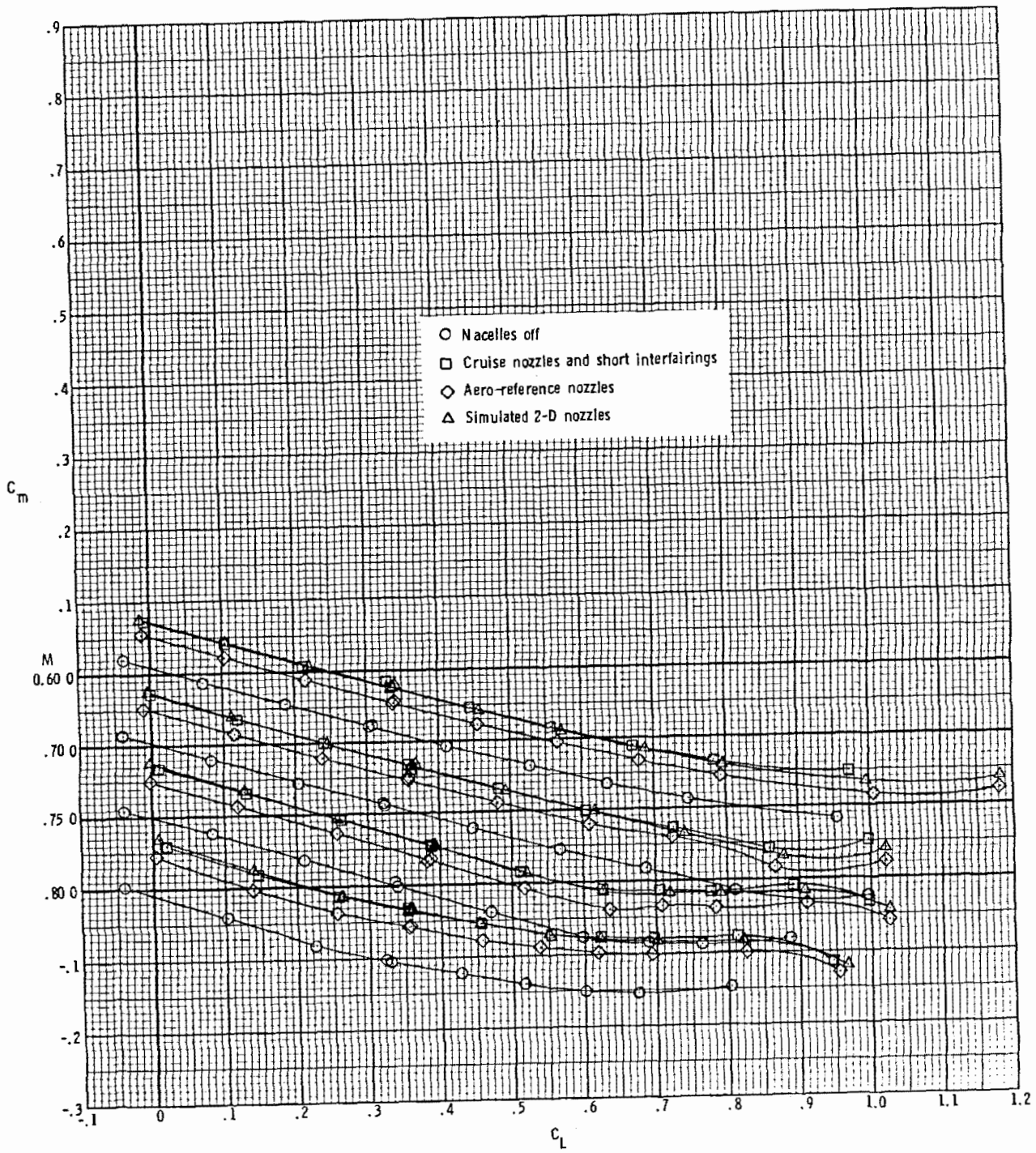

(b) Pitching-moment coefficient.

Figure 11.- Continued.

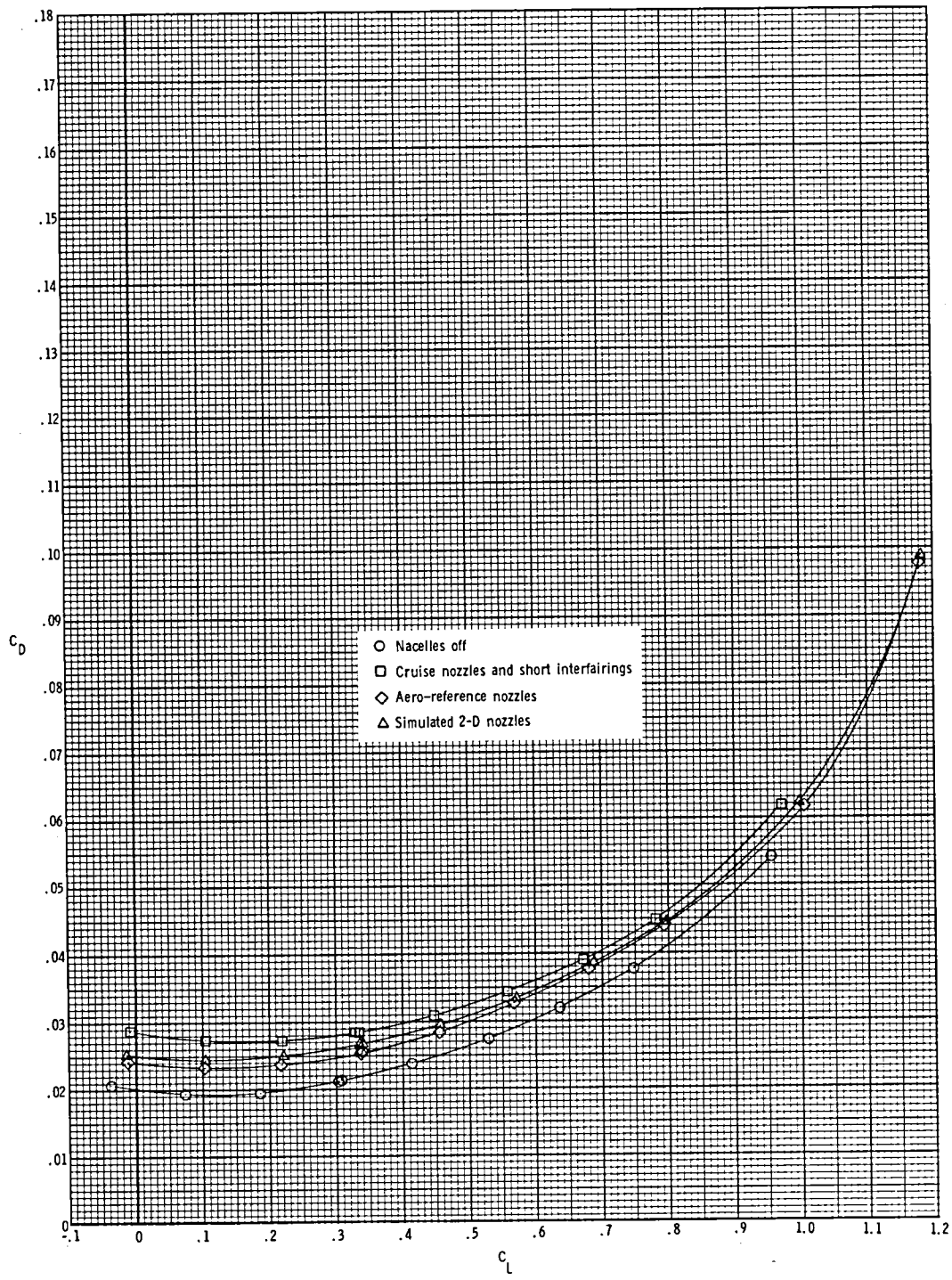

(c) Drag coefficient at M = 0.60.

Figure 11.- Continued.

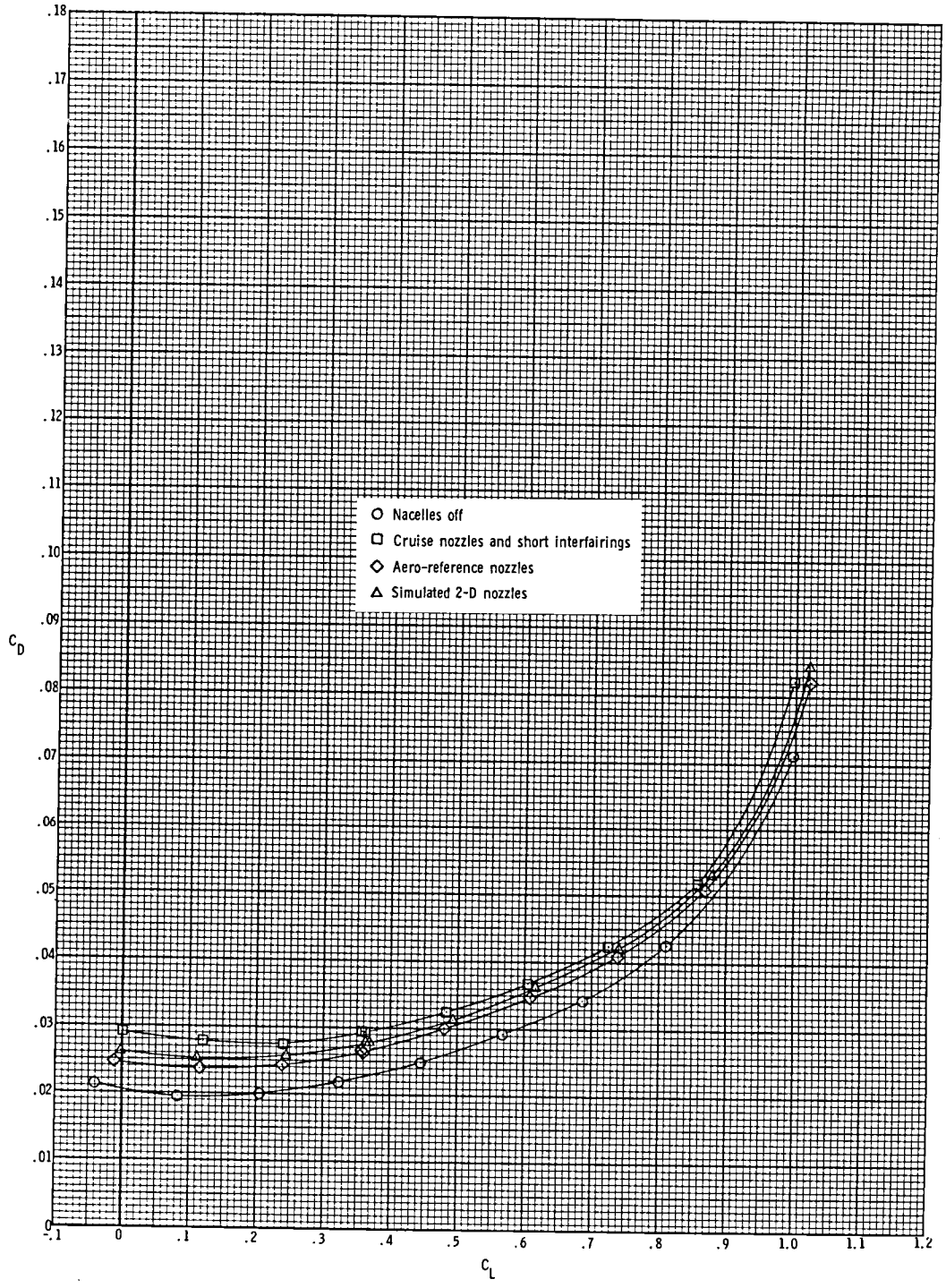

(d) Drag coefficient at M = 0.70.

Figure 11.- Continued.

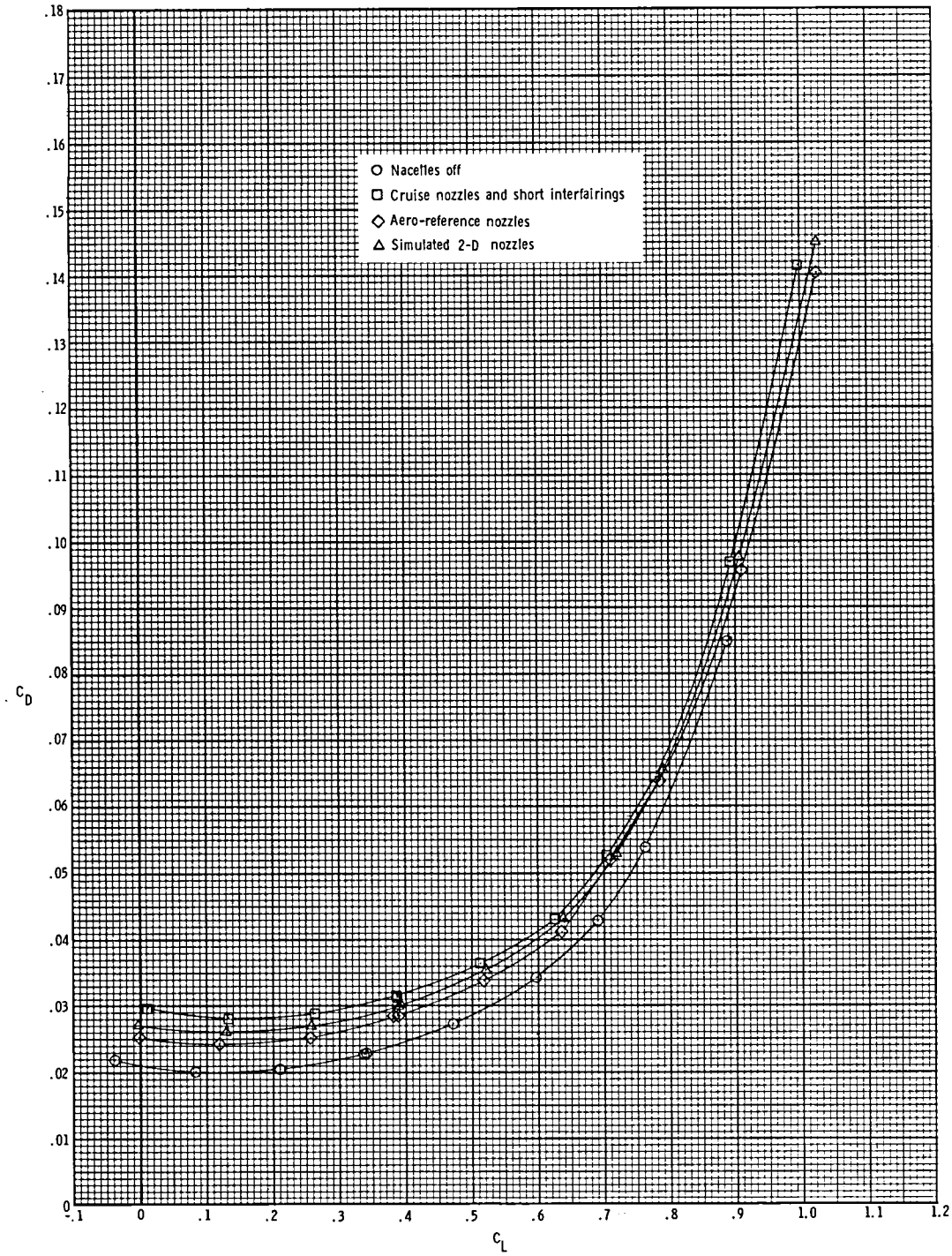

(e) Drag coefficient at M = 0.75.

Figure 11.- Continued.

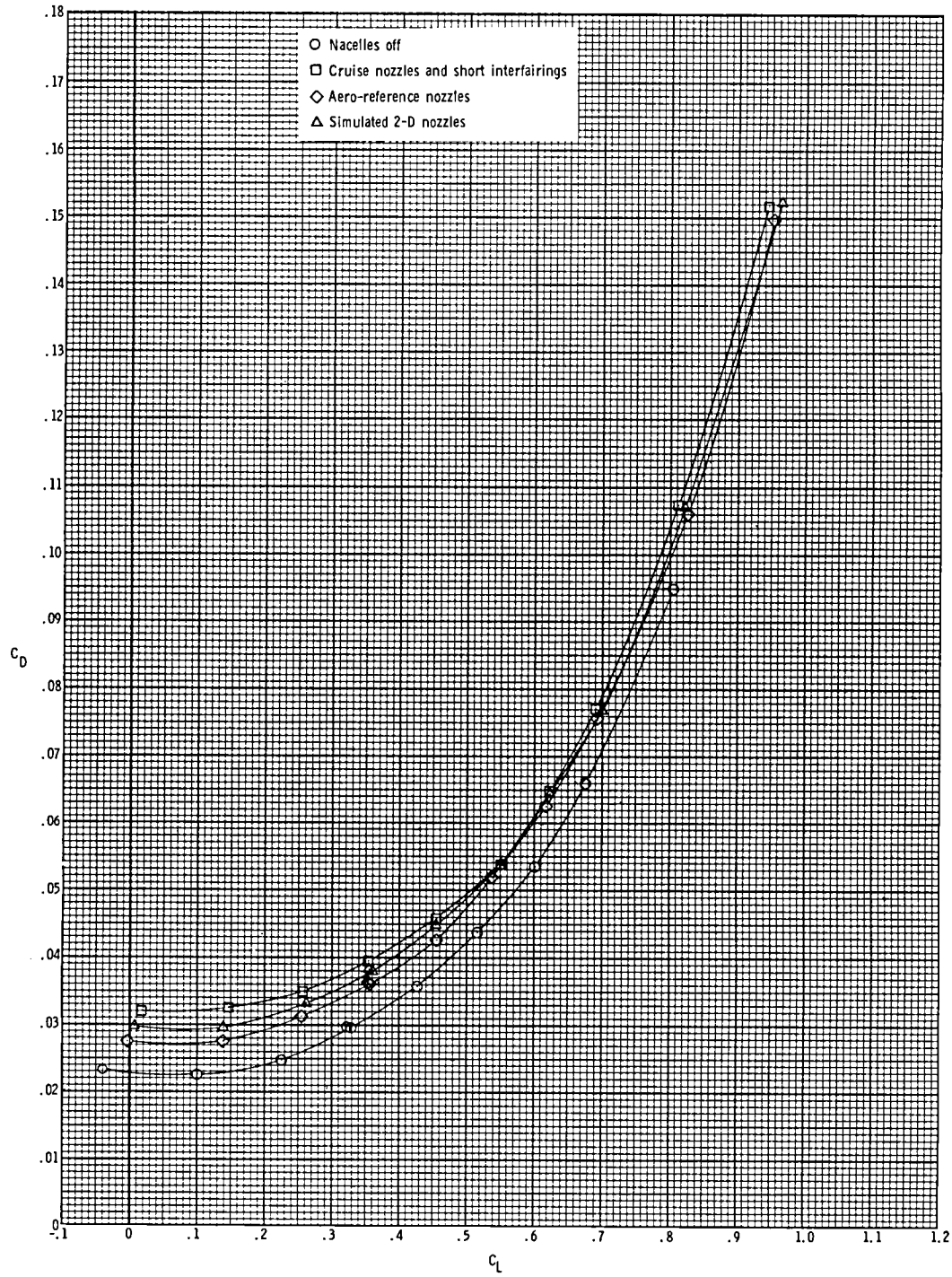

(f) Drag coefficient at M = 0.80.

Figure 11.- Concluded.

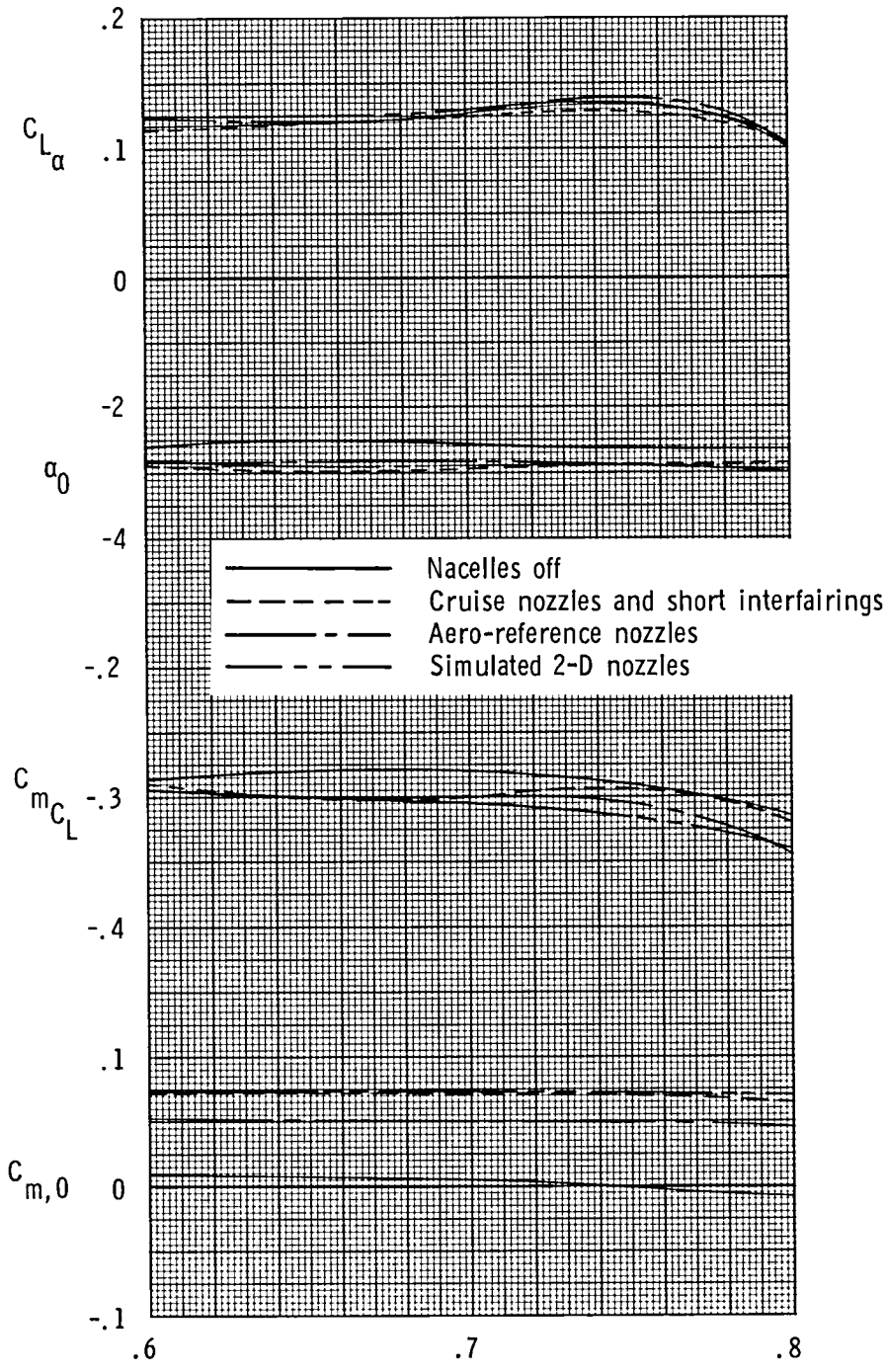

(a) C_{L_α}, α_0, $C_{m_{C_L}}$, and $C_{m,0}$.

Figure 12.- Effect of nacelles and of nozzle shape on model longitudinal parameters for model with wings swept 25°.

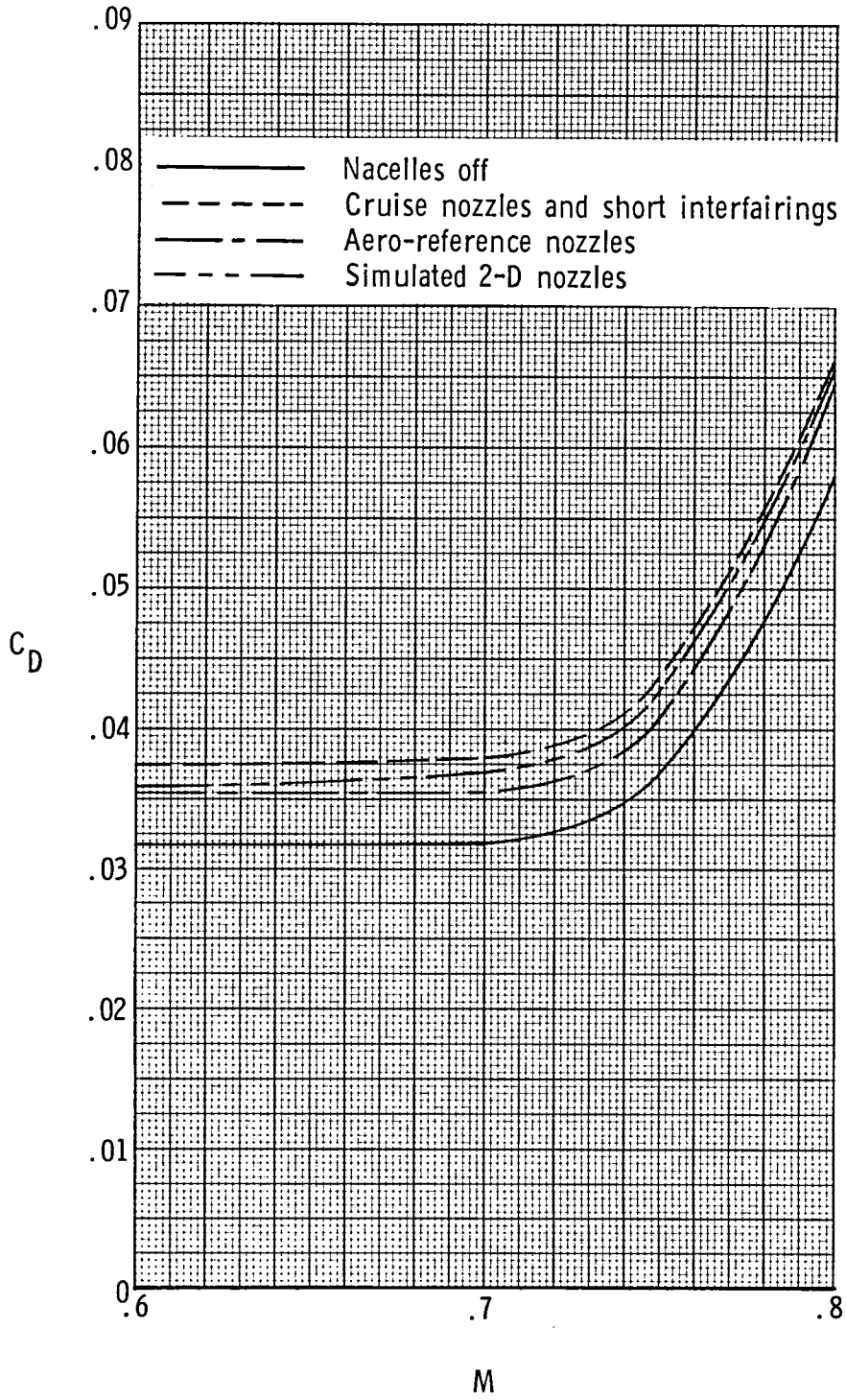

(b) Drag coefficient at $C_L = 0.63$.

Figure 12.- Concluded.

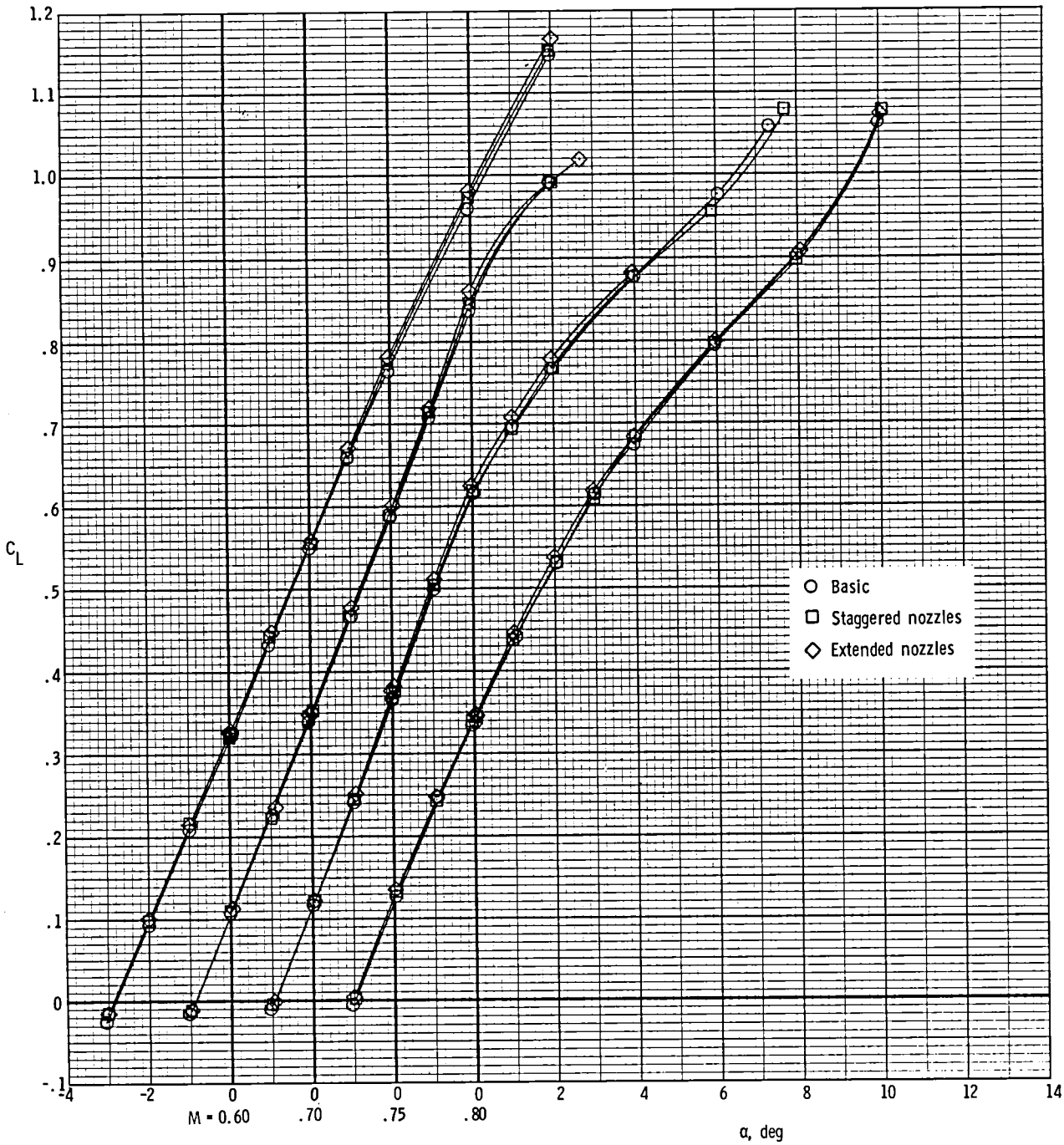

(a) Lift coefficient.

Figure 13.- Effect of staggered and extended nozzles on longitudinal aerodynamic characteristics of the model with cruise nozzles, short interfairing, and wings swept 25°.

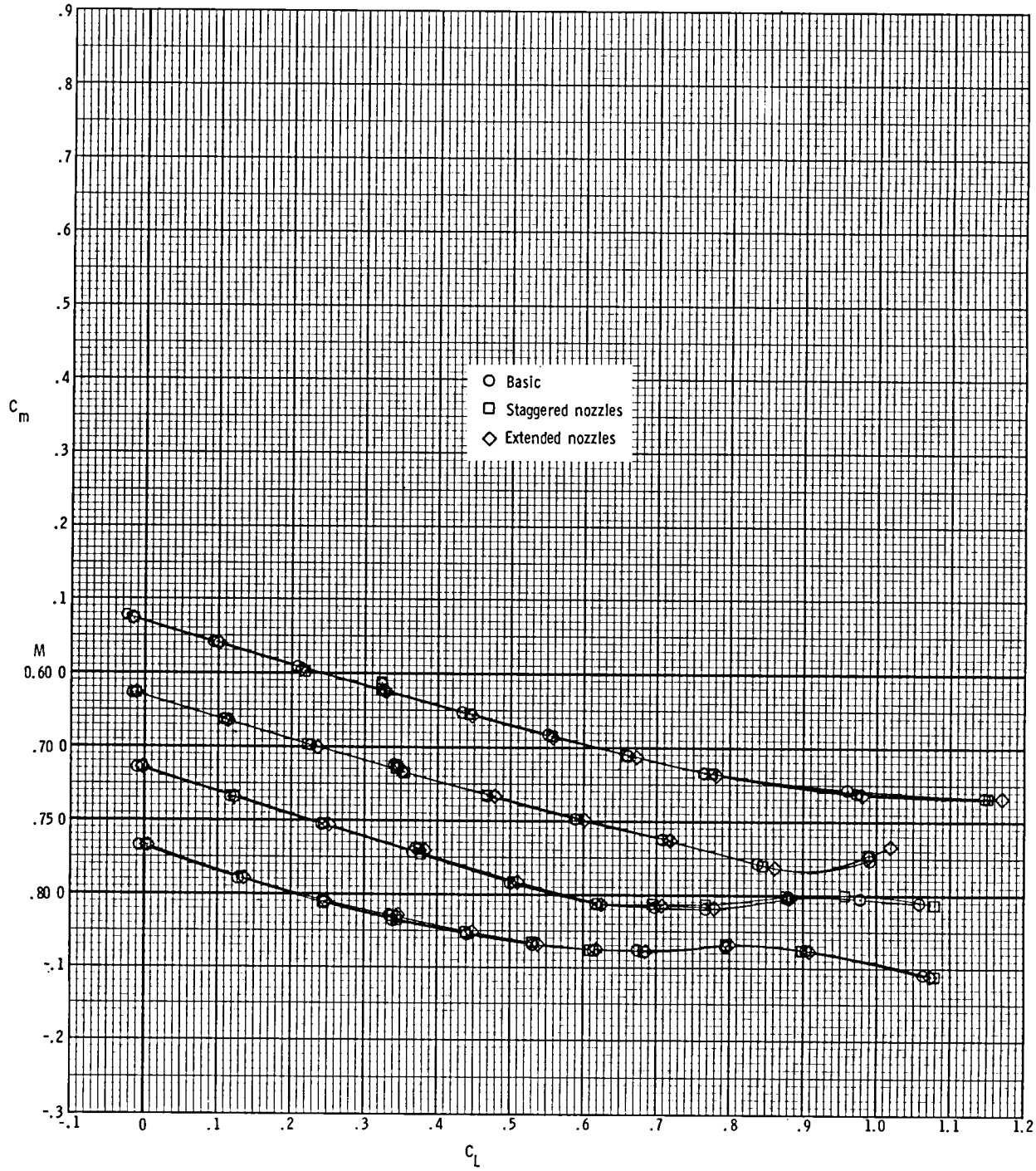

(b) Pitching-moment coefficient.

Figure 13.- Continued.

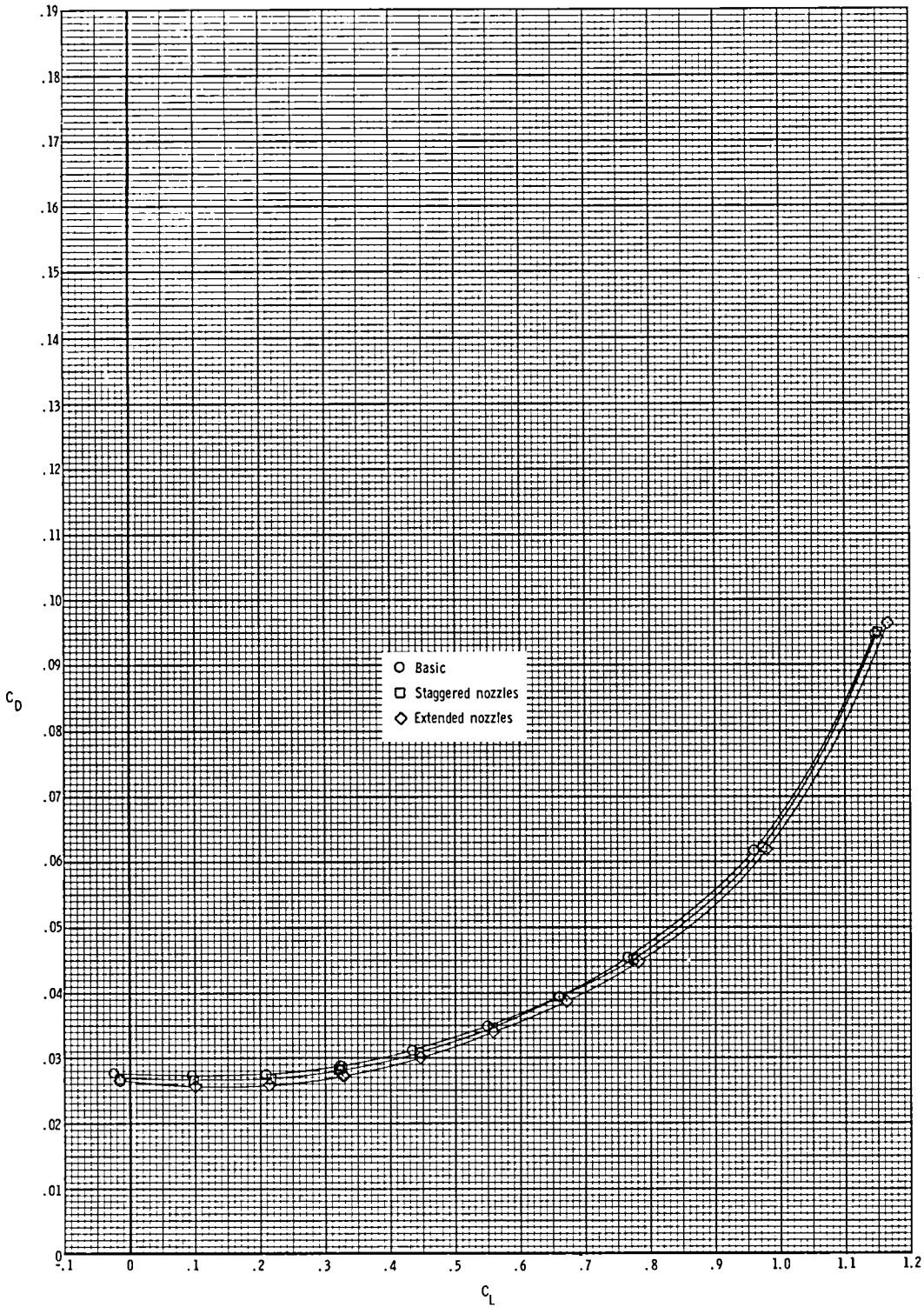

(c) Drag coefficient at M = 0.60.

Figure 13.- Continued.

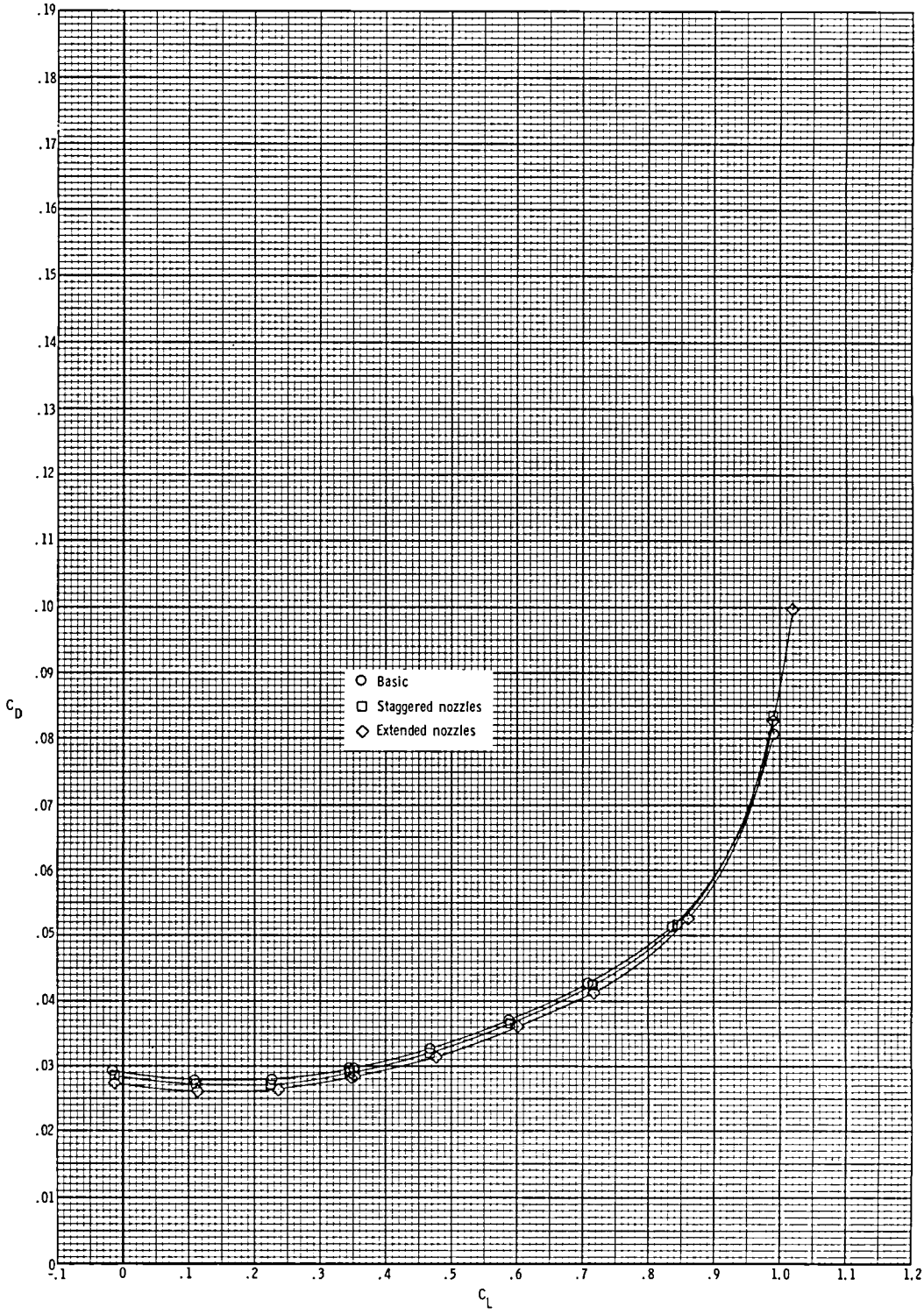

(d) Drag coefficient at M = 0.70.

Figure 13.- Continued.

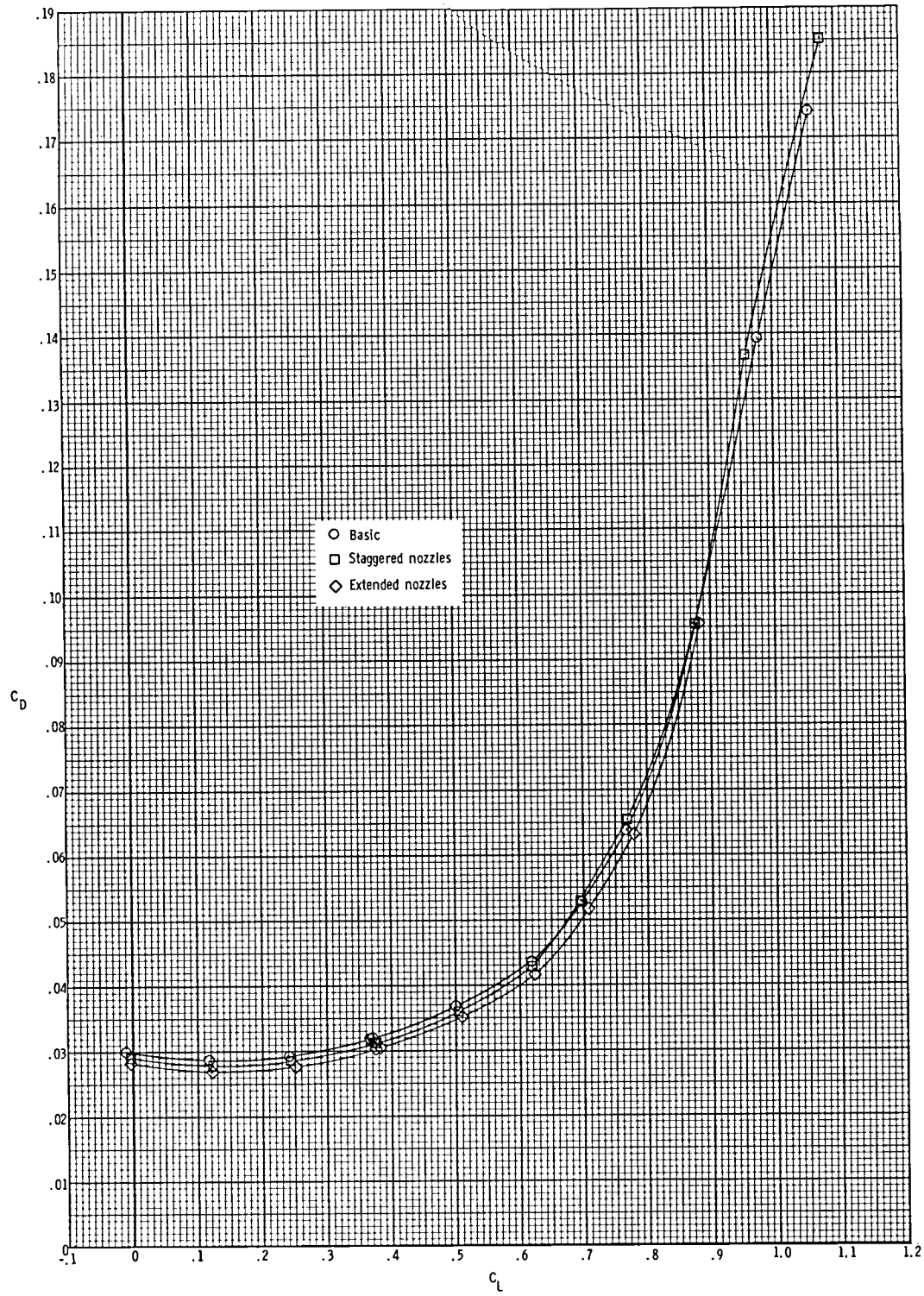

(e) Drag coefficient at M = 0.75.

Figure 13.- Continued.

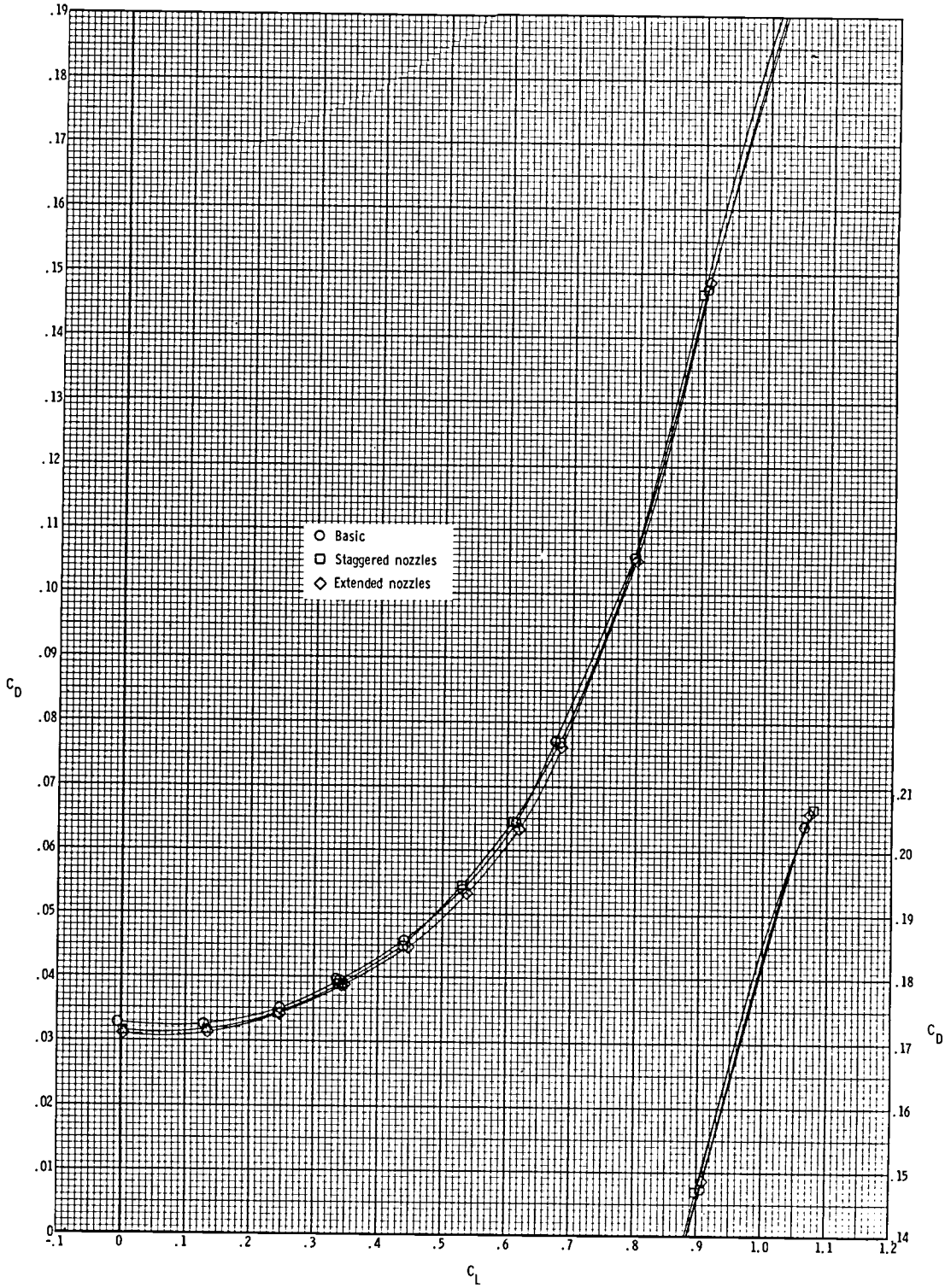

(f) Drag coefficient at M = 0.80.

Figure 13.- Concluded.

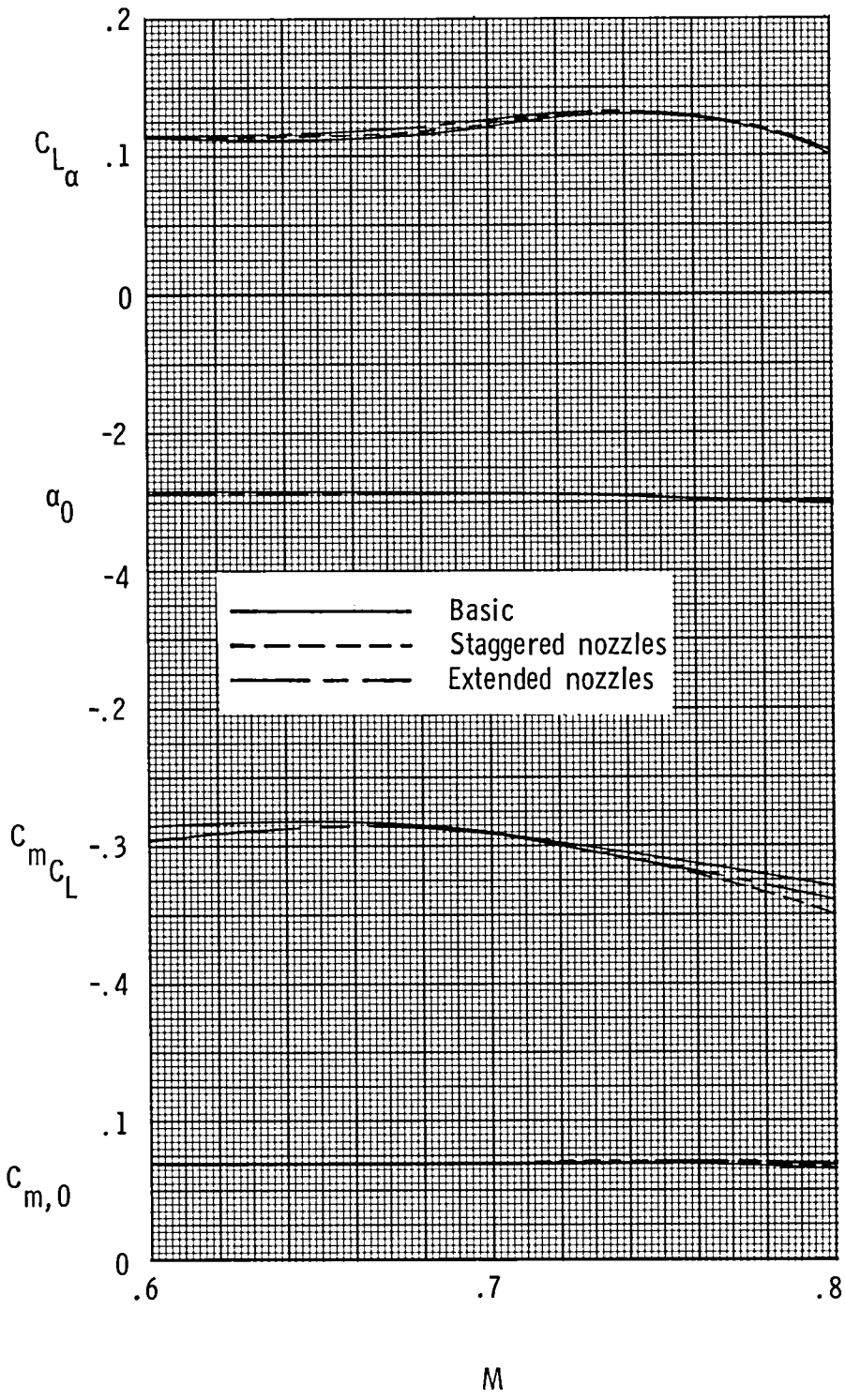

(a) C_{L_α}, α_0, $C_{m_{C_L}}$, and $C_{m,0}$.

Figure 14.- Effect of staggered and extended nozzles on model longitudinal parameters for model with cruise nozzles, short interfairing, and wings swept 25°.

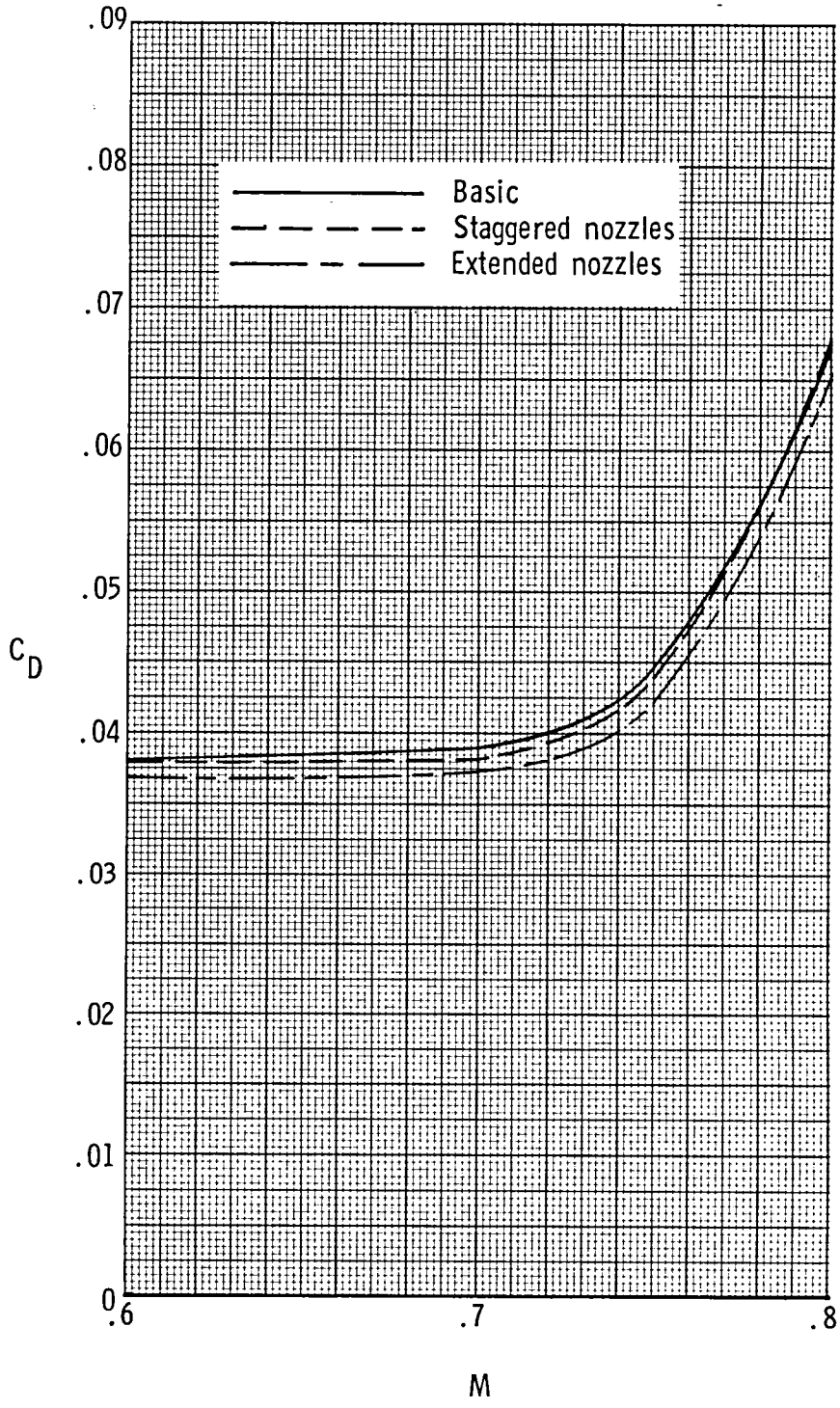

(b) Drag coefficient at $C_L = 0.63$.

Figure 14.- Concluded.

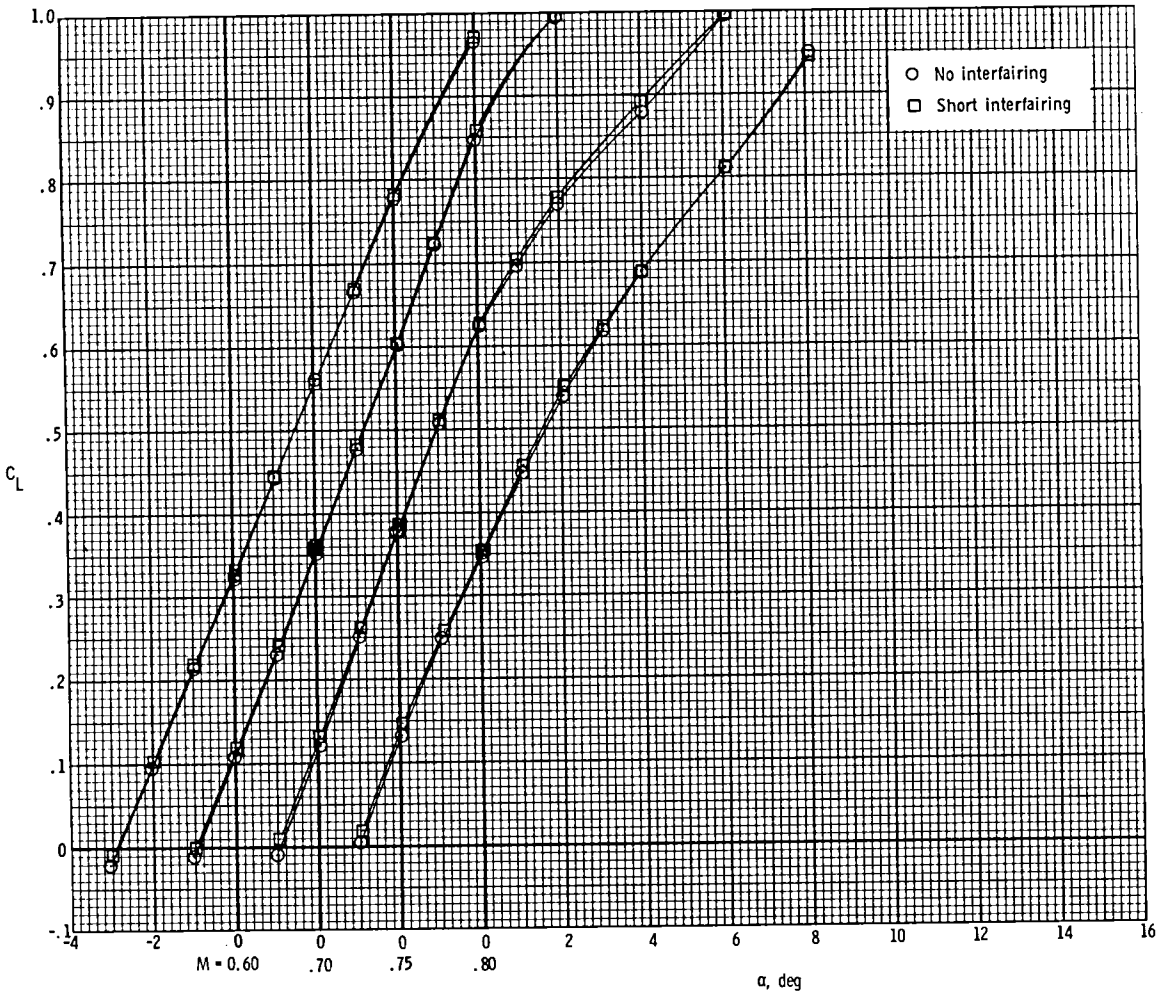

(a) Lift coefficient.

Figure 15.- Effect of short interfairing on longitudinal aerodynamic characteristics of the model with cruise nozzles and wings swept 25°.

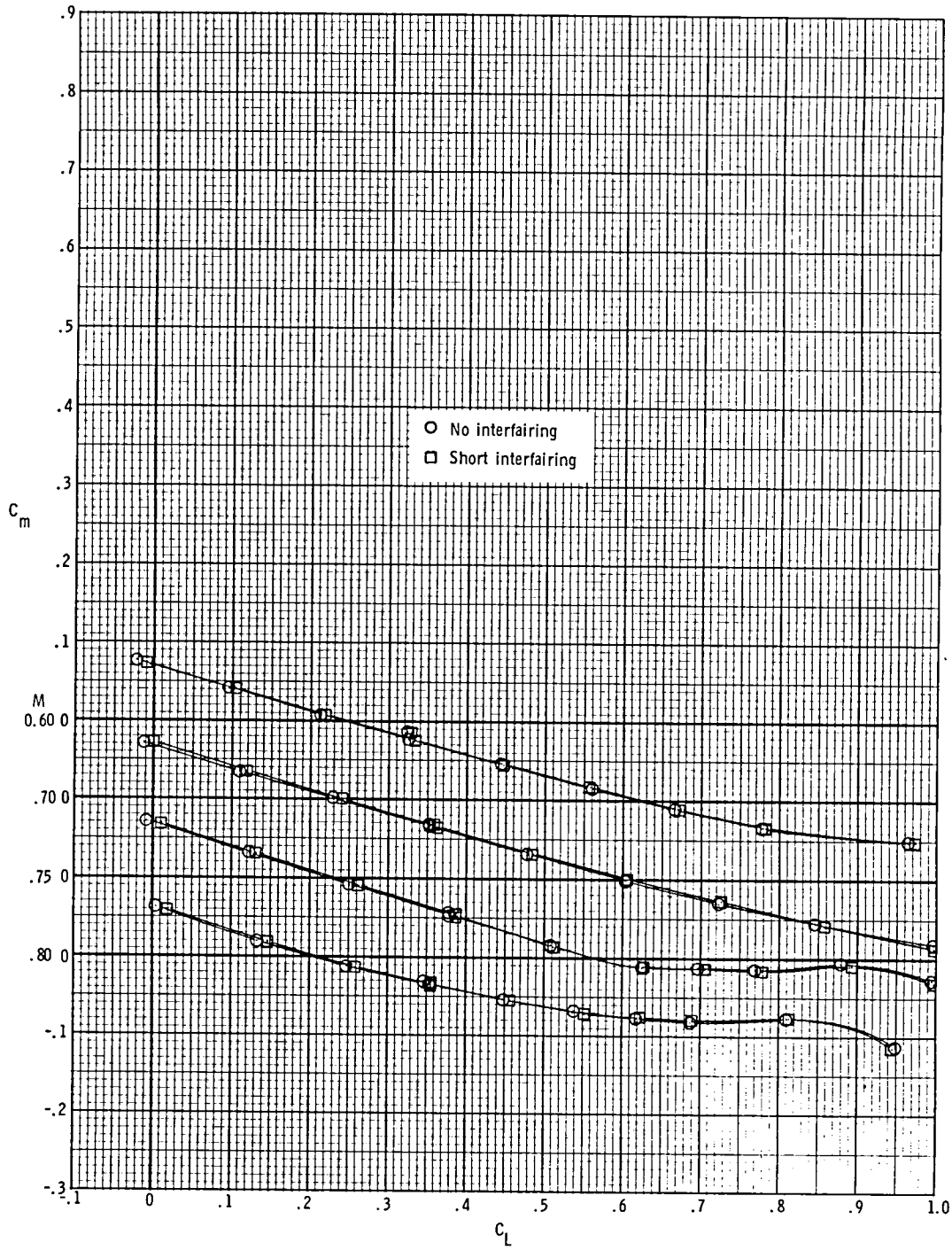

(b) Pitching-moment coefficient.

Figure 15.- Continued.

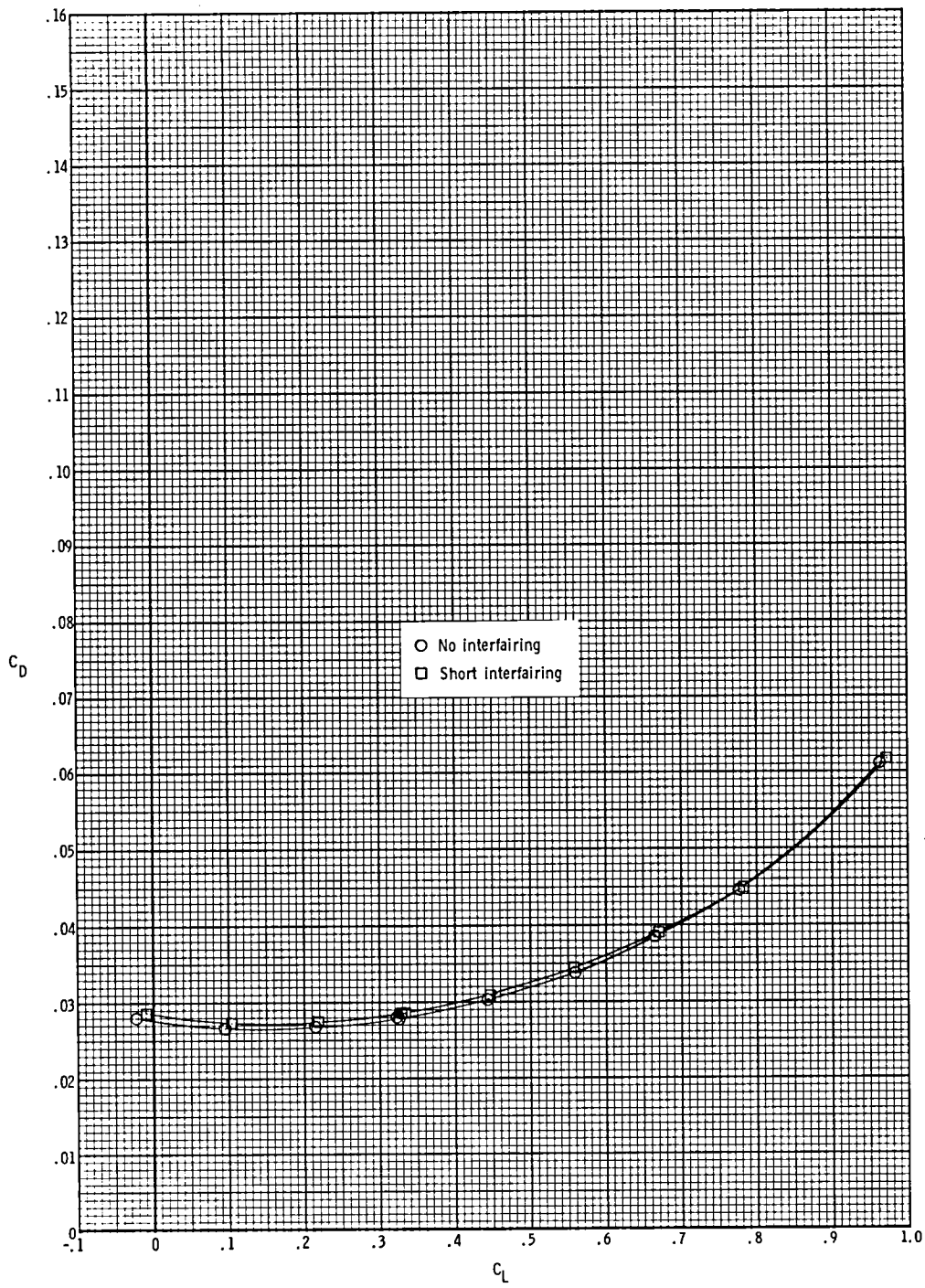

(c) Drag coefficient at M = 0.60.

Figure 15.- Continued.

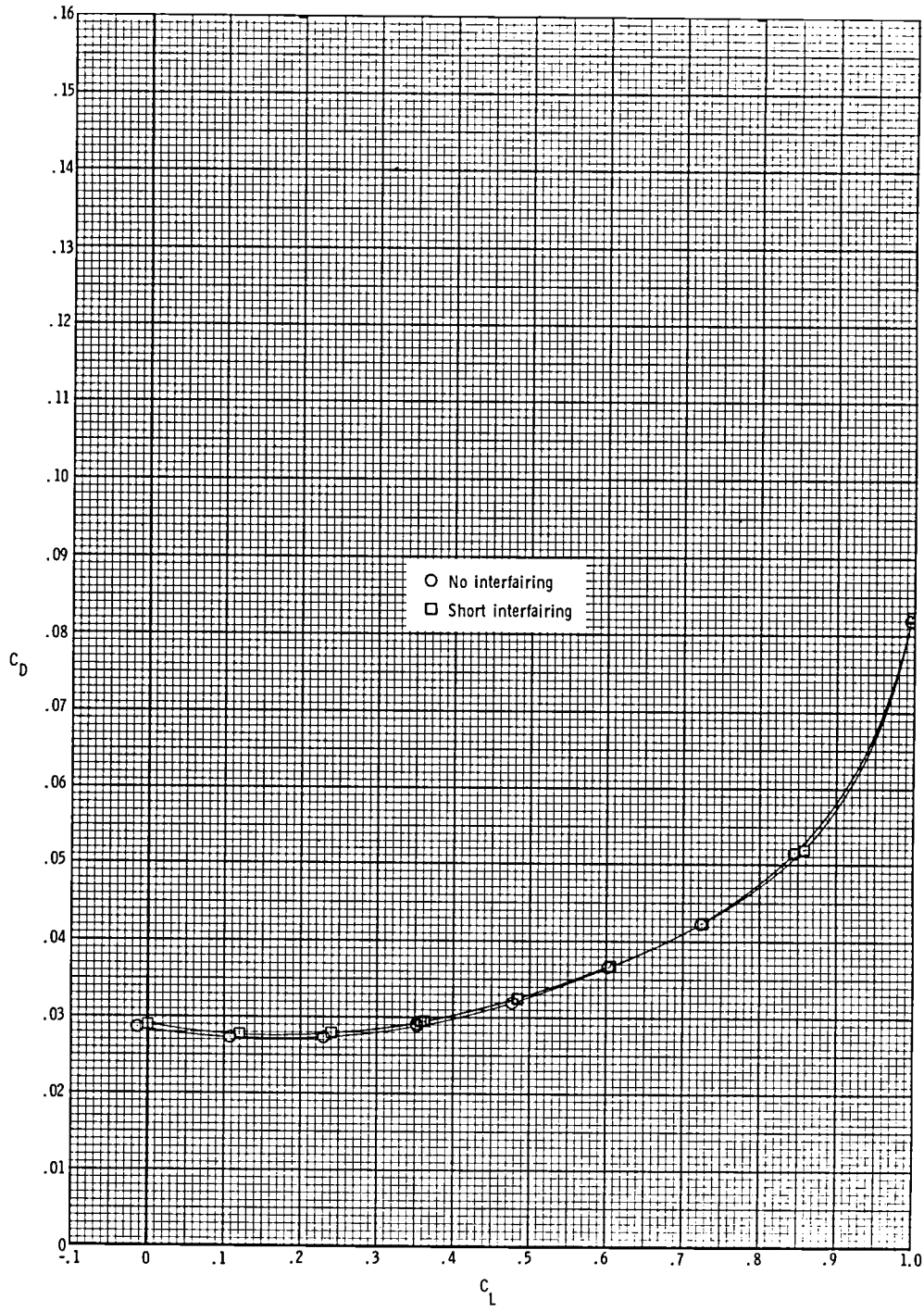

(d) Drag coefficient at M = 0.70.

Figure 15.- Continued.

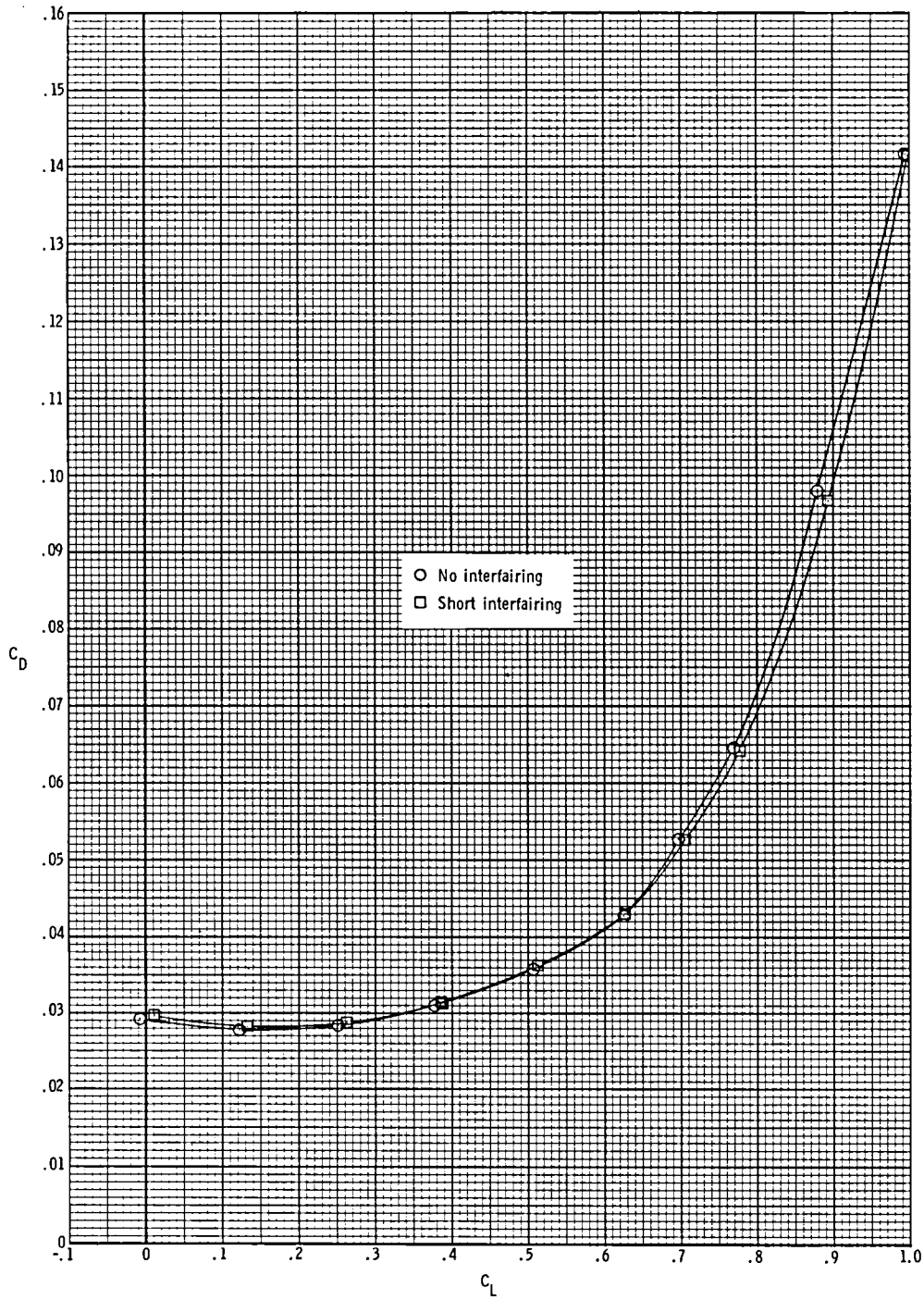

(e) Drag coefficient at M = 0.75.

Figure 15.- Continued.

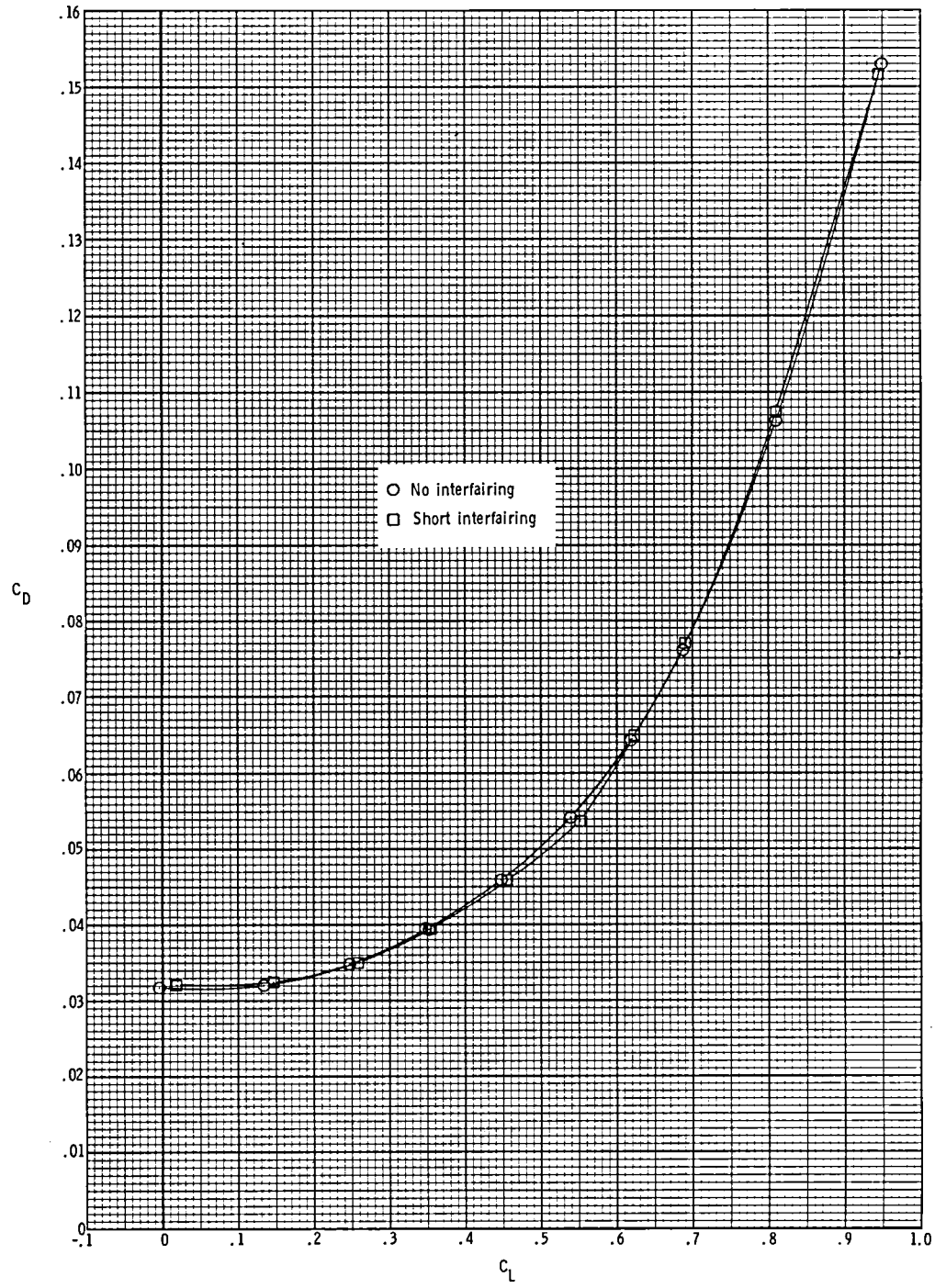

(f) Drag coefficient at M = 0.80.

Figure 15.- Concluded.

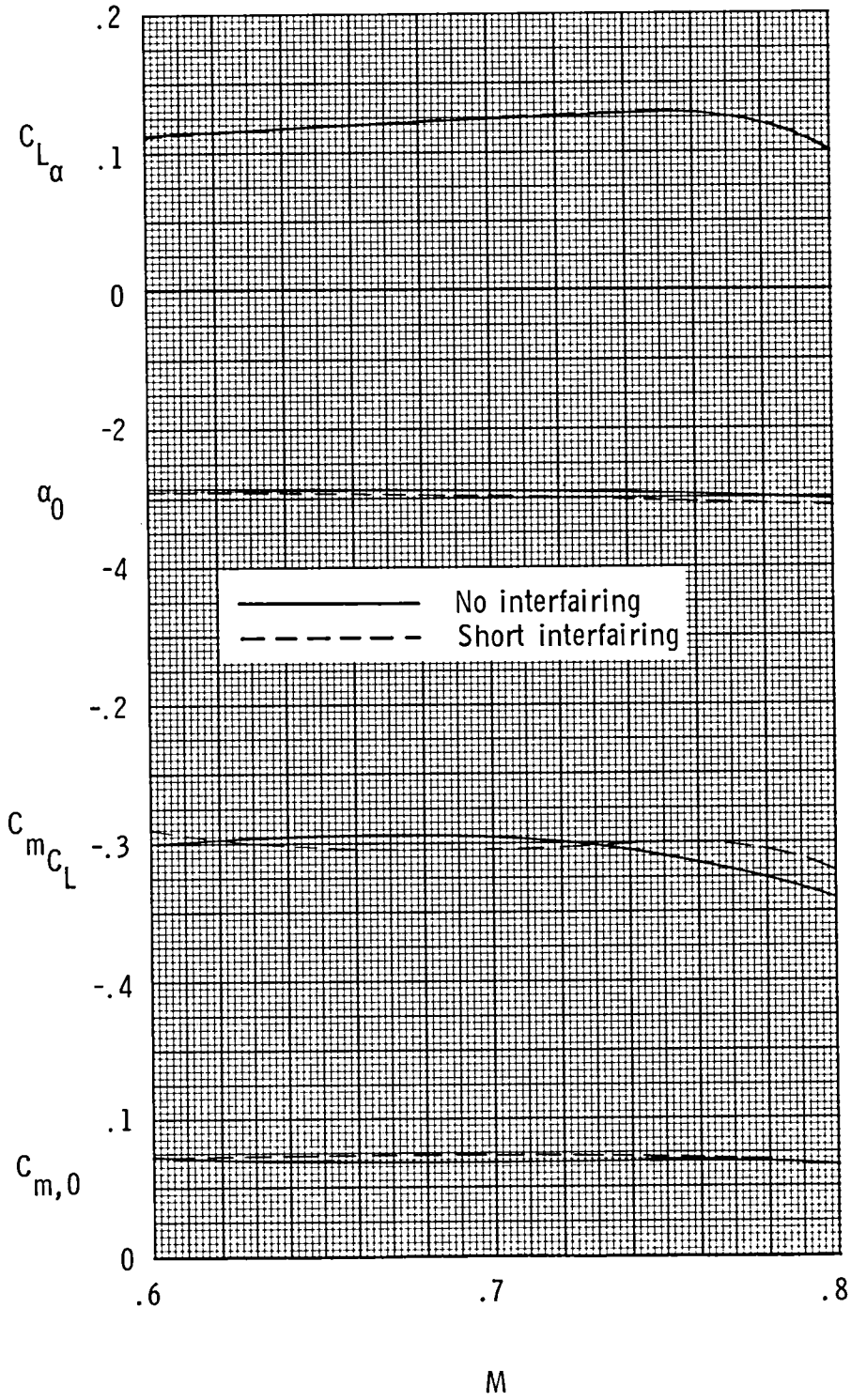

(a) C_{L_α}, α_0, $C_{m_{C_L}}$, and $C_{m,0}$.

Figure 16.- Effect of short interfairing on model longitudinal parameters for model with cruise nozzles and wings swept 25°.

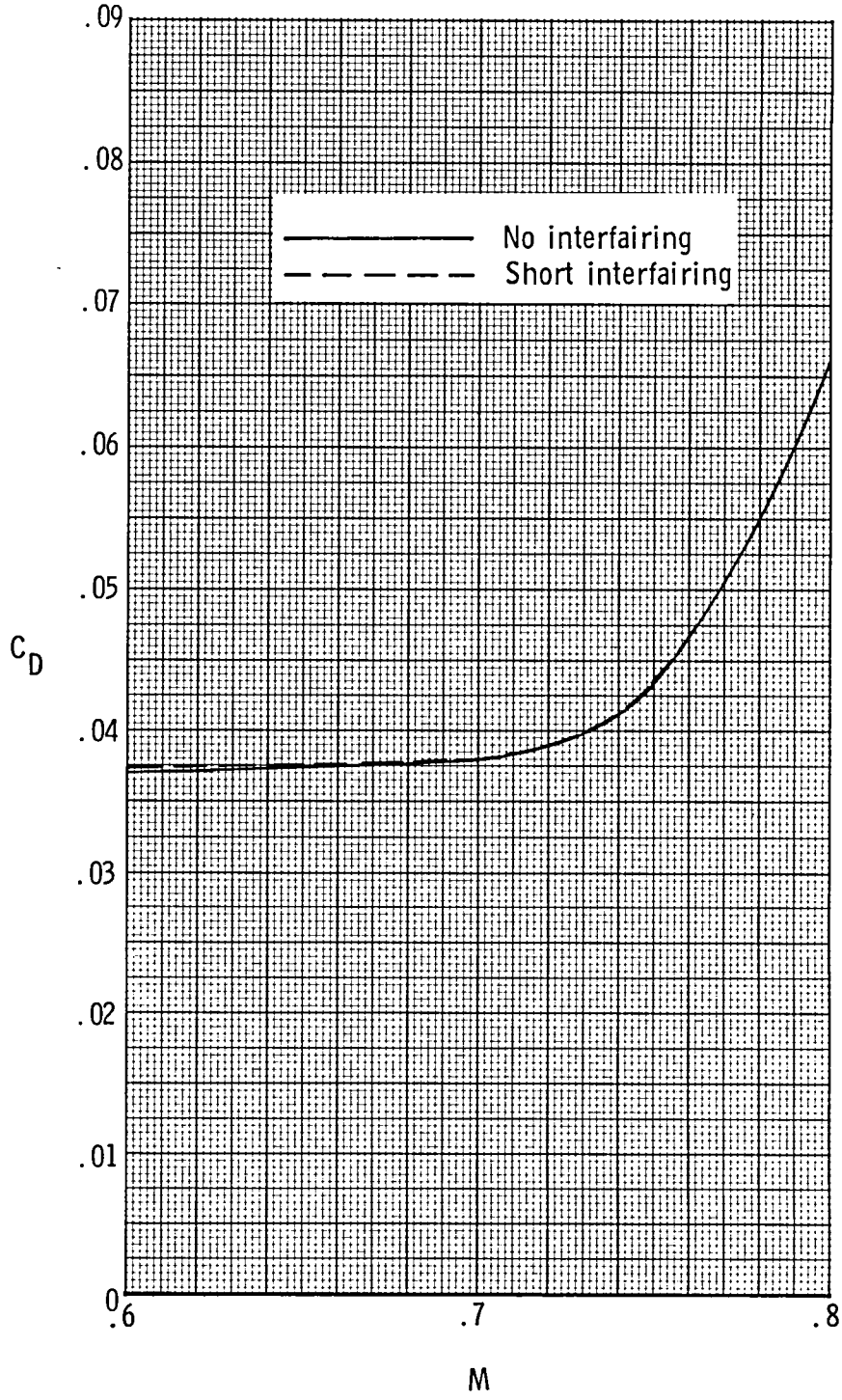

(b) Drag coefficient at $C_L = 0.63$.

Figure 16.- Concluded.

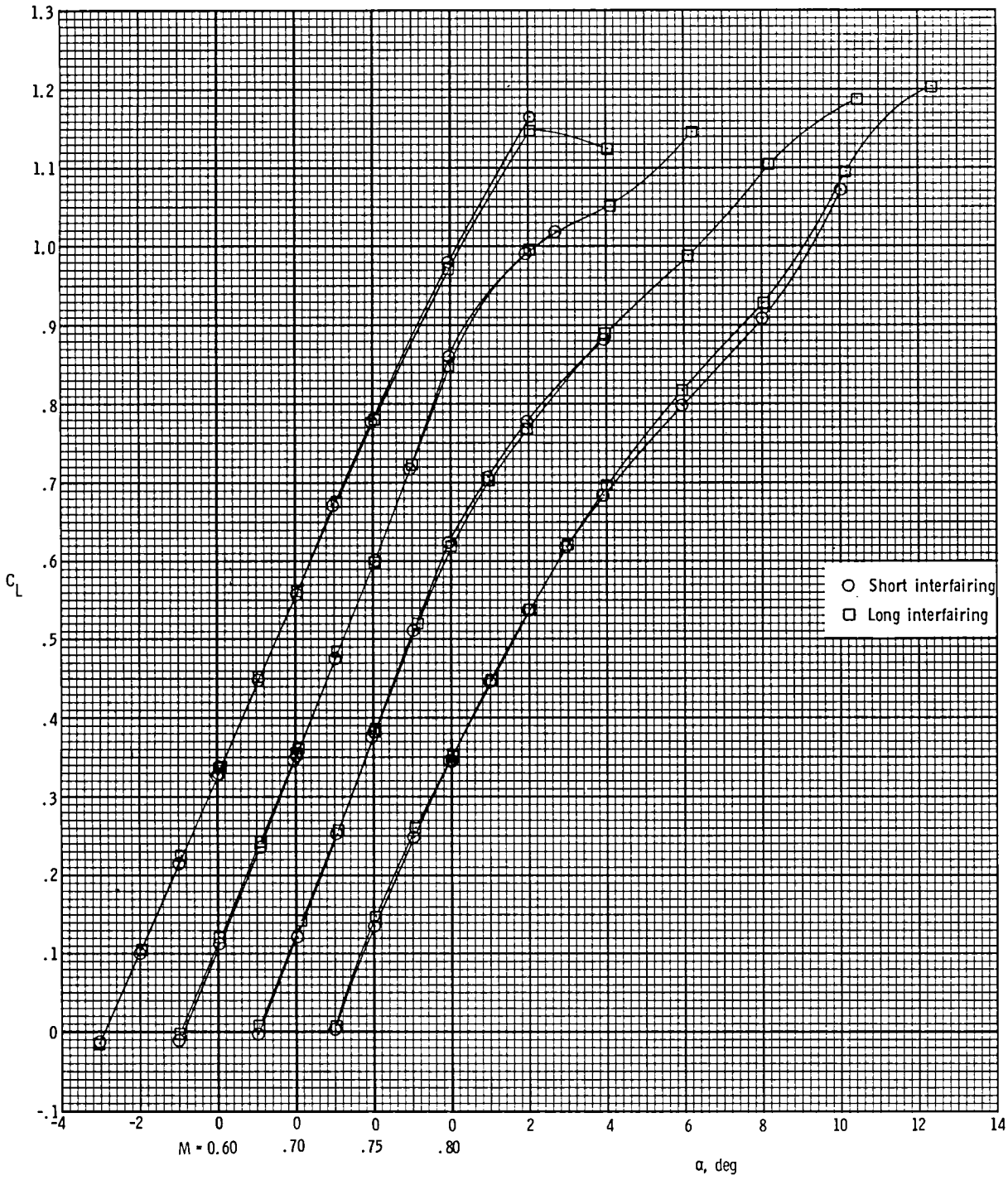

(a) Lift coefficient.

Figure 17.- Effect of lengthening interfairing on longitudinal aerodynamic characteristics of the model with cruise nozzles extended and wings swept 25°.

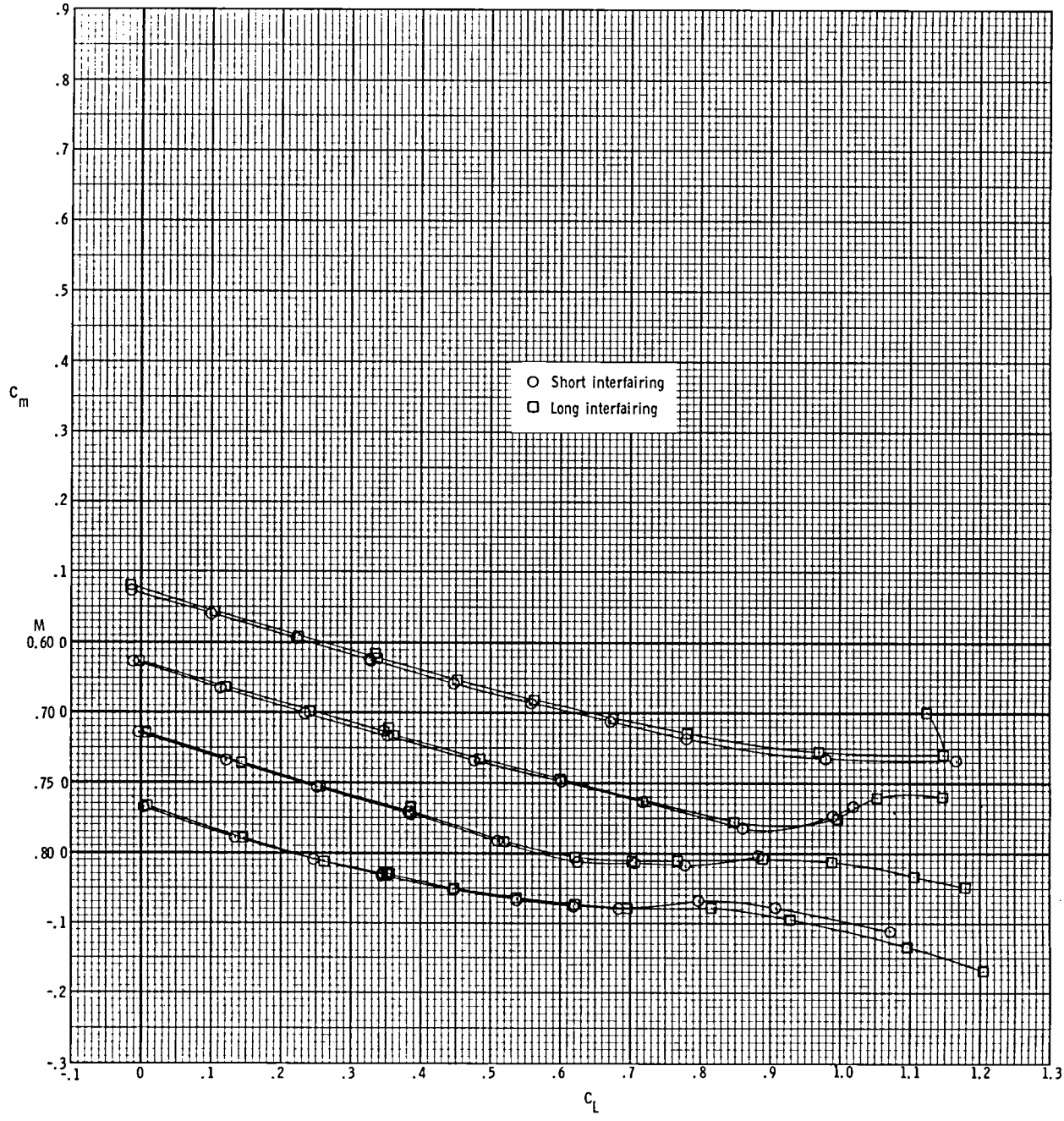

(b) Pitching-moment coefficient.

Figure 17.- Continued.

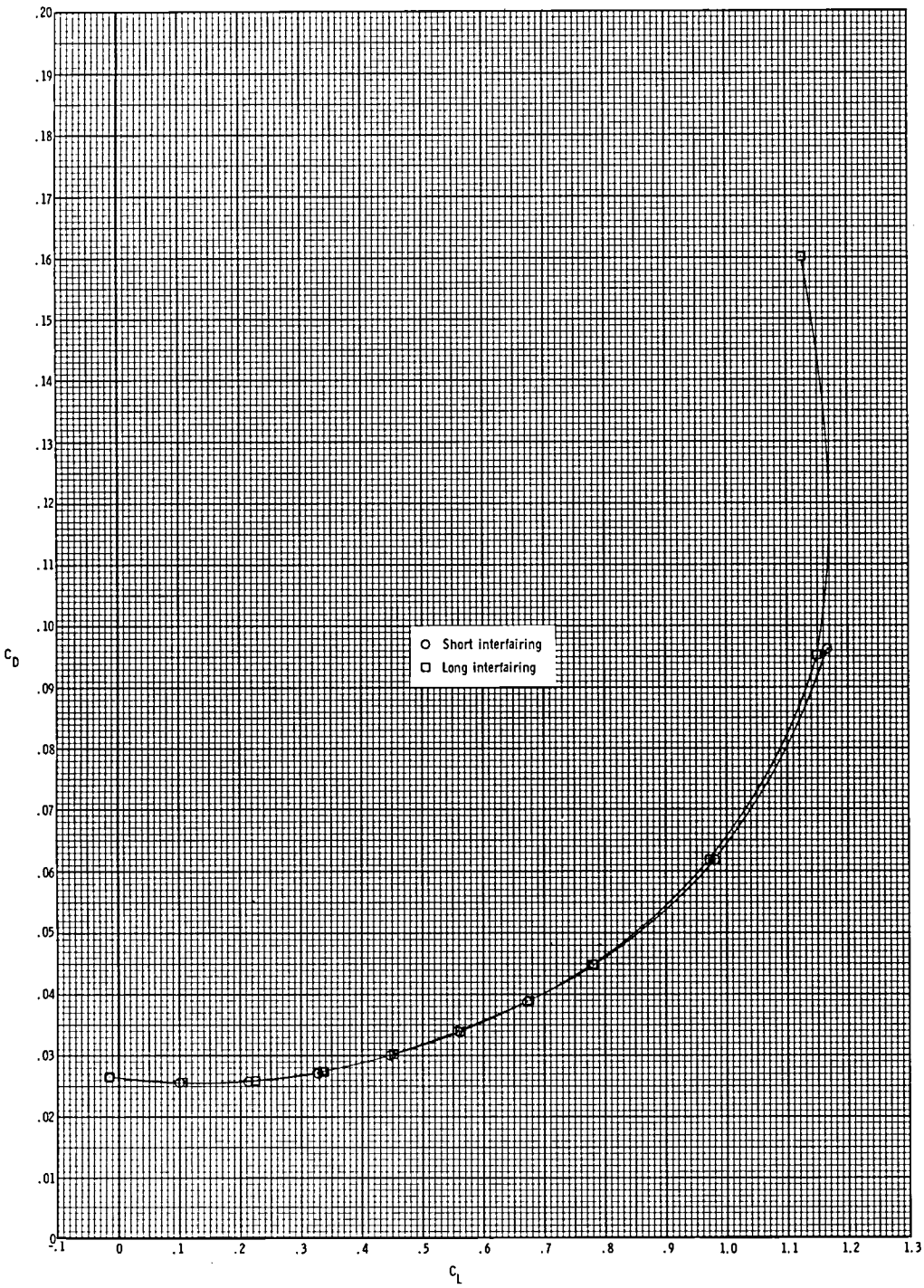

(c) Drag coefficient at M = 0.60.

Figure 17.- Continued.

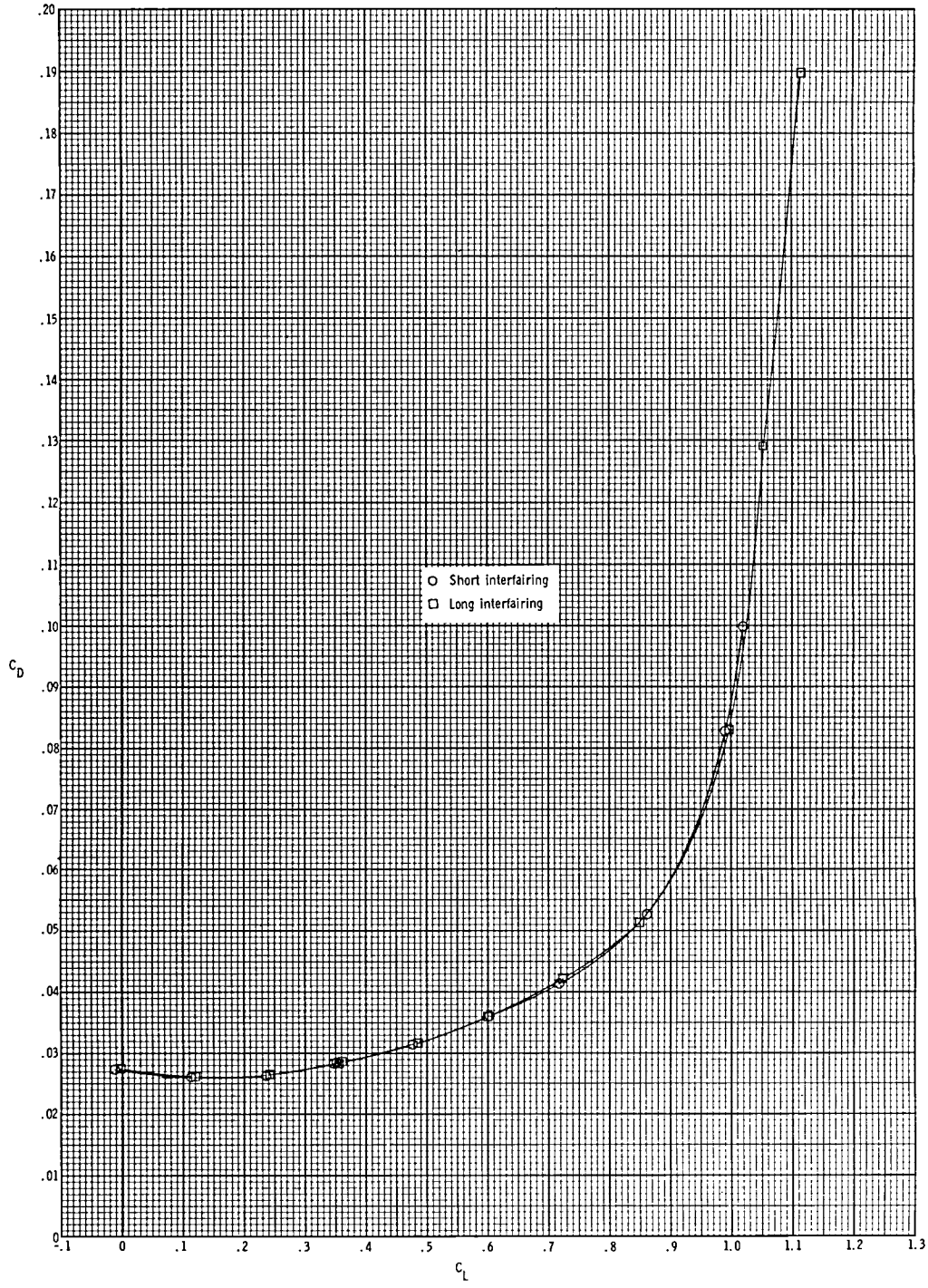

(d) Drag coefficient at M = 0.70.

Figure 17.- Continued.

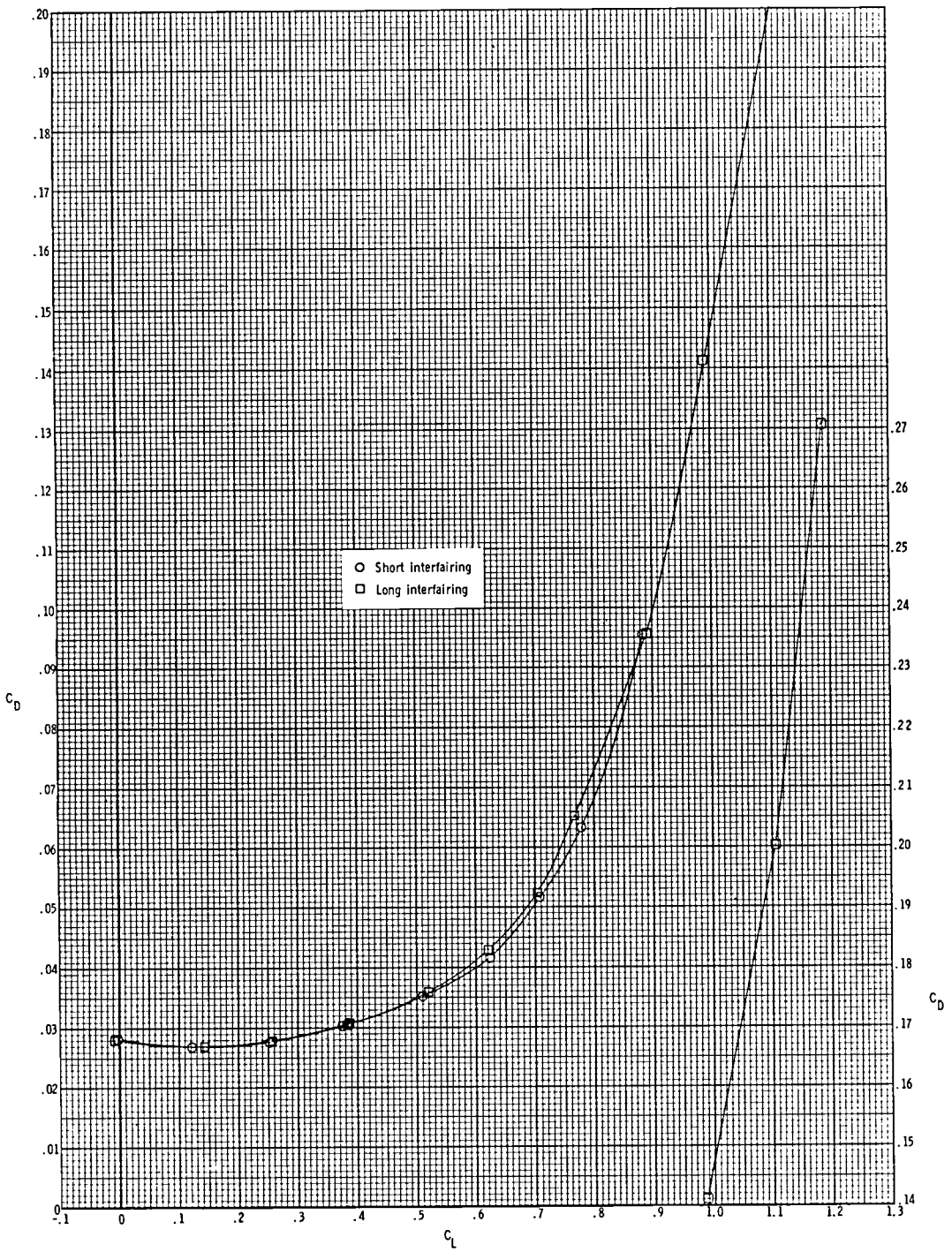

(e) Drag coefficient at M = 0.75.

Figure 17.- Continued.

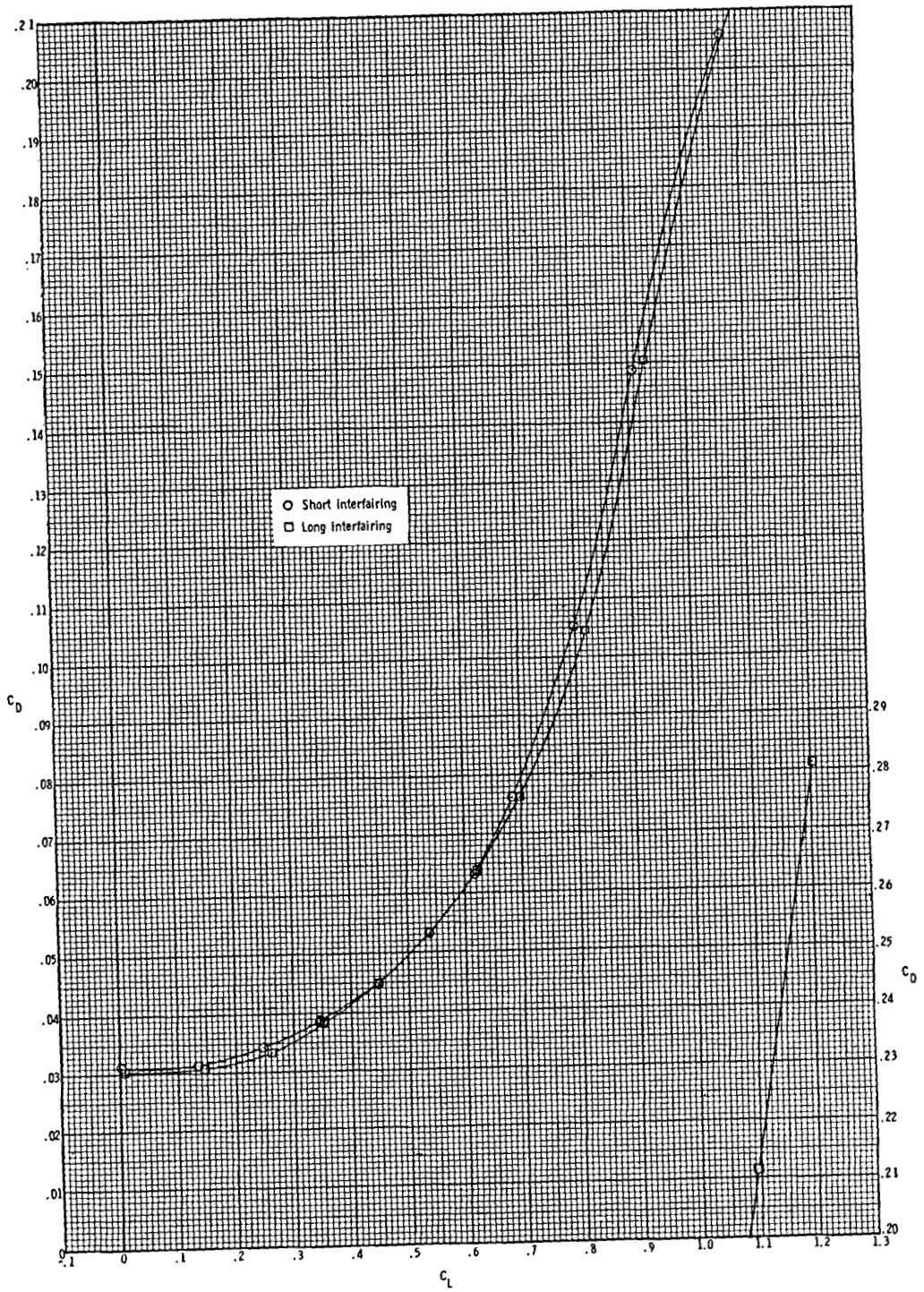

(f) Drag coefficient at M = 0.80.

Figure 17.- Concluded.

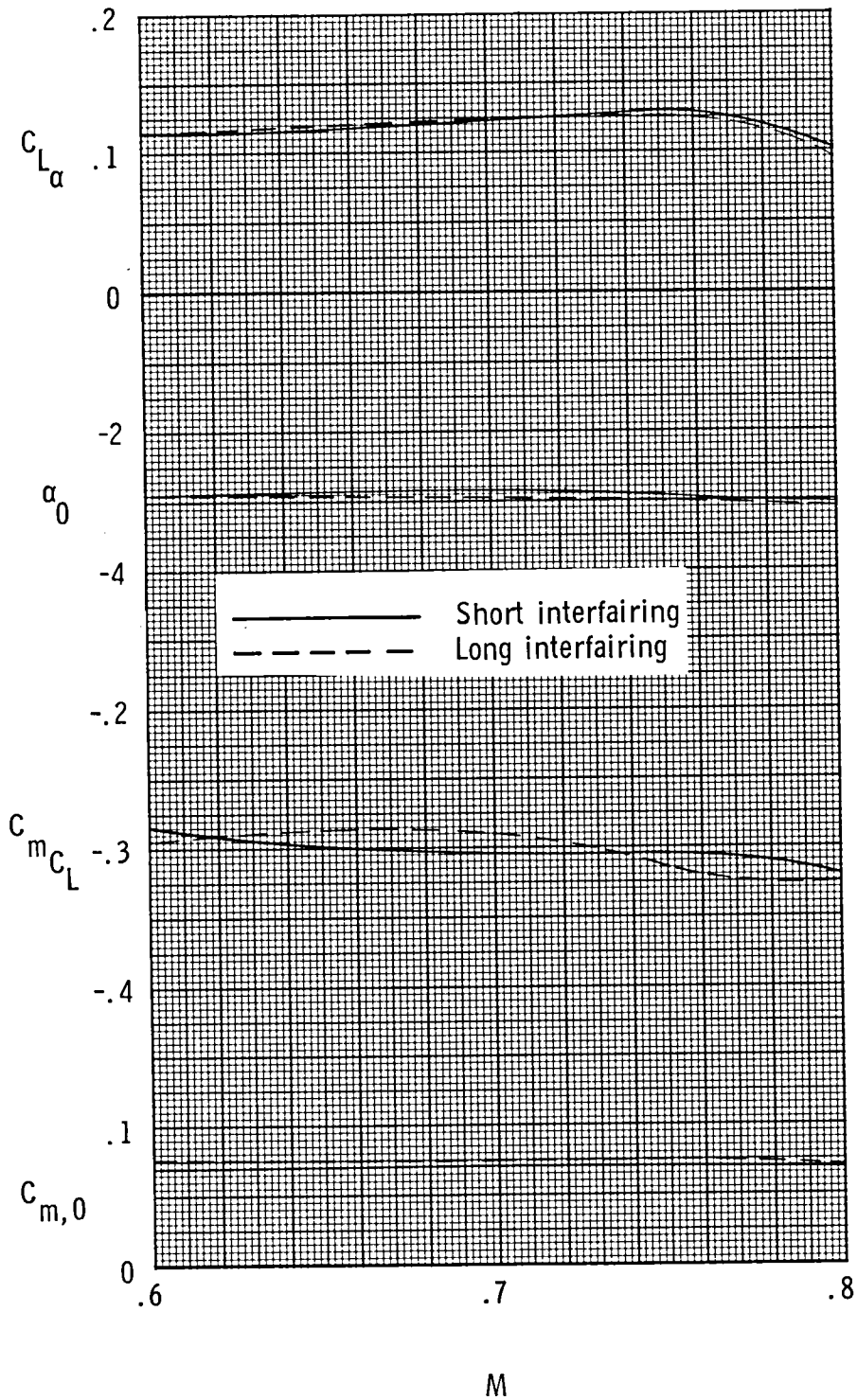

(a) C_{L_α}, α_0, $C_{m_{C_L}}$, and $C_{m,0}$.

Figure 18.- Effect of lengthening interfairing on model longitudinal parameters for model with cruise nozzles extended and wings swept 25°.

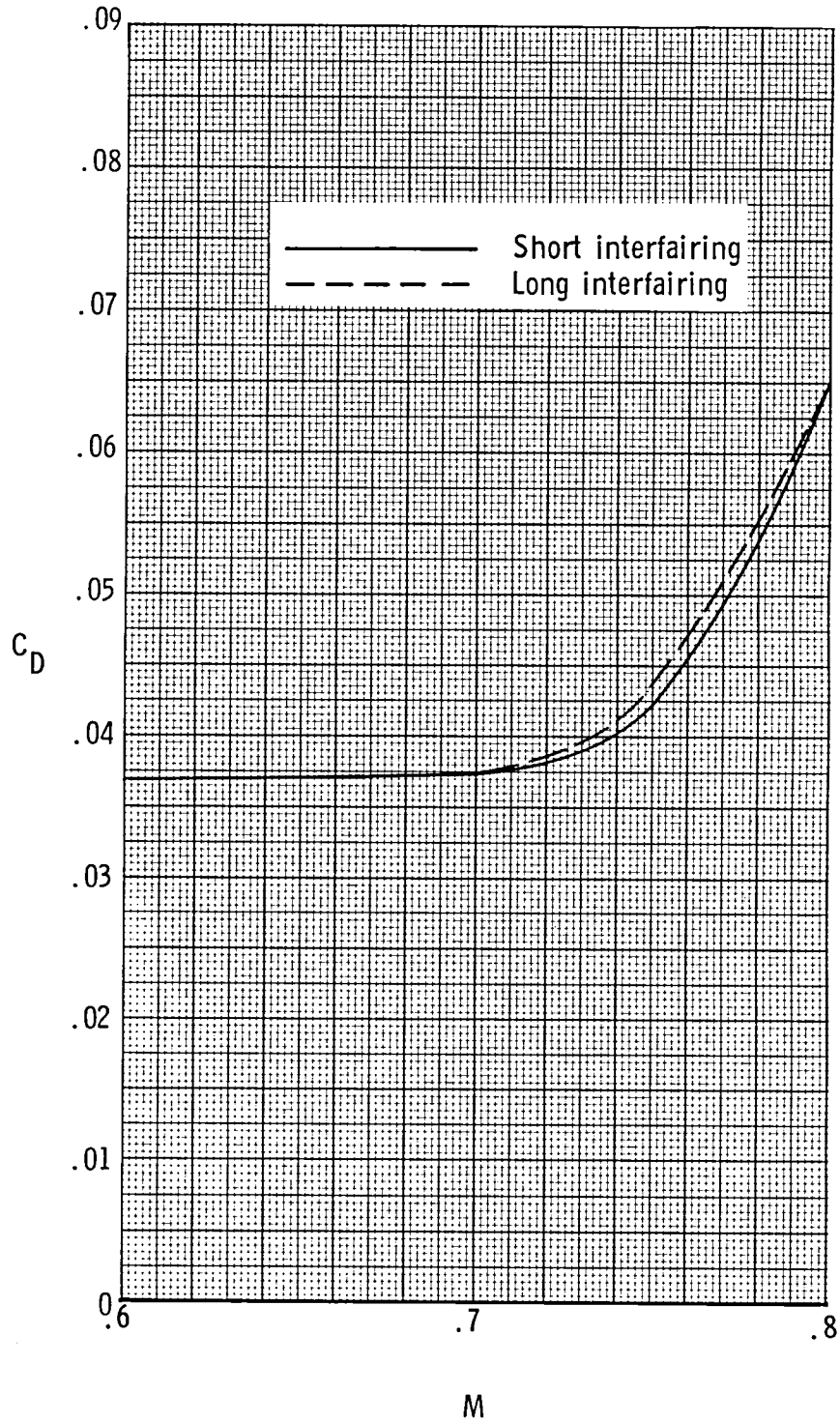

(b) Drag coefficient at $C_L = 0.63$.

Figure 18.- Concluded.

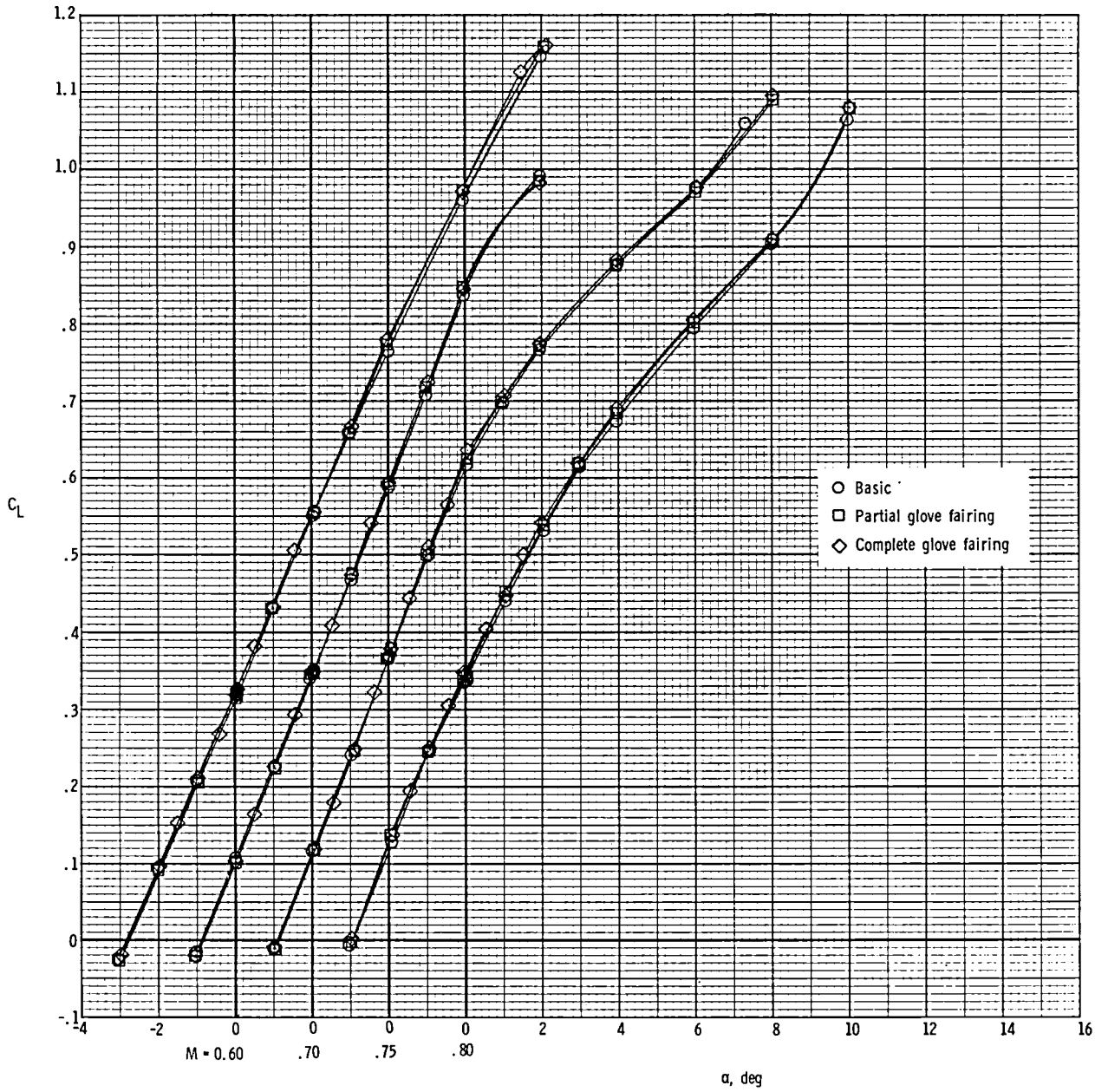

(a) Lift coefficient.

Figure 19.- Effect of fairing the upper surface of the wing glove on longitudinal aerodynamic characteristics of the model with cruise nozzles, short interfairing, and wings swept 25°.

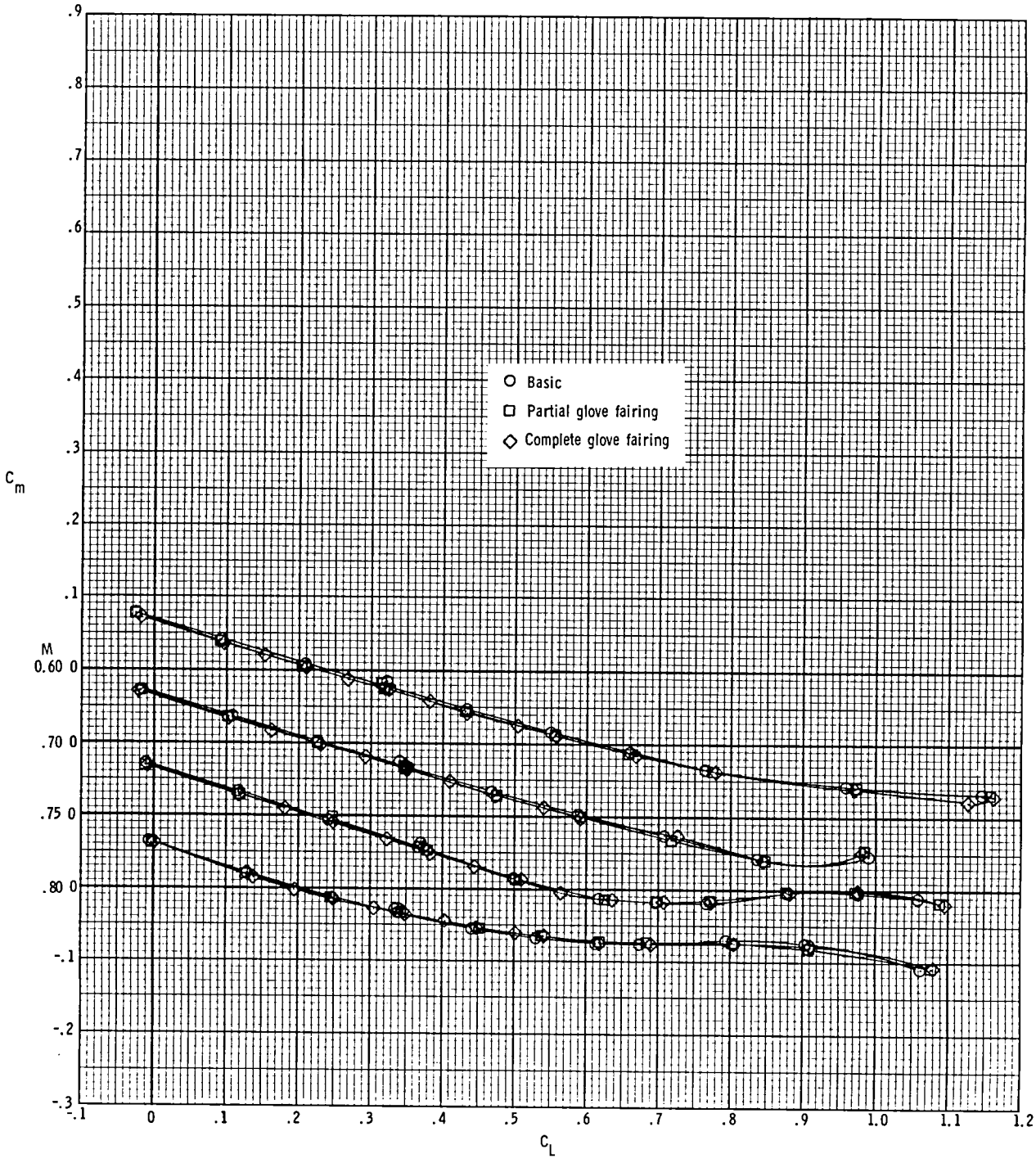

(b) Pitching-moment coefficient.

Figure 19.- Continued.

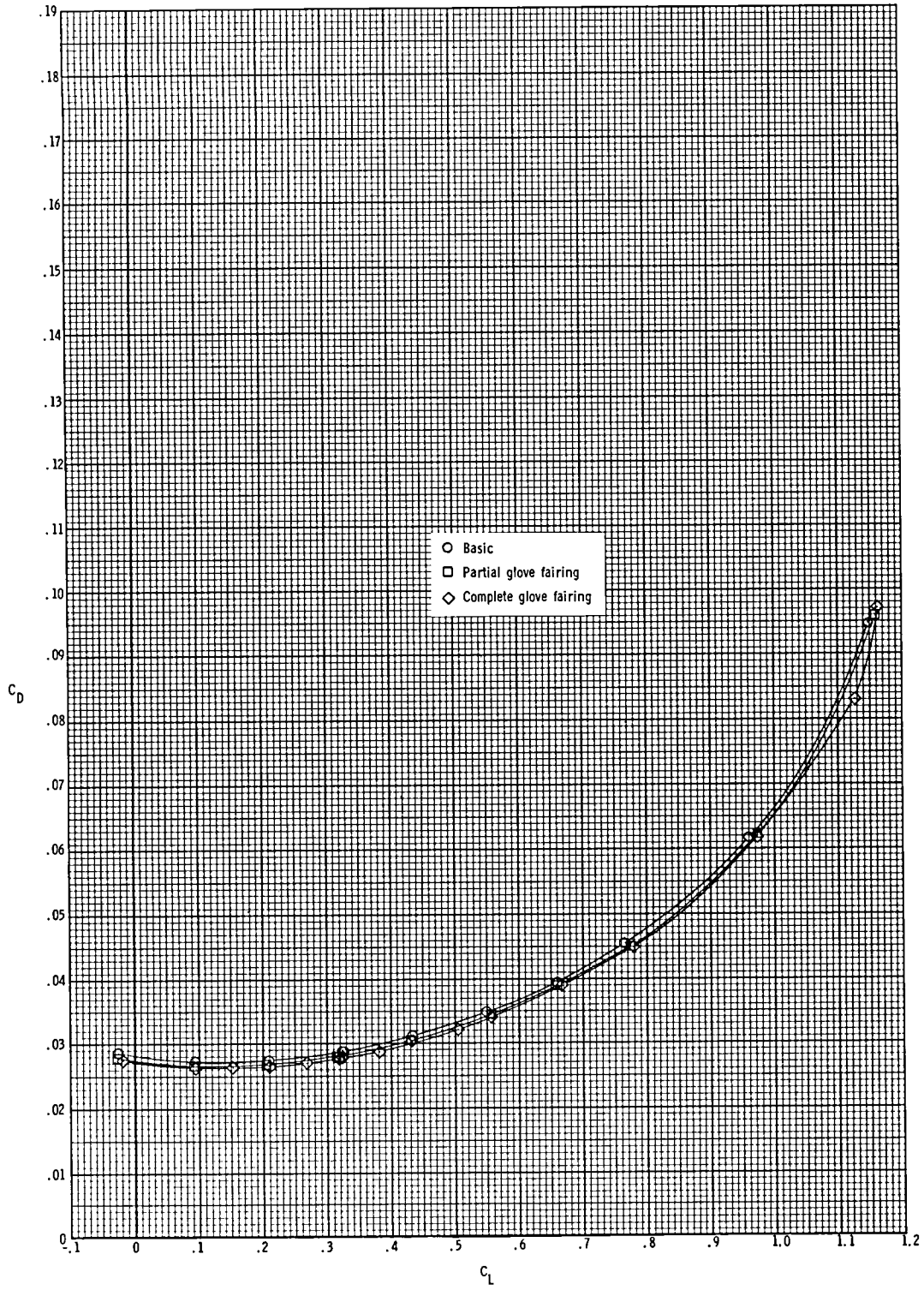

(c) Drag coefficient at M = 0.60.

Figure 19.- Continued.

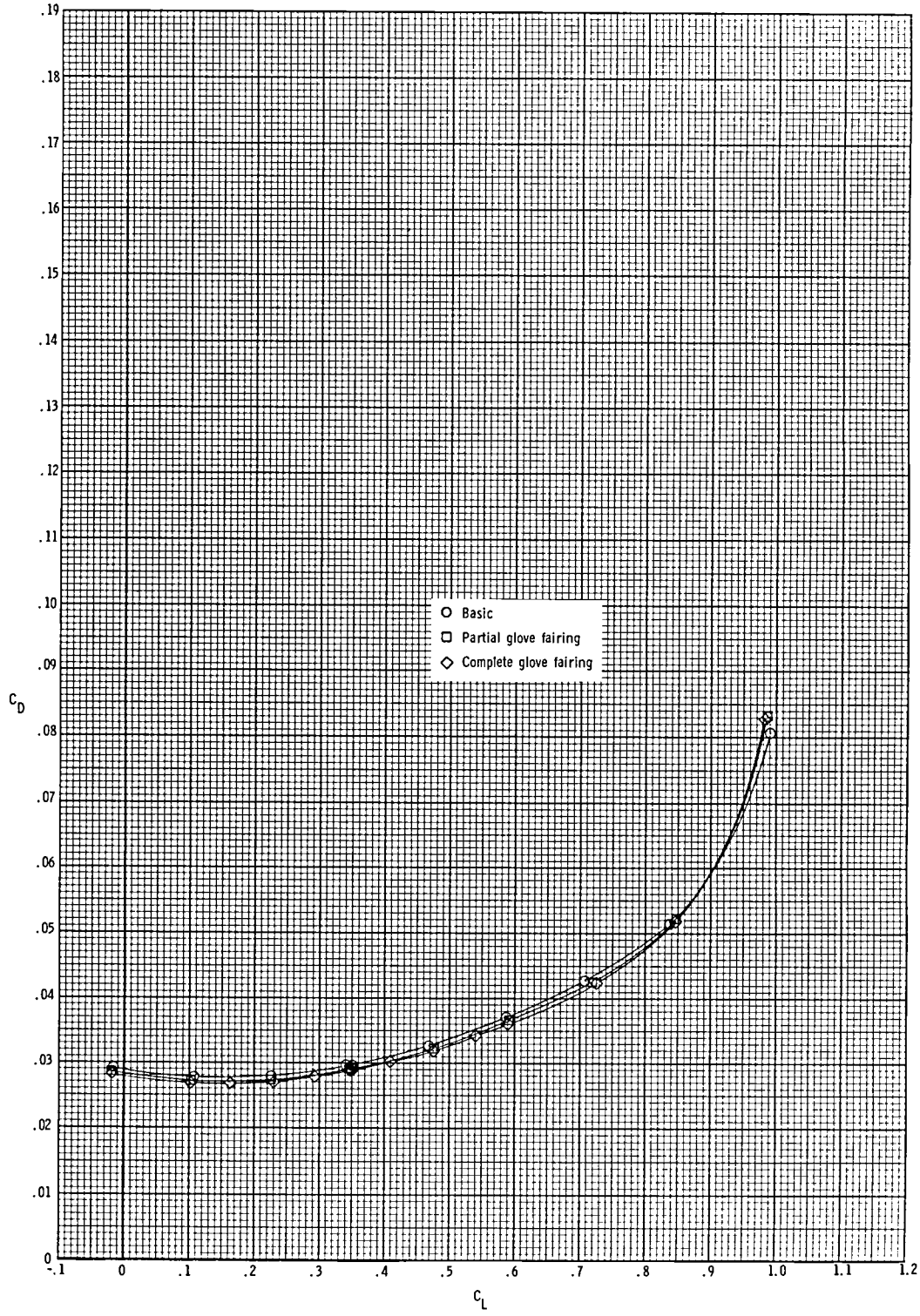

(d) Drag coefficient at M = 0.70.

Figure 19.- Continued.

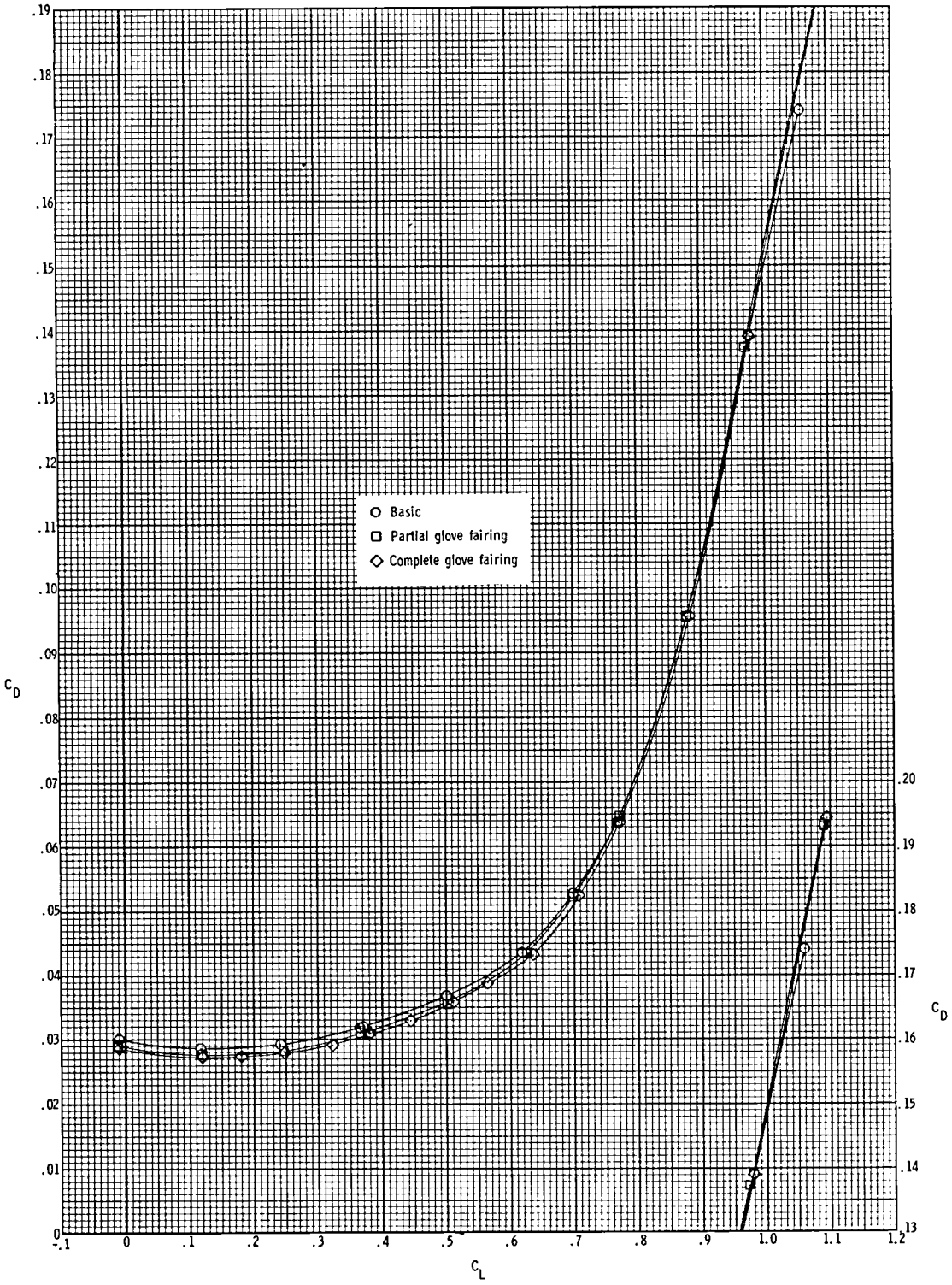

(e) Drag coefficient at M = 0.75.

Figure 19.- Continued.

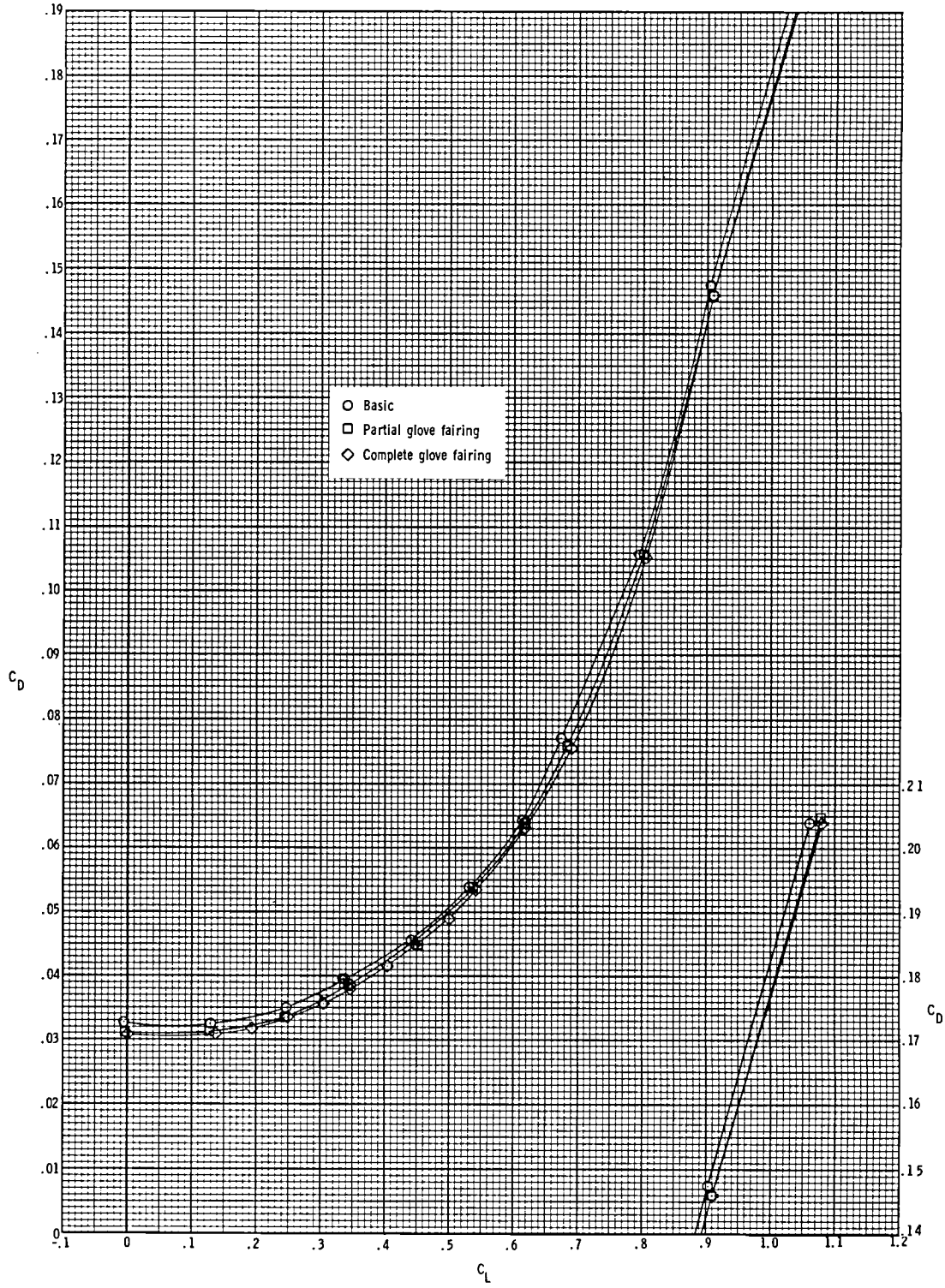

(f) Drag coefficient at M = 0.80.

Figure 19.- Concluded.

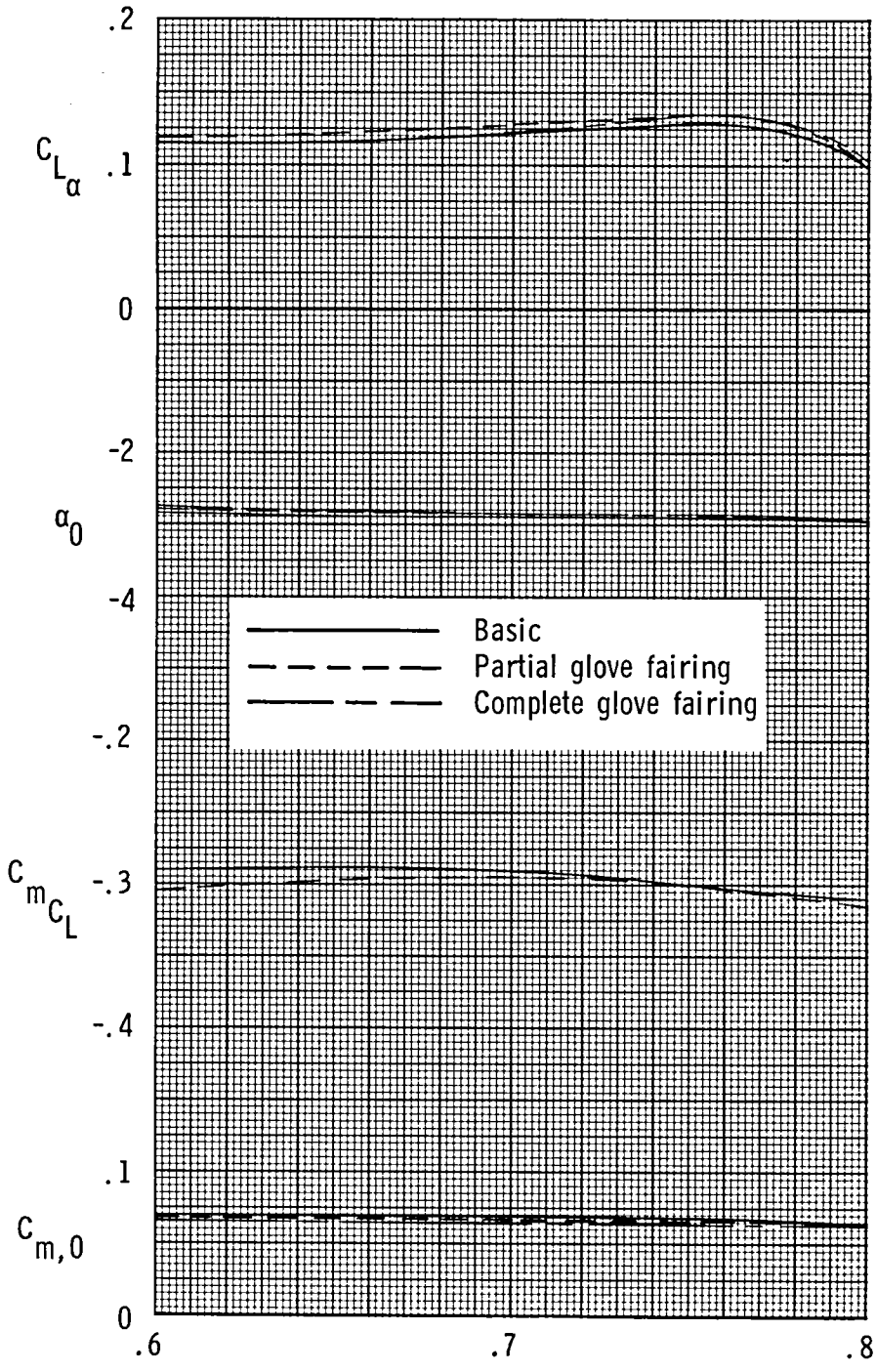

(a) C_{L_α}, α_0, $C_{m_{C_L}}$, and $C_{m,0}$.

Figure 20.- Effect of fairing the upper surface of the wing glove on model longitudinal parameters for model with cruise nozzles, short interfairing, and wings swept 25°.

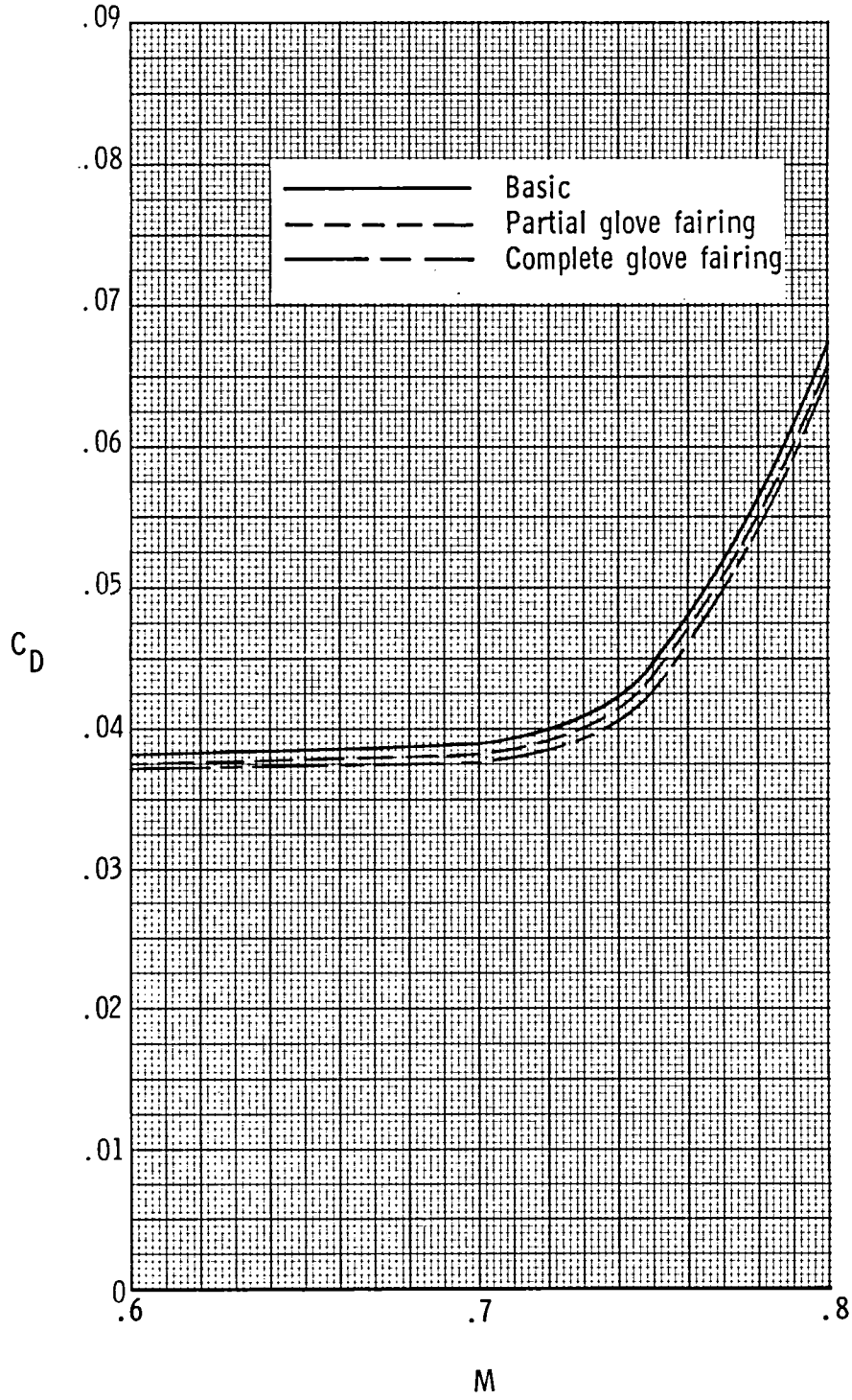

(b) Drag coefficient at $C_L = 0.63$.

Figure 20.- Concluded.

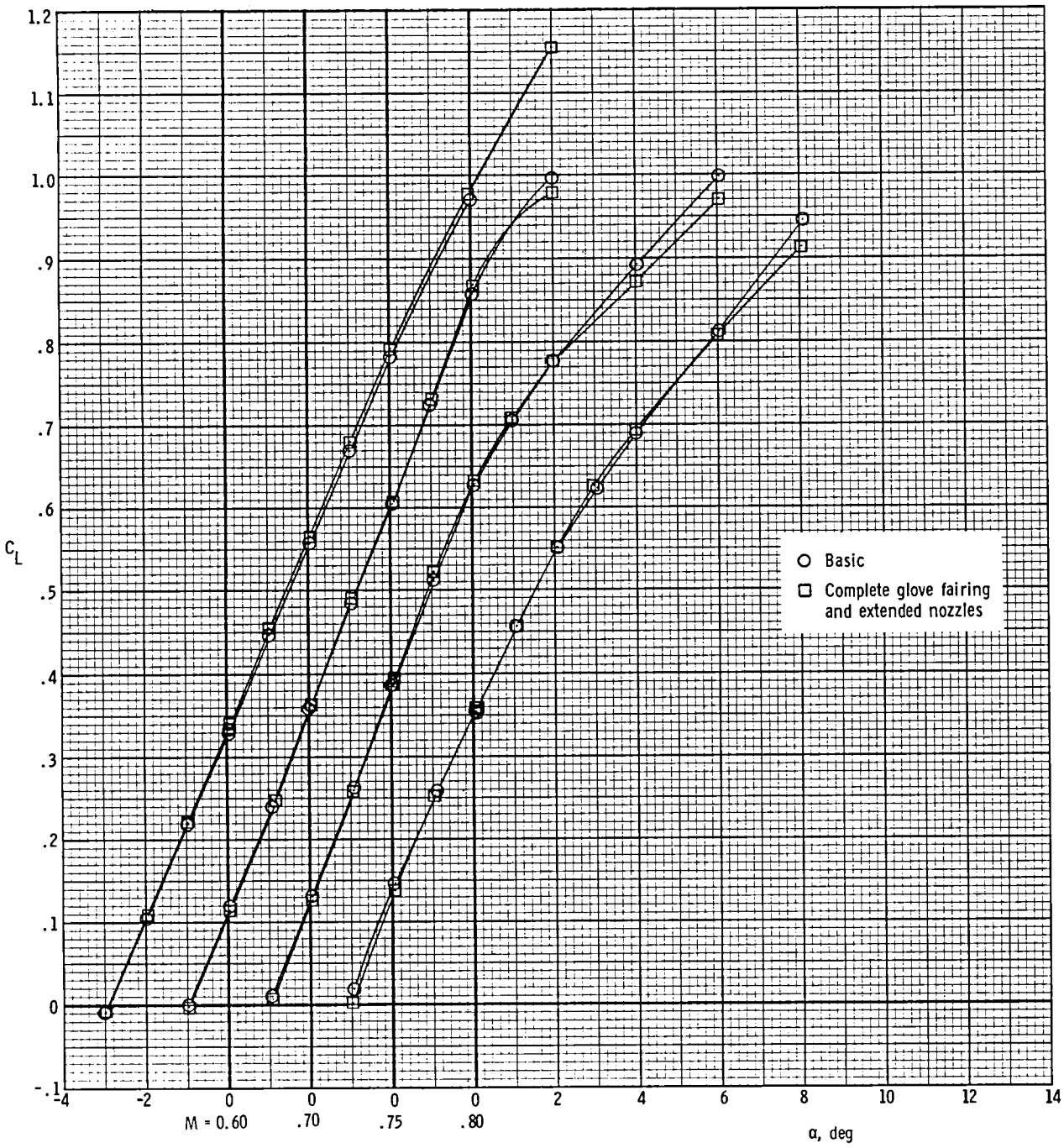

(a) Lift coefficient.

Figure 21.- Combined effect of complete glove fairing and extended nozzles on longitudinal aerodynamic characteristics of the model with cruise nozzles, short interfairing, and wings swept 25°.

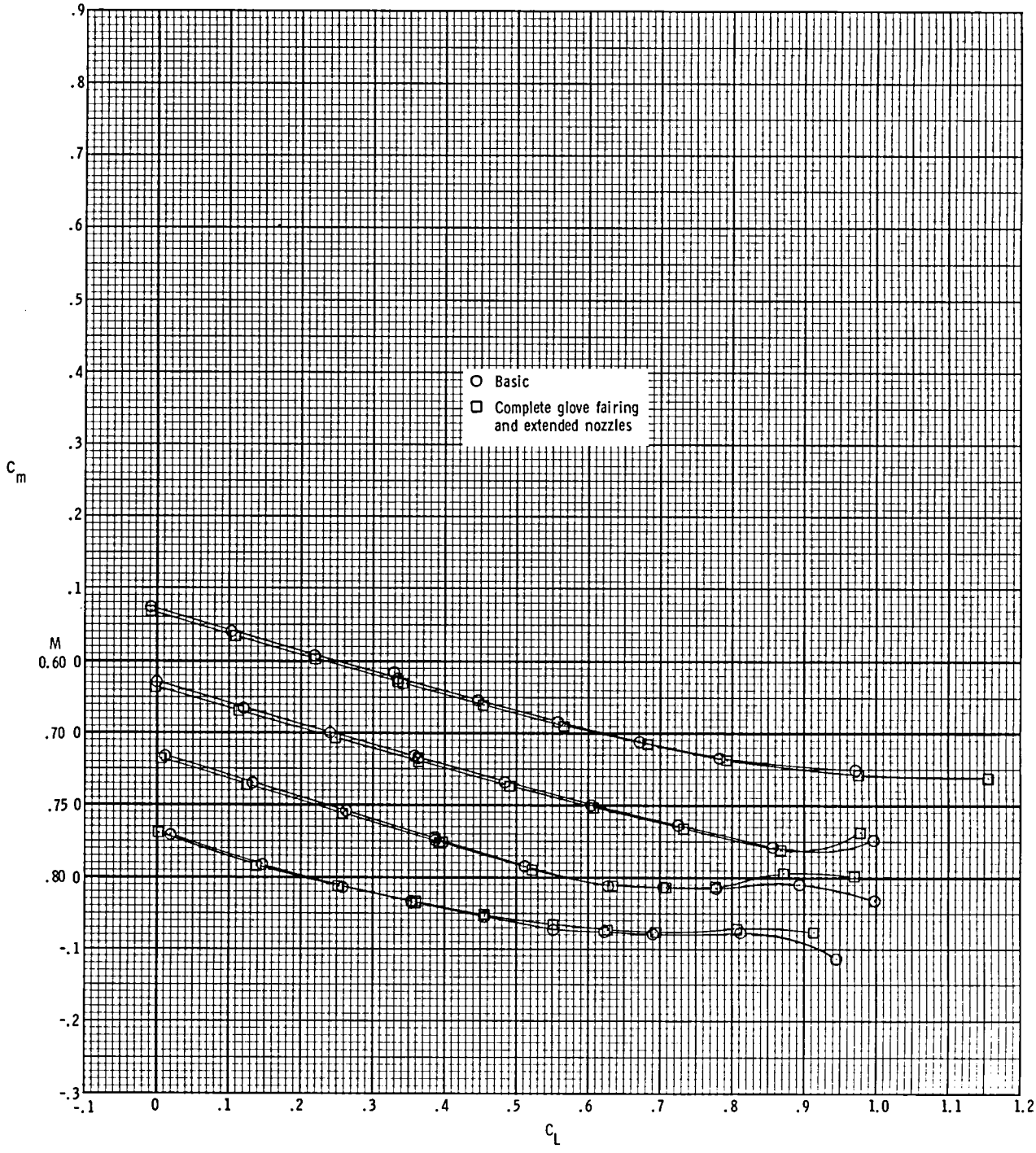

(b) Pitching-moment coefficient.

Figure 21.- Continued.

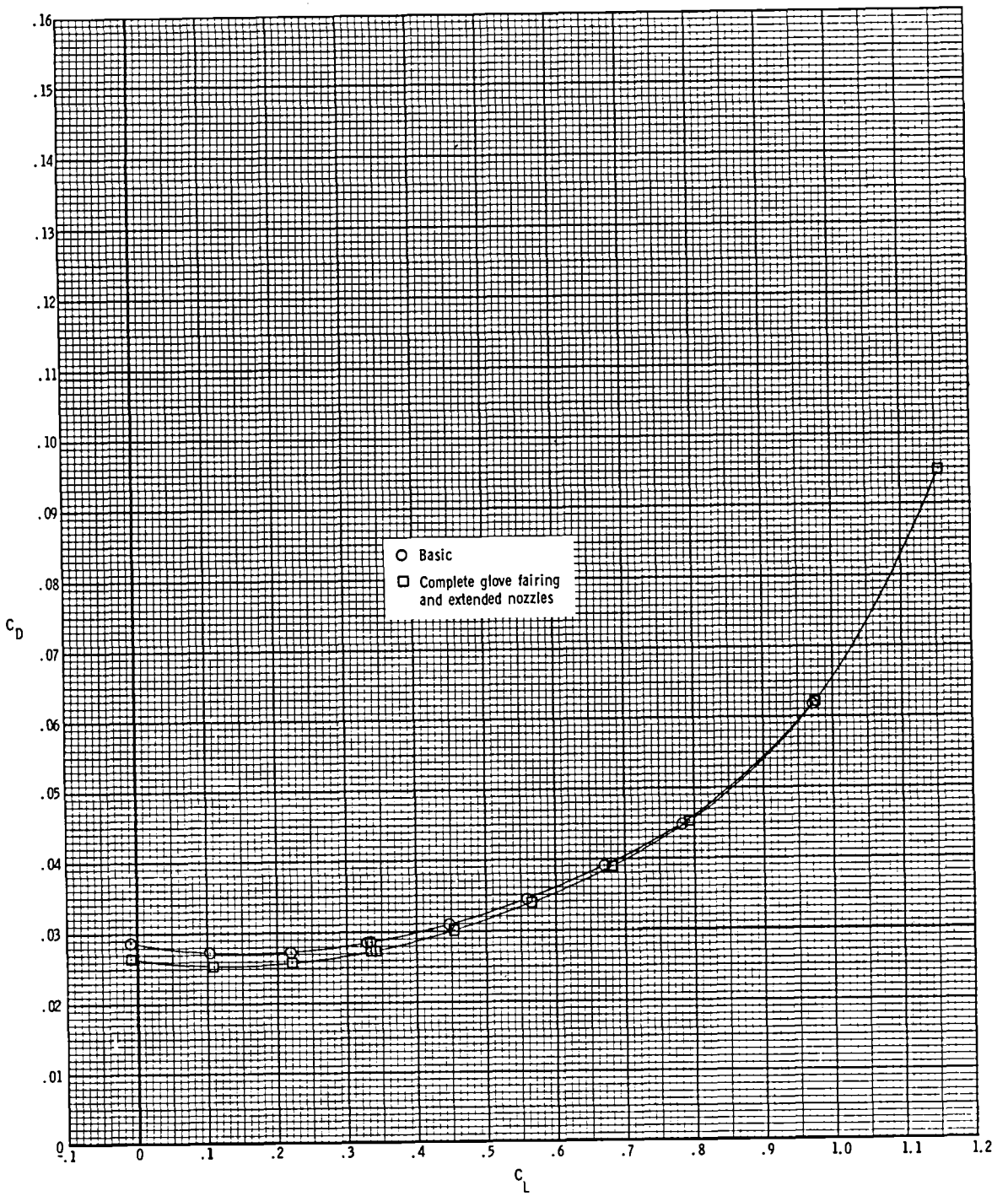

(c) Drag coefficient at M = 0.60.

Figure 21.- Continued.

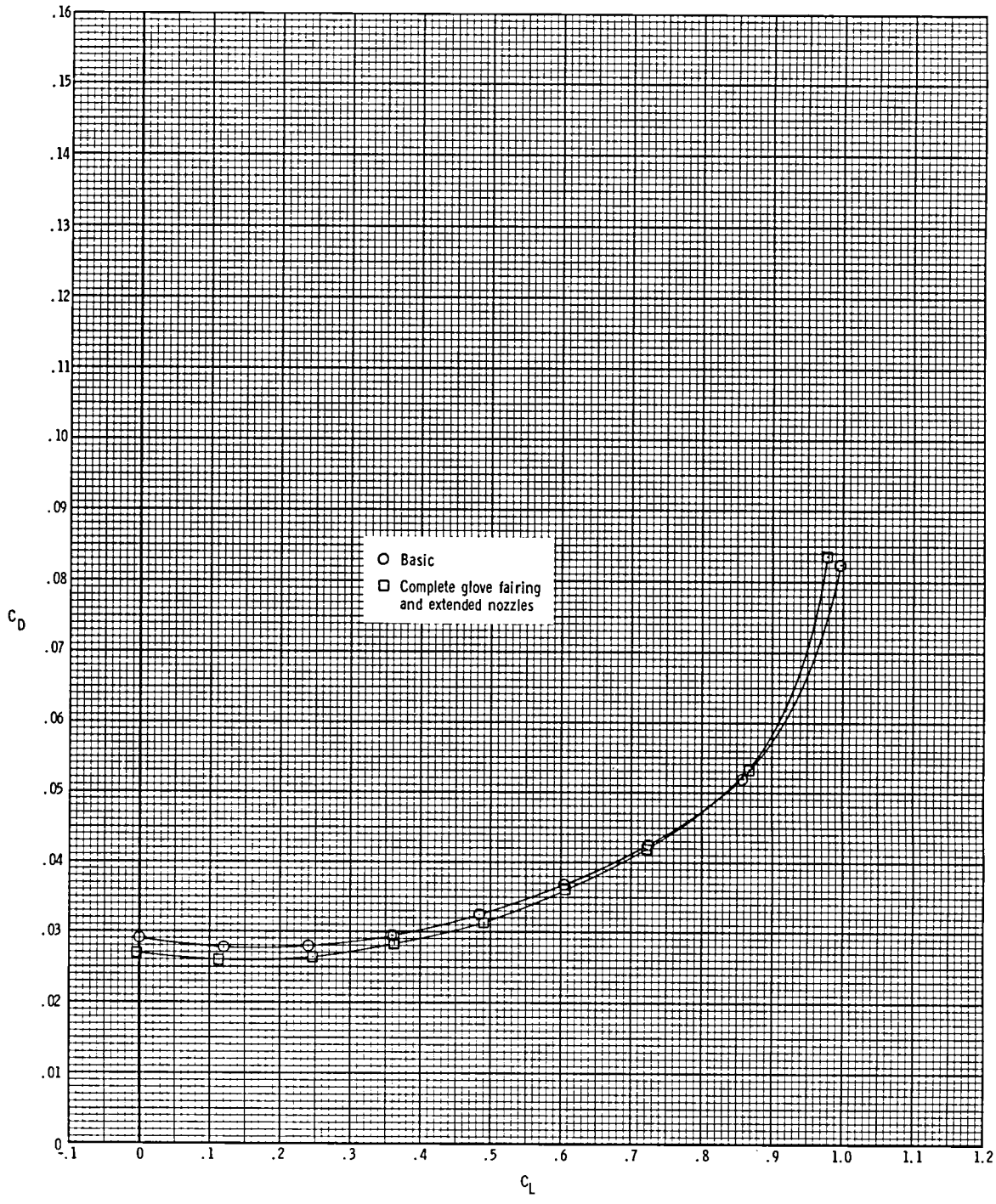

(d) Drag coefficient at M = 0.70.

Figure 21.- Continued.

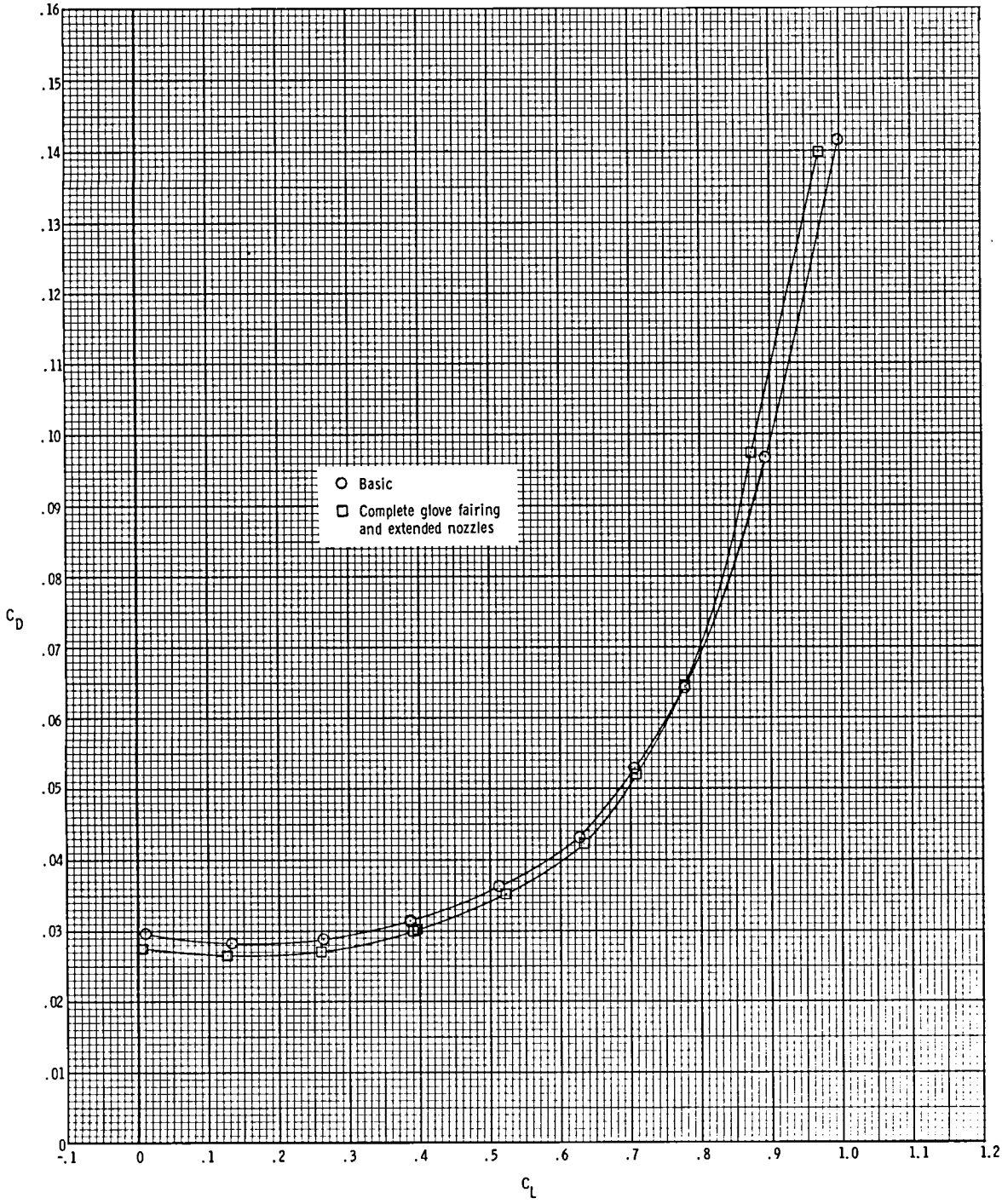

(e) Drag coefficient at M = 0.75.

Figure 21.- Continued.

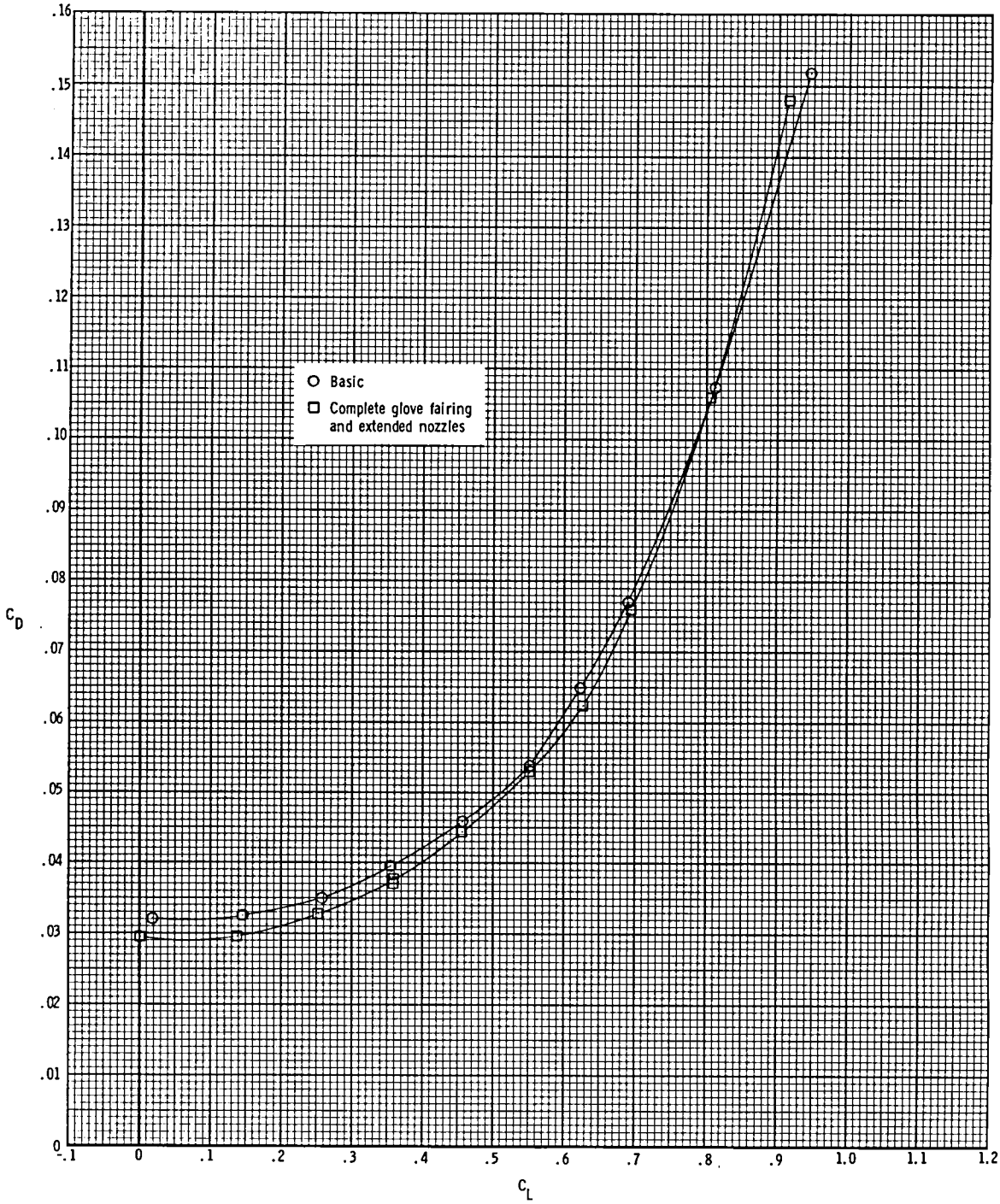

(f) Drag coefficient at M = 0.80.

Figure 21.- Concluded.

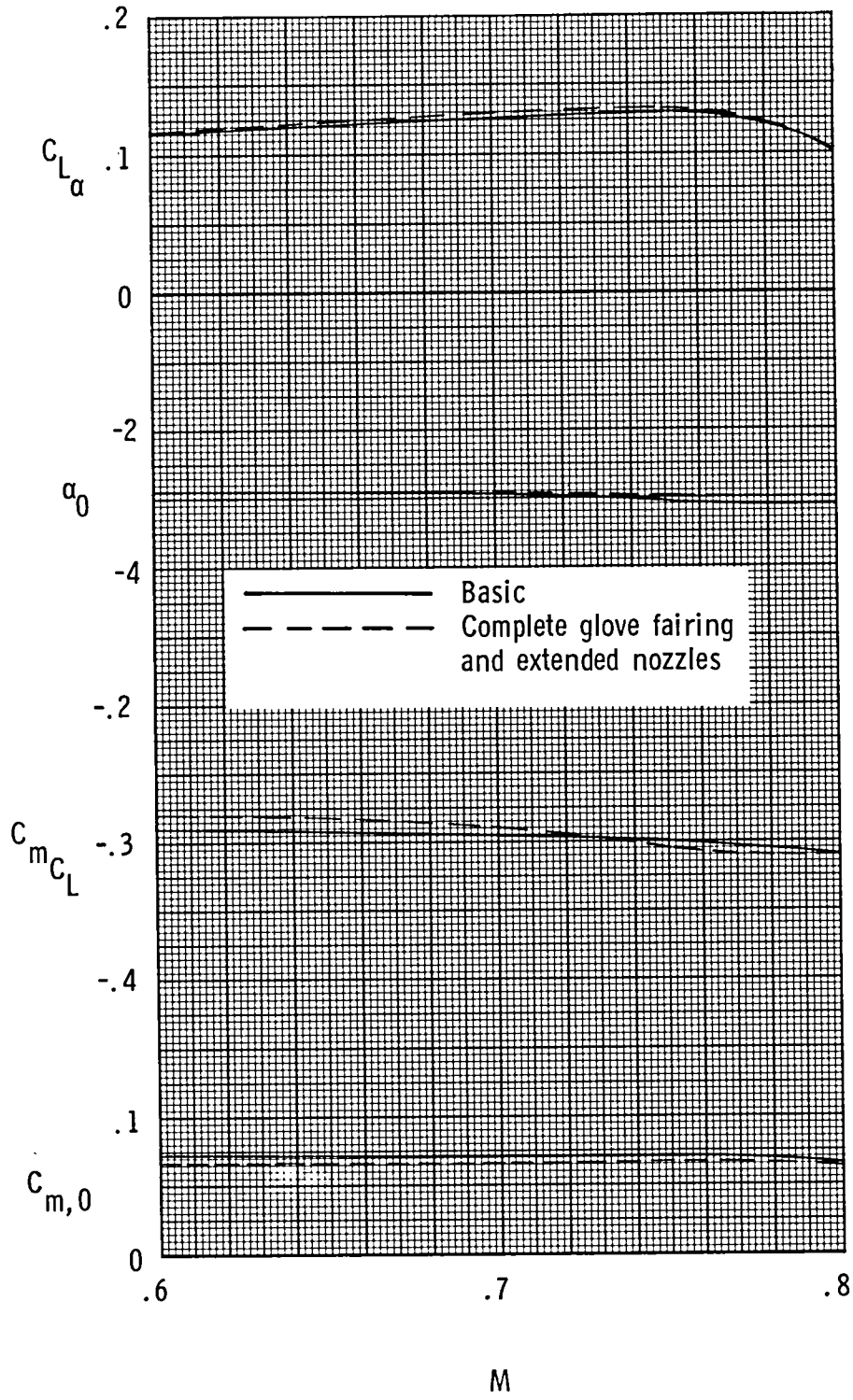

(a) C_{L_α}, α_0, $C_{m_{C_L}}$, and $C_{m,0}$.

Figure 22.- Combined effect of complete glove fairing and extended nozzles on model longitudinal parameters for model with cruise nozzles, short interfairing, and wings swept 25°.

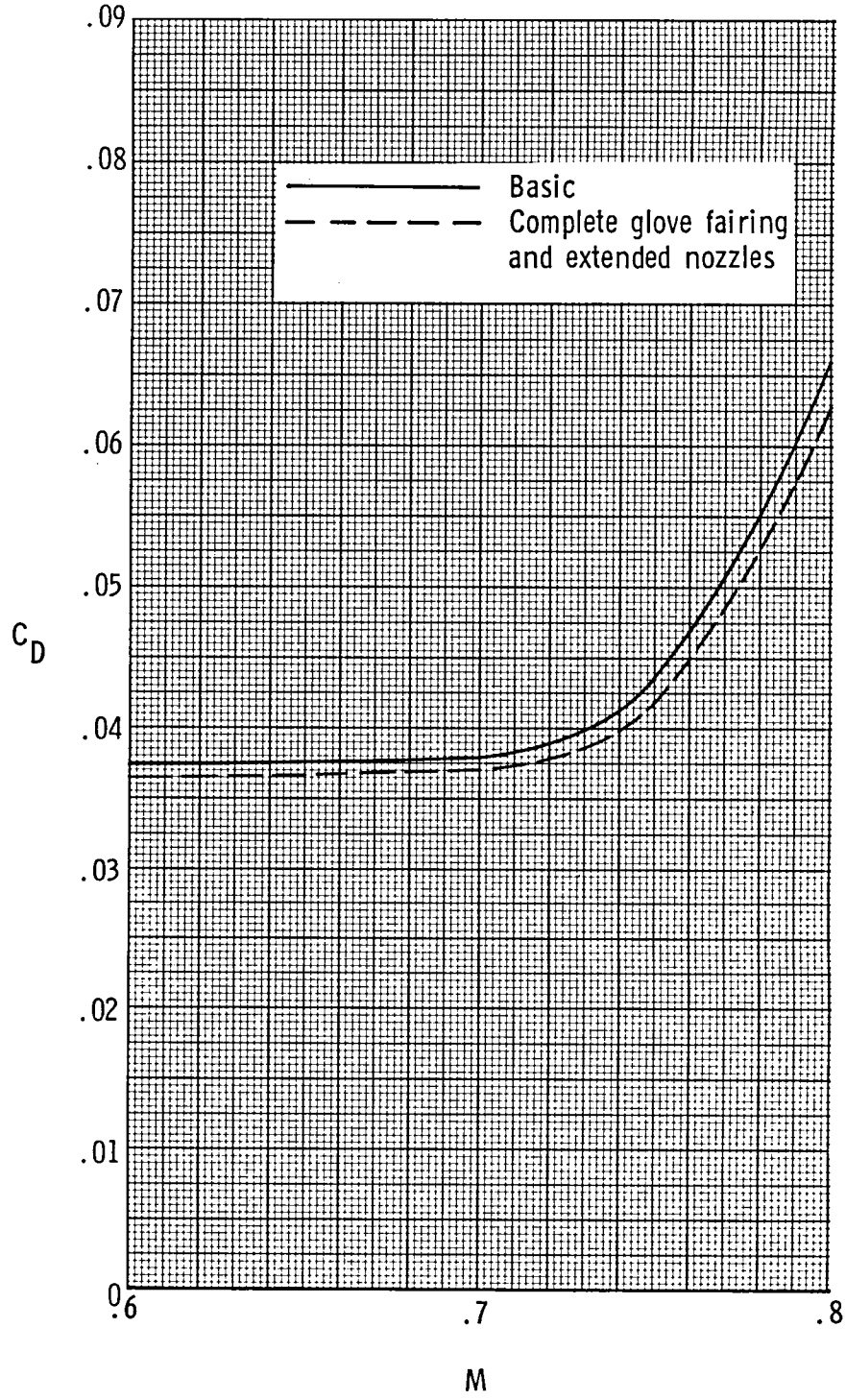

(b) Drag coefficient at $C_L = 0.63$.

Figure 22.- Concluded.

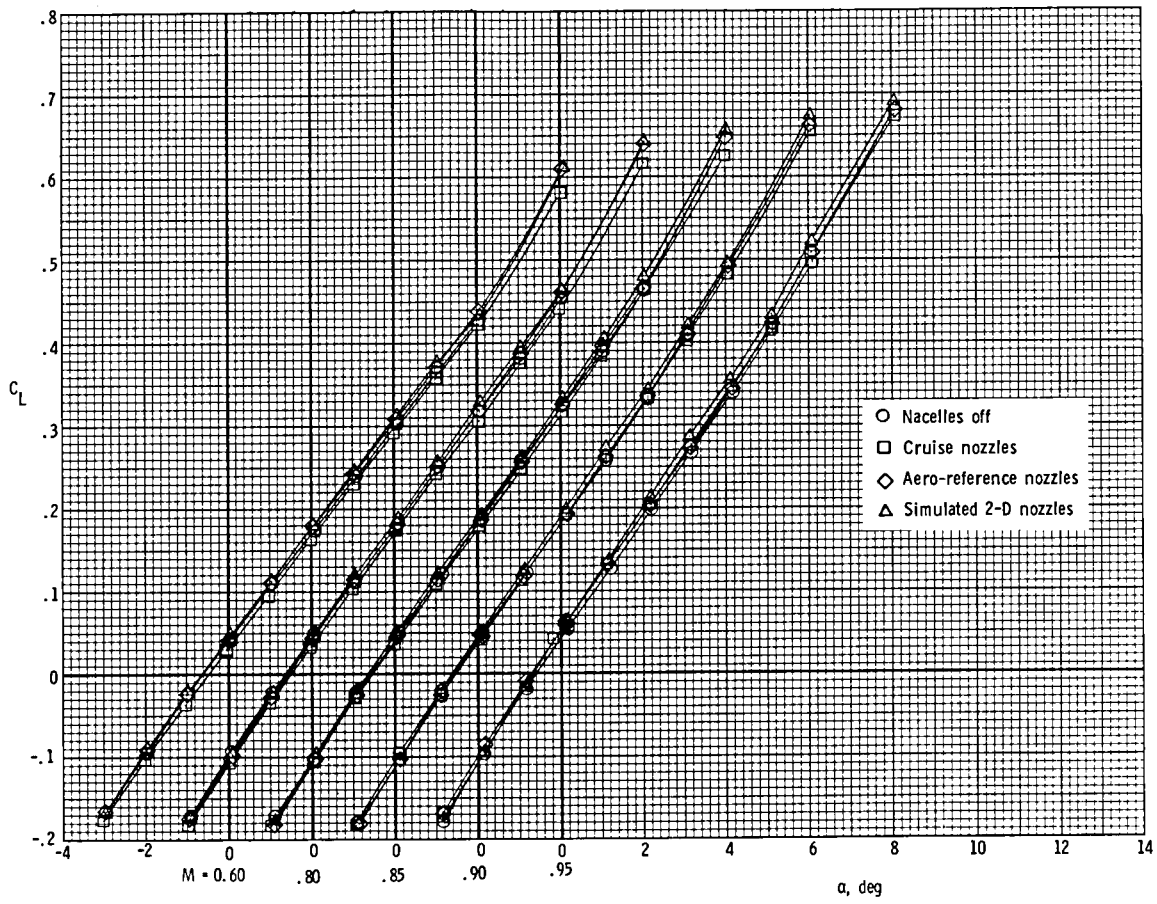

(a) Lift coefficient.

Figure 23.- Effect of nacelles and of nozzle shape on longitudinal aerodynamic characteristics of the model with wings swept 65°.

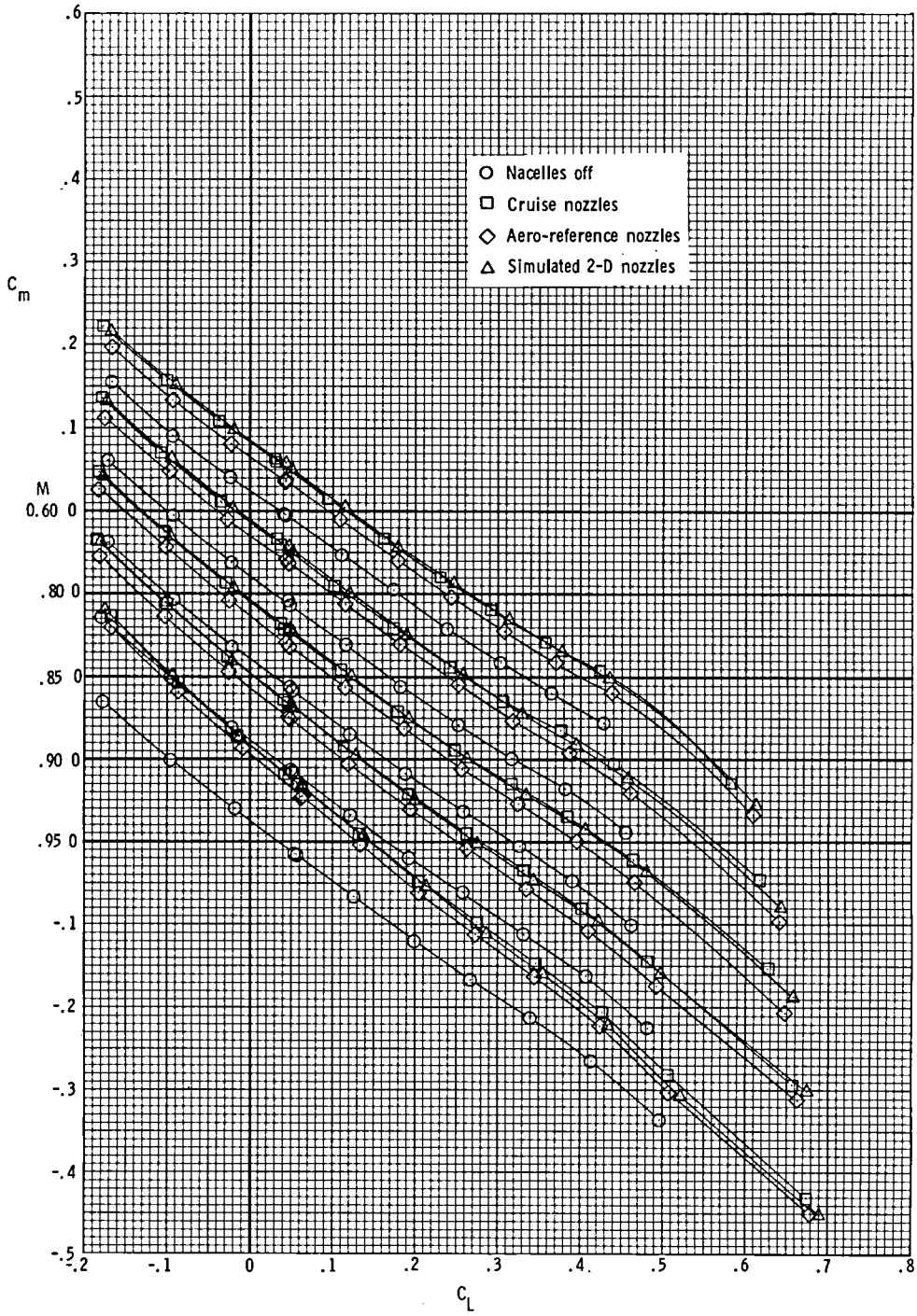

(b) Pitching-moment coefficient.

Figure 23.- Continued.

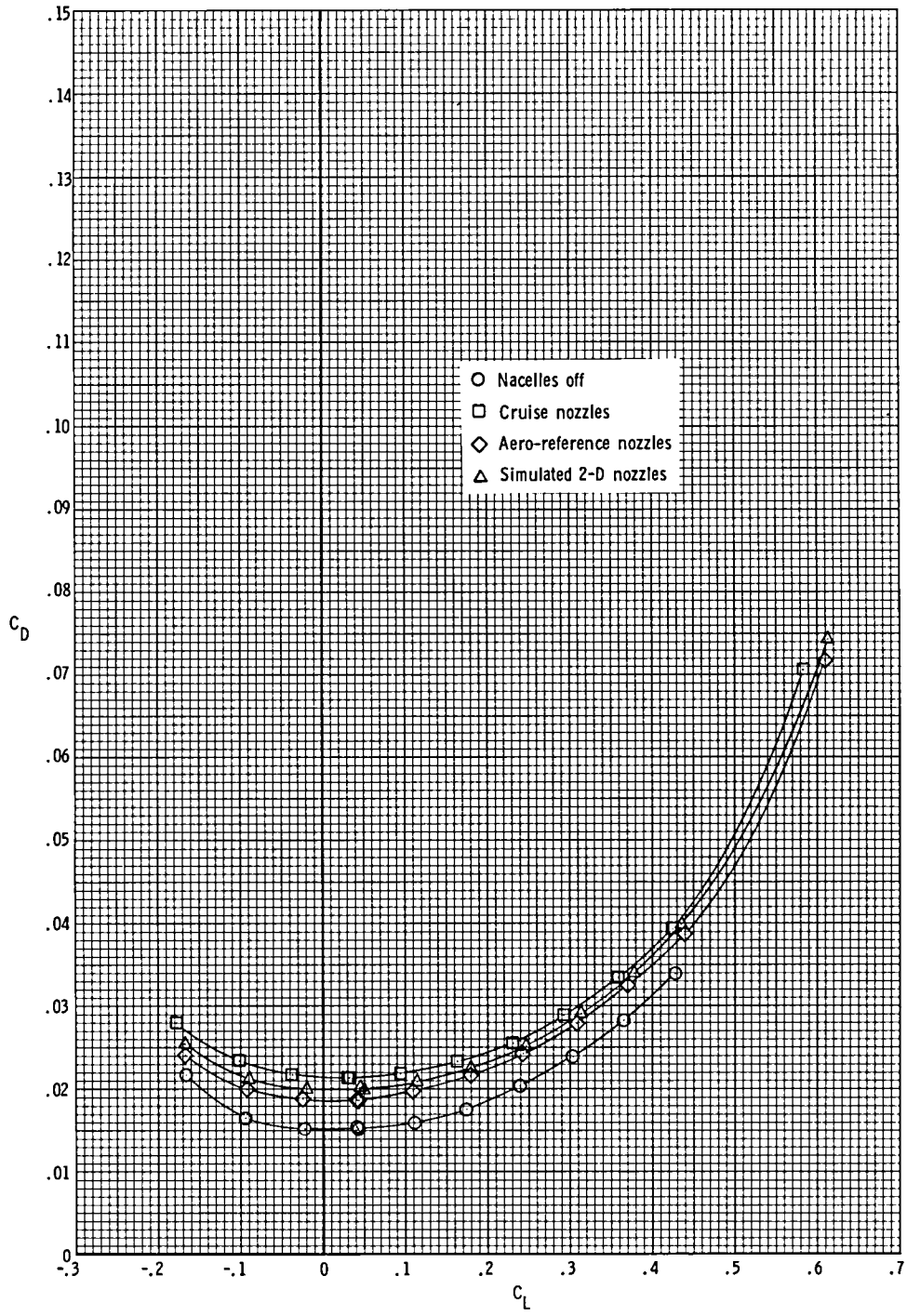

(c) Drag coefficient at M = 0.60.

Figure 23.- Continued.

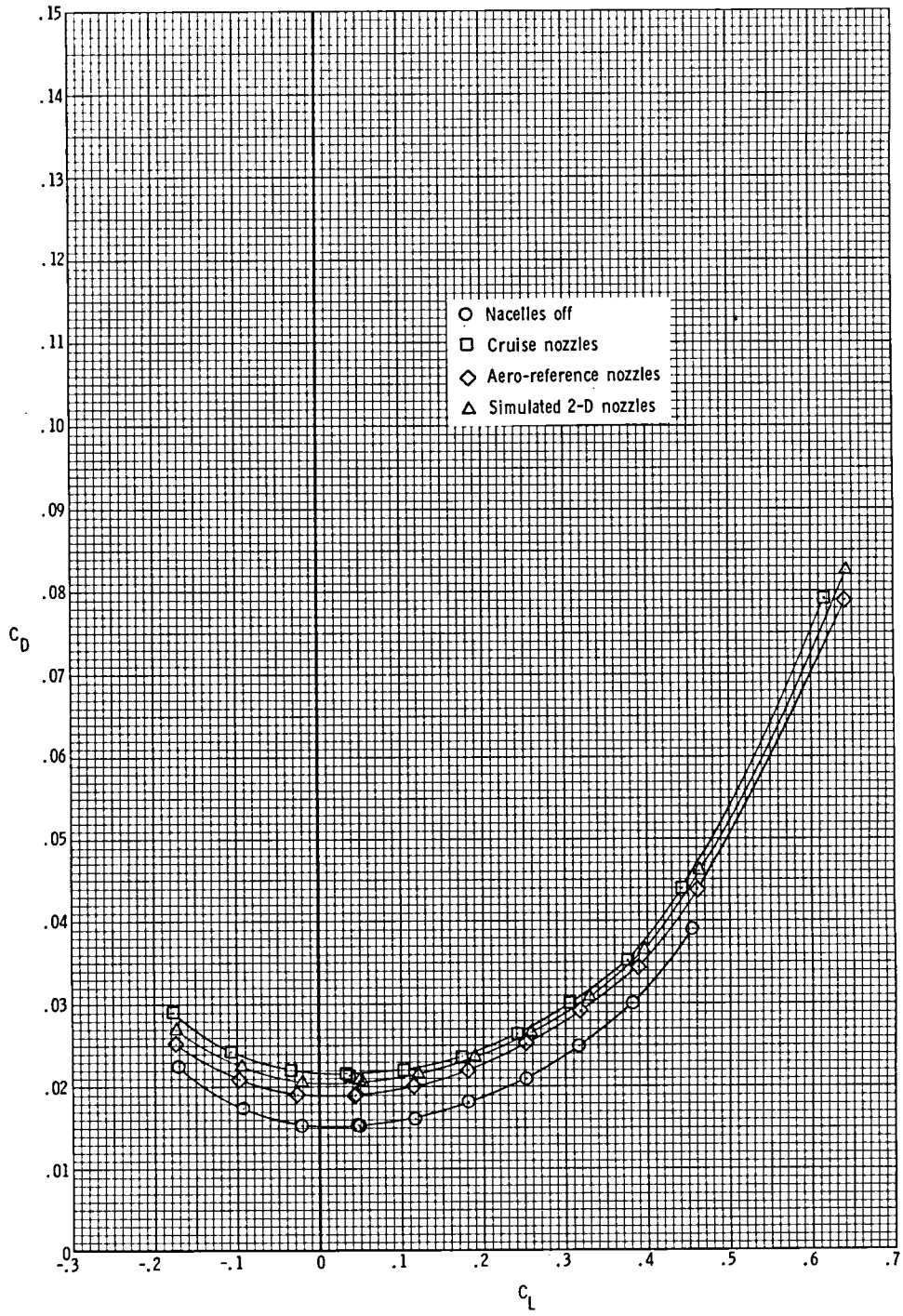

(d) Drag coefficient at M = 0.80.

Figure 23.- Continued.

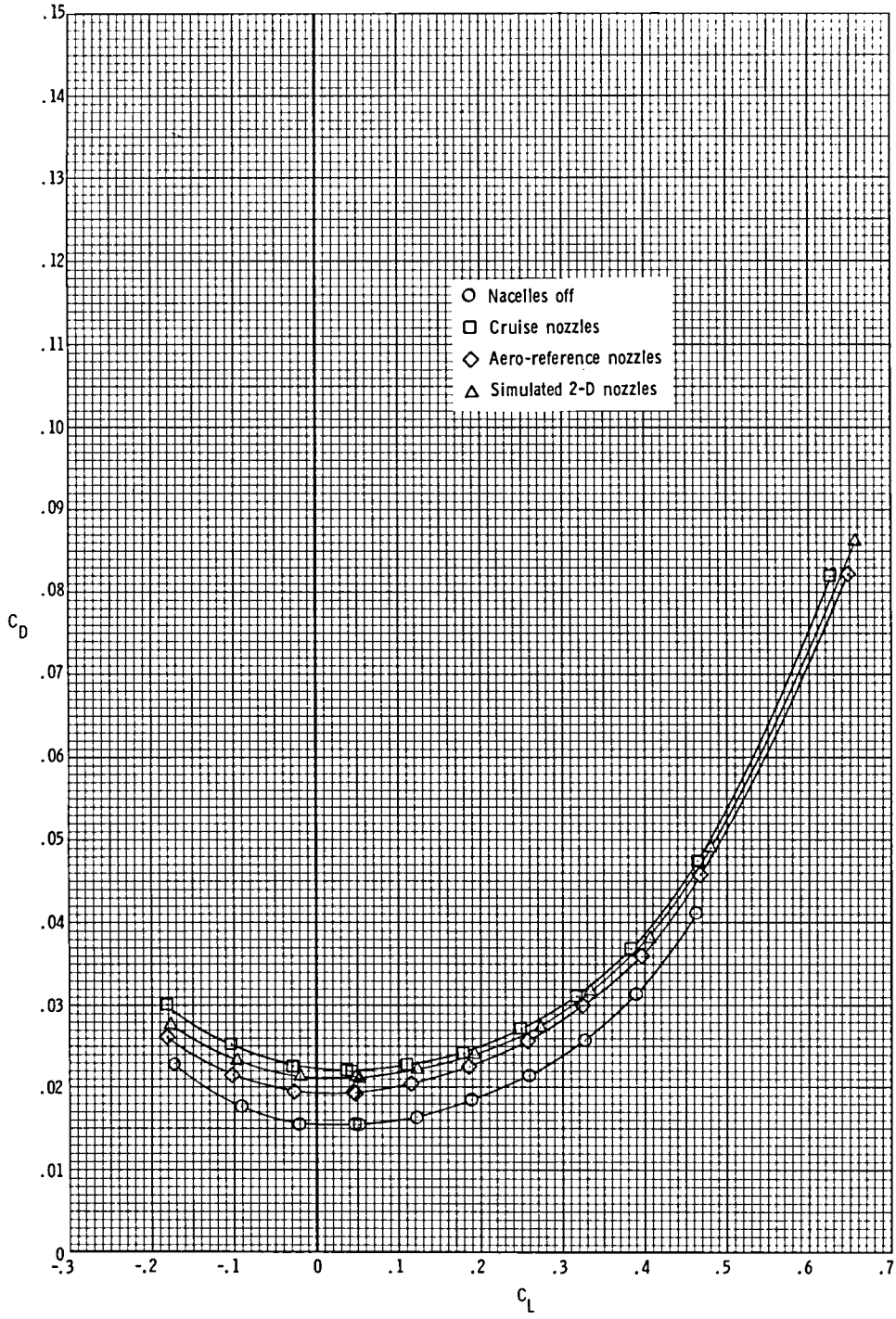

(e) Drag coefficient at M = 0.85.

Figure 23.- Continued.

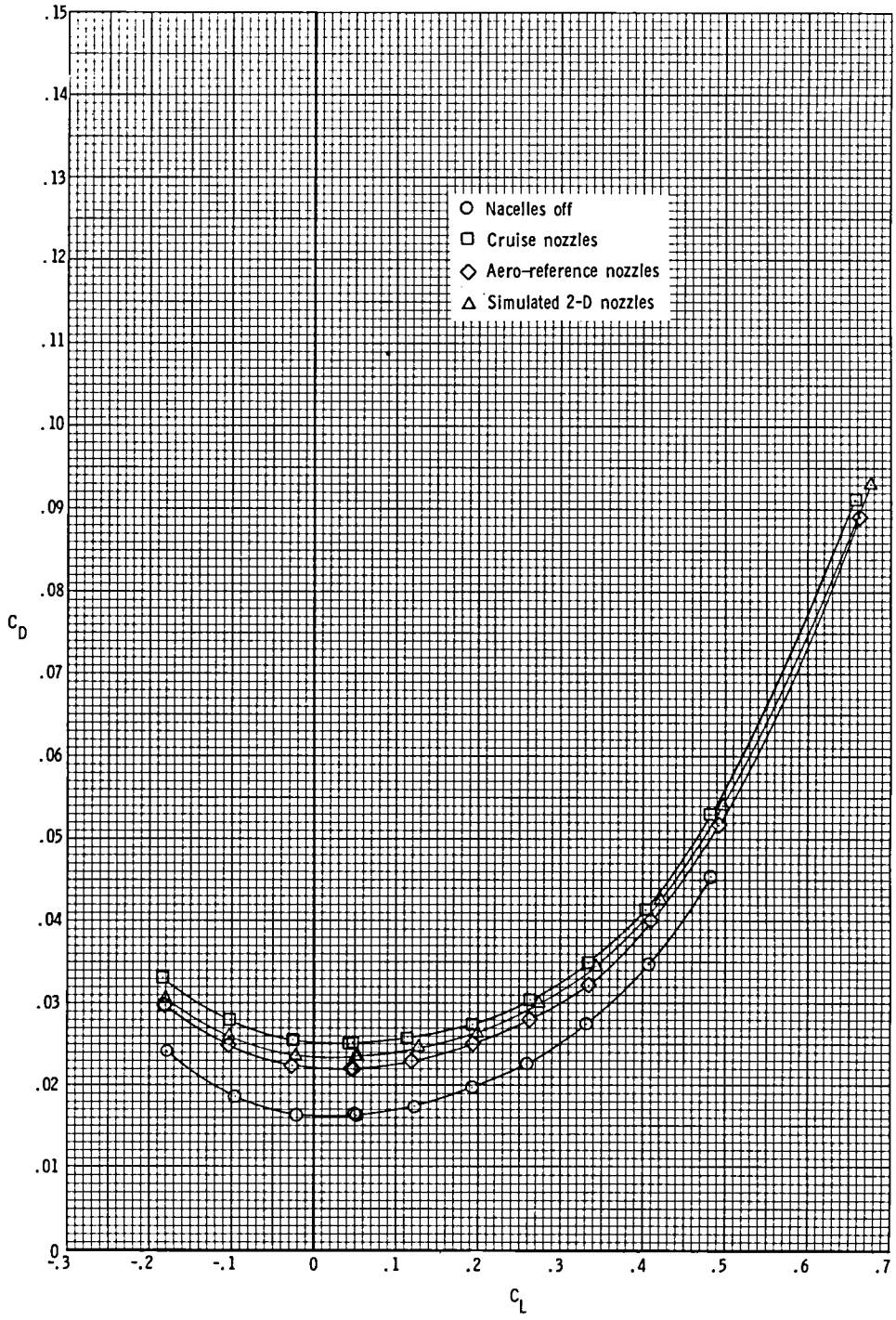

(f) Drag coefficient at M = 0.90.

Figure 23.- Continued.

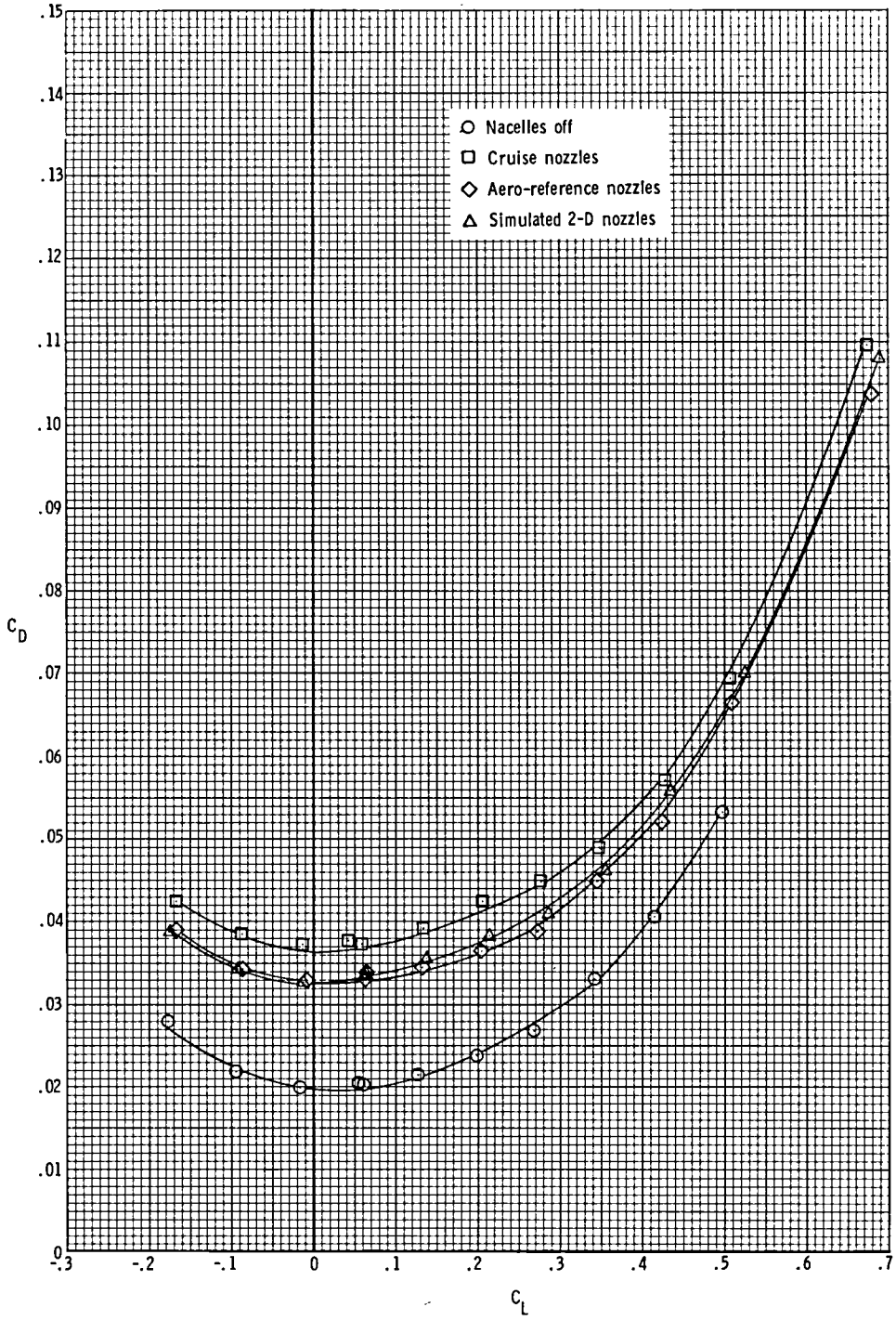

(g) Drag coefficient at M = 0.95.

Figure 23.- Concluded.

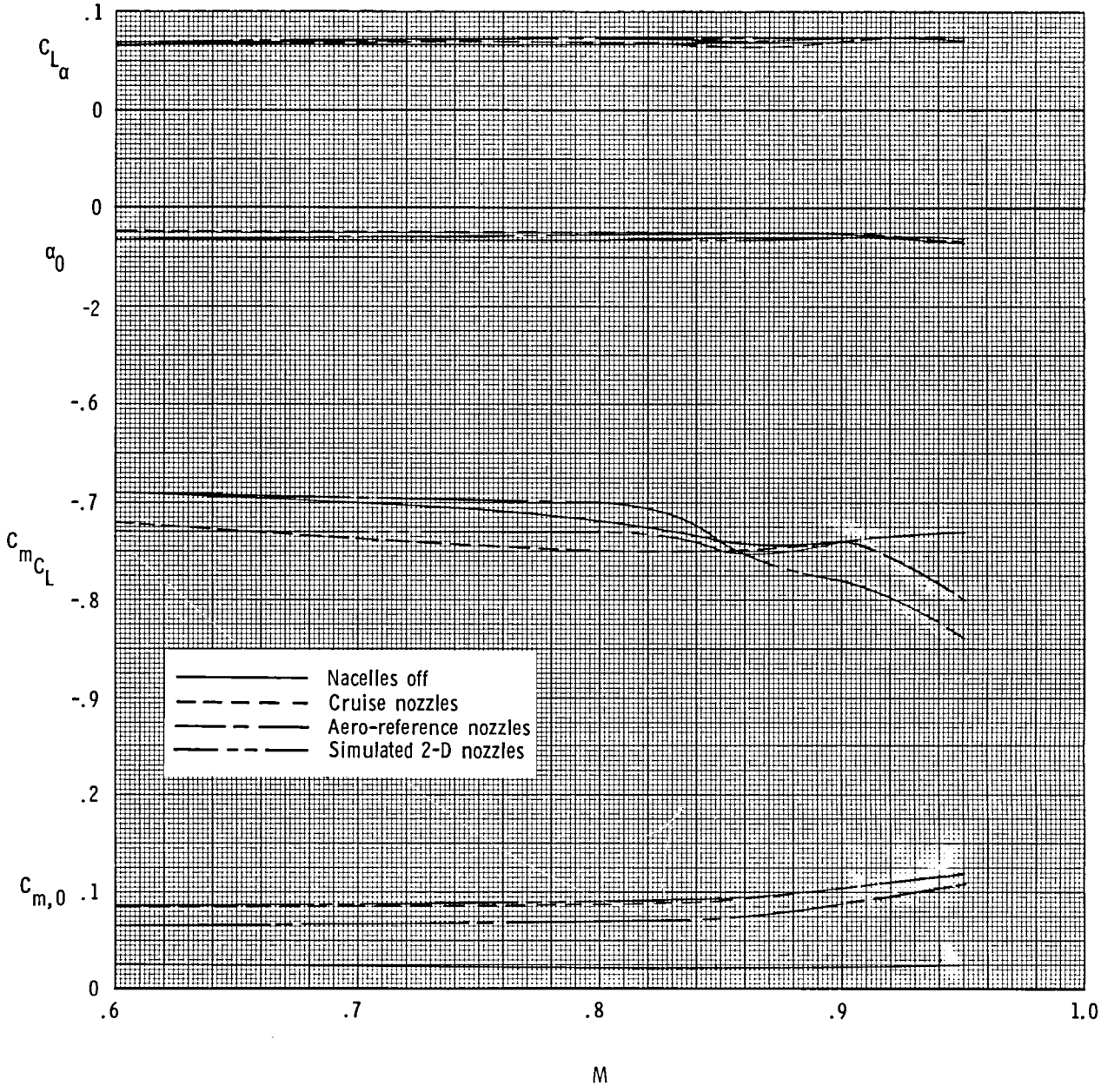

(a) $C_{L\alpha}$, α_0, $C_{m_{C_L}}$, and $C_{m,0}$.

Figure 24.- Effect of nacelles and of nozzle shape on model longitudinal parameters for model with wings swept 65°.

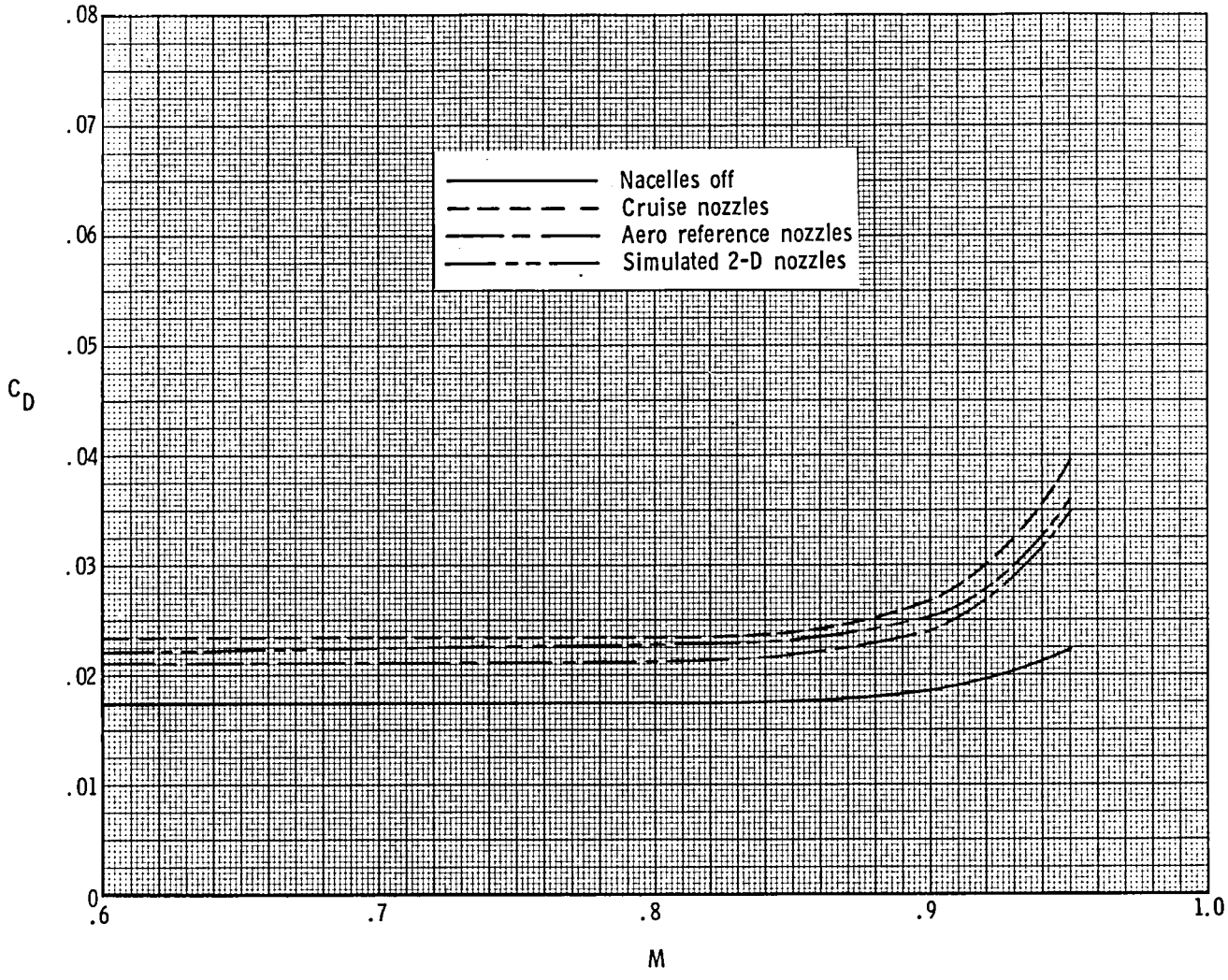

(b) Drag coefficient at $C_L = 0.16$.

Figure 24.- Concluded.

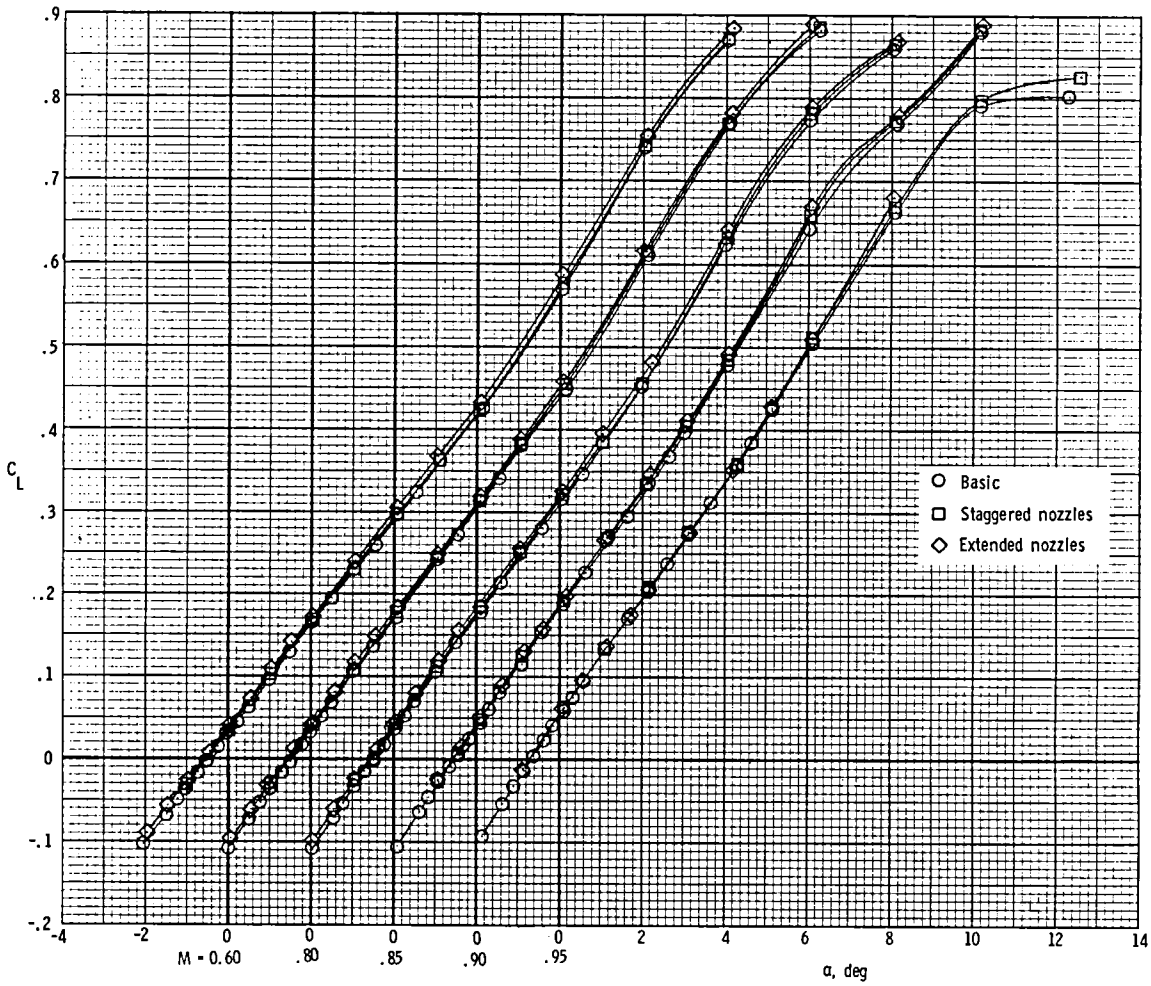

(a) Lift coefficient.

Figure 25.- Effect of staggered and extended nozzles on longitudinal aerodynamic characteristics of the model with cruise nozzles, short interfairing, and wings swept 65°.

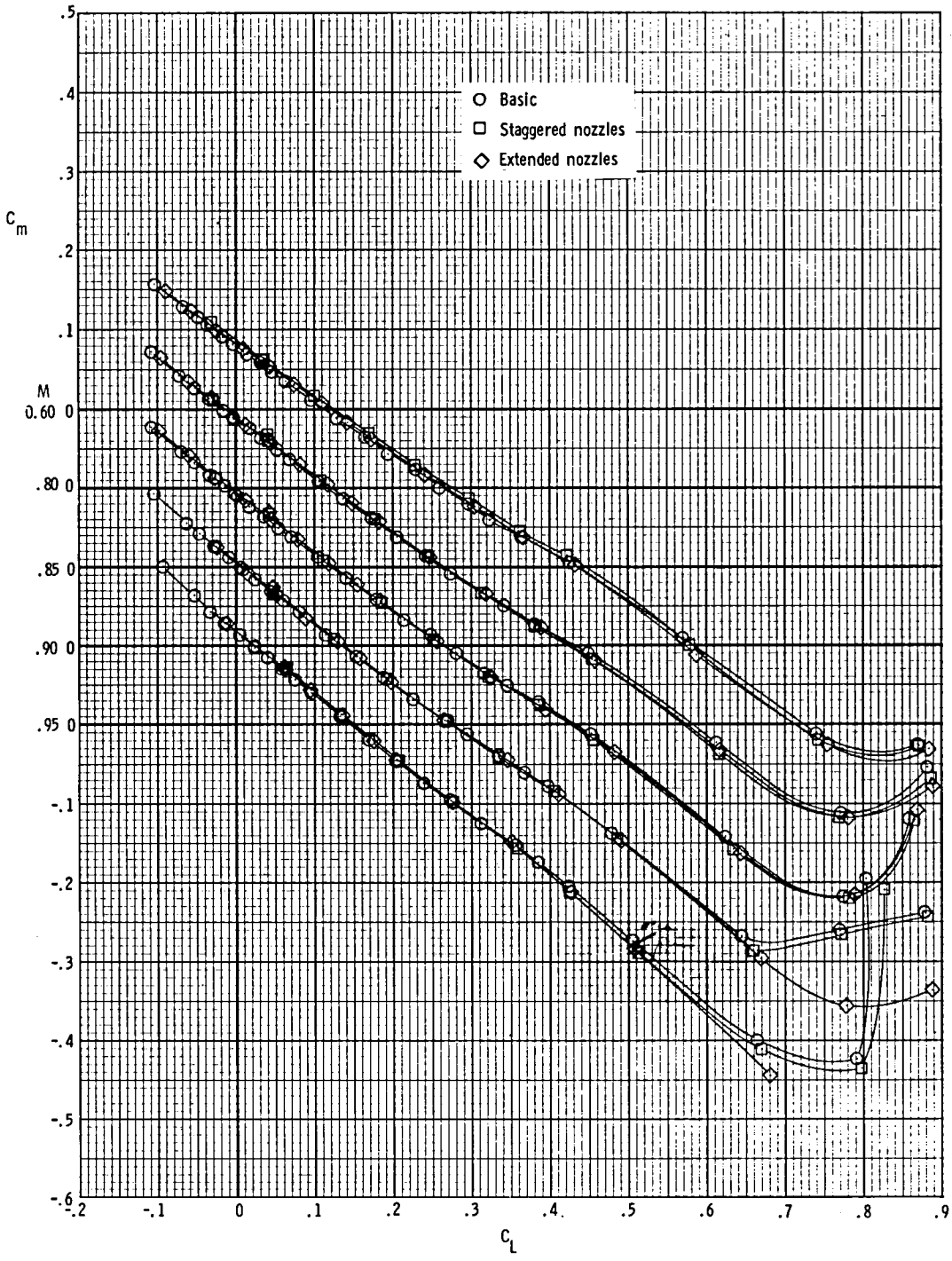

(b) Pitching-moment coefficient.

Figure 25.- Continued.

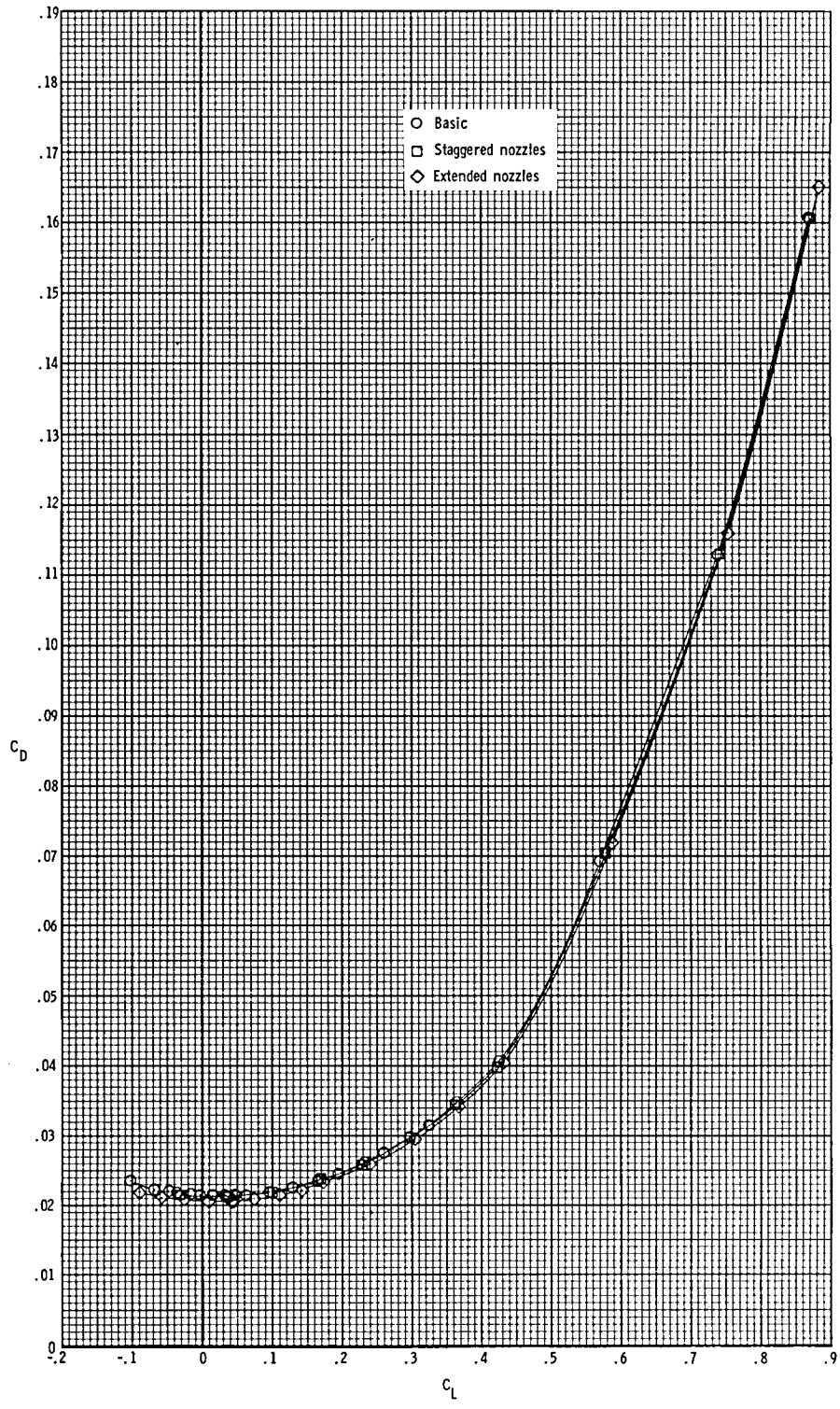

(c) Drag coefficient at M = 0.60.

Figure 25.- Continued.

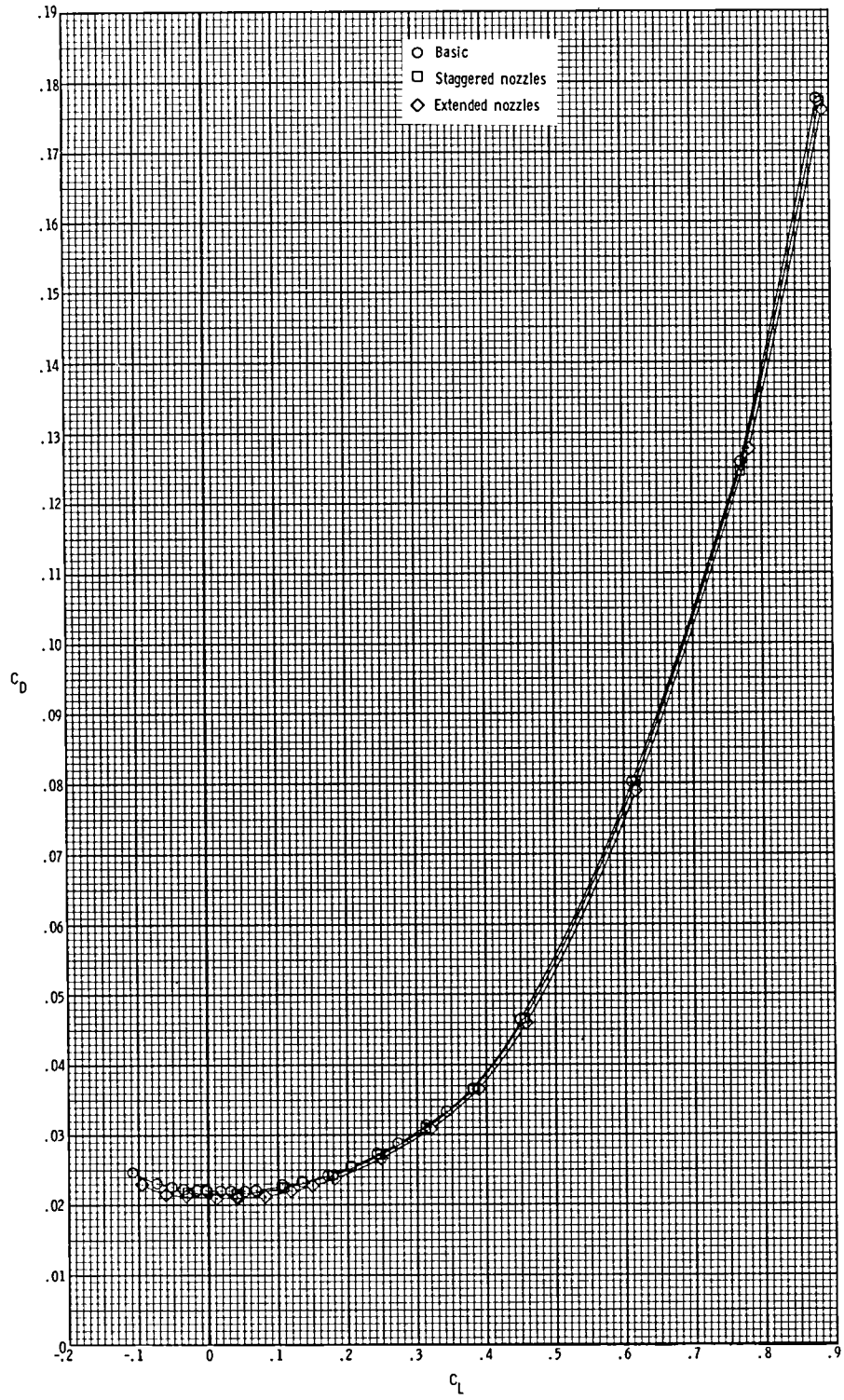

(d) Drag coefficient at M = 0.80.

Figure 25.- Continued.

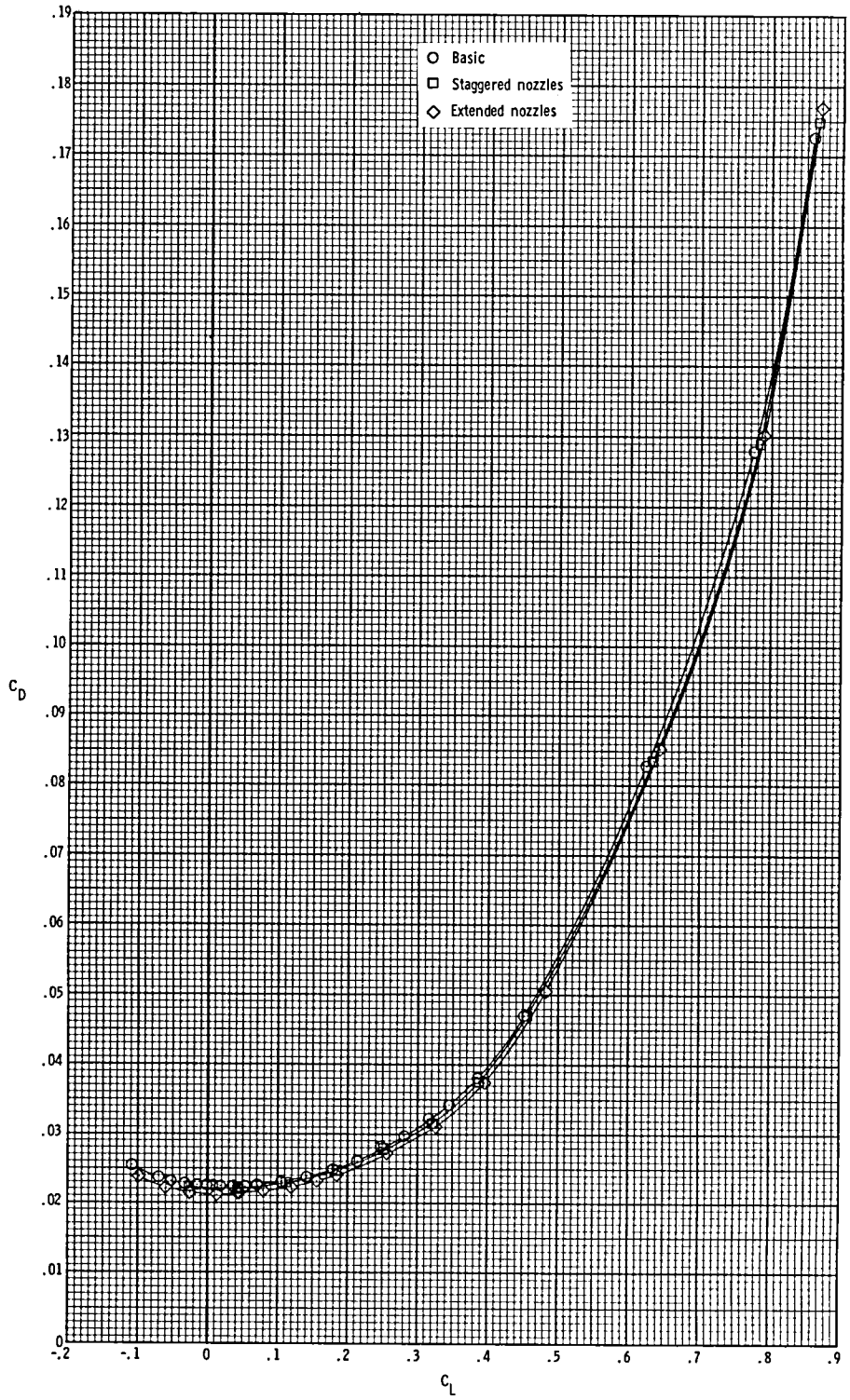

(e) Drag coefficient at M = 0.85.

Figure 25.- Continued.

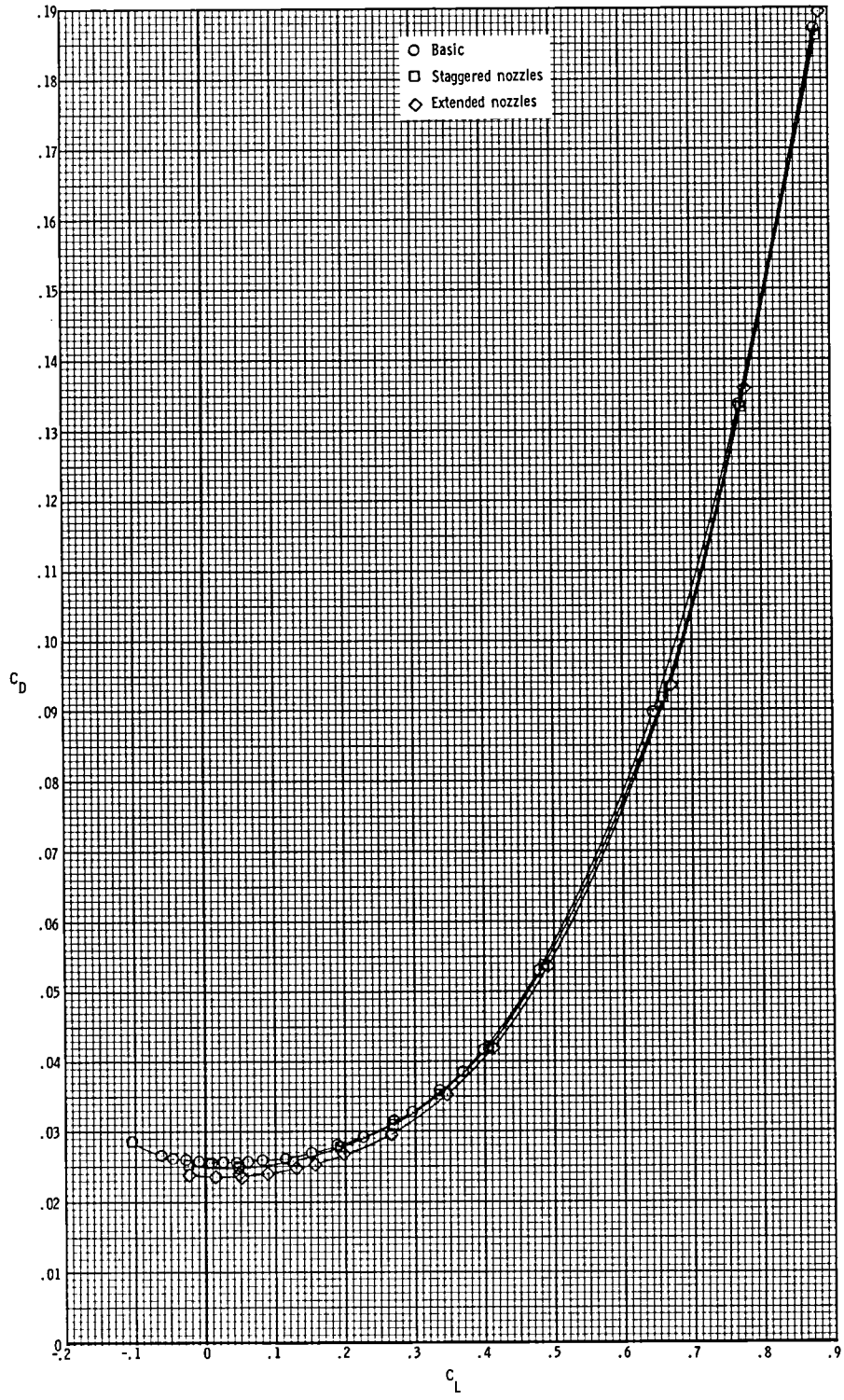

(f) Drag coefficient at M = 0.90.

Figure 25.- Continued.

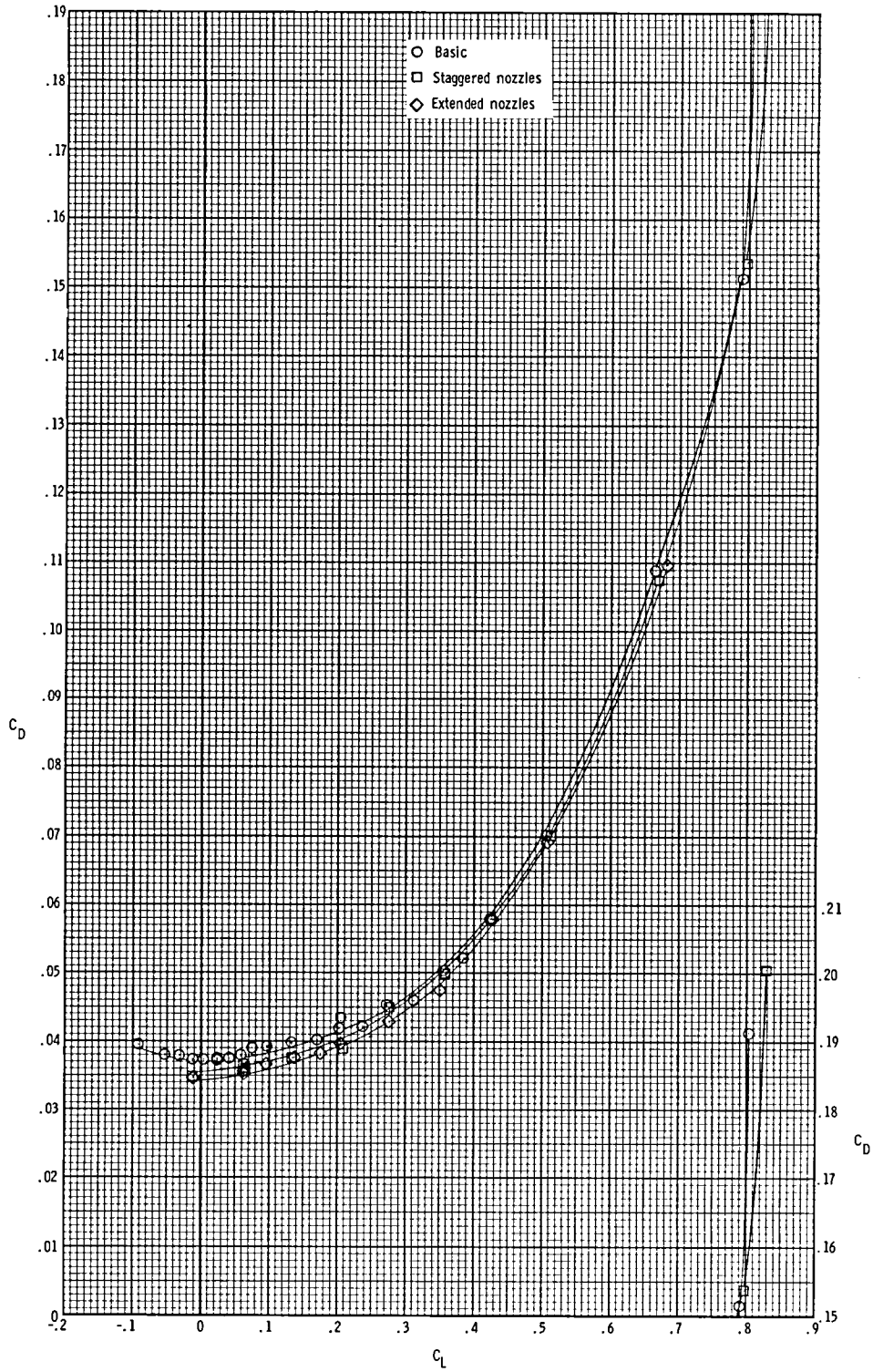

(g) Drag coefficient at M = 0.95.

Figure 25.- Concluded.

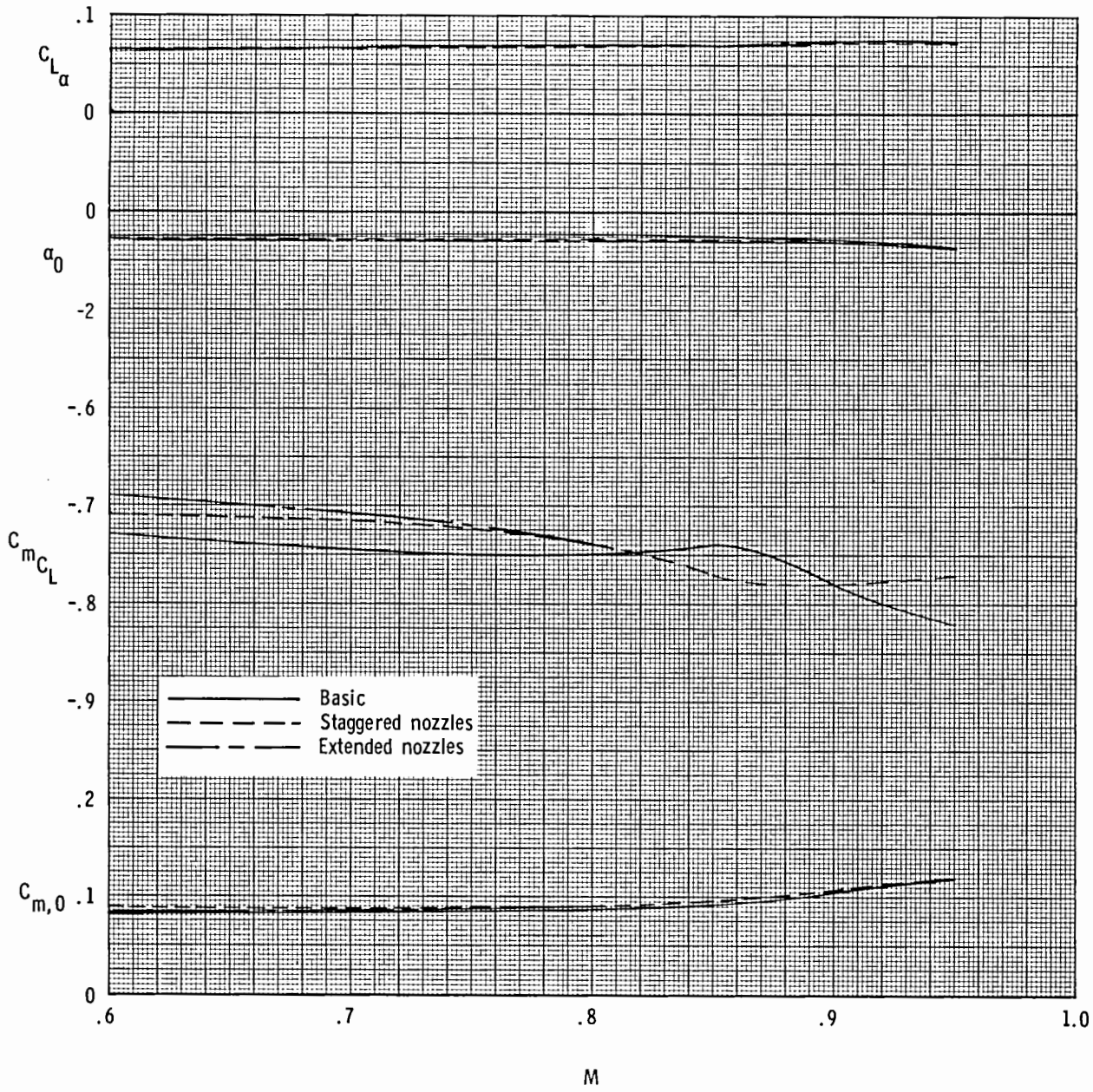

(a) C_{L_α}, α_0, $C_{m_{C_L}}$, and $C_{m,0}$.

Figure 26.- Effect of staggered and extended nozzles on model longitudinal parameters for model with cruise nozzles, short interfairing, and wings swept 65°.

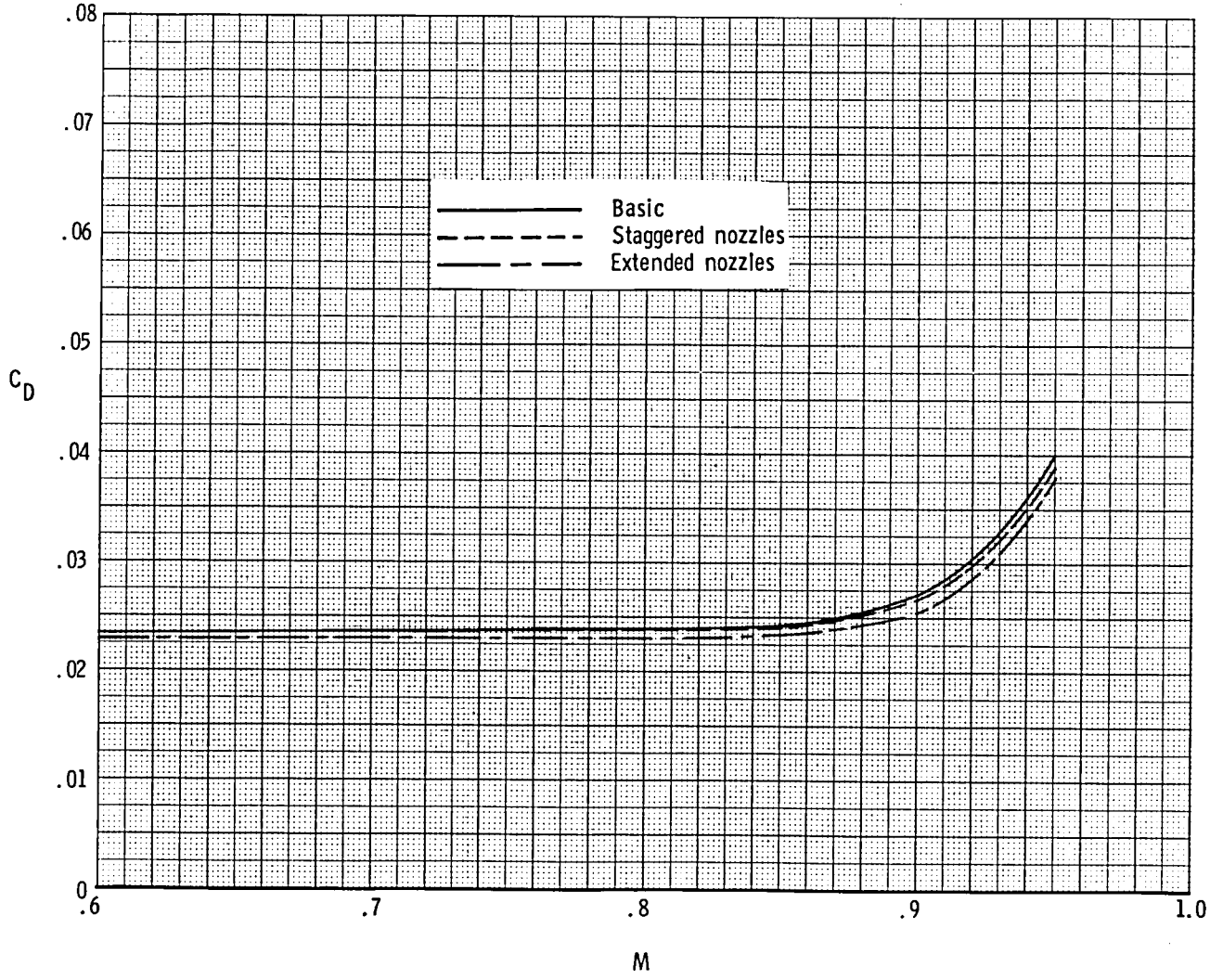

(b) Drag coefficient at $C_L = 0.16$.

Figure 26.- Concluded.

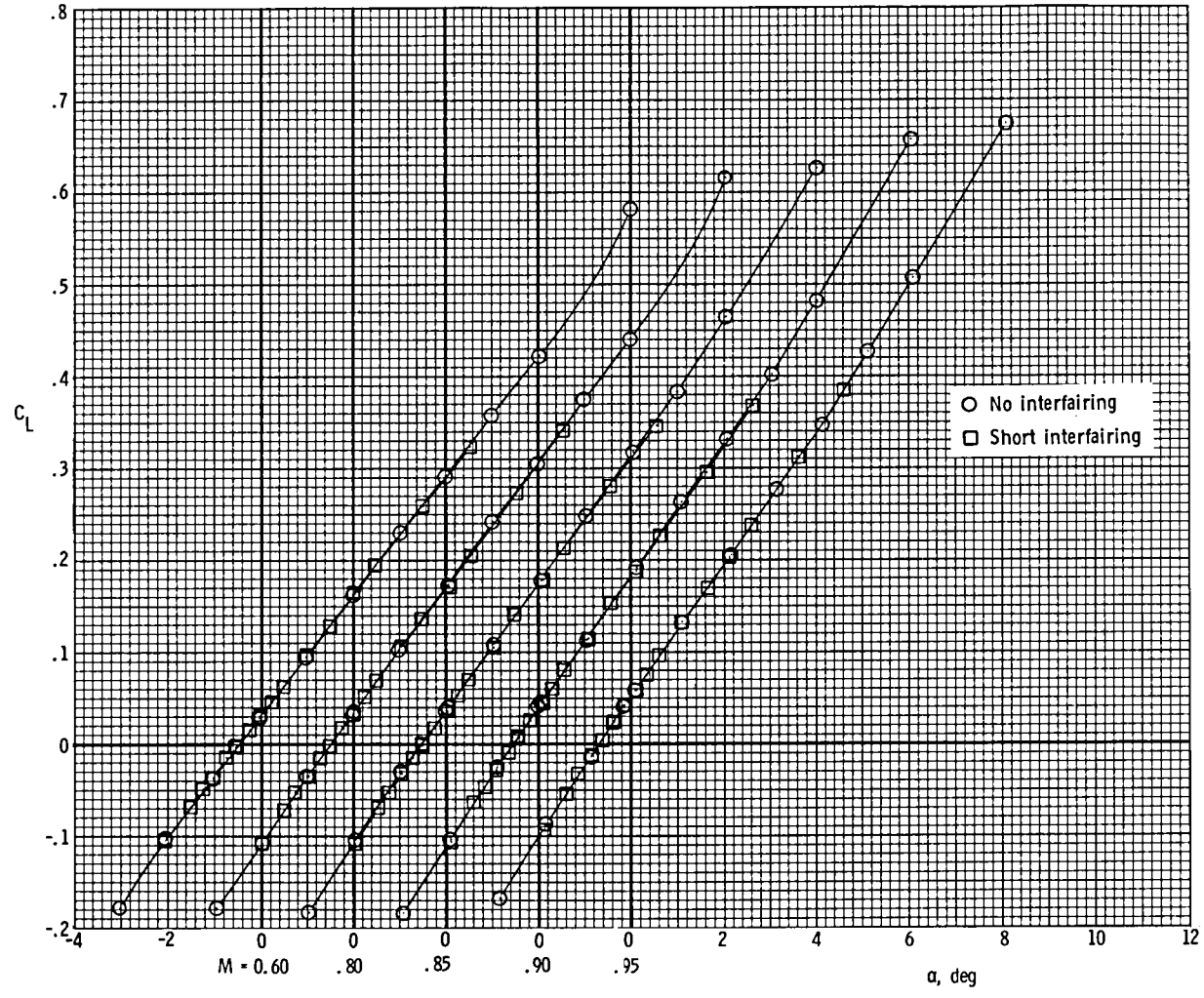

(a) Lift coefficient.

Figure 27.- Effect of short interfairing on longitudinal aerodynamic characteristics of the model with cruise nozzles and wings swept 65°.

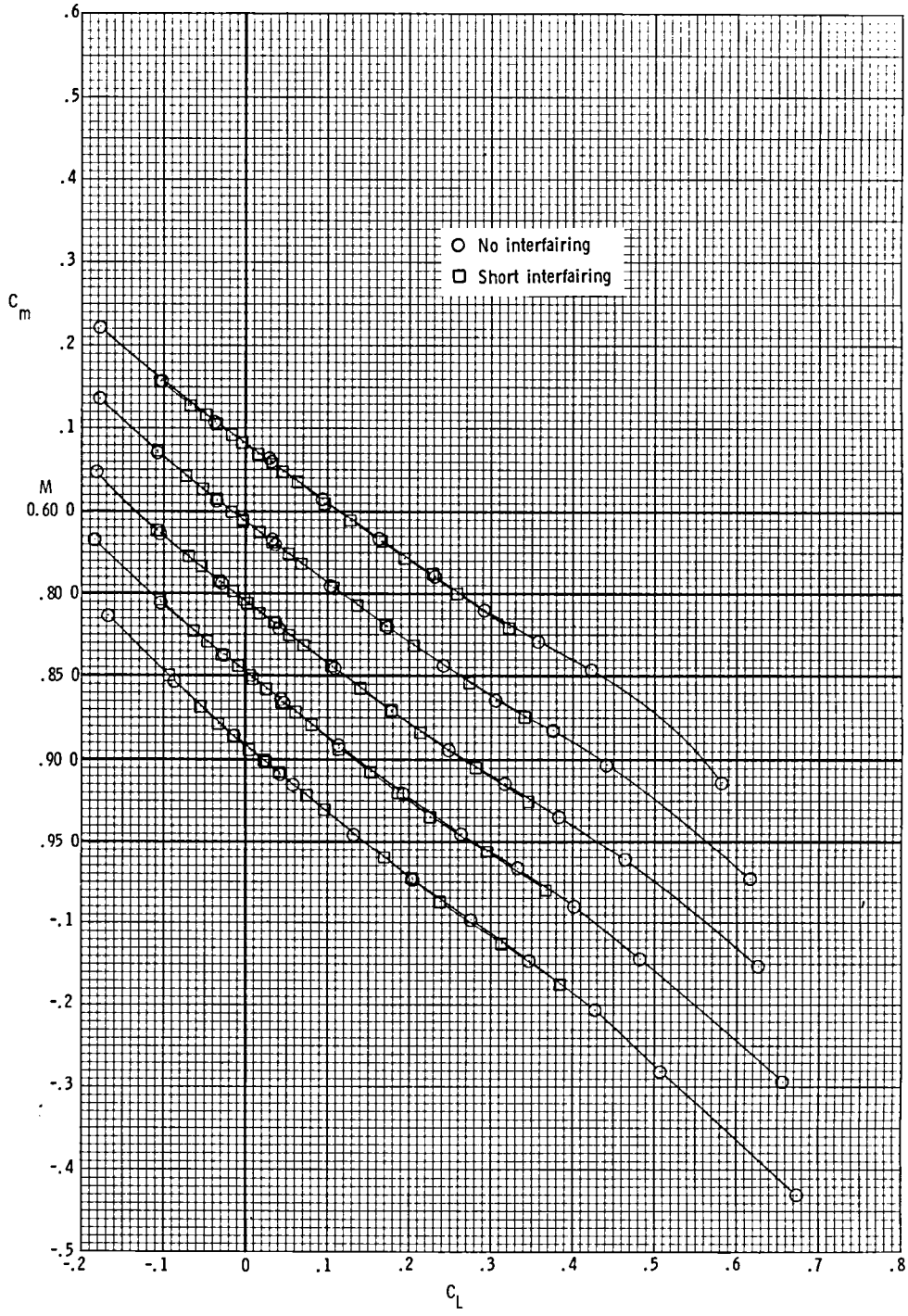

(b) Pitching-moment coefficient.

Figure 27.- Continued.

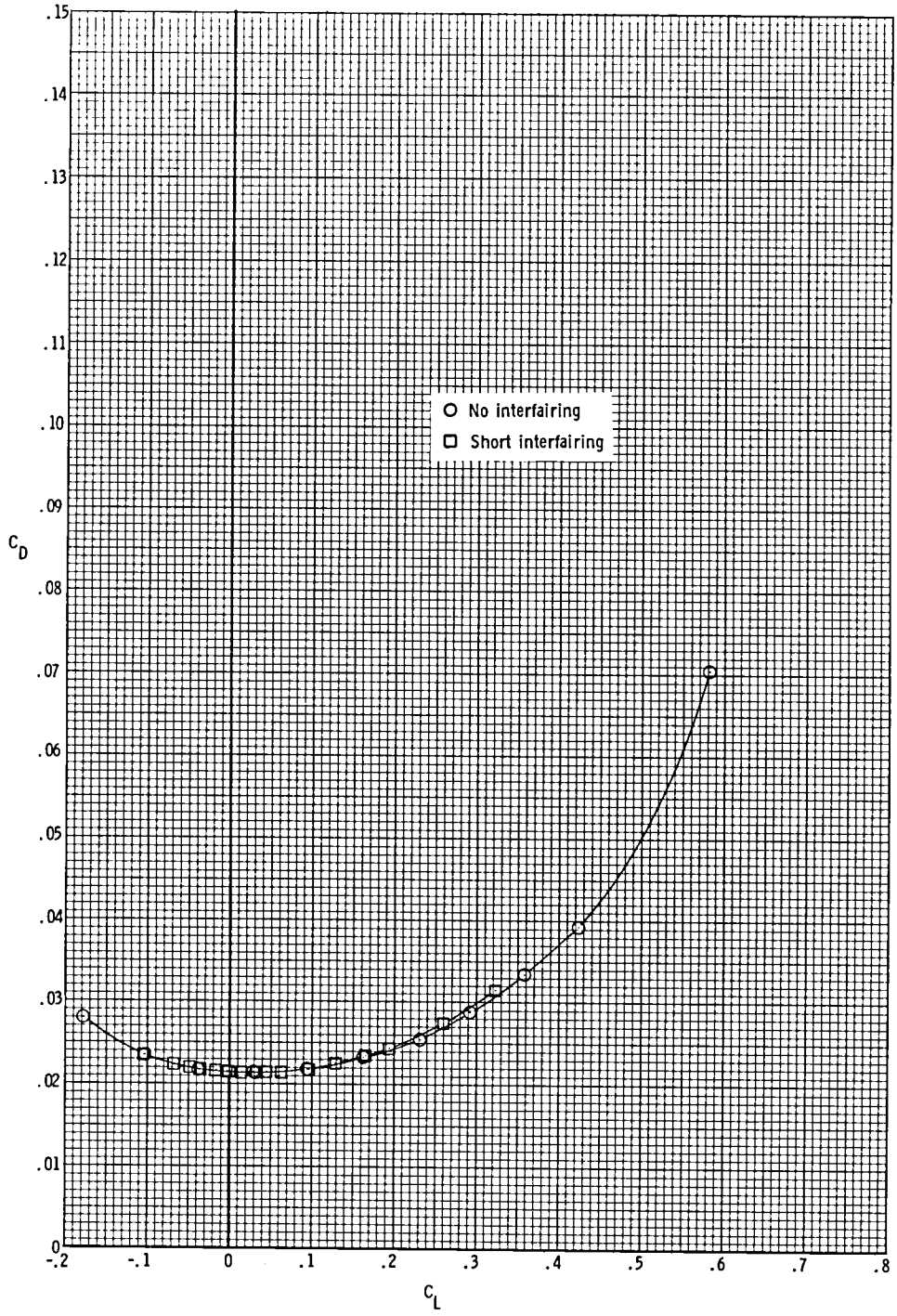

(c) Drag coefficient at M = 0.60.

Figure 27.- Continued.

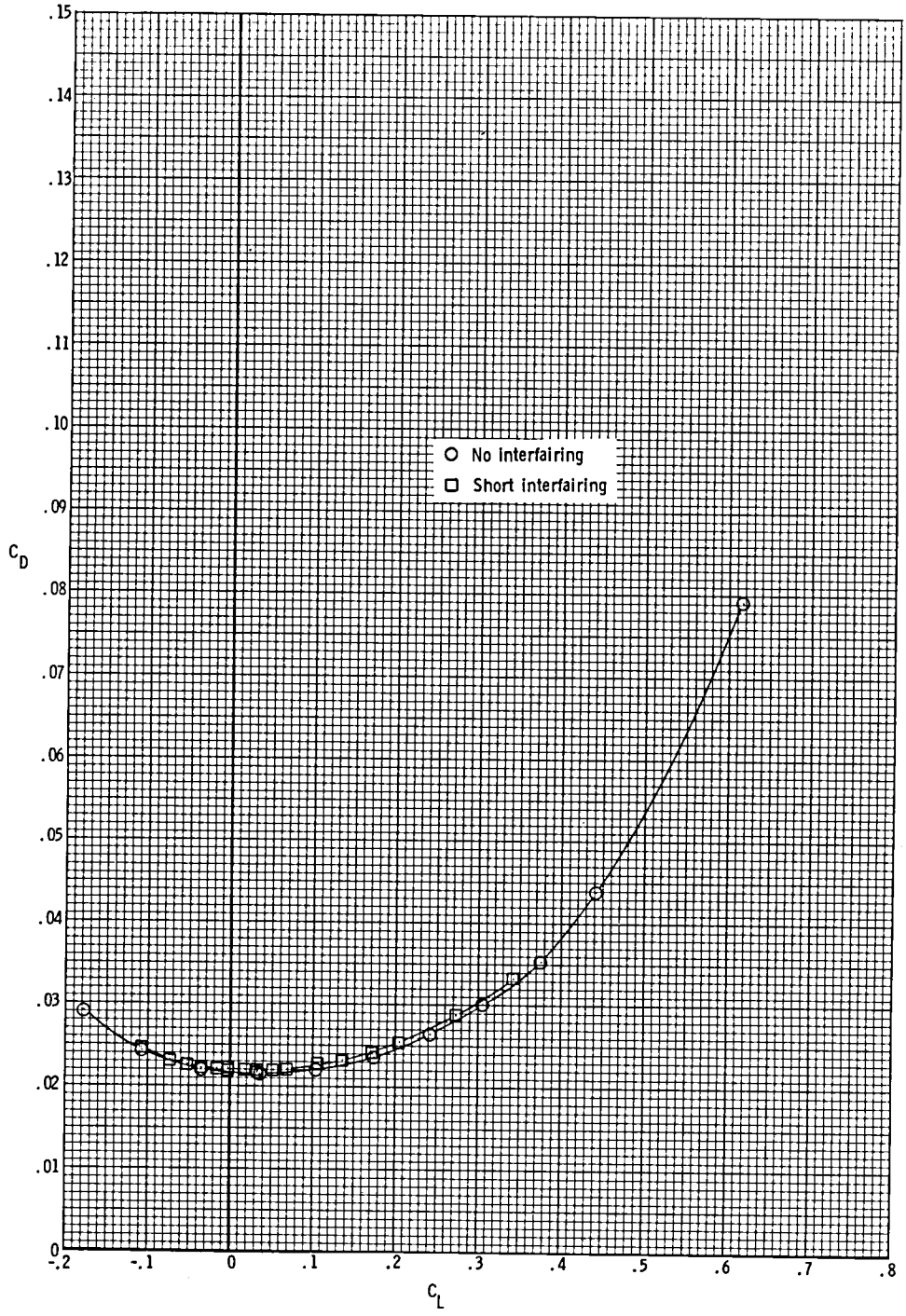

(d) Drag coefficient at M = 0.80.

Figure 27.- Continued.

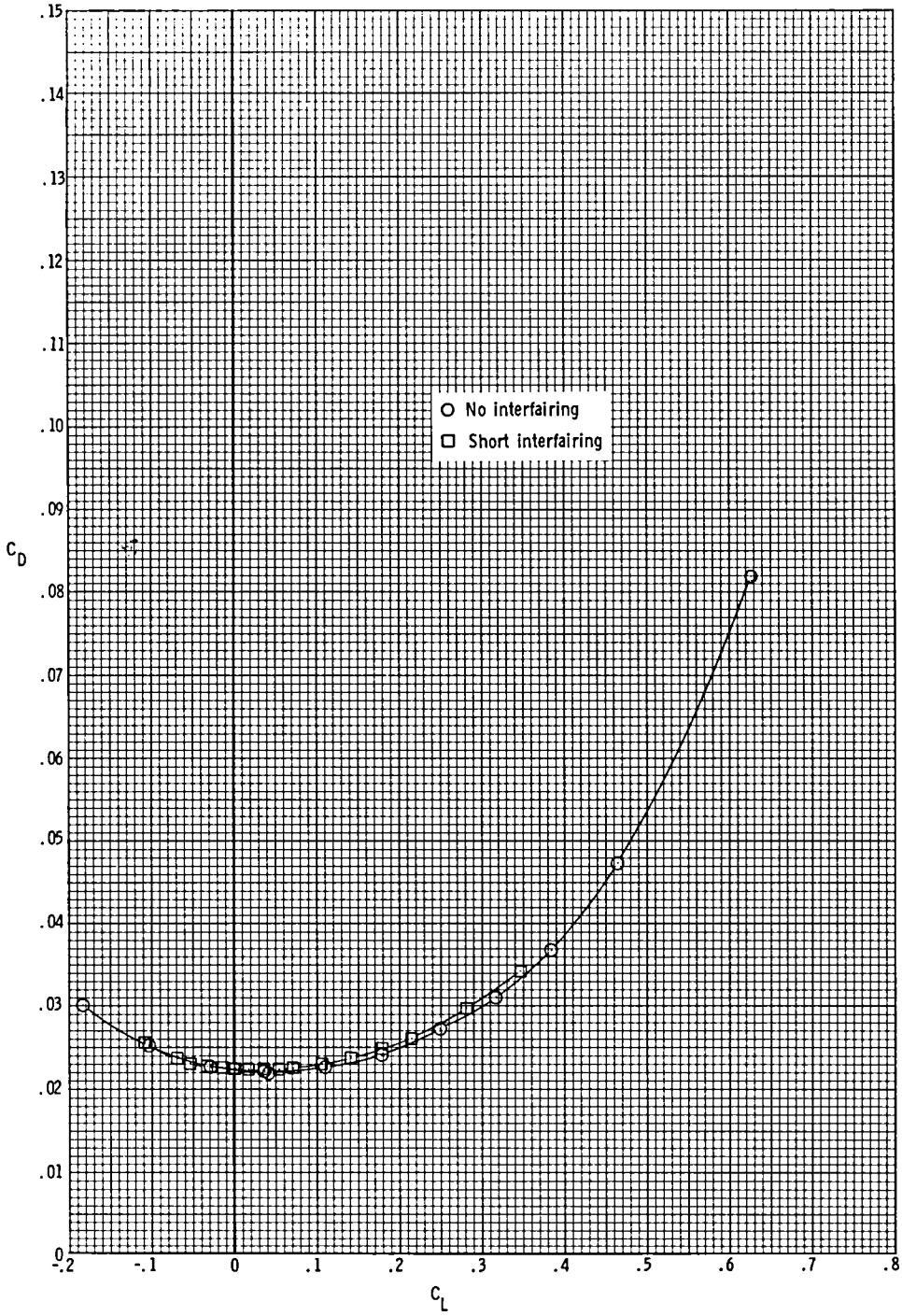

(e) Drag coefficient at M = 0.85.

Figure 27.- Continued.

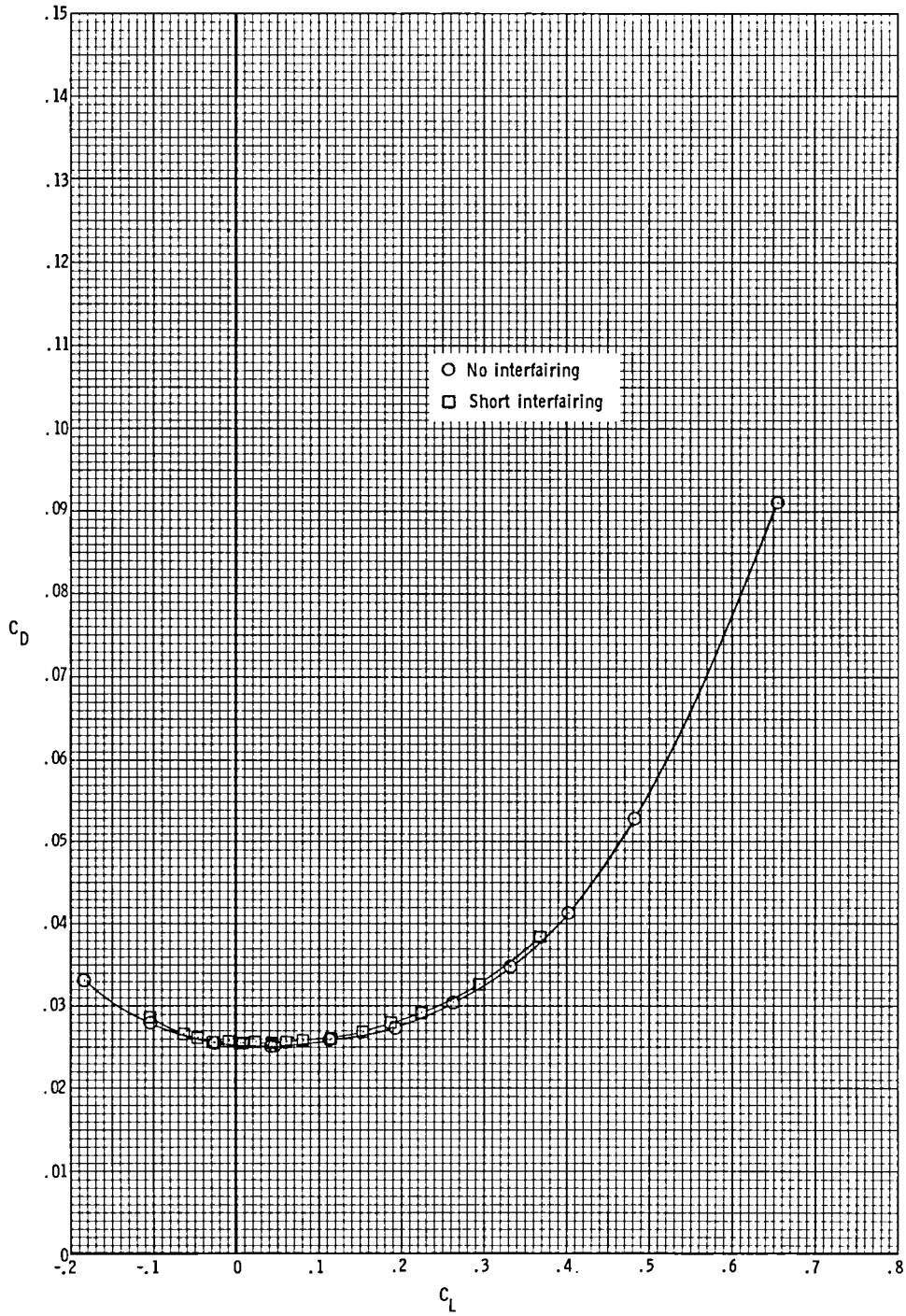

(f) Drag coefficient at M = 0.90.

Figure 27.- Continued.

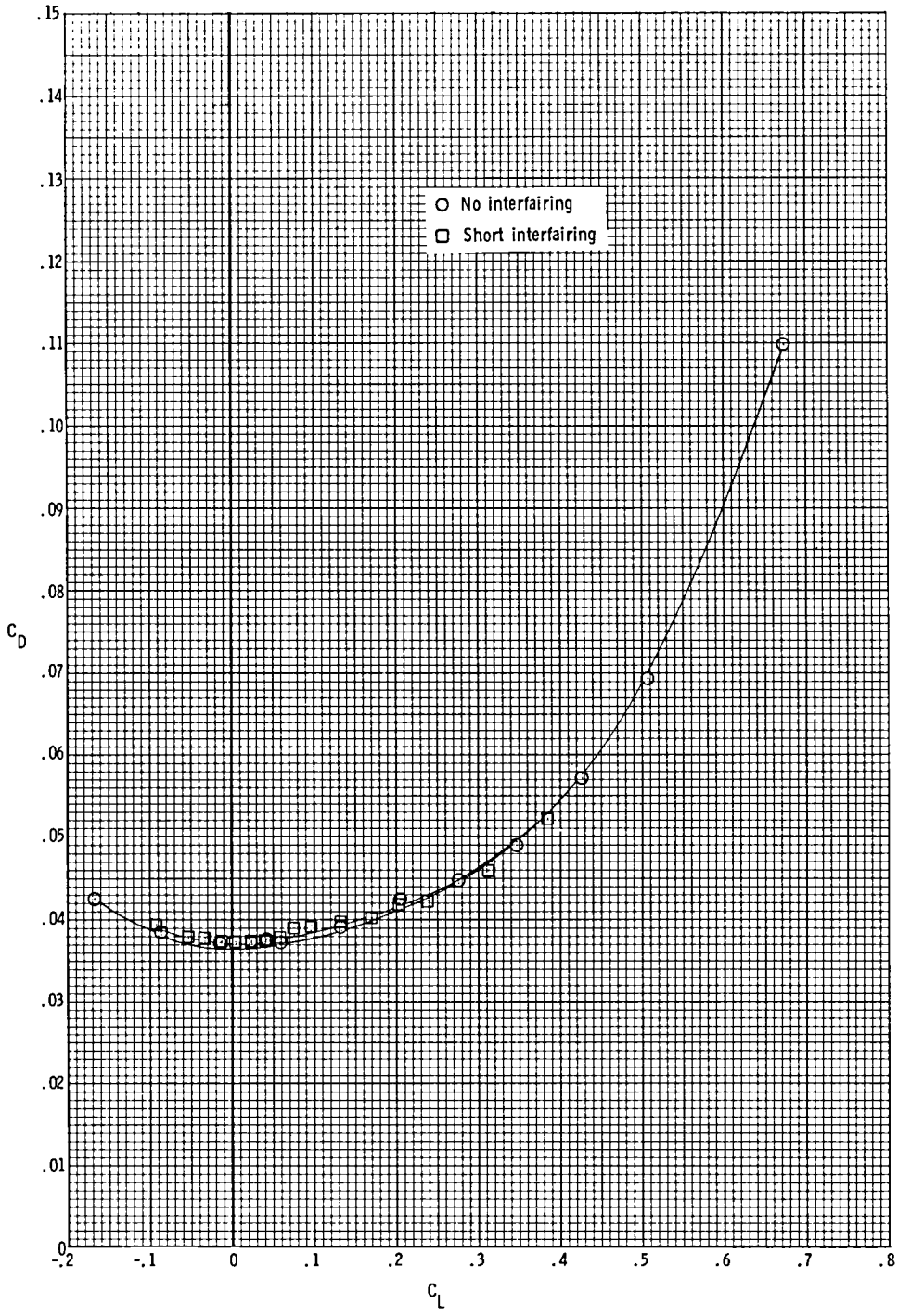

(g) Drag coefficient at M = 0.95

Figure 27.- Concluded.

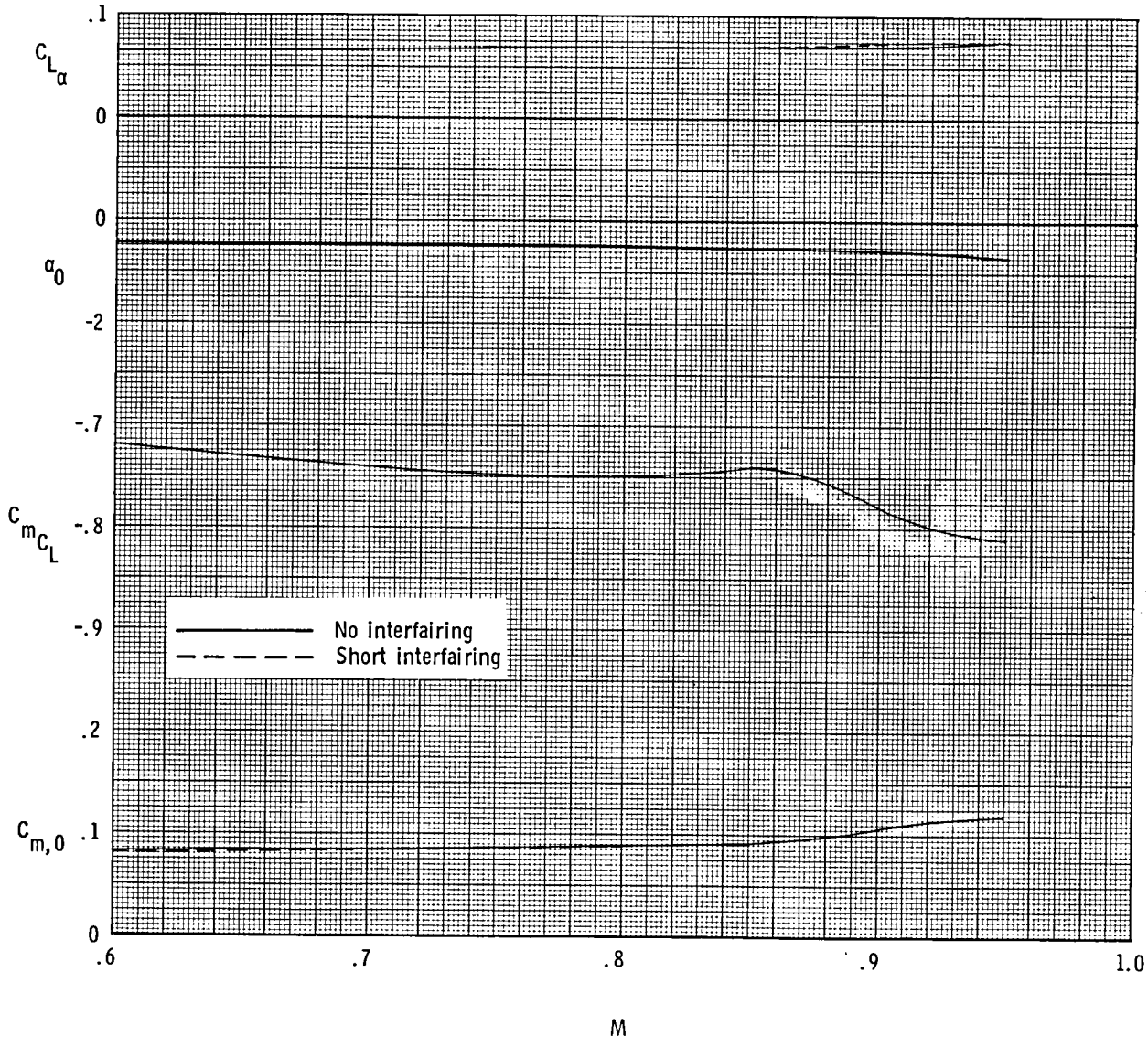

(a) C_{L_α}, α_0, $C_{m_{C_L}}$, and $C_{m,0}$.

Figure 28.- Effect of short interfairing on model longitudinal parameters for model with cruise nozzles and wings swept 65°

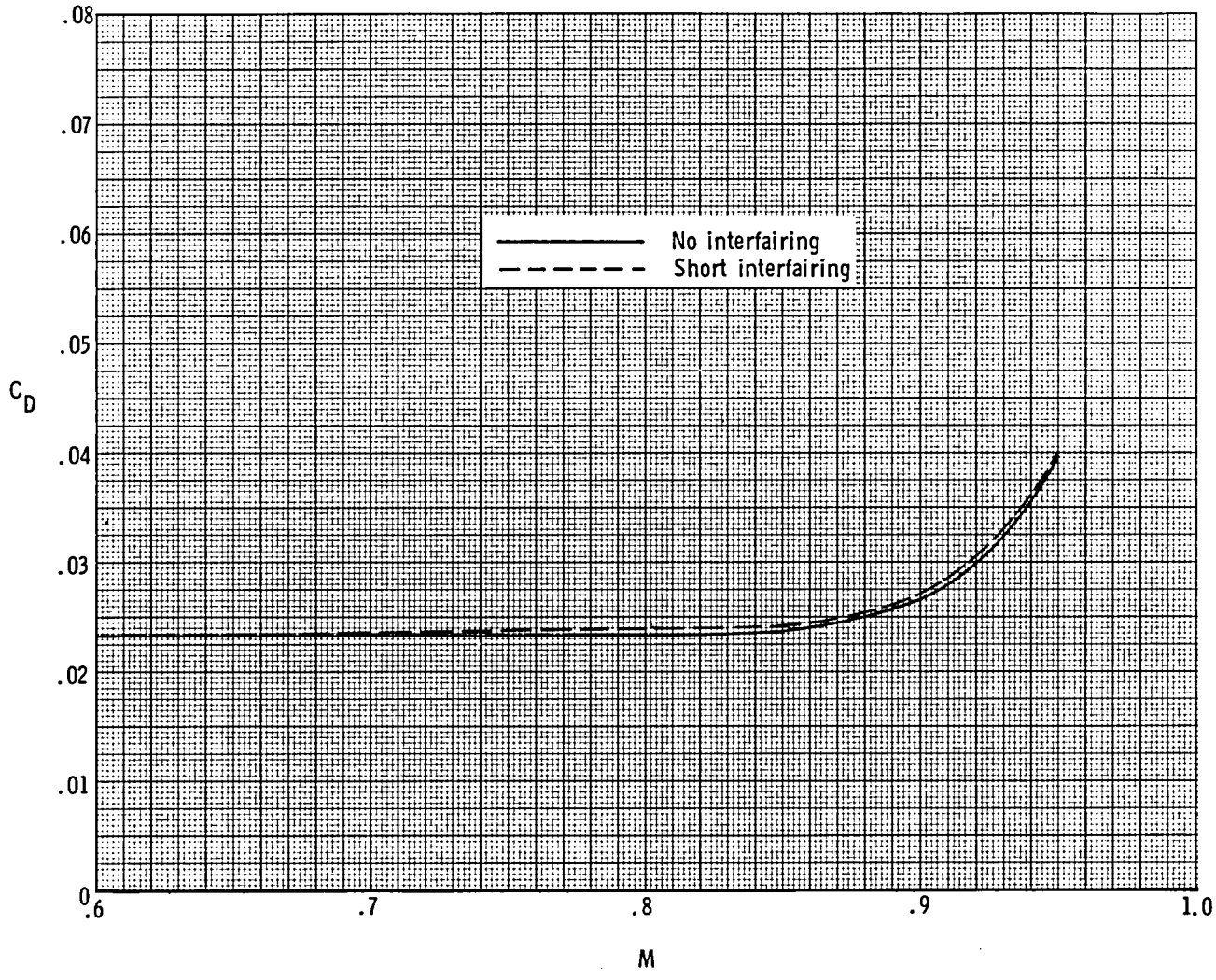

(b) Drag coefficient at $C_L = 0.16$.

Figure 28.- Concluded.

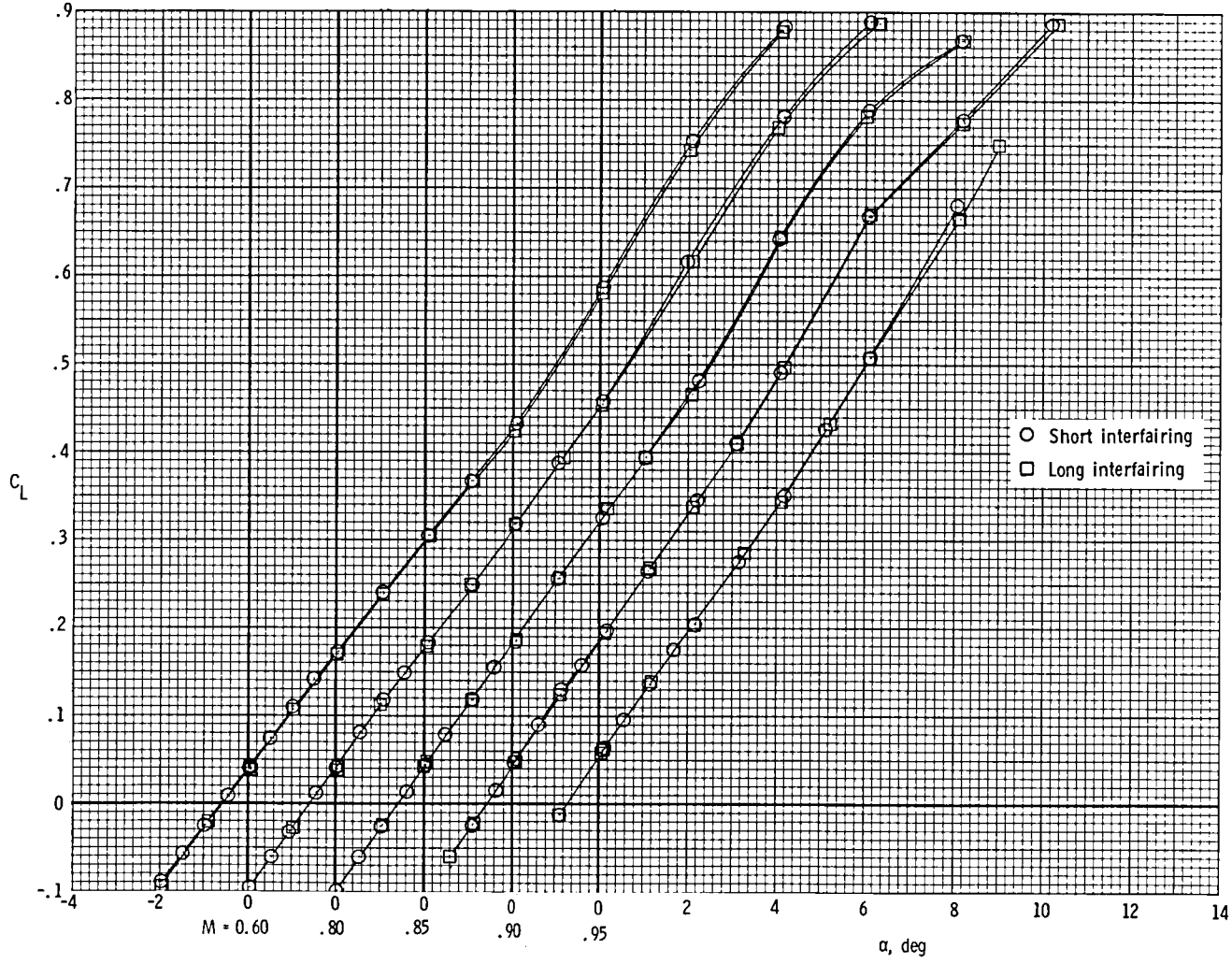

(a) Lift coefficient.

Figure 29.- Effect of lengthening interfairing on longtudinal aerodynamic characteristics of the model with cruise nozzles extended and wings swept 65°.

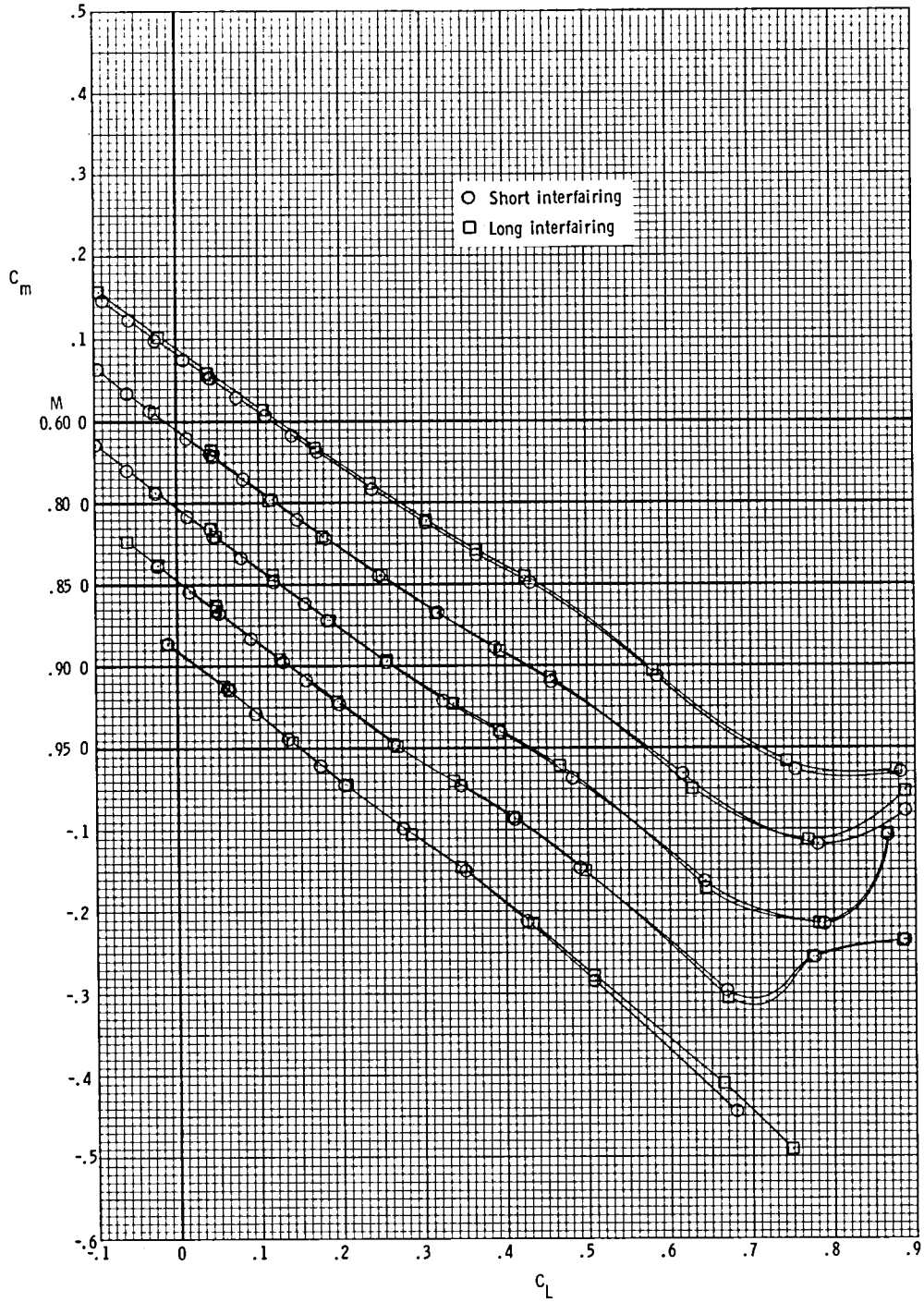

(b) Pitching-moment coefficient.

Figure 29.- Continued.

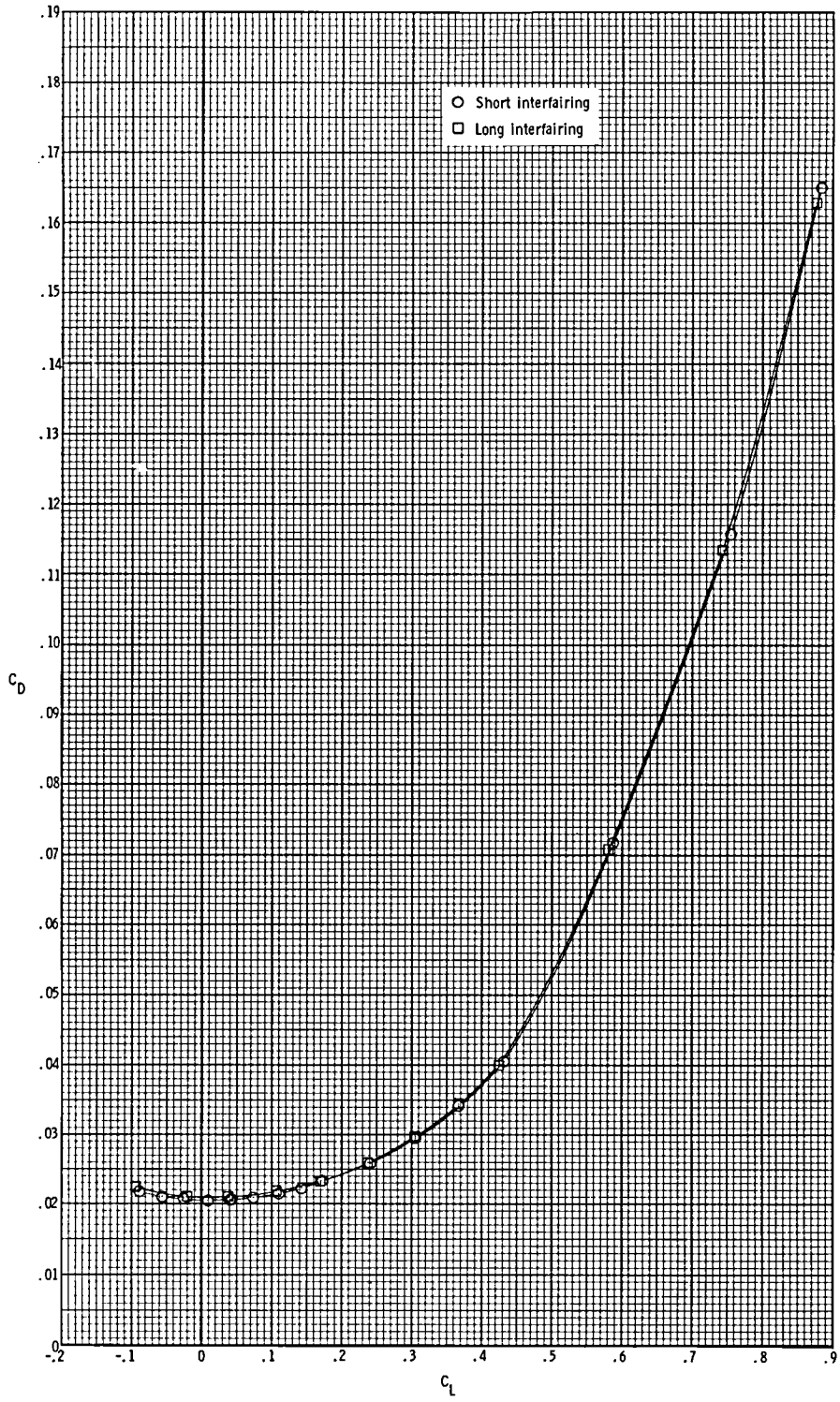

(c) Drag coefficient at M = 0.60.

Figure 29.- Continued.

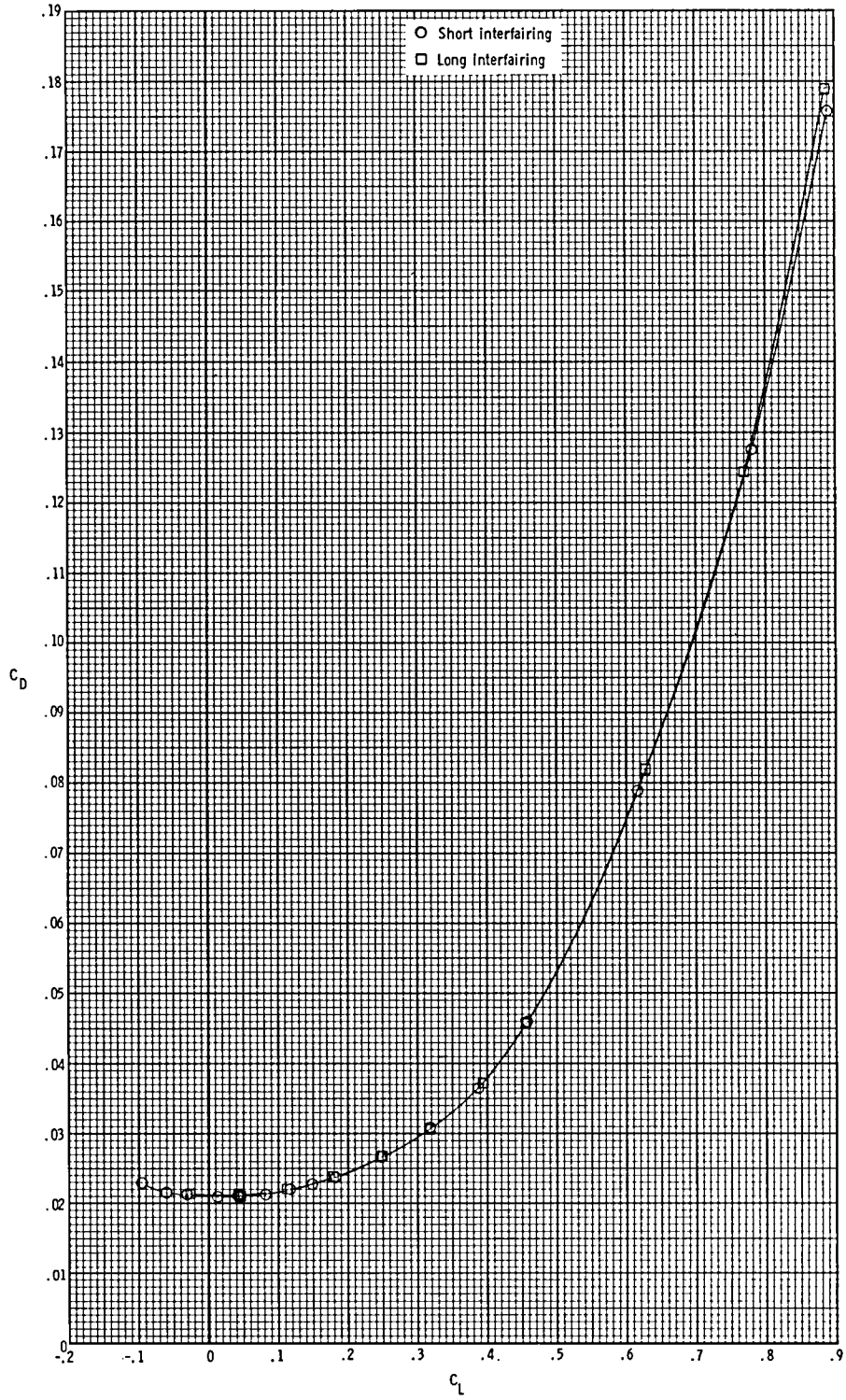

(d) Drag coefficient at M = 0.80.

Figure 29.- Continued.

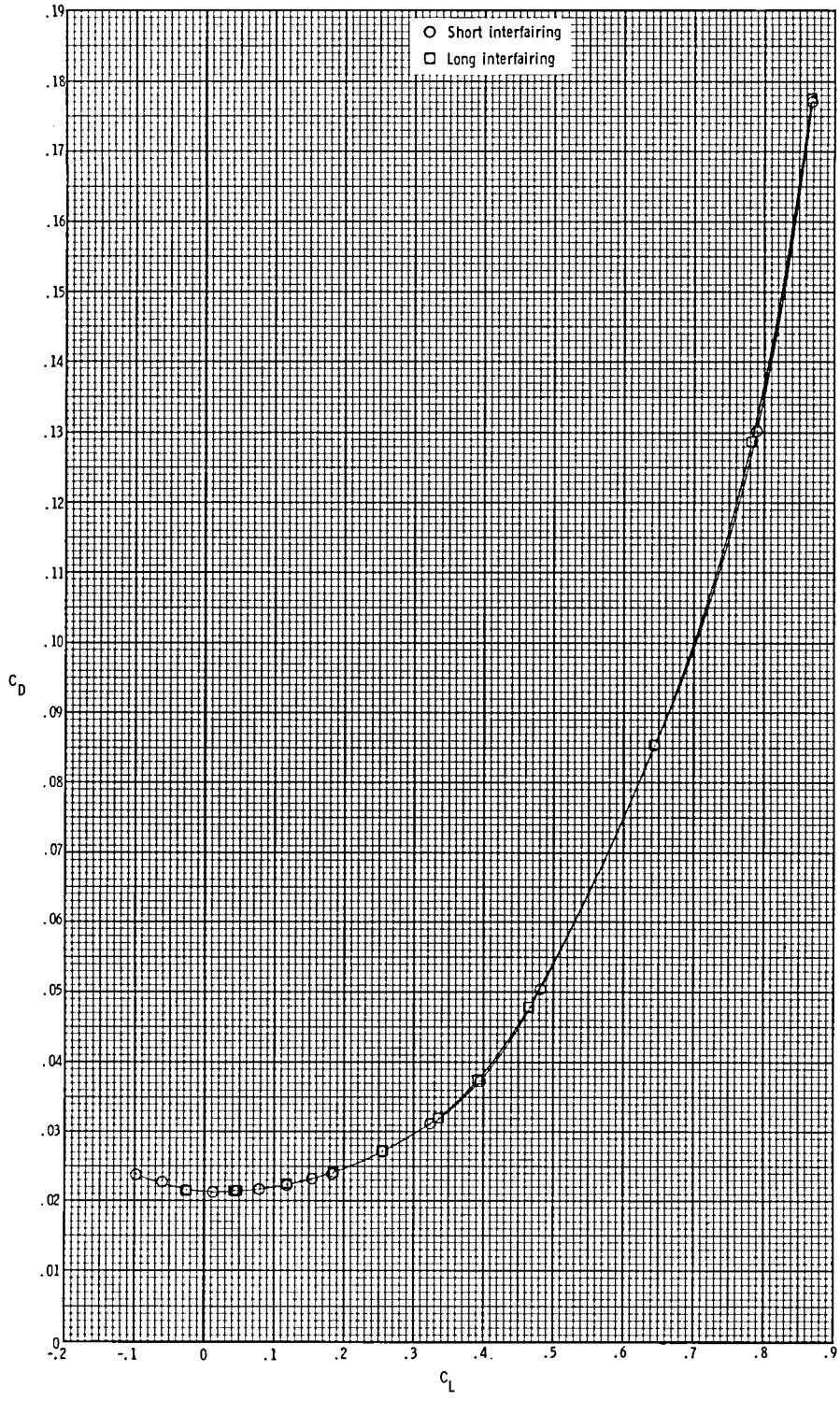

(e) Drag coefficient at M = 0.85.

Figure 29.- Continued.

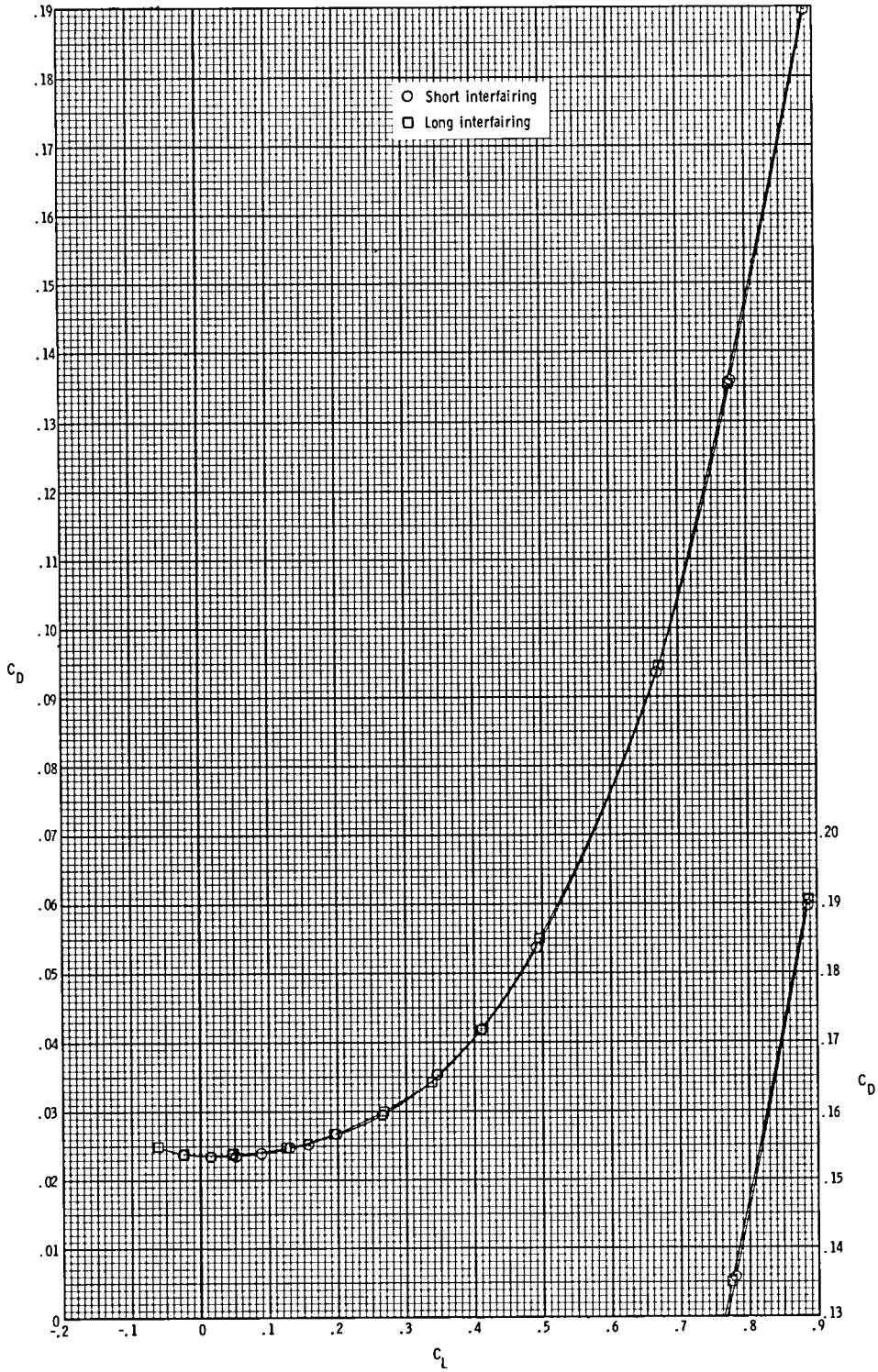

(f) Drag coefficient at M = 0.90.

Figure 29.- Continued.

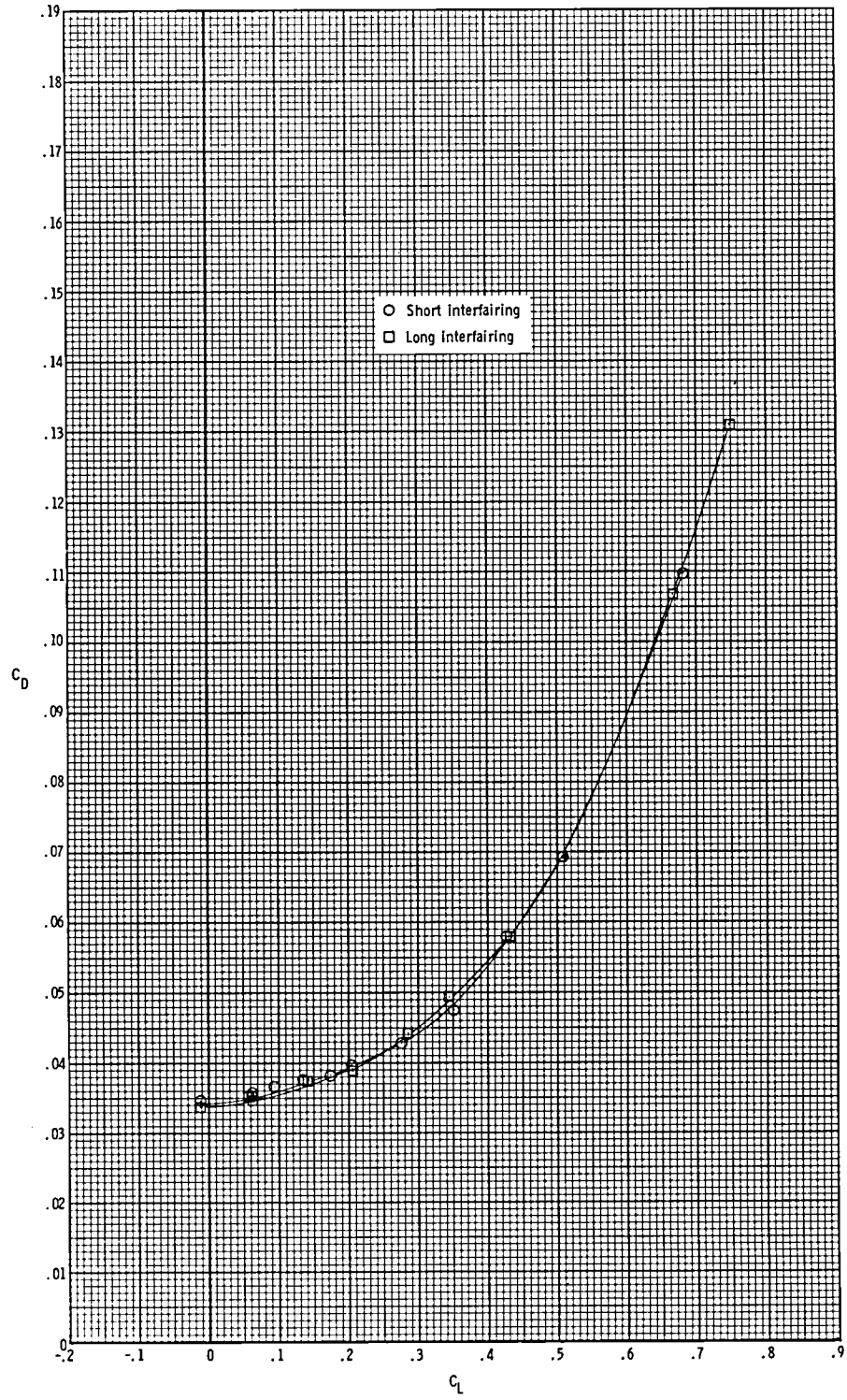

(g) Drag coefficient at M = 0.95.

Figure 29.- Concluded.

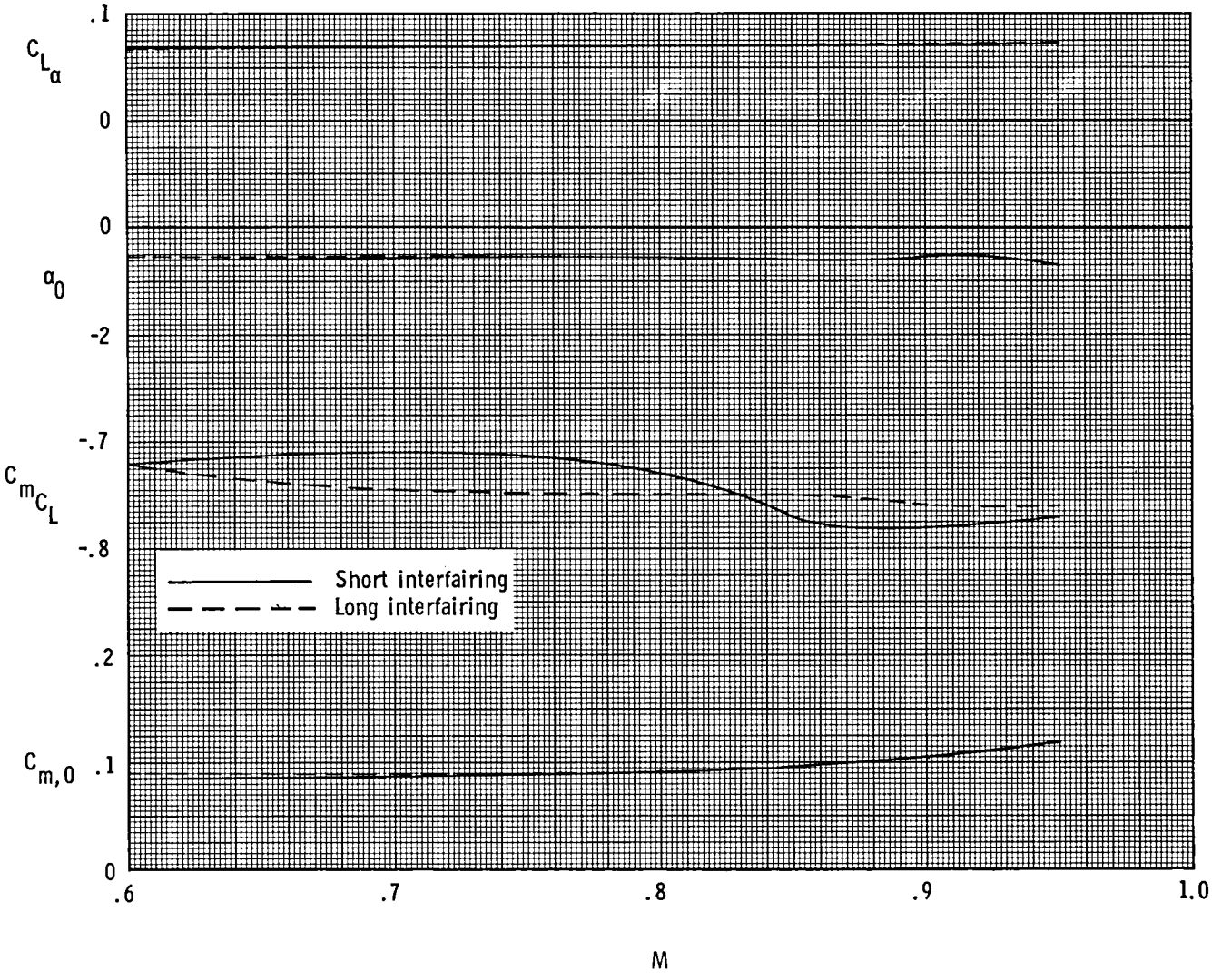

(a) $C_{L\alpha}$, α_0, $C_{m_{C_L}}$, and $C_{m,0}$.

Figure 30.- Effect of lengthening interfairing on model longitudinal parameters for the model with cruise nozzles extended and wings swept 65°.

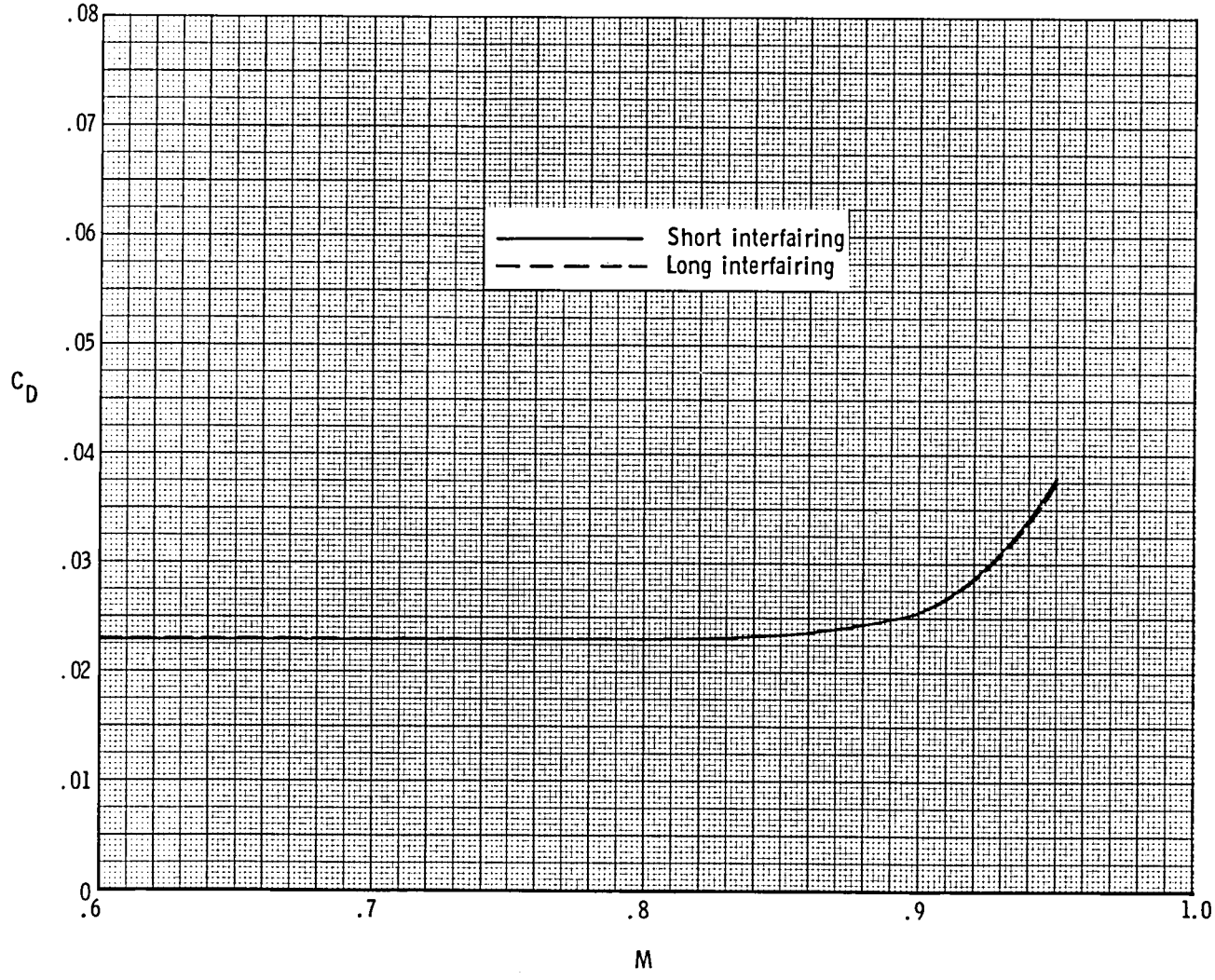

(b) Drag coefficient at $C_L = 0.16$.

Figure 30.- Concluded.

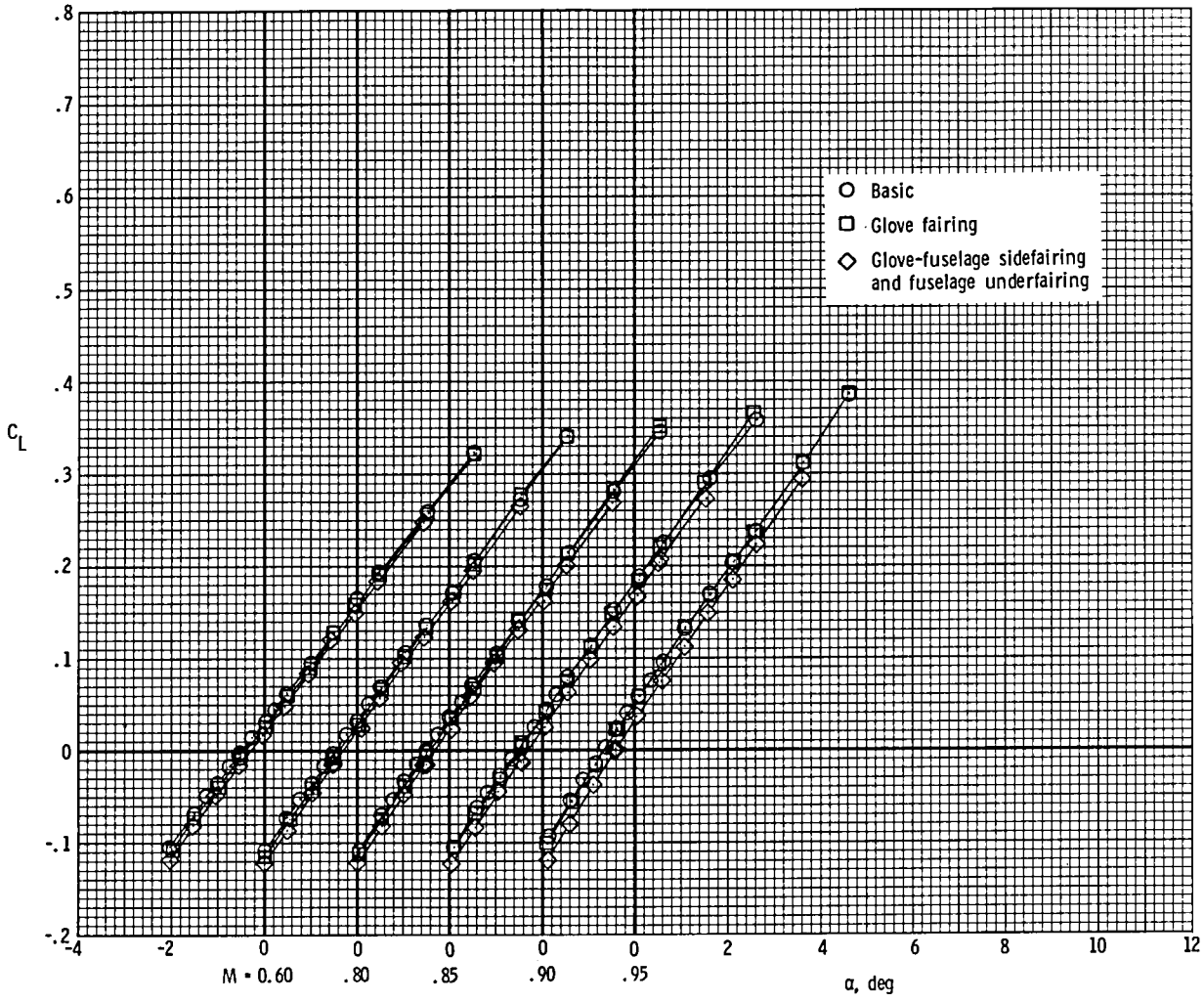

(a) Lift coefficient.

Figure 31.- Effect of fairing the upper surface of the wing glove and the fuselage on longitudinal aerodynamic characteristics of the model with cruise nozzles, short interfairing, and wings swept 65°.

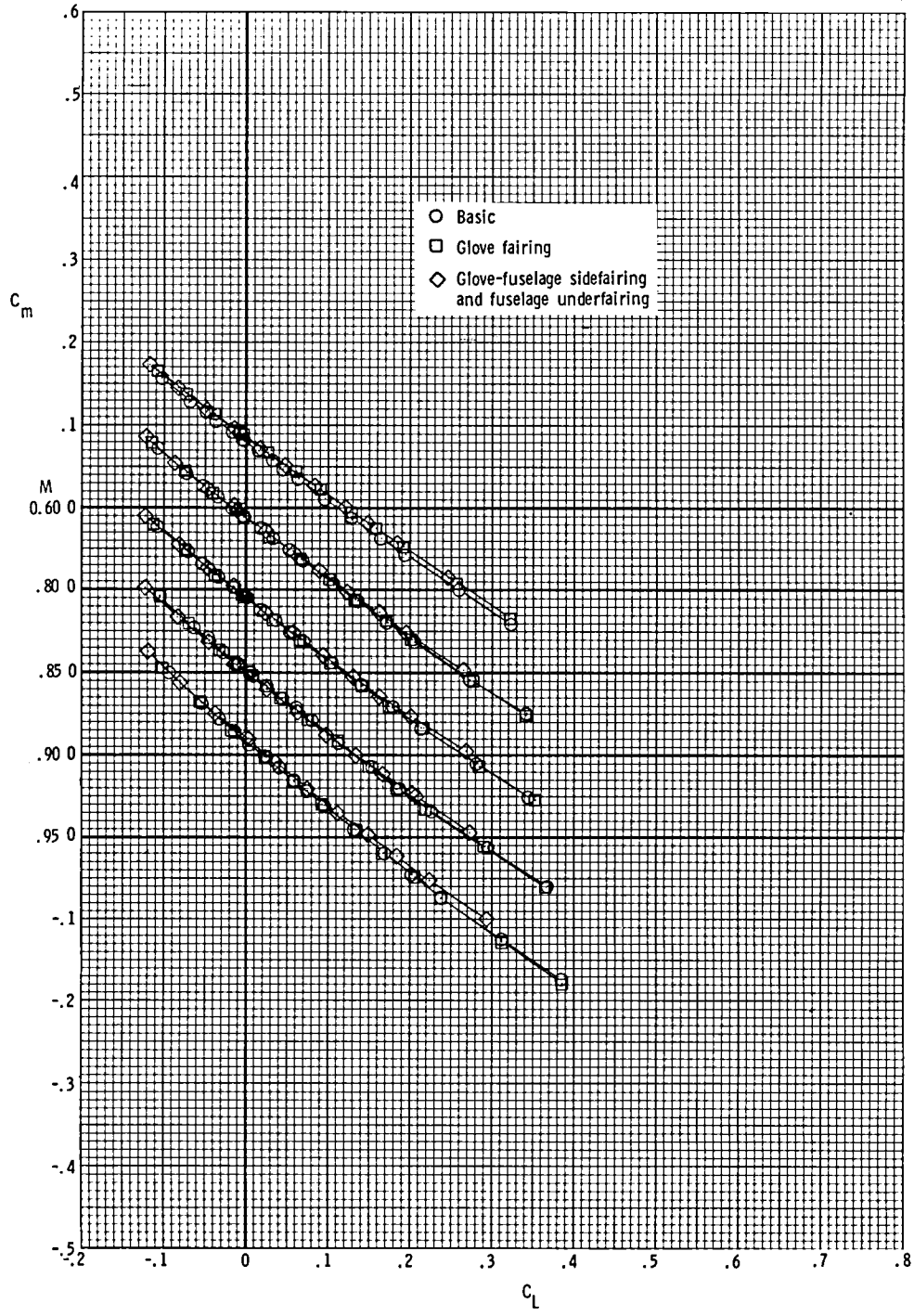

(b) Pitching-moment coefficient.

Figure 31.- Continued.

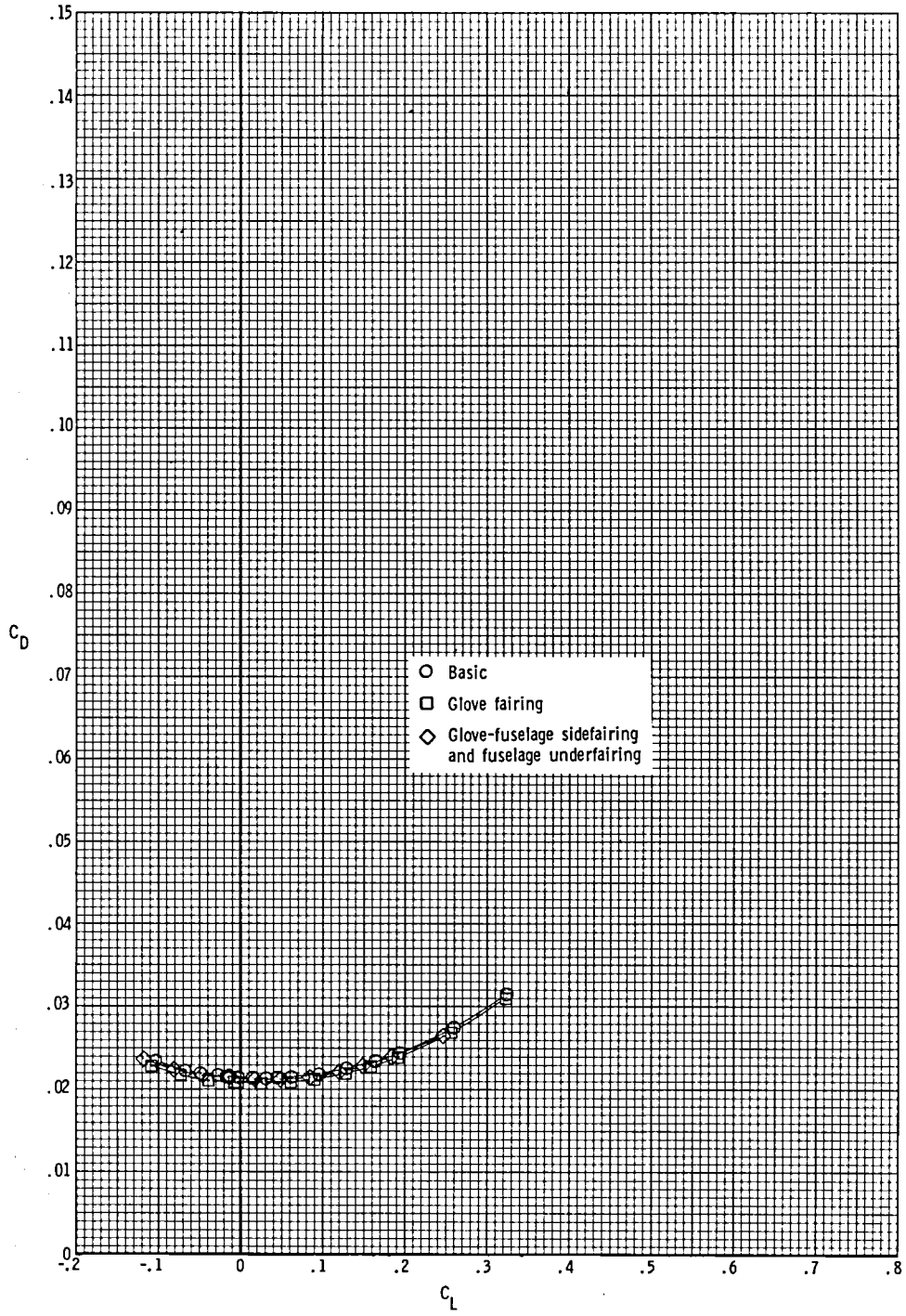

(c) Drag coefficient at M = 0.60.

Figure 31.- Continued.

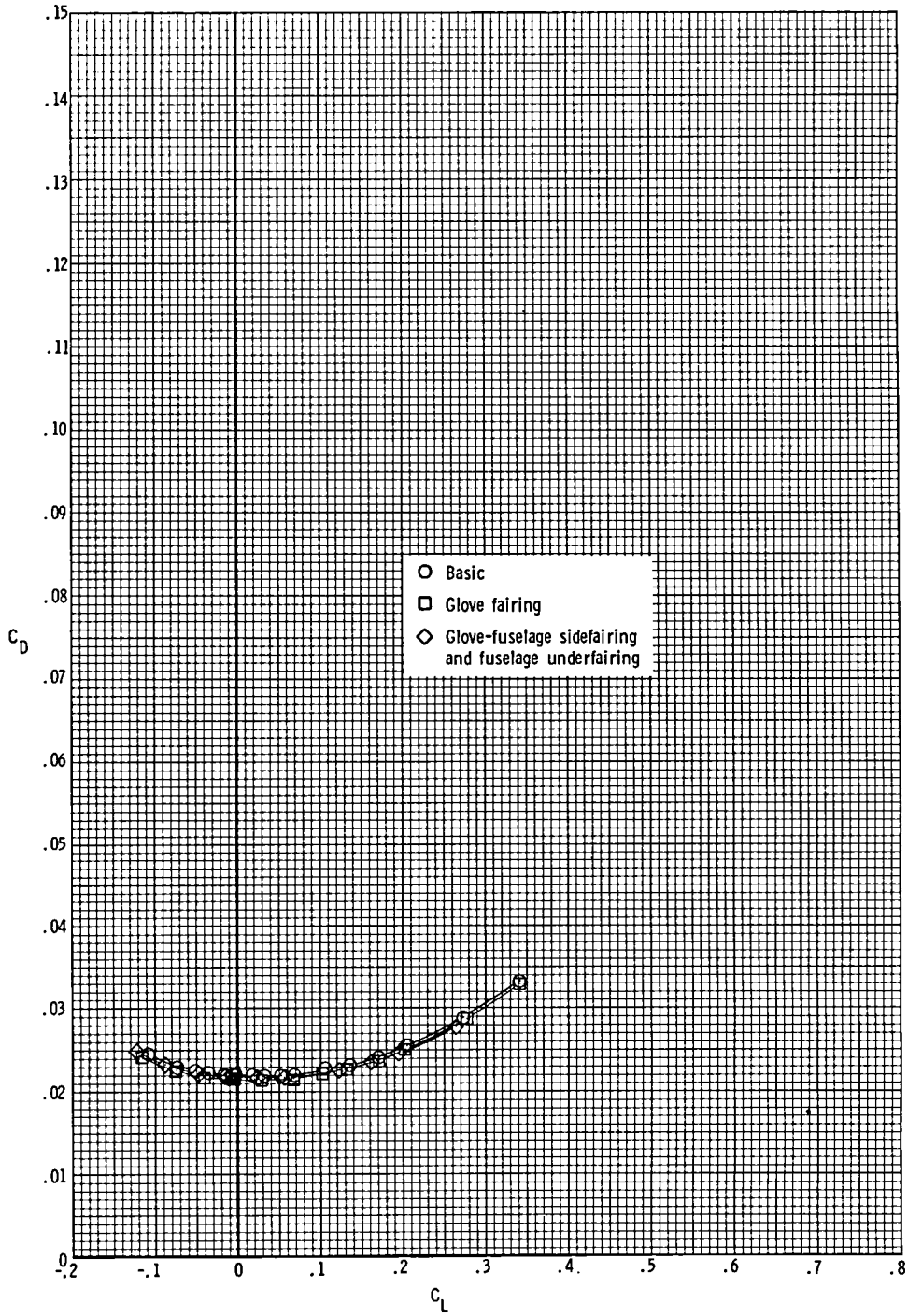

(d) Drag coefficient at M = 0.80.

Figure 31.- Continued.

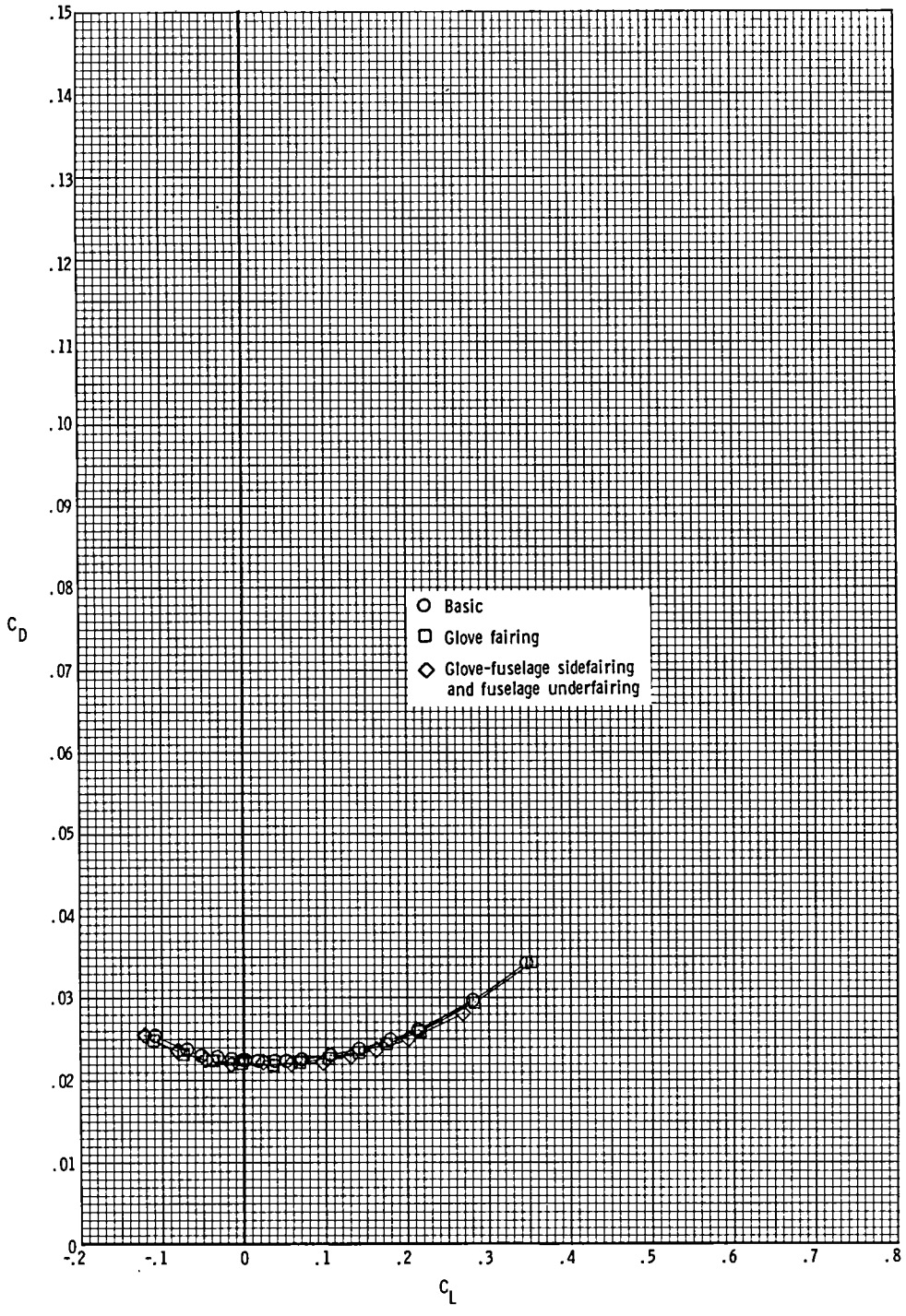

(e) Drag coefficient at M = 0.85.

Figure 31.- Continued.

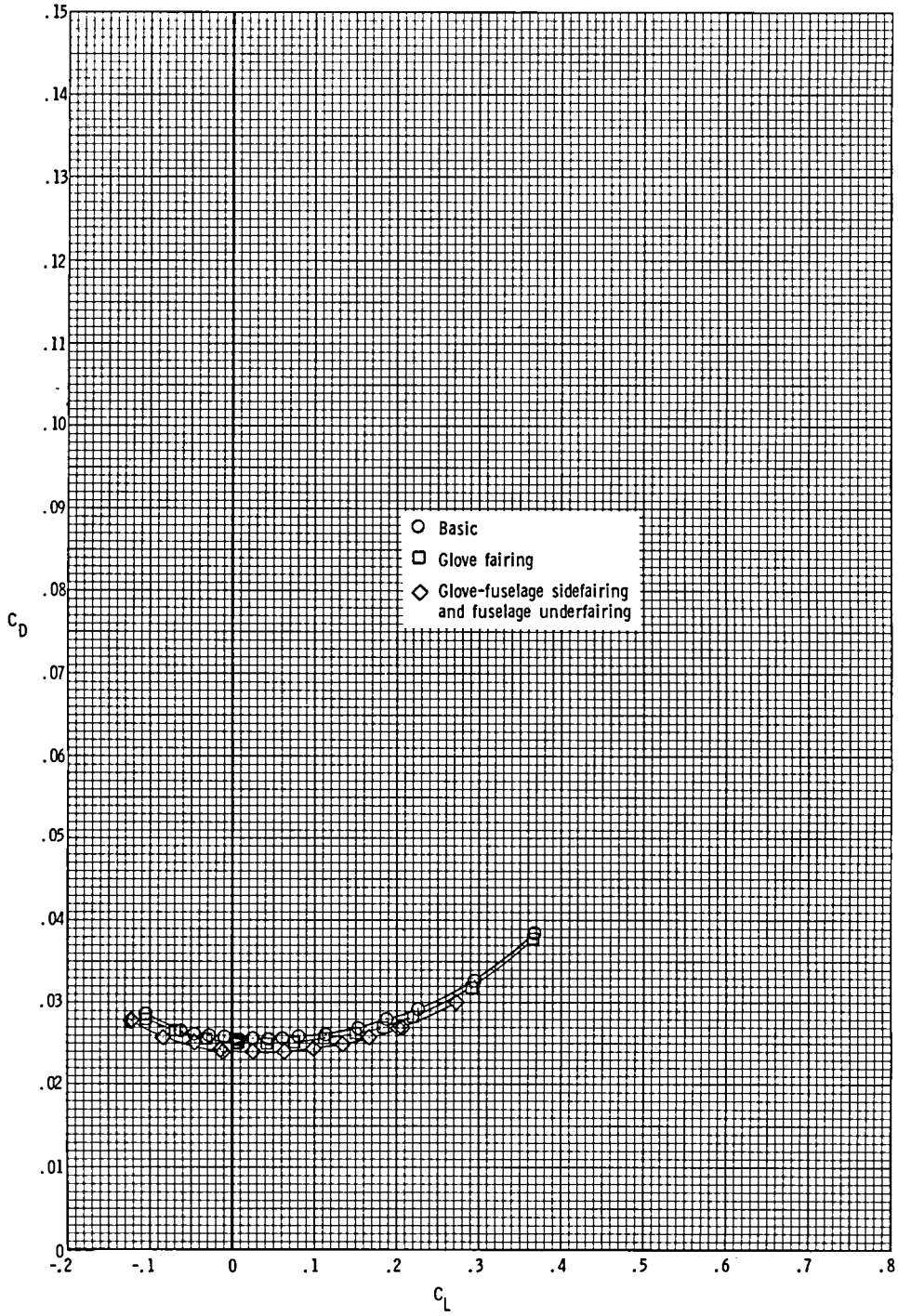

(f) Drag coefficient at M = 0.90.

Figure 31.- Continued.

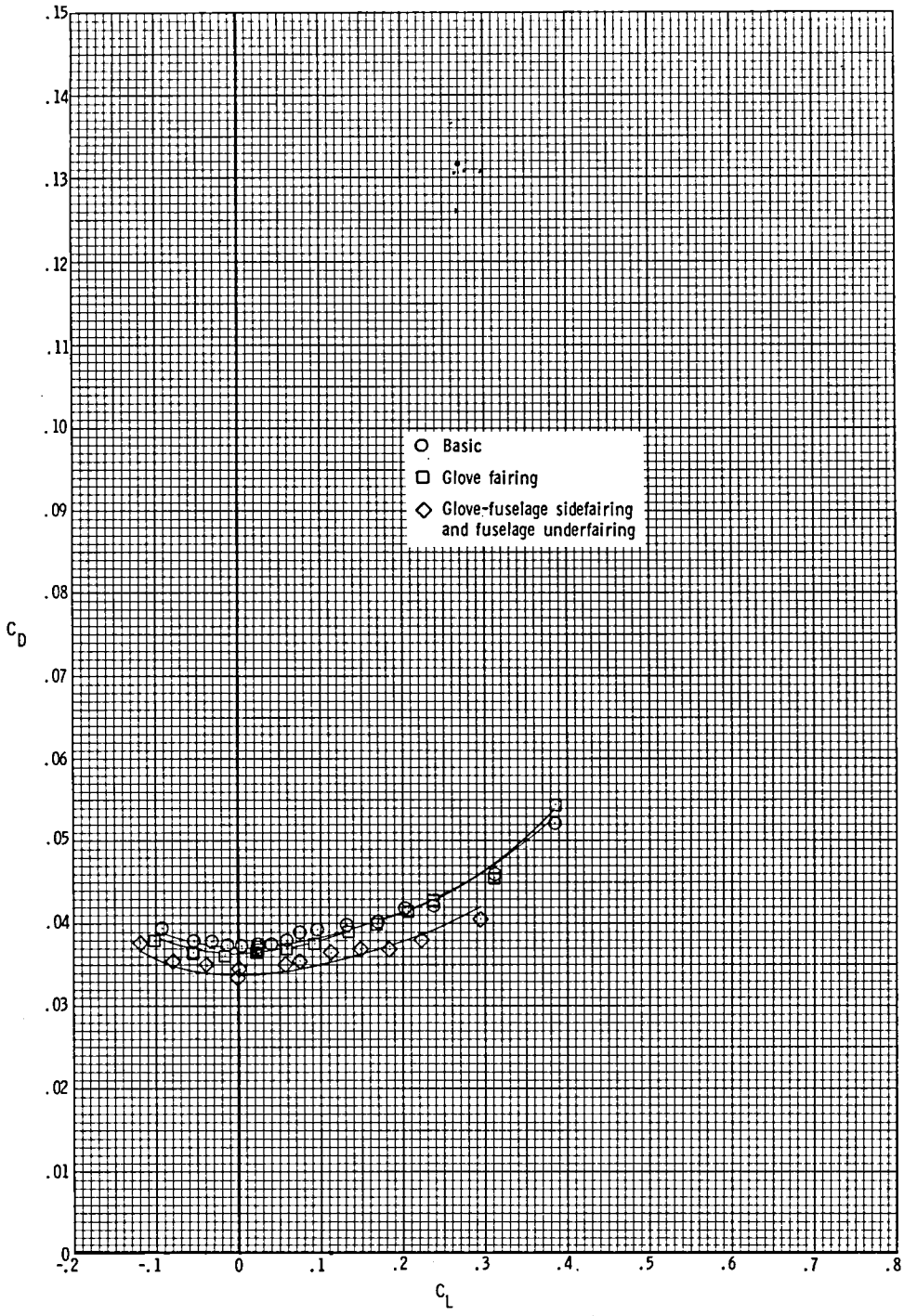

(g) Drag coefficient at M = 0.95.

Figure 31.- Concluded.

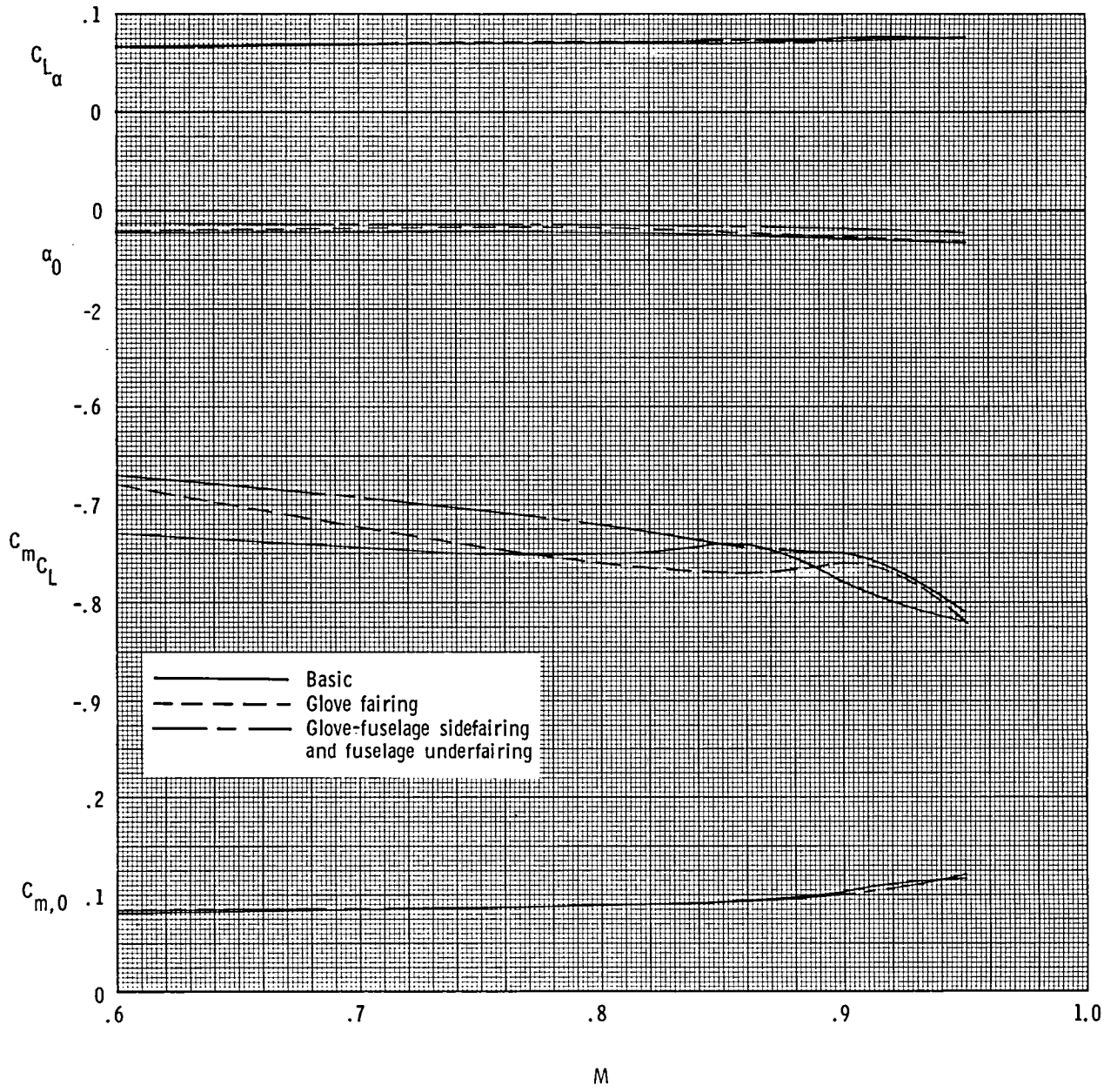

(a) C_{L_α}, α_0, $C_{m_{C_L}}$, and $C_{m,0}$.

Figure 32.- Effect of fairing the upper surface of the wing glove and the fuselage on model longitudinal parameters for model with cruise nozzles, short interfairing, and wings swept 65°.

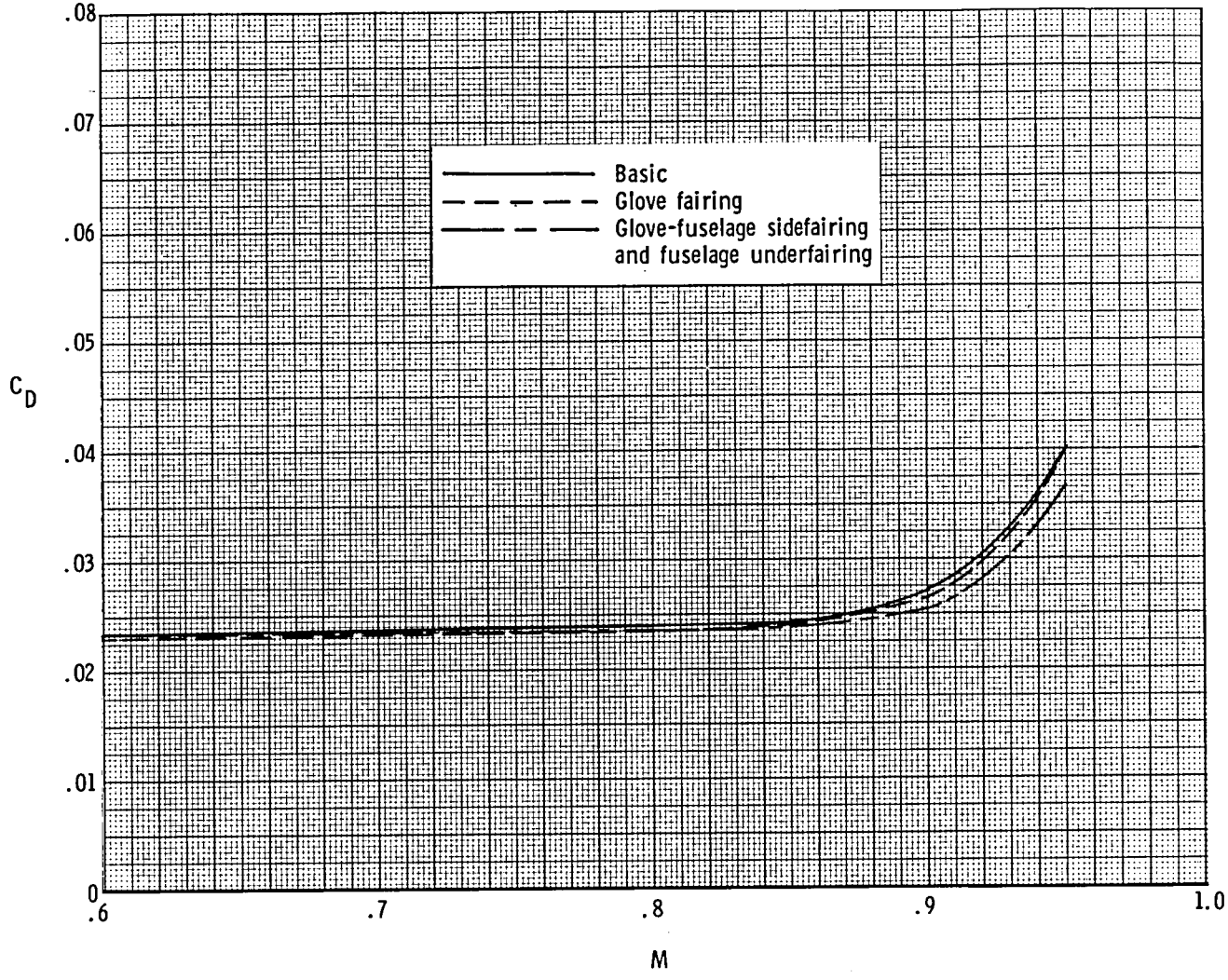

(b) Drag coefficient at $C_L = 0.16$.

Figure 32.- Concluded.

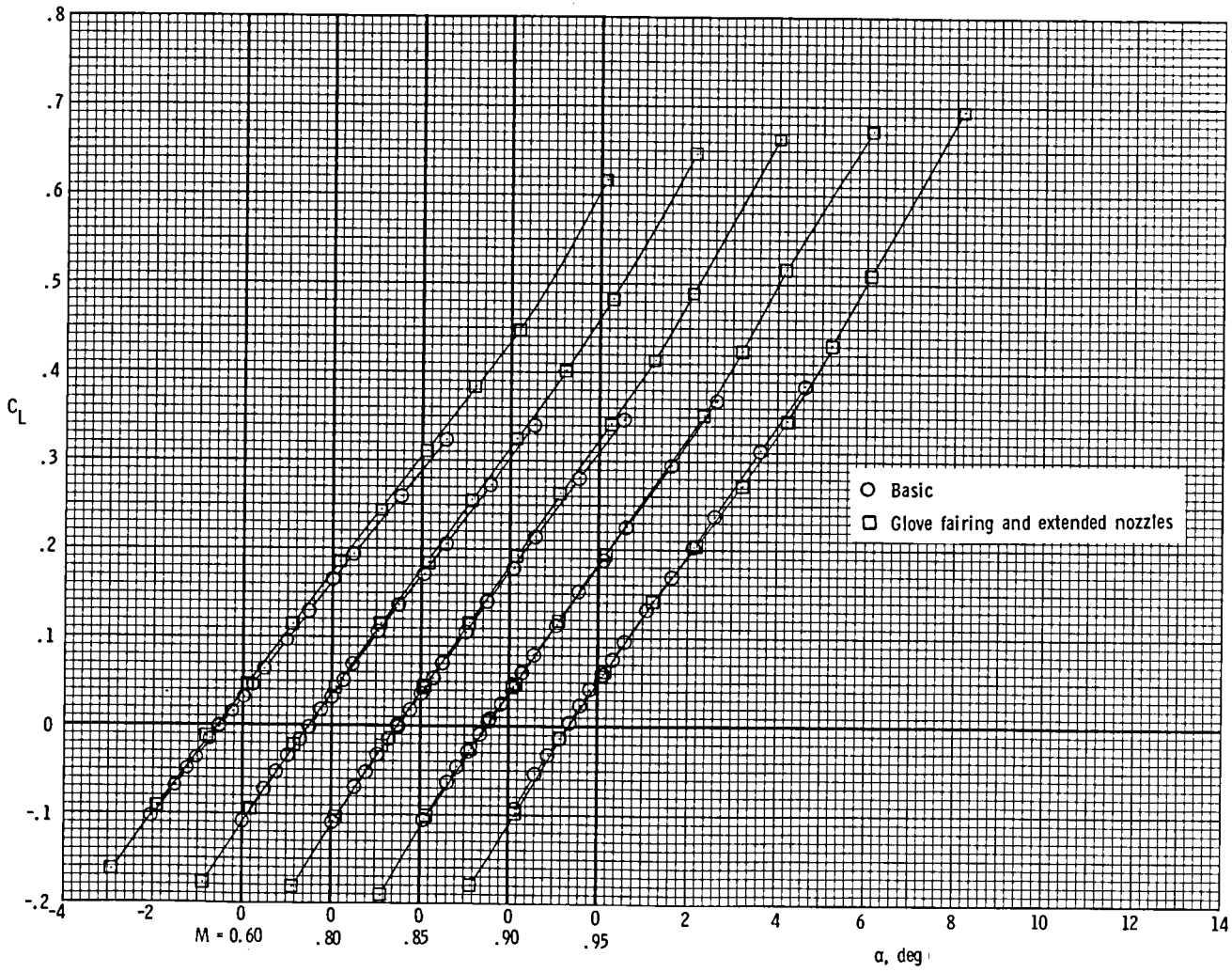

(a) Lift coefficient.

Figure 33.- Combined effect of fairing the upper surface of the wing glove and extending the nozzles on longitudinal aerodynamic characteristics of the model with cruise nozzles, short interfairing, and wings swept 65°.

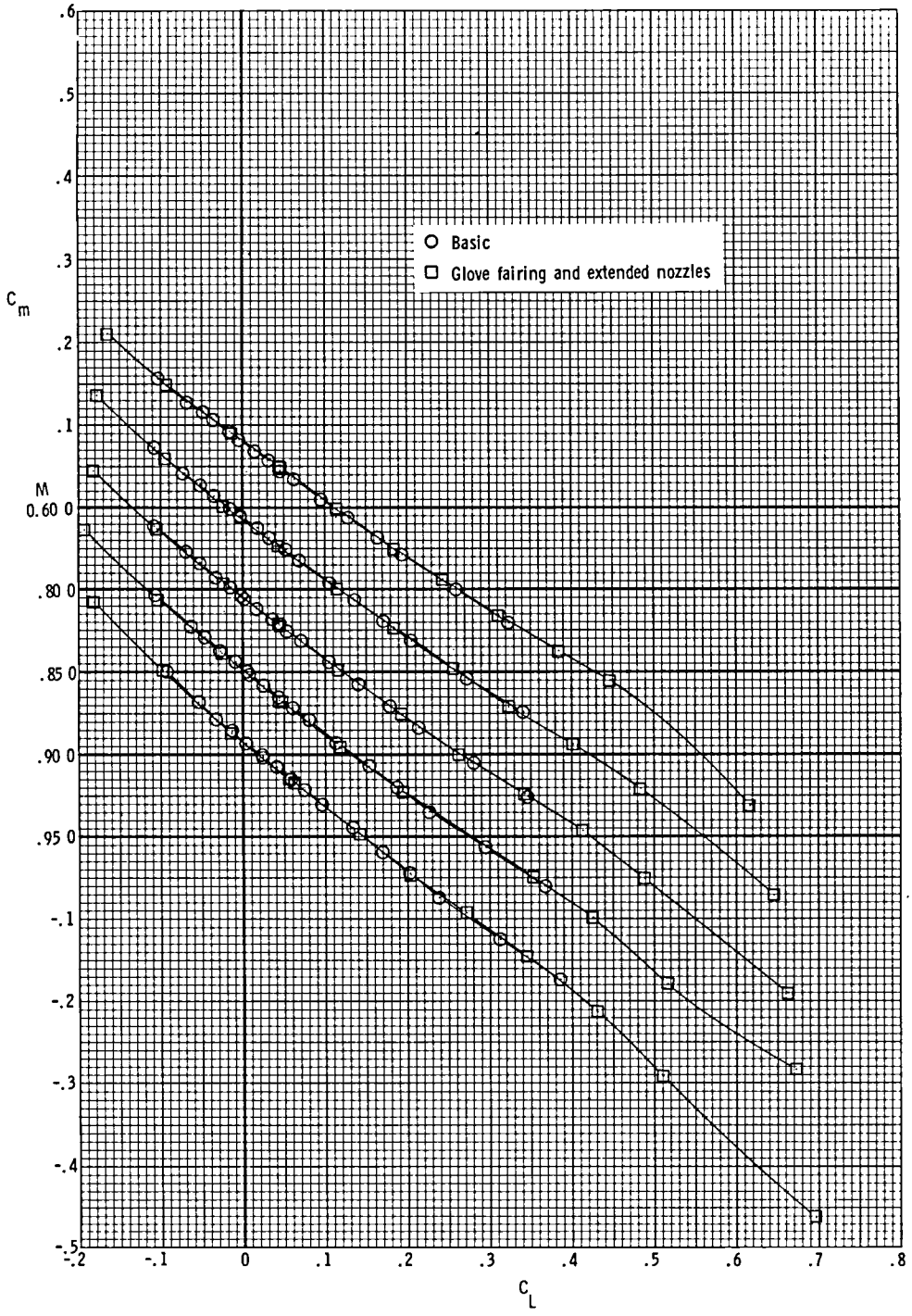

(b) Pitching-moment coefficient.

Figure 33.- Continued.

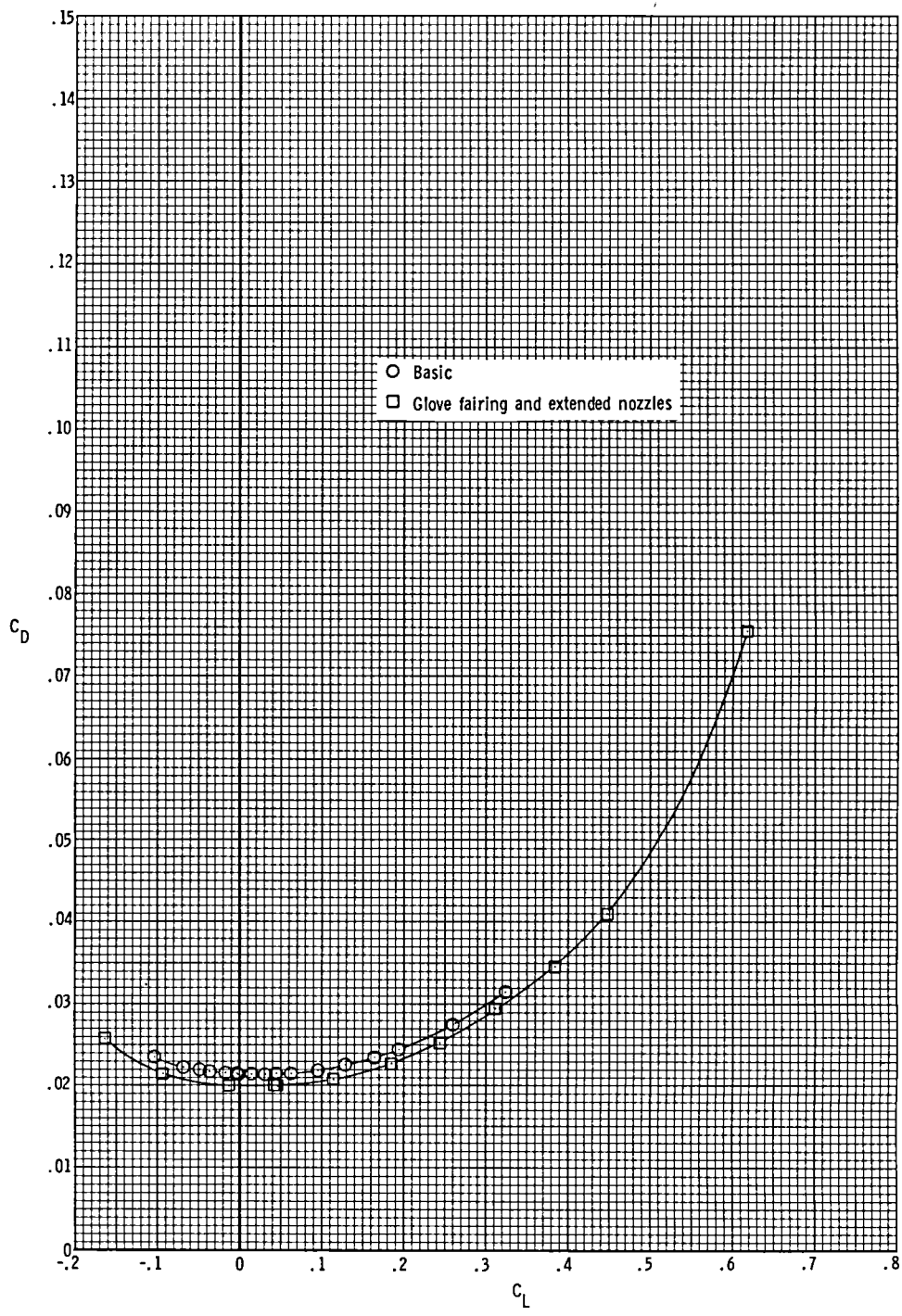

(c) Drag coefficient at M = 0.60.

Figure 33.- Continued.

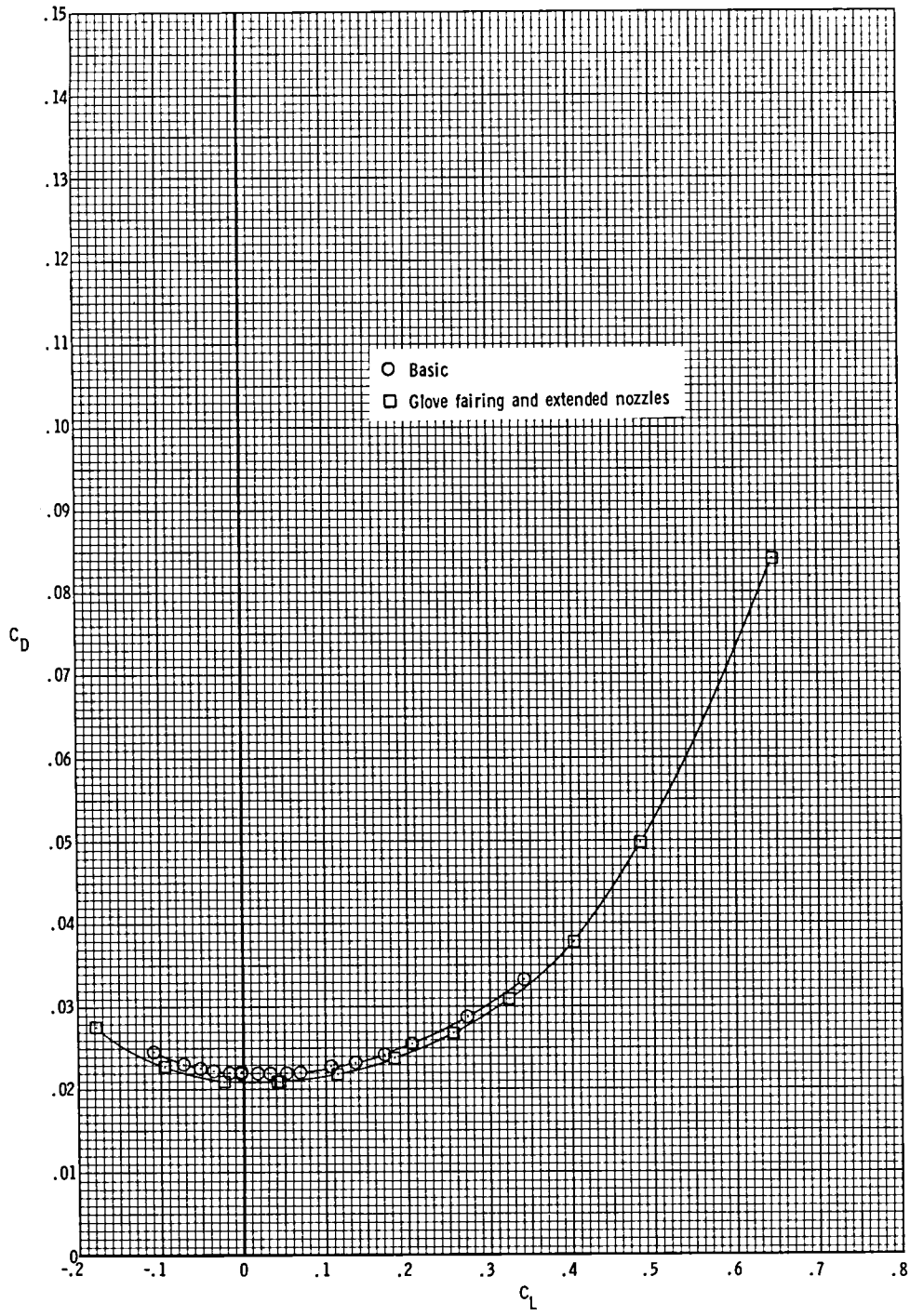

(d) Drag coefficient at M = 0.80.

Figure 33.- Continued.

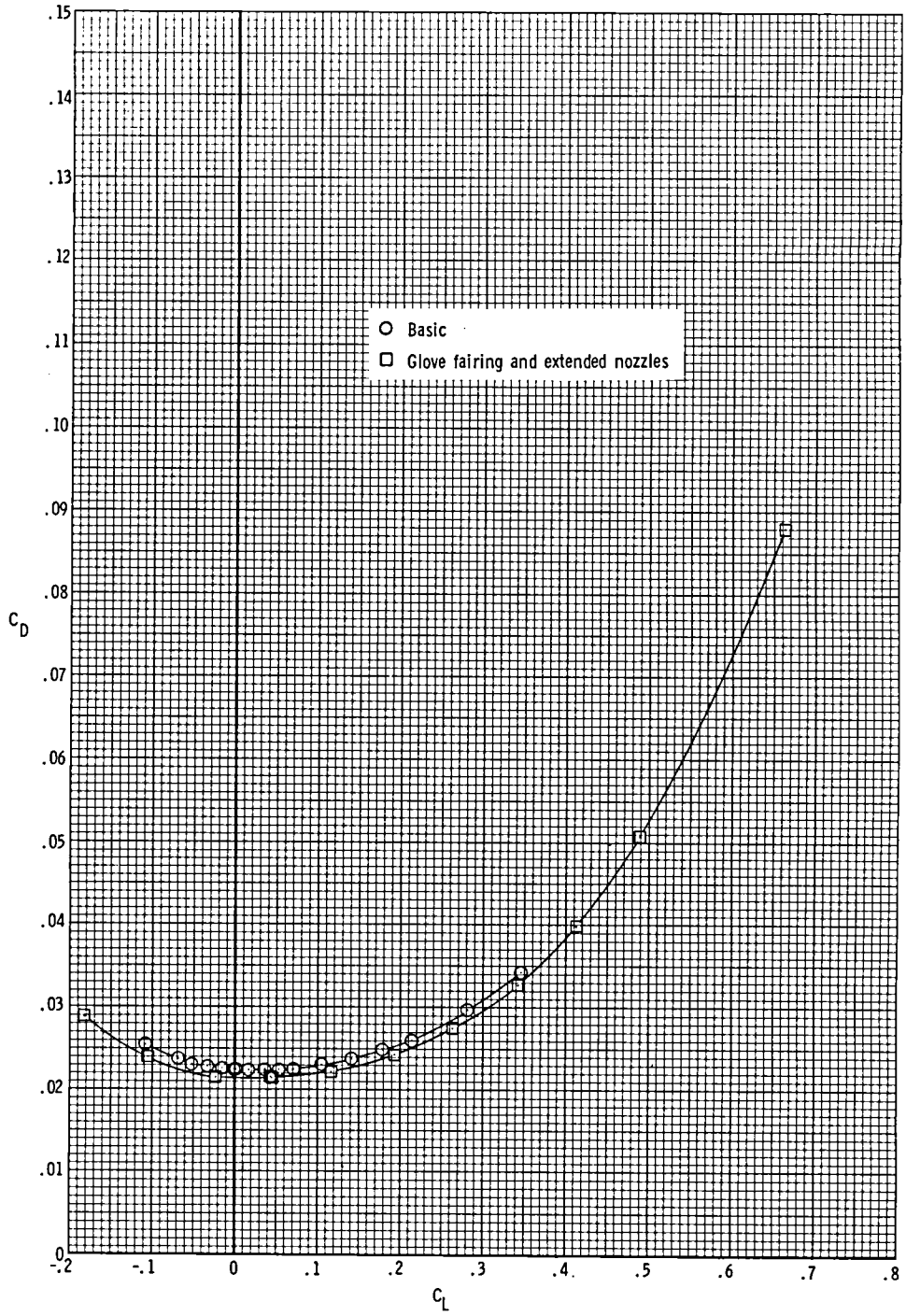

(e) Drag coefficient at M = 0.85.

Figure 33.- Continued.

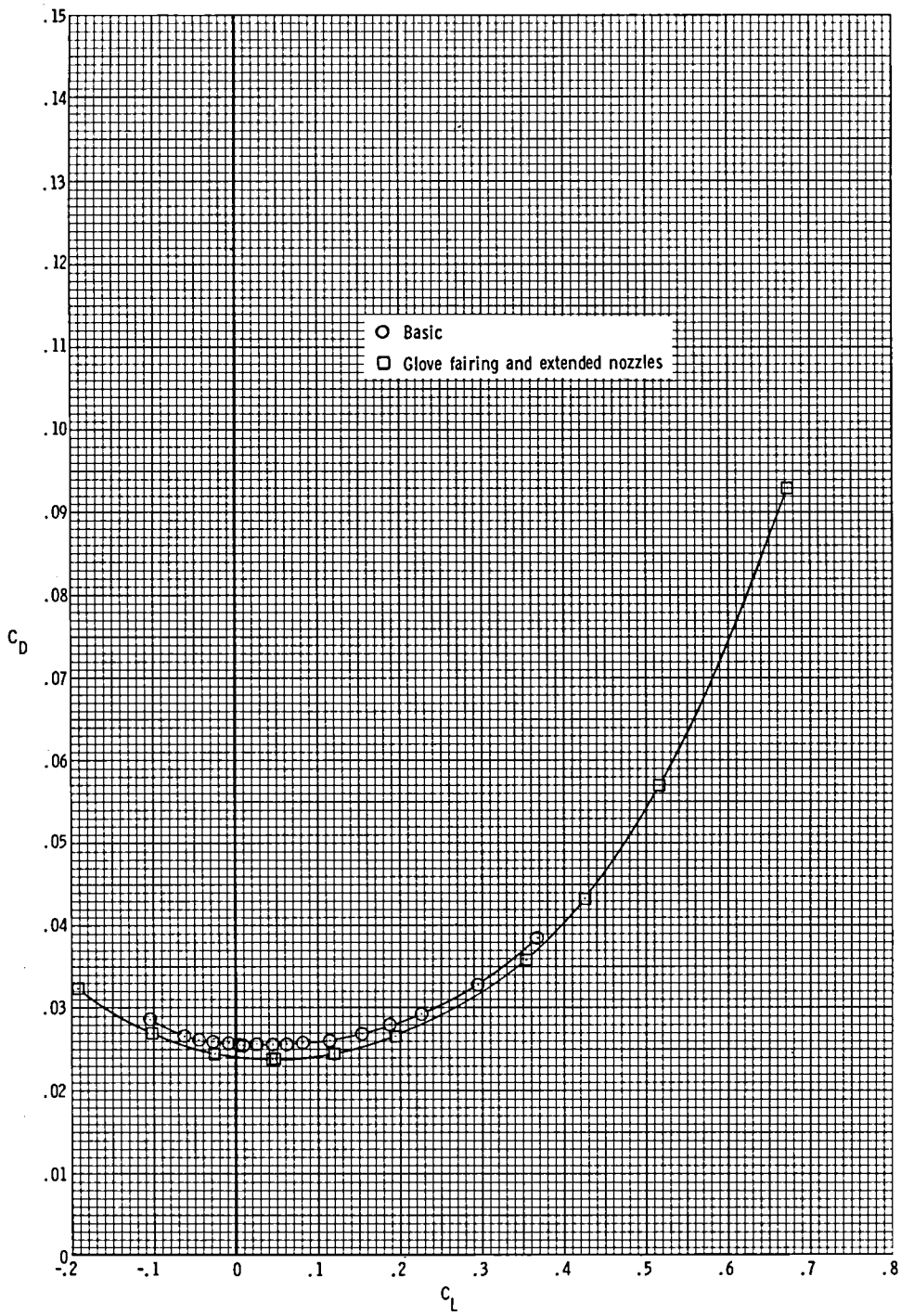

(f) Drag coefficient at M = 0.90.

Figure 33.- Continued.

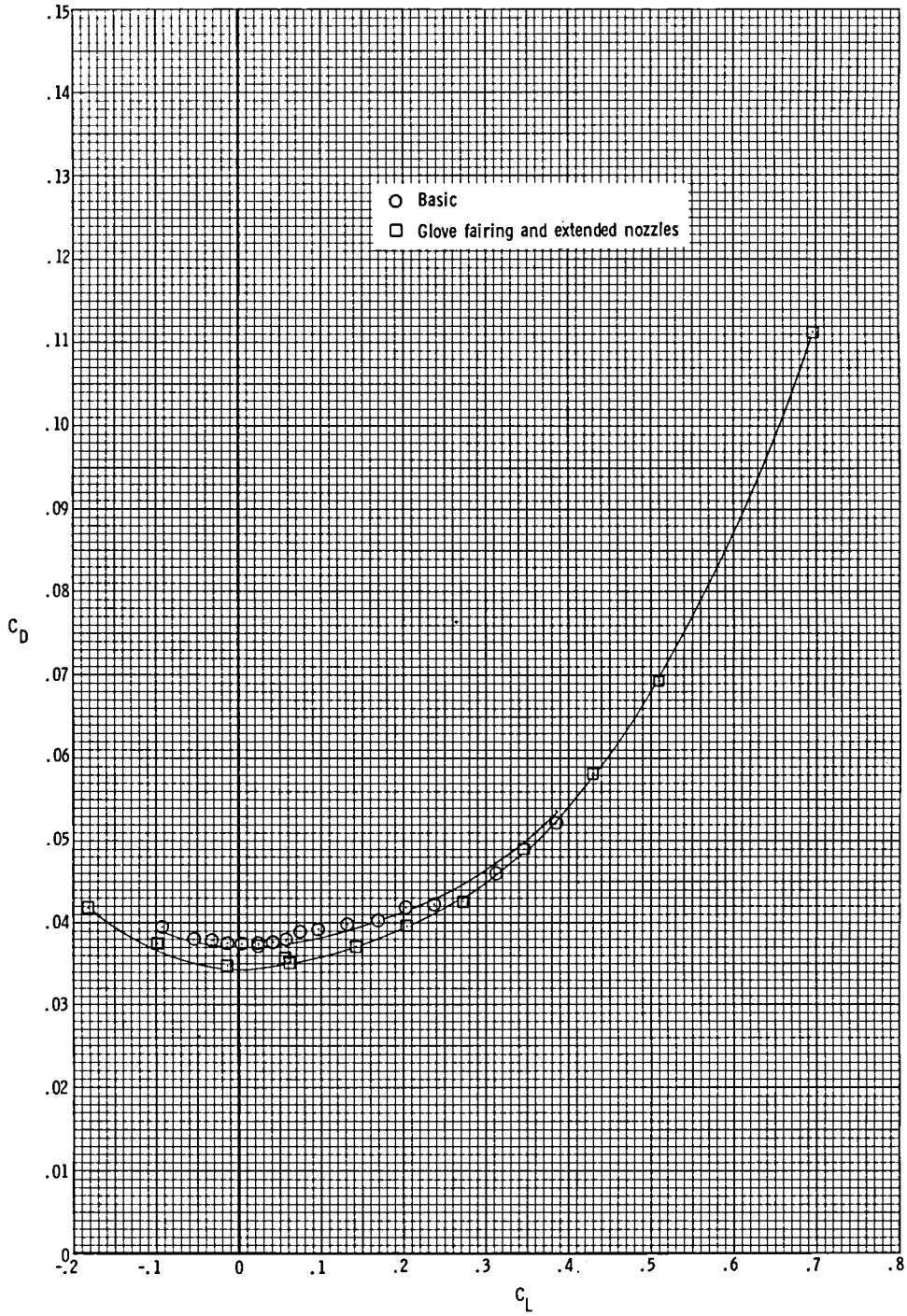

(g) Drag coefficient at M = 0.95.

Figure 33.- Concluded.

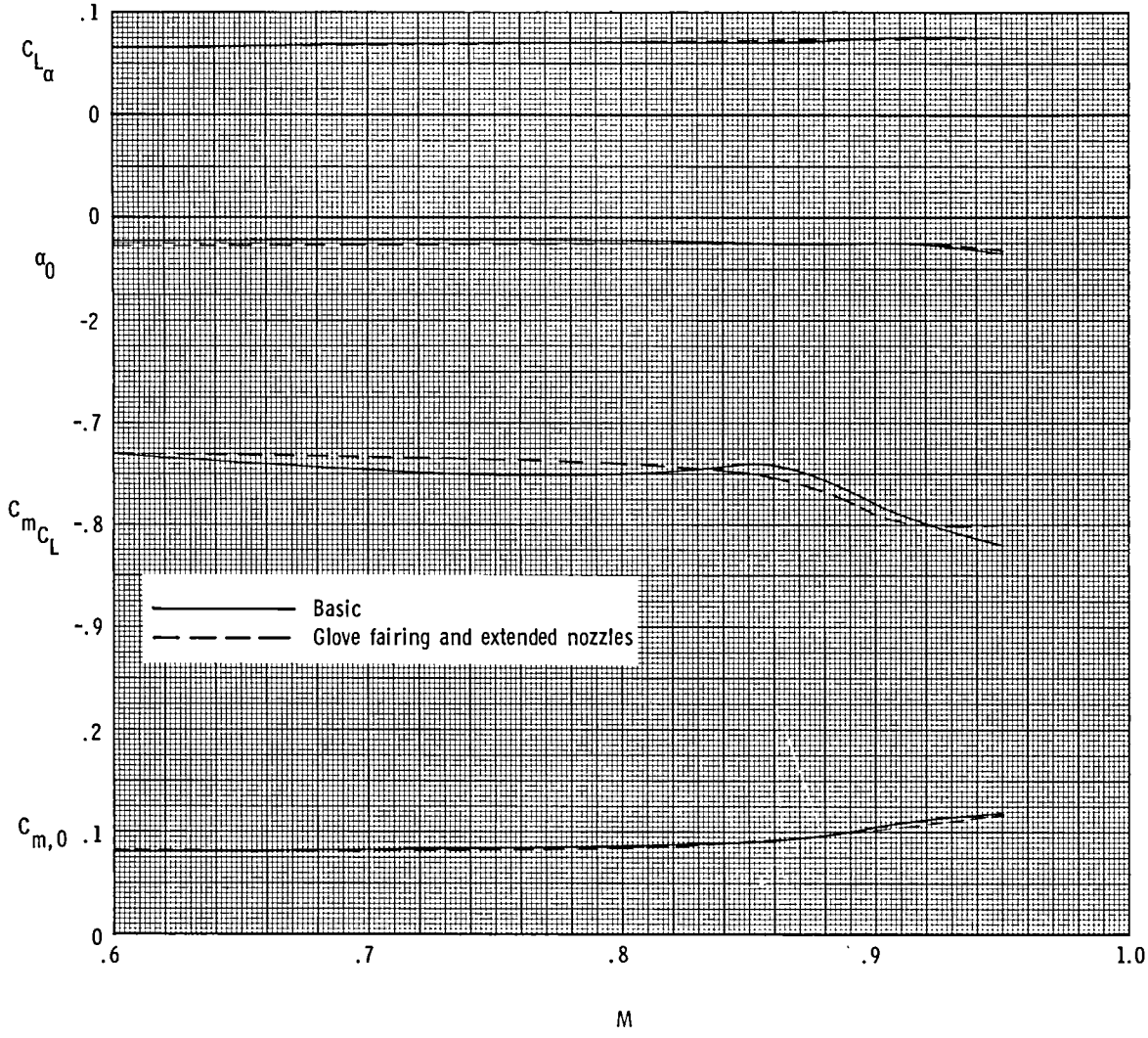

(a) C_{L_α}, α_0, $C_{m_{C_L}}$, and $C_{m,0}$.

Figure 34.- Combined effect of fairing the upper surface of the wing glove and extending the nozzles on model longitudinal parameters for model with cruise nozzles, short interfairing, and wings swept 65°.

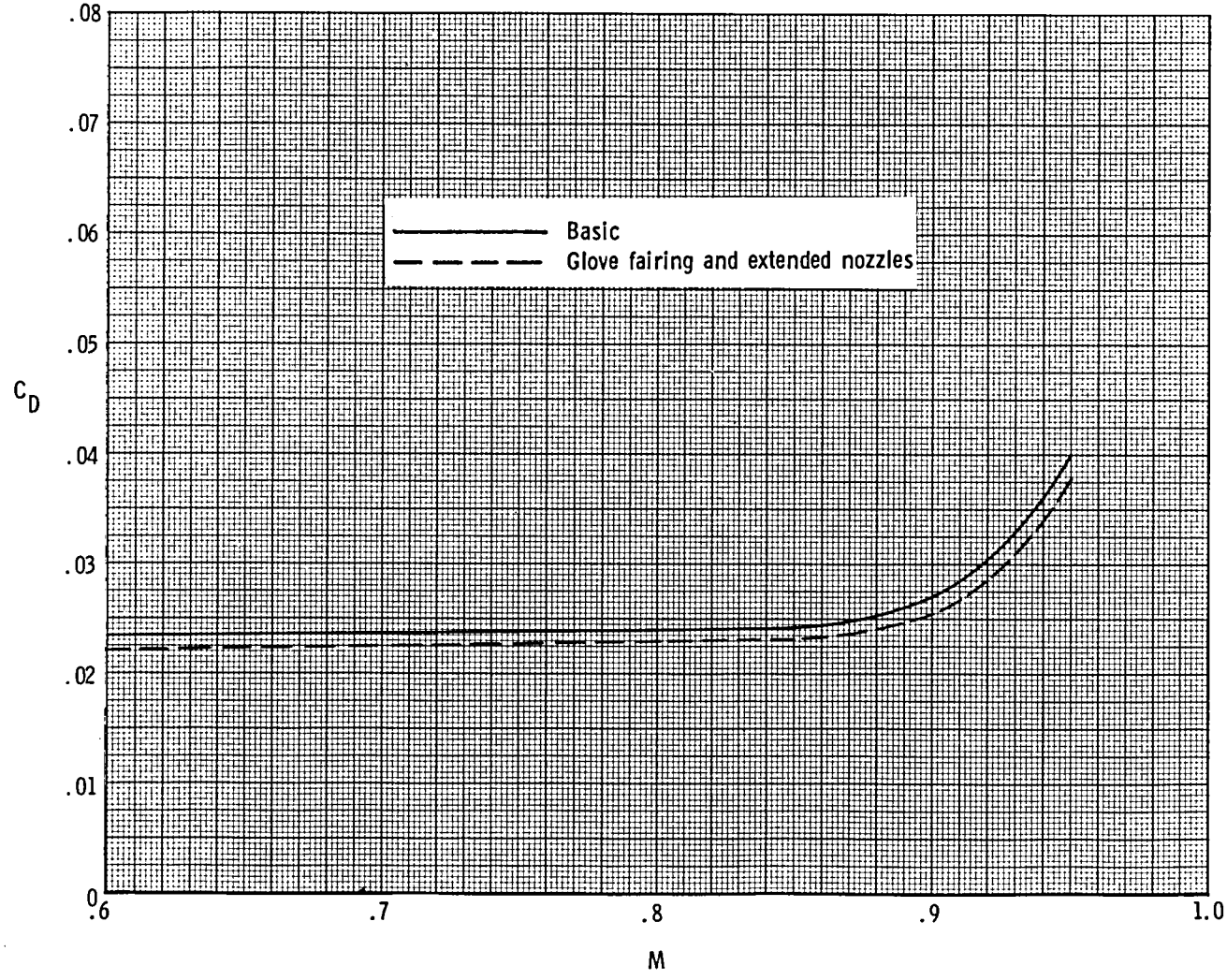

(b) Drag coefficient at $C_L = 0.16$.

Figure 34.- Concluded.

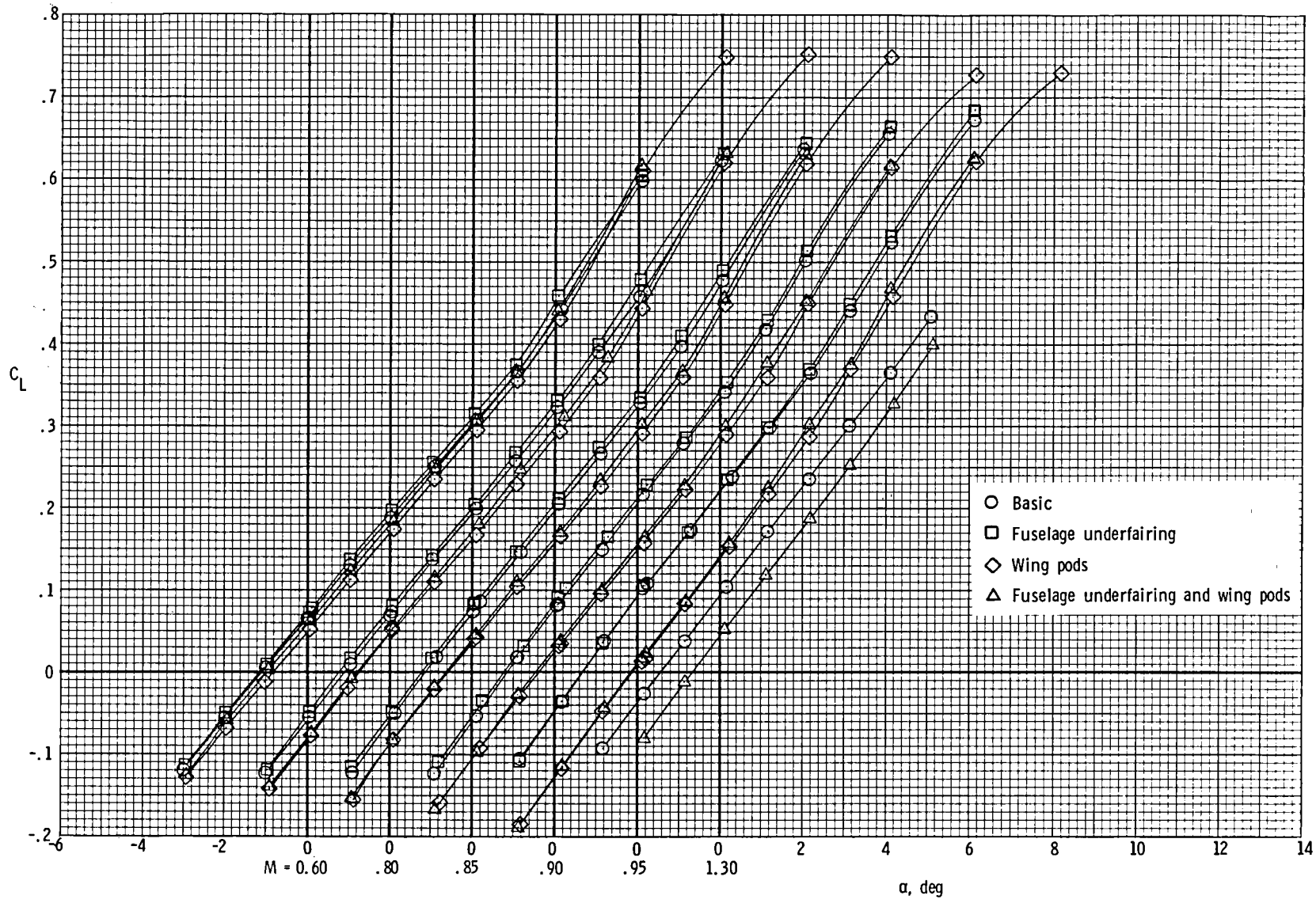

(a) Lift coefficient.

Figure 35.- Effect of fuselage underfairing and wing pods on longitudinal aerodynamic characteristics of the model with cruise nozzles, short interfairing, and wings swept 67.5°.

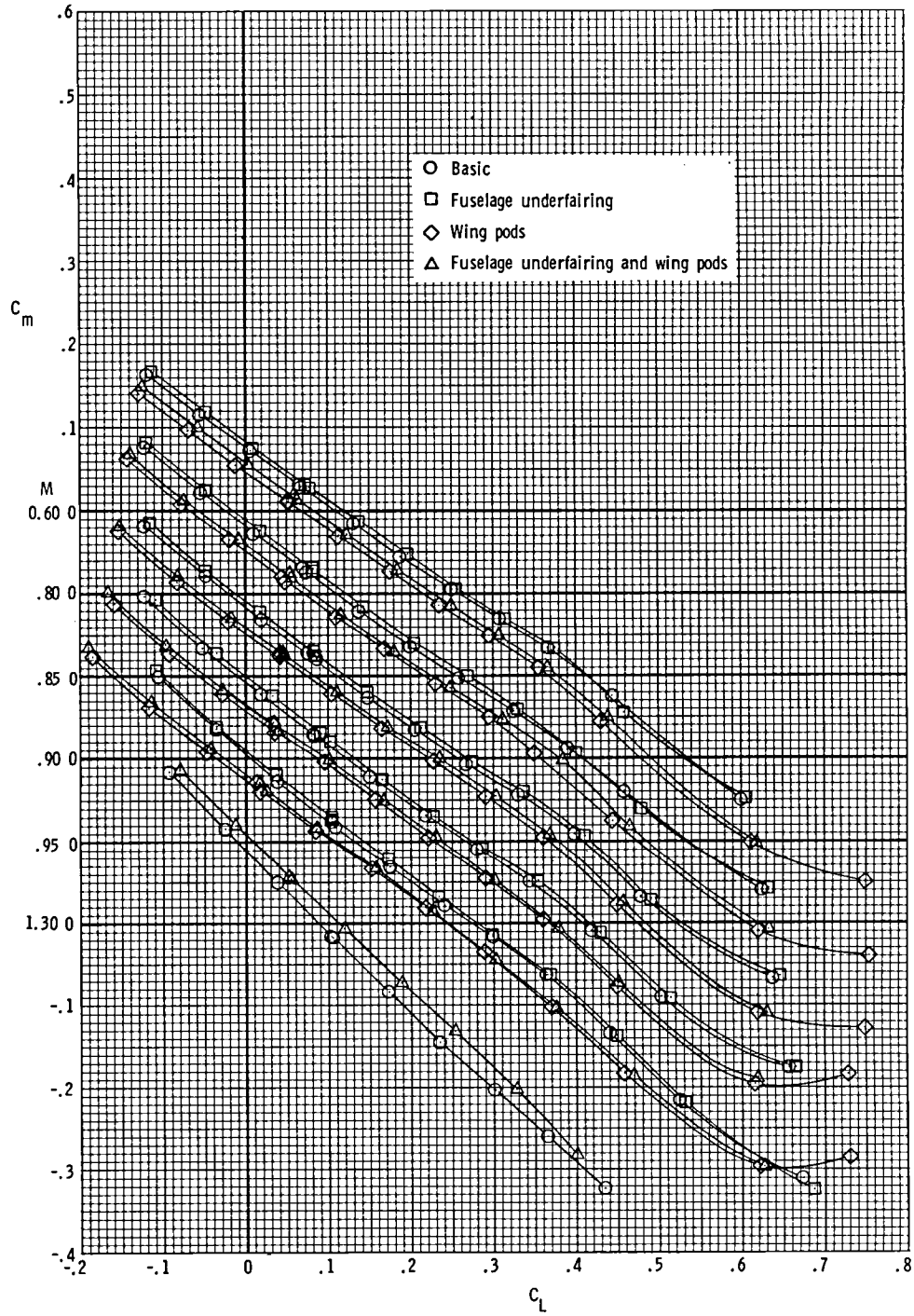

(b) Pitching-moment coefficient.

Figure 35.- Continued.

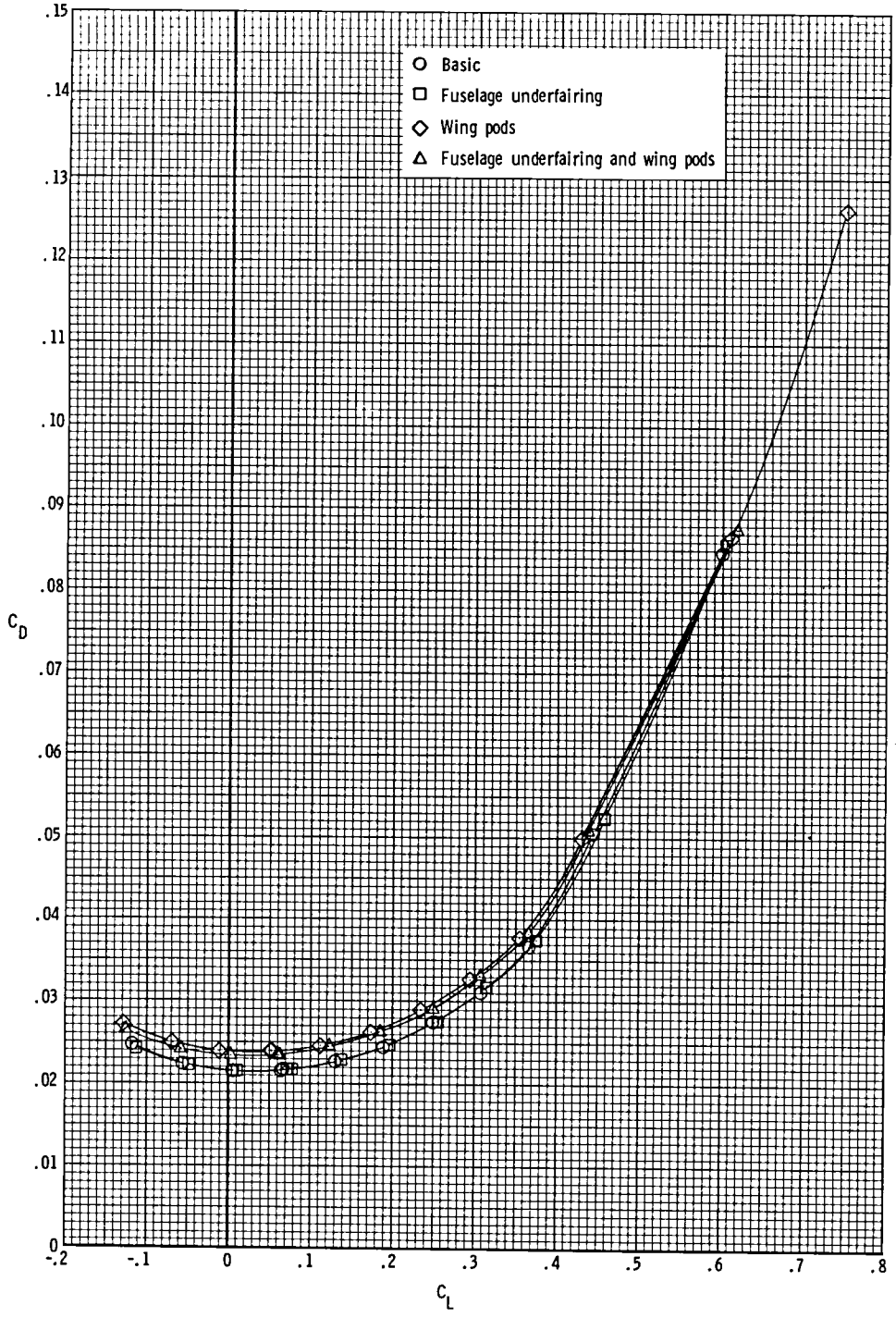

(c) Drag coefficient at M = 0.60.

Figure 35.- Continued.

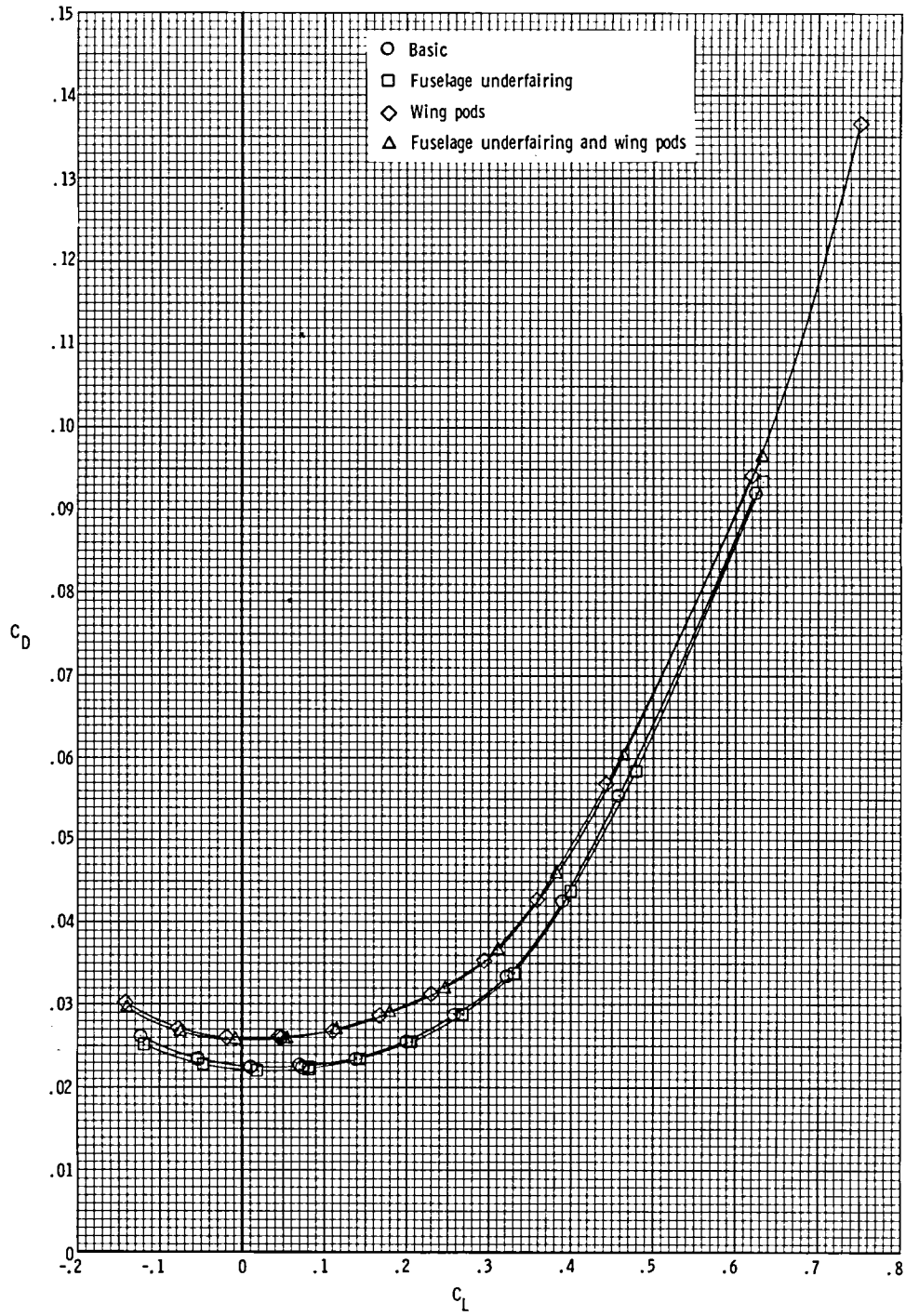

(d) Drag coefficient at M = 0.80.

Figure 35.- Continued.

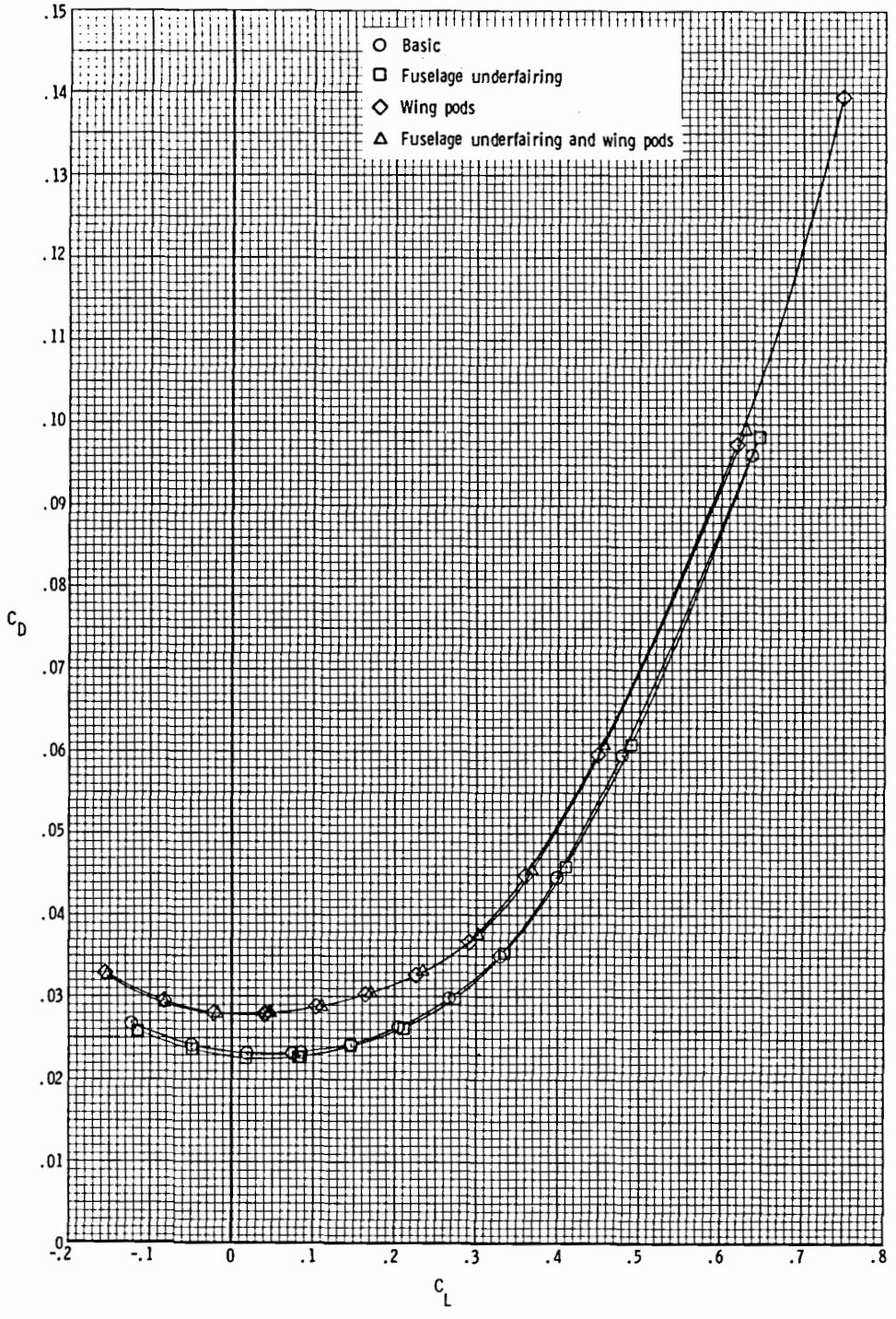

(e) Drag coefficient at M = 0.85.

Figure 35.- Continued.

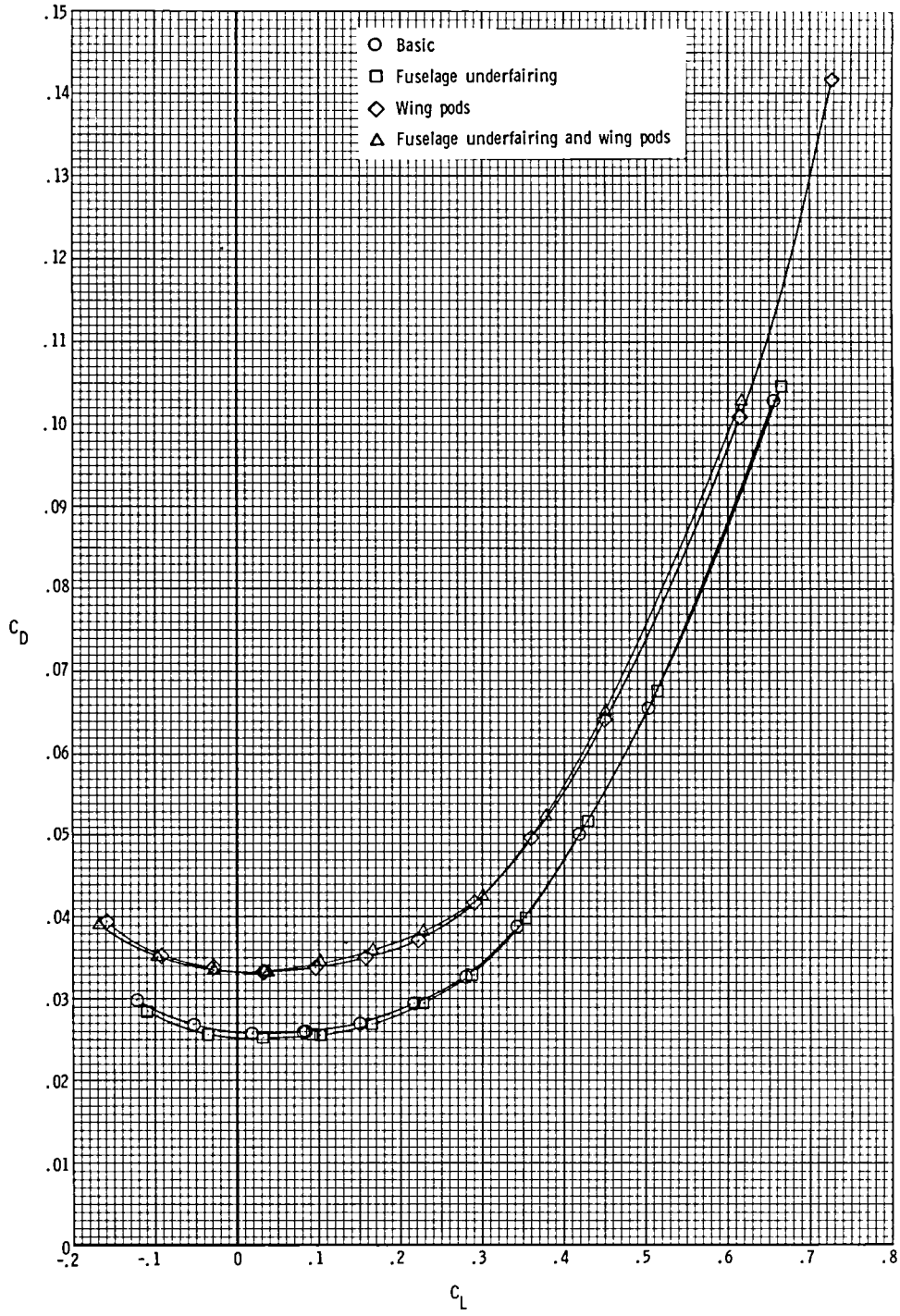

(f) Drag coefficient at M = 0.90.

Figure 35.- Continued.

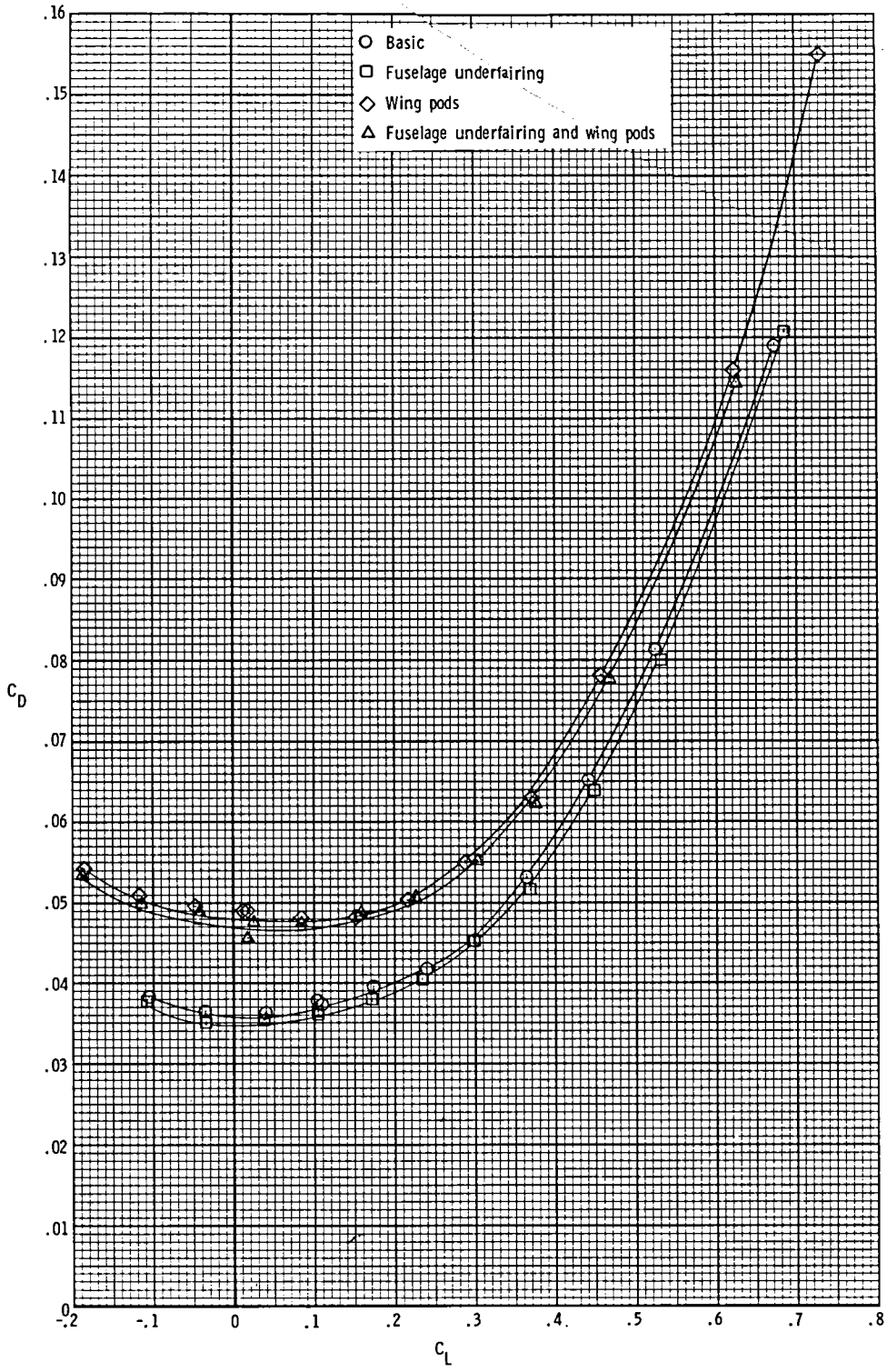

(g) Drag coefficient at M = 0.95.

Figure 35.- Continued.

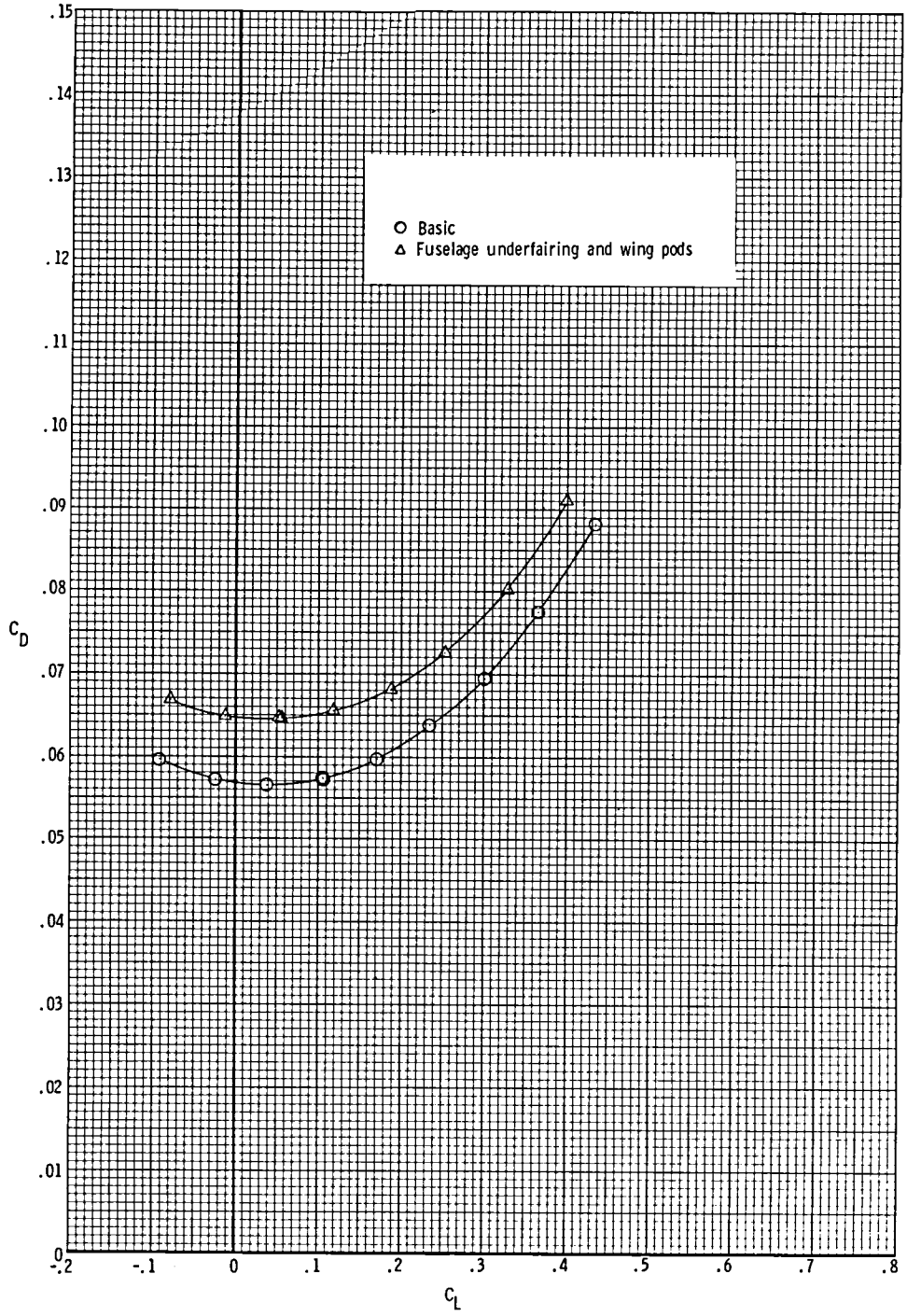

(h) Drag coefficient at M = 1.30.

Figure 35.- Concluded.

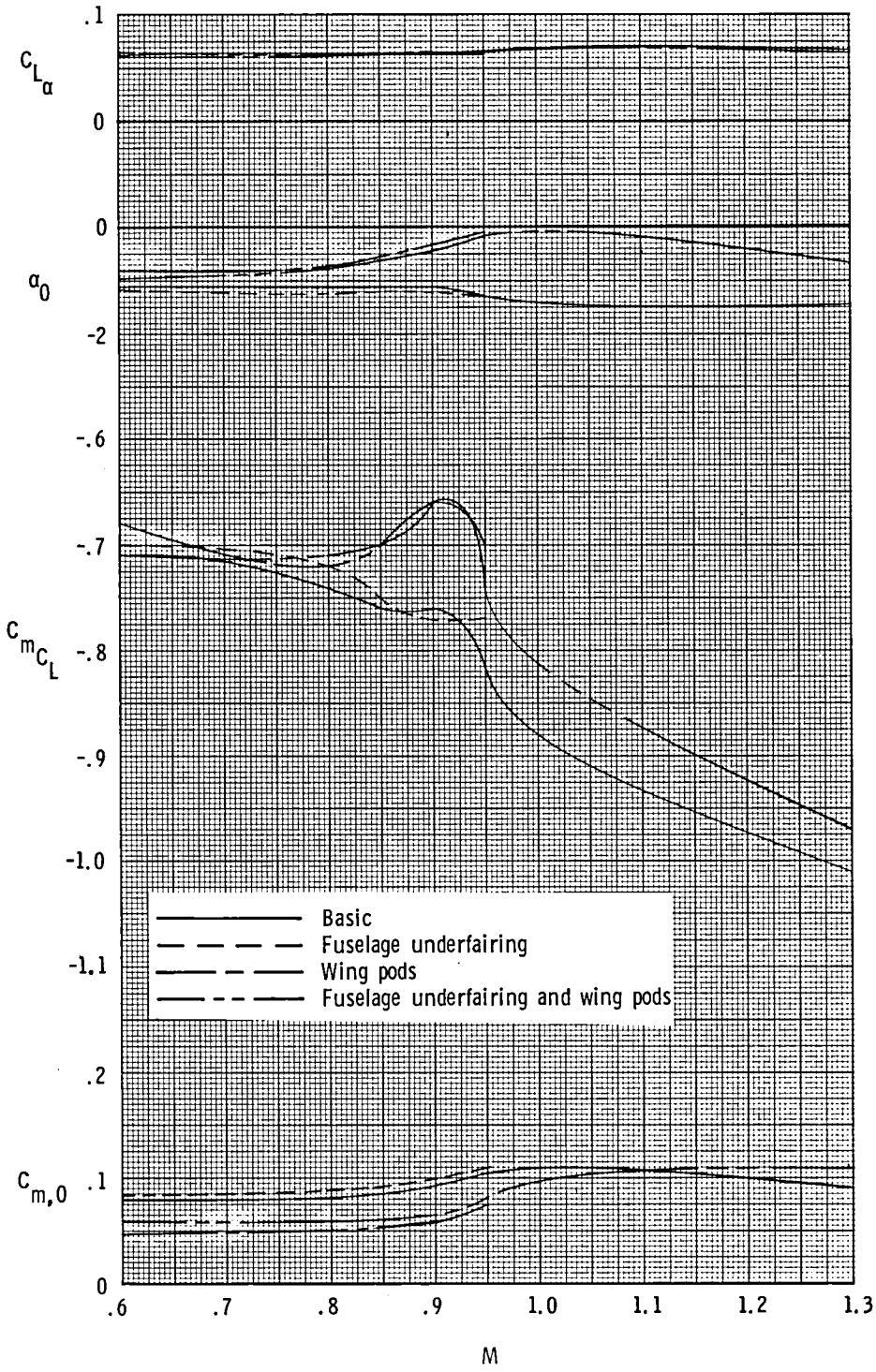

(a) C_{L_α}, α_0, $C_{m_{C_L}}$, and $C_{m,0}$.

Figure 36.- Effect of fuselage underfairing and wing pods on model longitudinal parameters for model with cruise nozzles, short interfairing, and wings swept 67.5°.

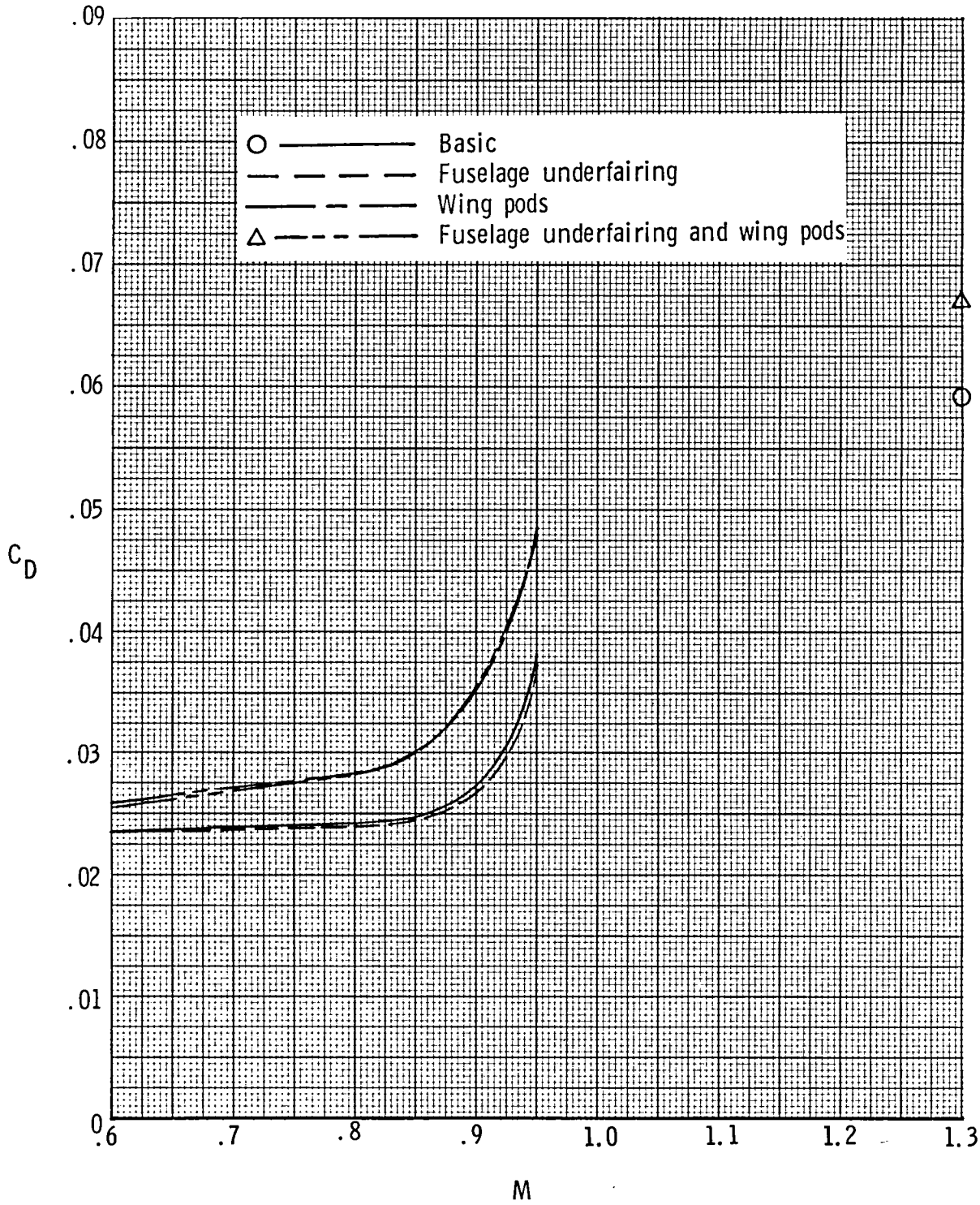

(b) Drag coefficient at $C_L = 0.16$.

Figure 36.- Concluded.

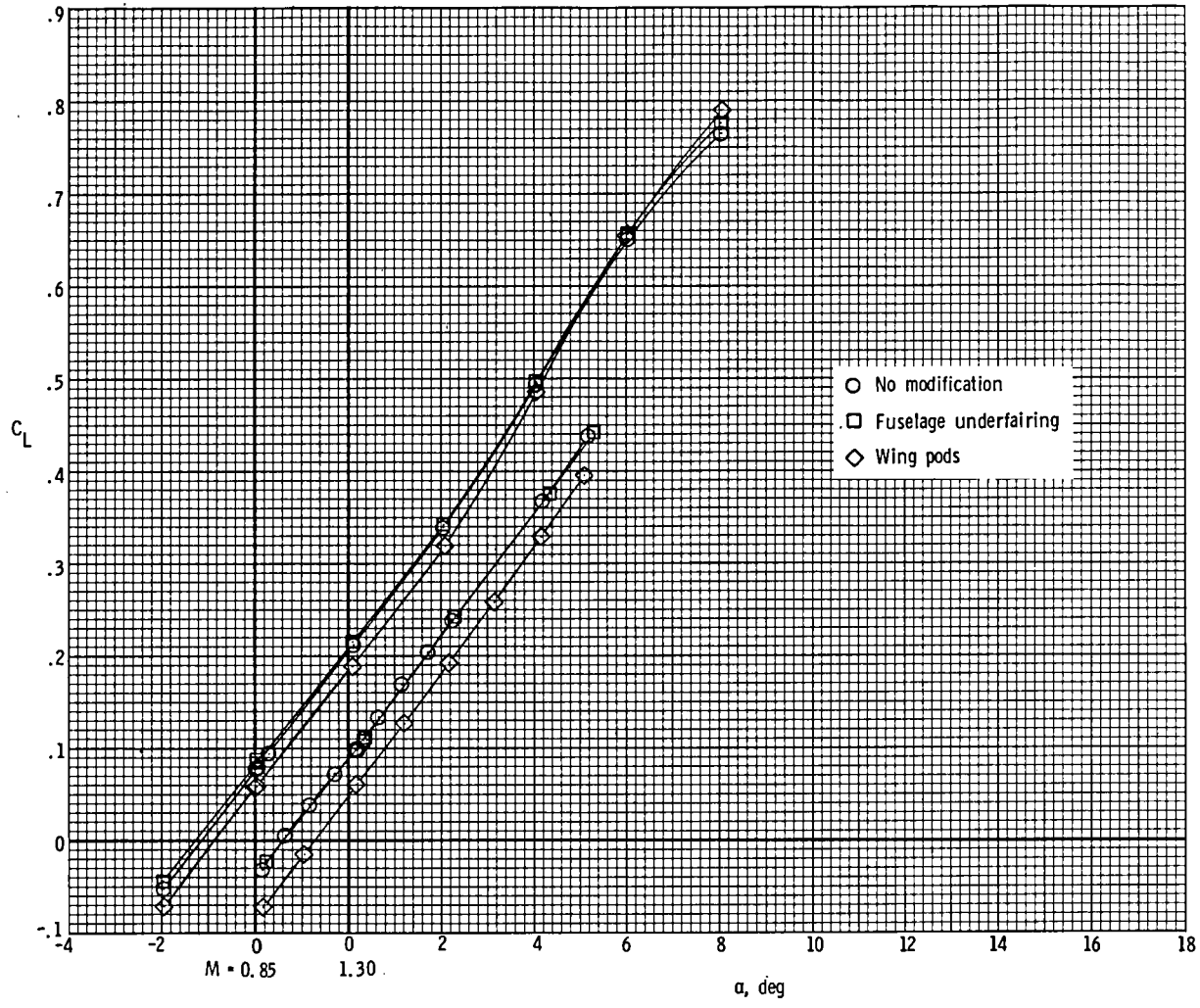

(a) Lift coefficient.

Figure 37.- Effect of fuselage underfairing and wing pods on the longitudinal aerodynamic characteristics of the model with aero-reference nozzles, short interfairing, and wings swept 67.5°.

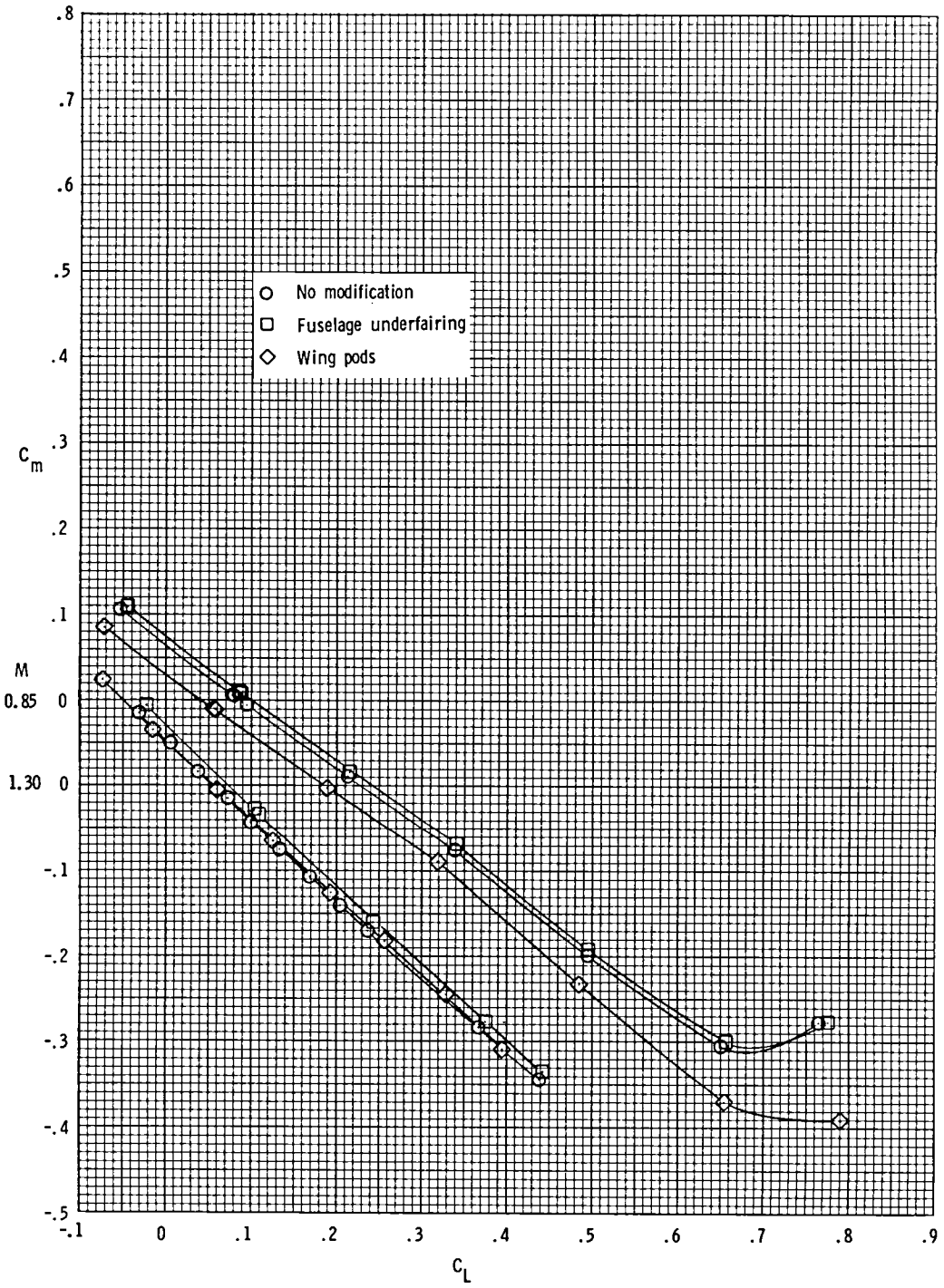

(b) Pitching-moment coefficient.

Figure 37.- Continued.

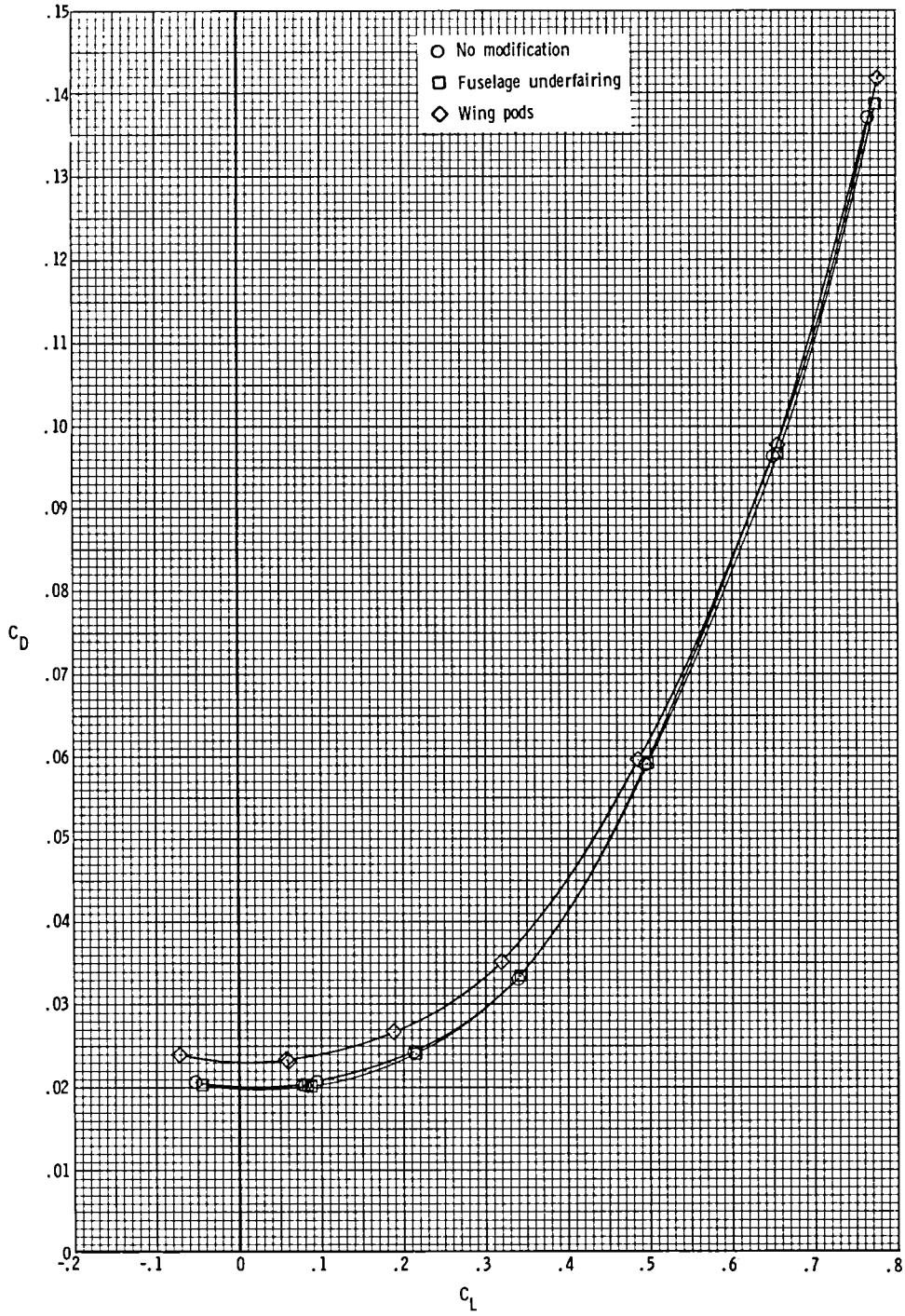

(c) Drag coefficient at M = 0.85.

Figure 37.- Continued.

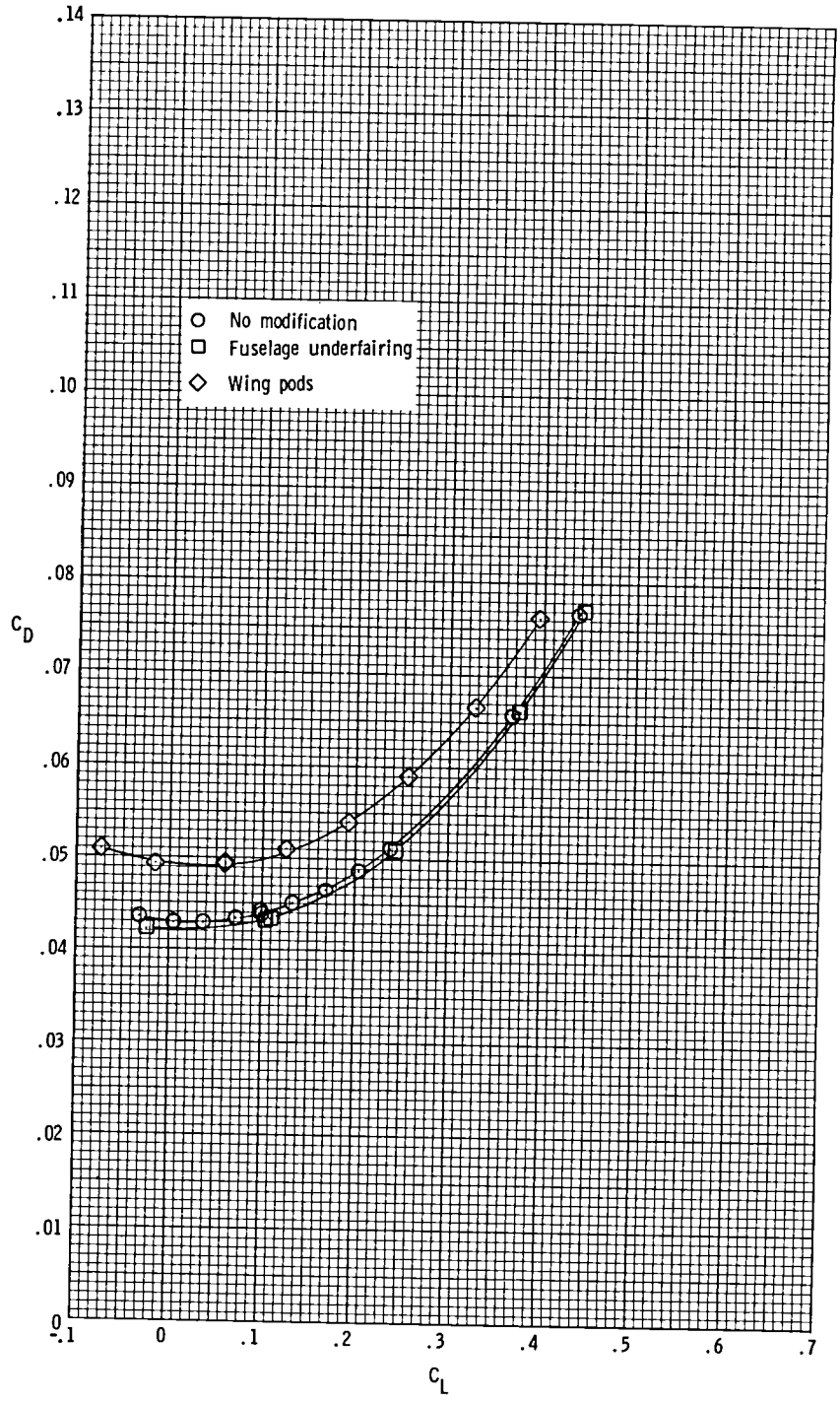

(d) Drag coefficient at M = 1.30.

Figure 37.- Concluded.

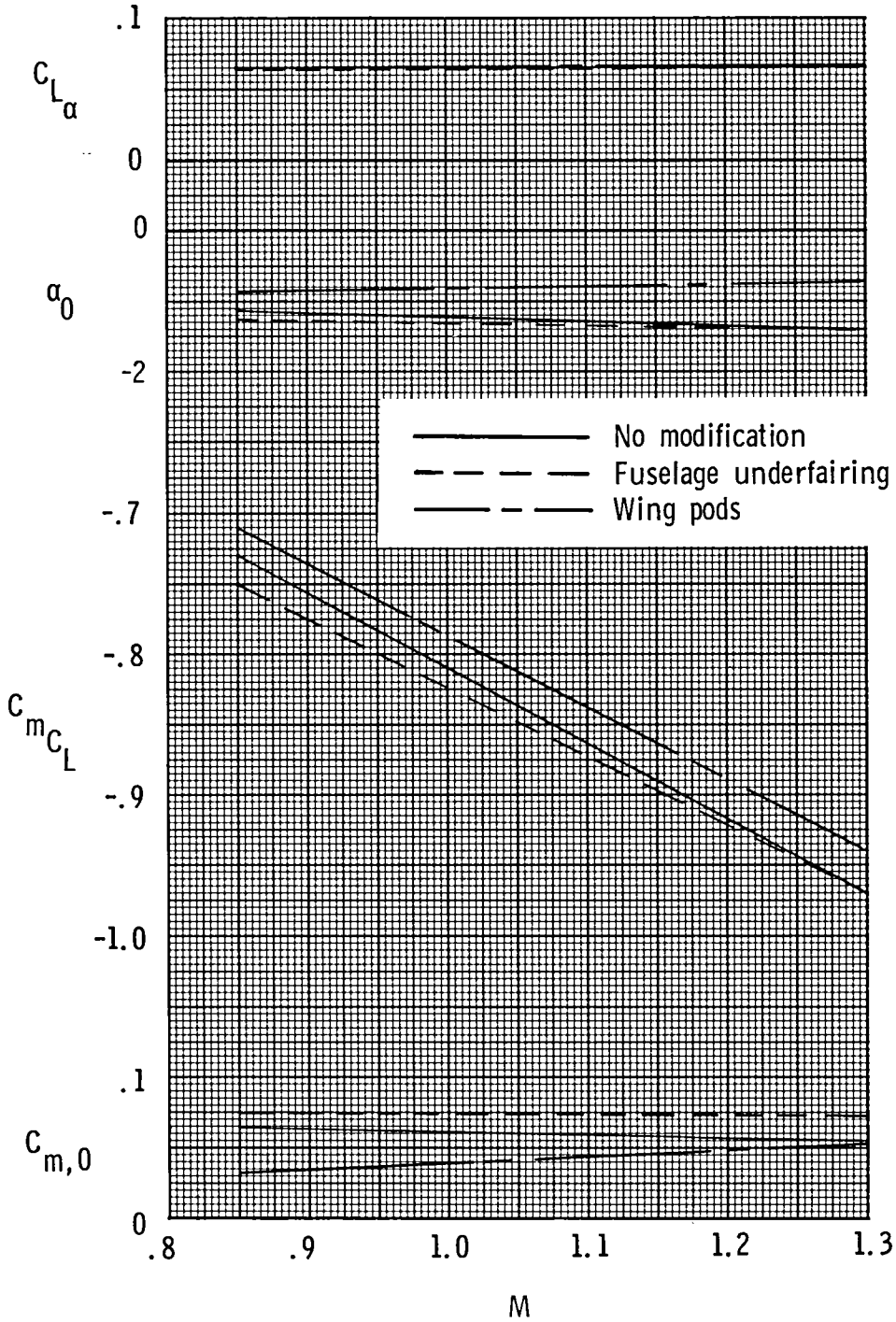

Figure 38.- Effect of fuselage underfairing and wing pods on model longitudinal parameters for model with aero-reference nozzles, short interfairing, and wings swept 67.5°. (Data for two Mach numbers only and faired with a straight line.)

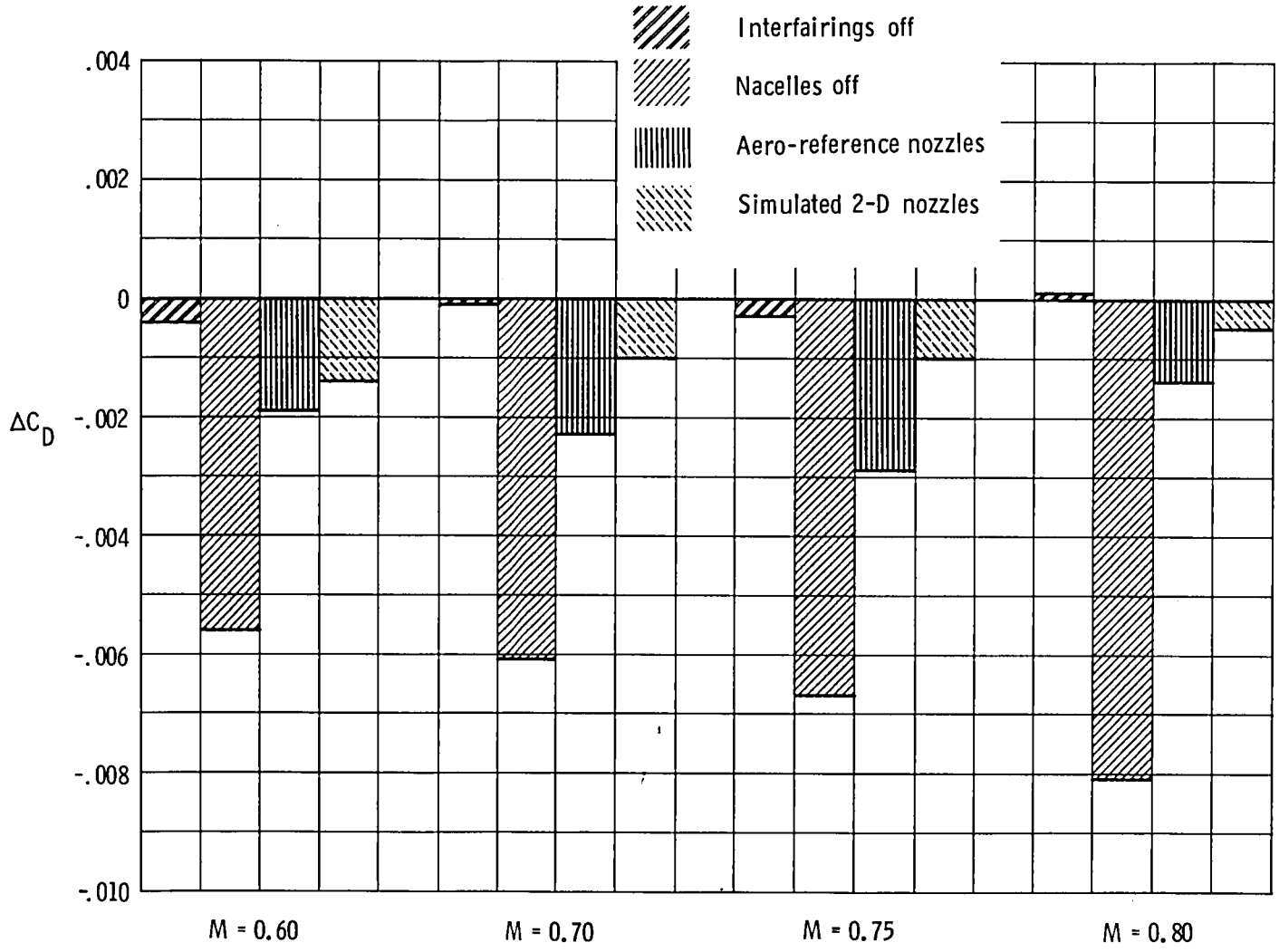

Figure 39.- Effect of nacelles and nozzle shape on incremental drag at $C_L = 0.63$ for model with wings swept 25°.

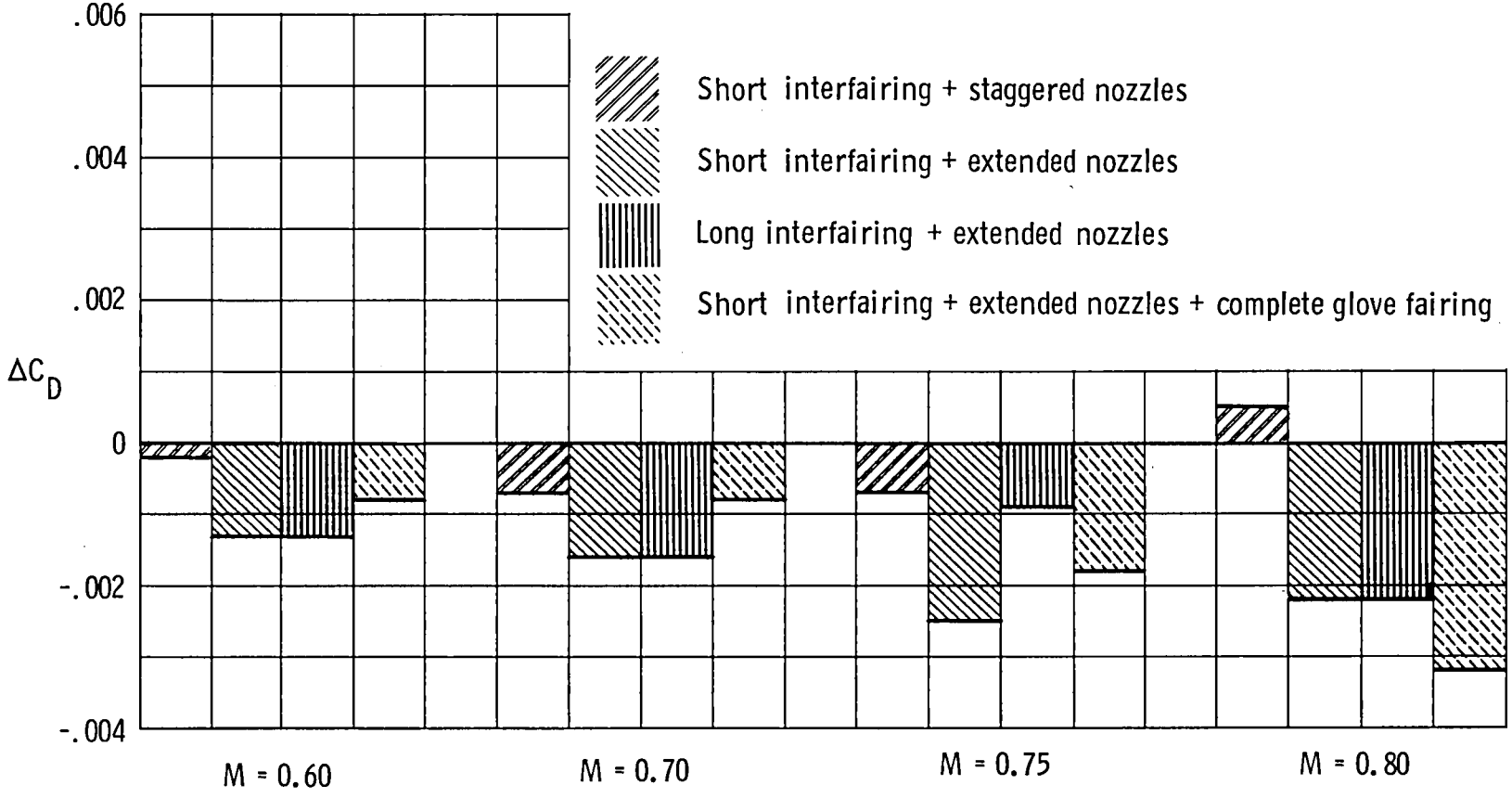

Figure 40.- Effect of staggered and extended nozzles, interfairing length, and complete glove fairing on incremental drag at $C_L = 0.63$ for model with wings swept 25°.

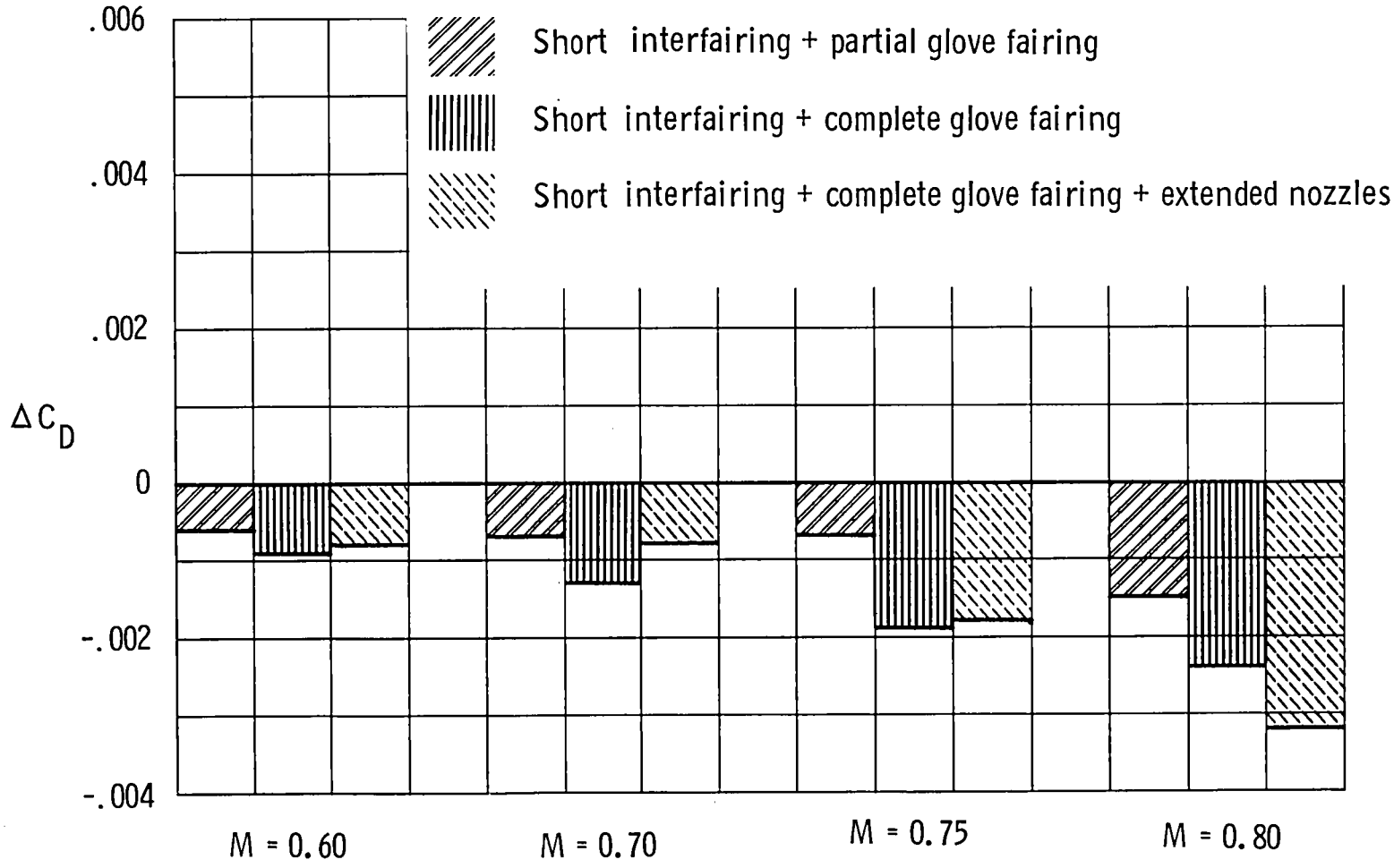

Figure 41.- Effect of glove fairing on incremental drag at $C_L = 0.63$ for model with wings swept 25°.

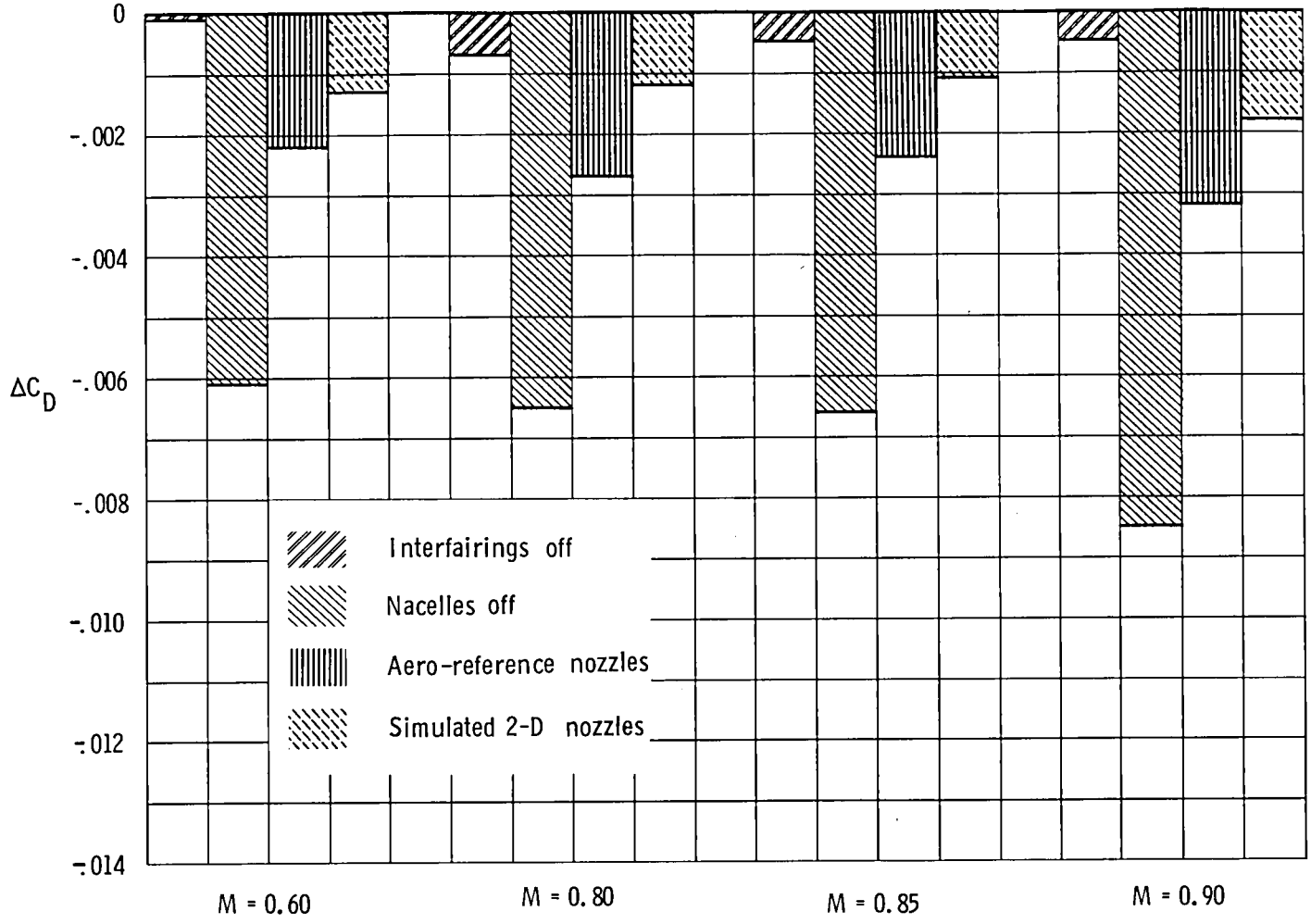

(a) M = 0.60 to 0.90.

Figure 42.- Effect of nacelles and nozzle shape on incremental drag at C_L = 0.16 for model with wings swept 65°.

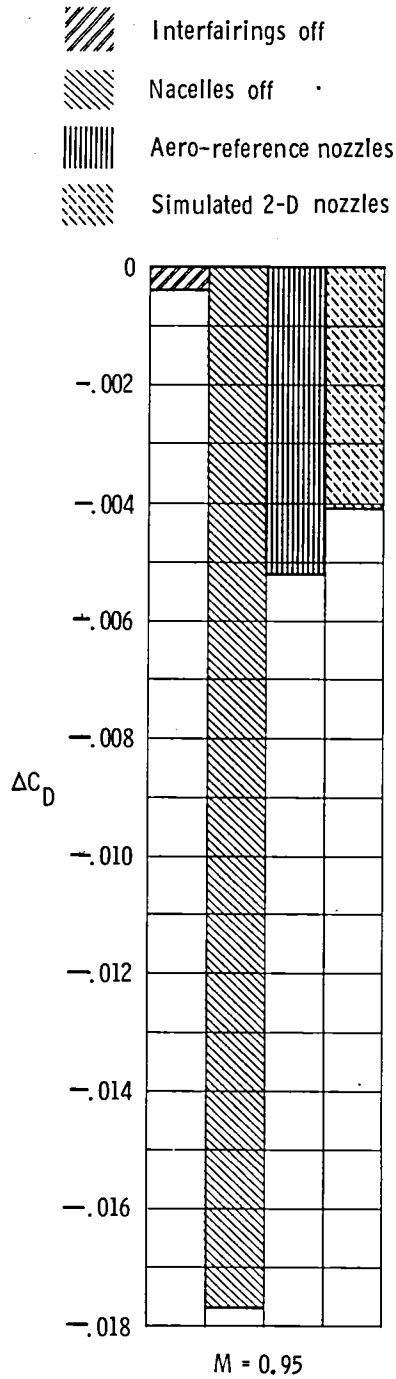

(b) M = 0.95.

Figure 42.- Concluded.

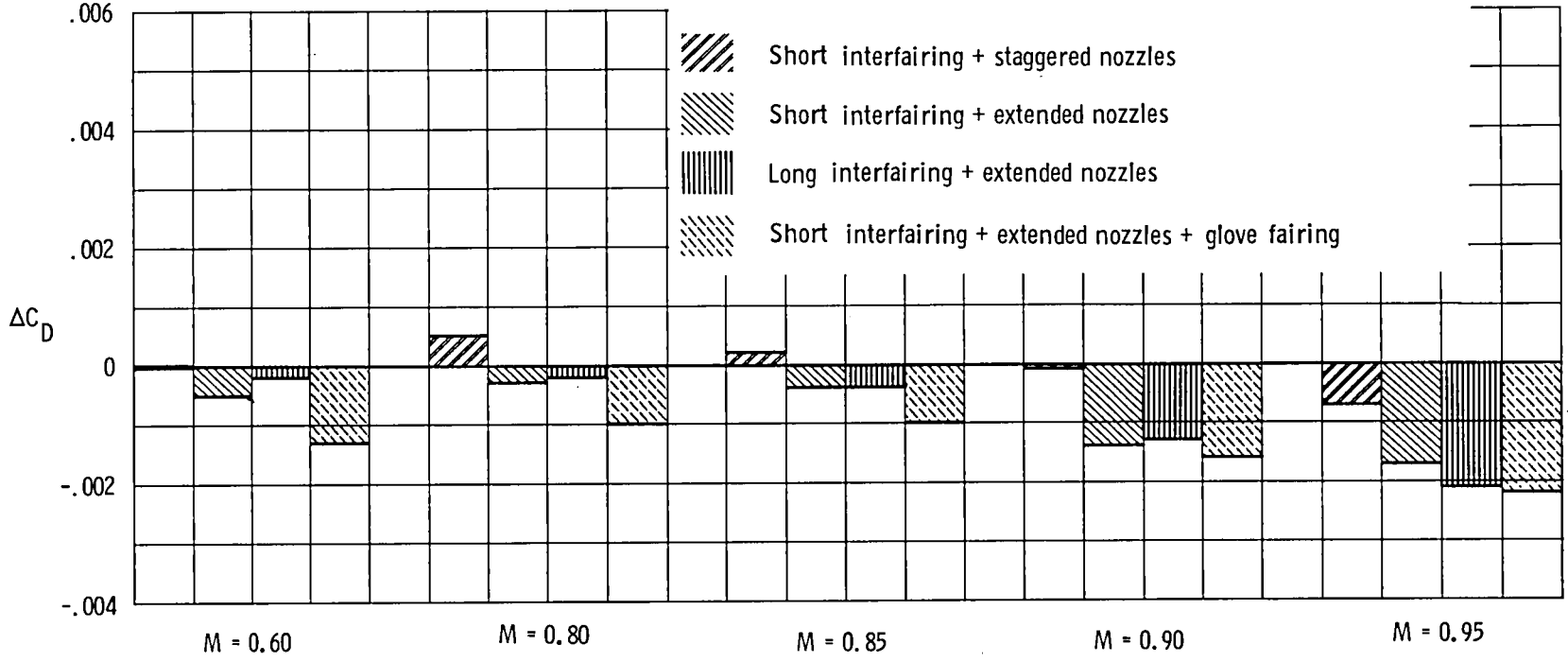

Figure 43.- Effect of staggered and extended nozzles, interfairing length, and glove fairing on incremental drag at $C_L = 0.16$ for model with wings swept 65°.

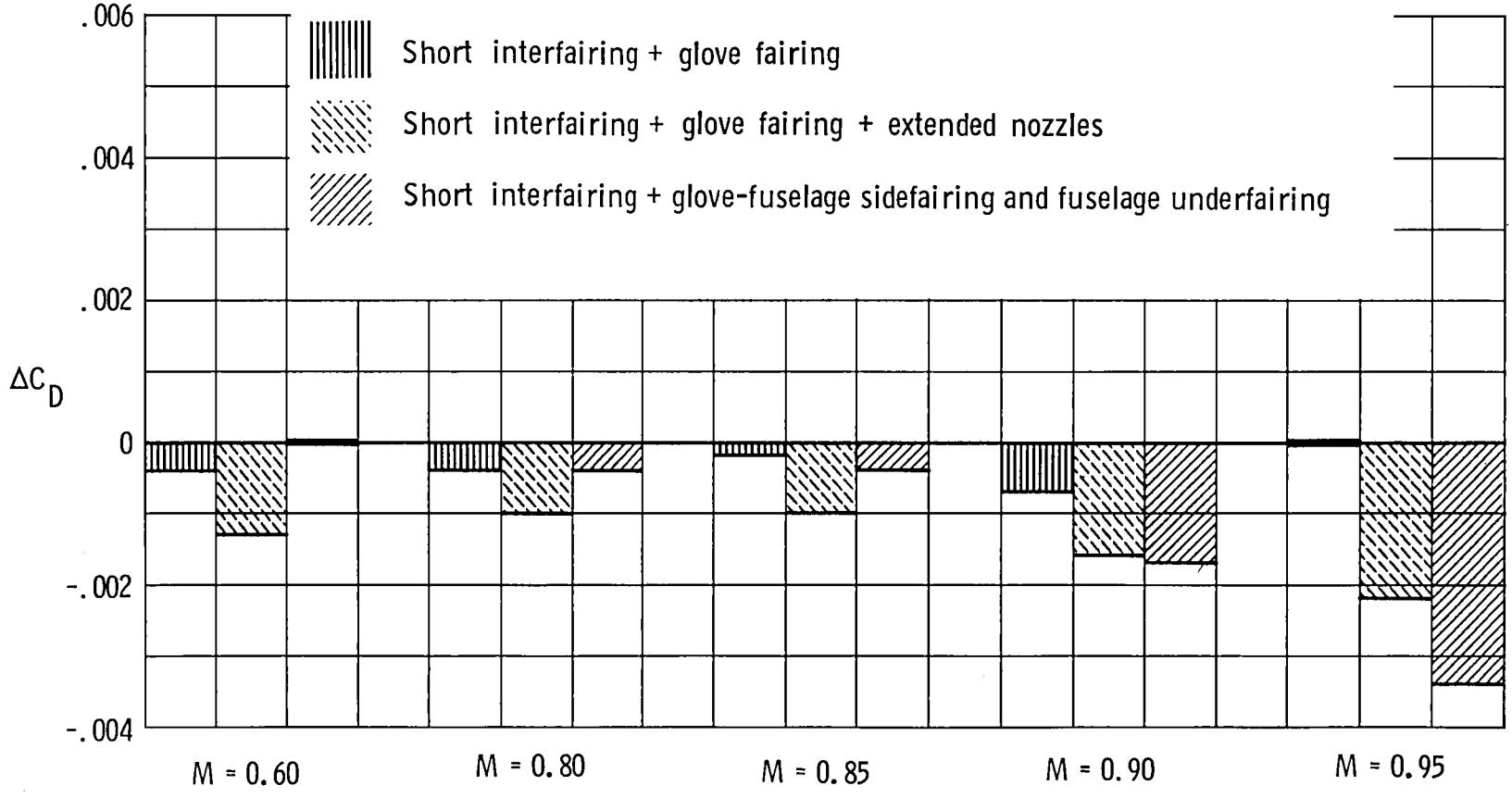

Figure 44.- Effect of glove and fuselage fairings on incremental drag at $C_L = 0.16$ for model with wings swept 65°.

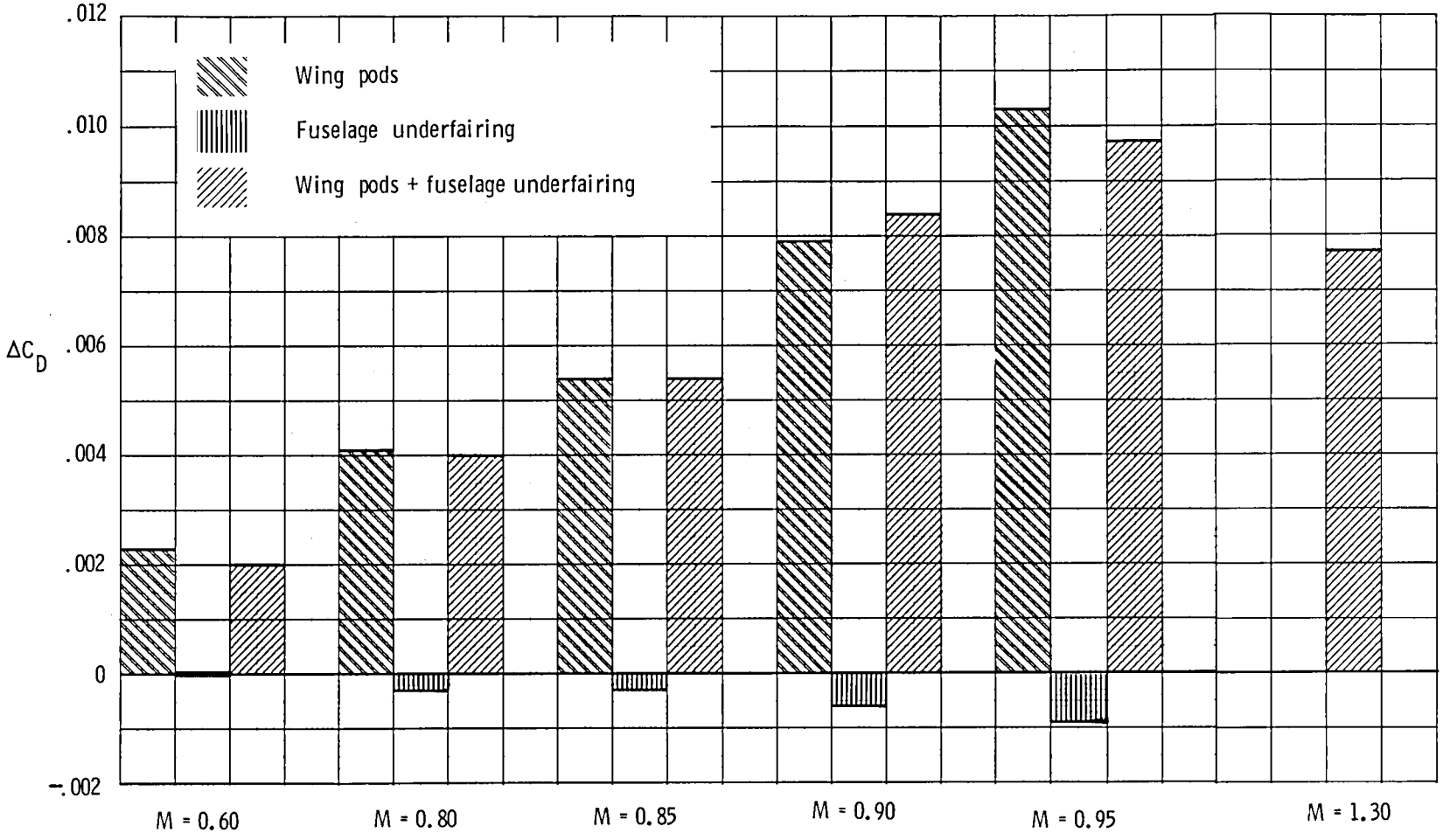

Figure 45.- Effect of wing pods, fuselage underfairing, and a combination of the two on incremental drag at $C_L = 0.16$ for model with wings swept 67.5°.

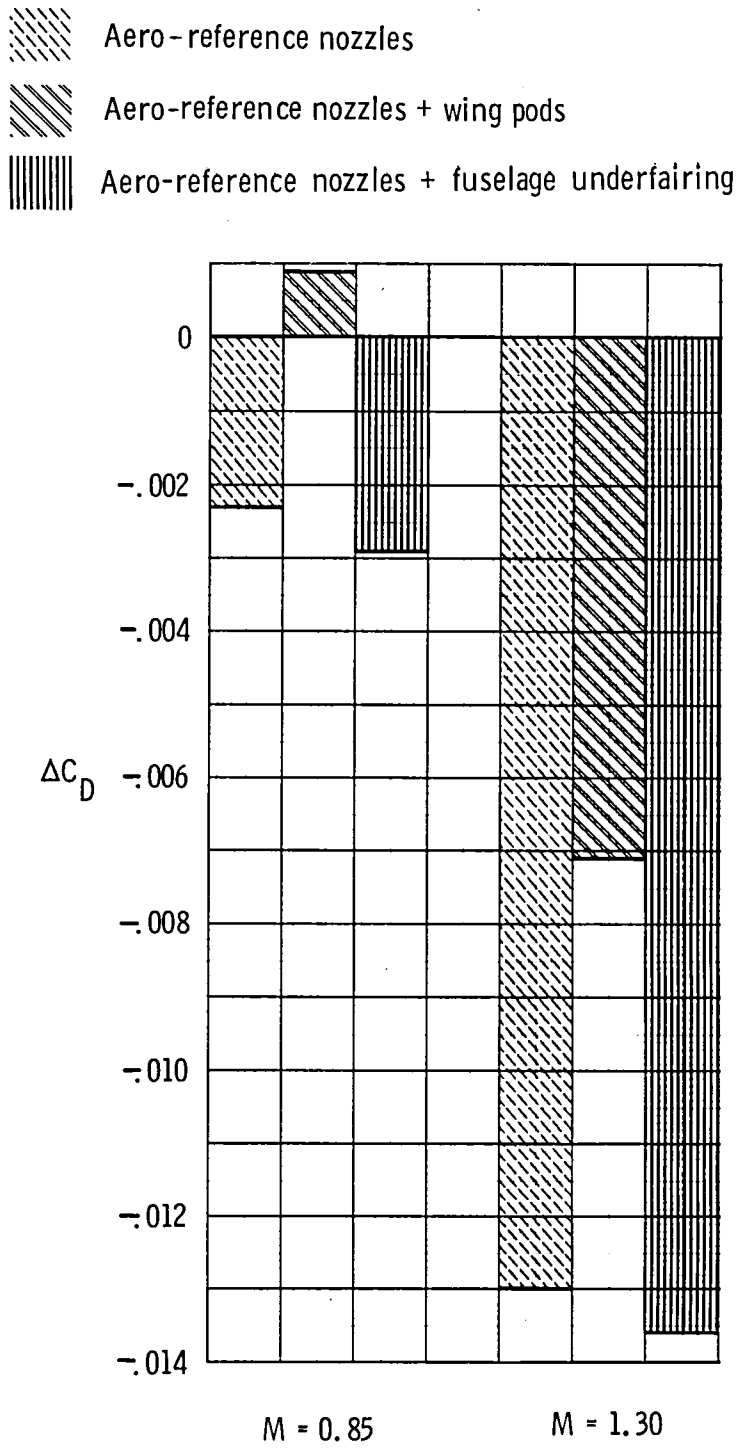

Figure 46.- Effect of aero-reference nozzles, wing pods, and fuselage underfairing on incremental drag at $C_L = 0.16$ for model with wings swept 67.5°.

1. Report No.	2. Government Accession No.	3. Recipient's Catalog No.
NASA TM-80129		

4. Title and Subtitle	5. Report Date
EFFECT OF SEVERAL AIRFRAME/NOZZLE MODIFICATIONS ON THE DRAG OF A VARIABLE-SWEEP BOMBER CONFIGURATION	October 1979
	6. Performing Organization Code

7. Author(s)	8. Performing Organization Report No.
Richard J. Re and David E. Reubush	L-13043
	10. Work Unit No. 505-04-13-02
9. Performing Organization Name and Address	11. Contract or Grant No.
NASA Langley Research Center Hampton, VA 23665	
	13. Type of Report and Period Covered
12. Sponsoring Agency Name and Address	Technical Memorandum
National Aeronautics and Space Administration Washington, DC 20546	14. Sponsoring Agency Code

15. Supplementary Notes

16. Abstract

An investigation of a 0.06-scale model of a variable-sweep bomber airplane was conducted in the Langley 16-foot transonic tunnel to identify possible modifications to the configuration which would result in reduced drag. The modifications, some of which were tested in combination, included simulated two-dimensional nozzles; staggered and extended nozzles; short, long, and no interfairings between the nozzles; partial and complete wing-glove fairings; glove-fuselage sidefairing; fuselage underfairing; and wing pods. Tests were conducted at Mach numbers from 0.60 to 1.30 at angles of attack in the range from -4° to 12° with the wings swept 25°, 65°, and 67.5°. Of the modifications tested, the staggered nozzles and the changes in interfairing lengths had little or no effect on the drag, the wing pods increased the drag, and the rest of the modifications reduced the drag.

17. Key Words (Suggested by Author(s))	18. Distribution Statement
Variable-sweep bomber Drag reduction	Unclassified - Unlimited Subject Category 02

19. Security Classif. (of this report)	20. Security Classif. (of this page)	21. No. of Pages	22. Price*
Unclassified	Unclassified	168	$8.00

* For sale by the National Technical Information Service, Springfield, Virginia 22161

NASA-Langley, 1979

National Aeronautics and
Space Administration

Washington, D.C.
20546

Official Business
Penalty for Private Use, $300

SPECIAL FOURTH CLASS MAIL
BOOK

Postage and Fees Paid
National Aeronautics and
Space Administration
NASA-451

NASA

POSTMASTER: If Undeliverable (Section 158 Postal Manual) Do Not Return